Stratigraphic Modelling and Chronology at the Site of Soyo, Northern Mongolia

Michael Everett
Bachelor of Science (Adv.) and Bachelor of Arts (Honours)

A dissertation submitted to
the Department of Archaeology, Flinders University
for the degree of
Doctor of Philosophy

February 2024

Declaration

I certify that this thesis:

1. does not incorporate without acknowledgement any material previously submitted for a degree or diploma in any university; and

2. the research within will not be submitted for any other future degree or diploma without the permission of Flinders University; and

3. to the best of my knowledge and belief, does not contain any material previously published or written by another person except where due reference is made in the text.

Signed
Michael Everett
31 July 2023

Abstract

The archaeology of Mongolia is relatively less known than many other parts of the world. In particular, there is limited understanding of chronology prior to the Late Bronze Age. This is despite the Neolithic and Early Bronze Age being the probable time for the emergence of pastoralism which is a major ongoing research question in Mongolian archaeology.

Part of the difficulty is due to the unstratified nature of many Mongolian sites meaning archaeological material is difficult to arrange into a relative chronological system to examine diachronic trends. The site of Soyo, in the Darkhad basin of northern Mongolia, presents a rare opportunity to study a stratified Neolithic site in Mongolia. Previous research at the site has revealed an extensive site formation history from as early as 13,000 years ago and occupation from at least the Neolithic period at 6500-6000 years ago contained within multiple generations of palaeosols. However, the complex and disturbed stratigraphy at this site within a former glacial valley has so far hindered efforts to construct a site-wide stratigraphic model and chronological framework.

This thesis presents new stratigraphic modelling of Soyo using geophysical, sedimentological and radiocarbon results. Electrical resistivity tomography and magnetometry surveys were conducted in 2019 alongside excavations for stratigraphic control. This is combined with previously collected ground-penetrating radar data to construct a model for the stratigraphy at Soyo. Sediment analyses are used to infer depositional environments for each layer and radiocarbon dates (both new and old) provide ages for the layers and the archaeological material they contain.

The results of this thesis challenge previously held assumptions about age of much of the stratigraphy at Soyo. While extensive periods of previously missing stratigraphy have been accounted for here, it was also found that the there are likely to be significant periods not represented because of erosion or non-deposition. Furthermore, much of the complex stratigraphy at Soyo does not extend far laterally because the site experienced periods of deposition and erosion in localised areas rather than site-wide. It is argued here that the Neolithic and Early Bronze Age strata at Soyo are partially missing because of erosion or non-deposition which reduces the ability of the site to inform archaeologists about diachronic changes in that period of Mongolia's history. It is suggested also that changes in

lithic technology at Soyo that had previously been tentatively assigned to the Early Bronze Age probably date to the Early Iron Age.

Special thanks to

- Dr Ian Moffat (principle supervisor) for his excellent supervision, research group meeting and discussions, and for his voluminous feedback.
- Dr Julia Clark (supervisor) for her invaluable feedback, for previous archaeological reports from Soyo and for leading the 2019 field season to Soyo.
- Dr Martin Polkinghorne (supervisor) for his feedback and support for the past few years.
- Jamsranjav Bayarsaikhan for leading the 2019 field season to Soyo.
- Rob Koch for help with geopositioning at Soyo and post-processing afterwards.
- Zee for the use of his photographs taken at and around Soyo.
- All other staff and students who attended the 2019 field season to Soyo for their help and especially for digging and logging all those stratigraphic excavations.
- Chantal Wight for access to the Flinders University archaeology lab and for various help with using equipment.
- Ms Curtis, my highschool history teacher, who set me down the path of research with some much needed toughness.
- Australian Institute for Nuclear Science and Engineering (AINSE) for grants for radiocarbon and cosmogenic dating.
- Australian Government Research Training Program Scholarship (RTP).
- New Colombo Plan (Department of Foreign Affairs and Trade) for the funds to attend the 2019 Soyo field season.

"When I had journeyed half our life's way,
I found myself within a shadowed forest,
for I had lost the path that does not stray.
Ah, it is hard to speak of what it was,
that savage forest, dense and difficult,
which even in recall renews my fear:
so bitter — death is hardly more severe!
But to retell the good discovered there,
I'll also tell the other things I saw."

– Dante Alighieri *La Commedia*
Translated by Allen Mandelbaum
Everyman's Library (1995)

To the Virgil who guided me up the steep and savage ascent to the threshold of completion.

Contents

Chapter 1

Introduction

1.1 The Problem - The Solution

Research on the archaeology of Mongolia has flourished in recent decades. There has been a slew of theses written on pre-Iron Age Mongolia in the last two decades (Wright 2006, Houle 2010, Janz 2012, Clark 2014, Vella 2018, Gribble 2021) and yet understanding of this part of Mongolia's past remains obscured. This is even more so the case for pre-Bronze Age, Holocene Mongolia on which there is very little known. This stands in contrast to other geographic areas such as the Near East and Europe where those early time periods are intensively studied.

The biggest problem lies with the difficulty in establishing an accurate chronology of events and trends due to the lack of well stratified sites that were inhabited over a long period of time. Because of the high prevalence of mobility among the nomadic pastoralists living there, sites are scattered in the landscape rather than being built up successively through intensive occupation of single locations. This has led to an emphasis on landscape-level approaches (Honeychurch *et al*. 2007, Seitsonen *et al*. 2018, Schneider et al. 2020) but it hampers regional chronologies as it is difficult to determine temporal relations between spatially disparate sites. Furthermore, sites that are reused tend to become palimpsests of multiple periods of occupation as is often the case with the remains of nomadic pastoralists (Cribb 1991, p. 80). It is unusual to find sites in Mongolia with thick, datable strata.

The site of Soyo (fig. 1.1), however, appears to offer a rare chance to study early Mongolian archaeology in a stratified context. Soyo was discovered in 2002 in the Darkhad region of northern Mongolia by the American-Mongolian Deer Stone Project and further investigations were conducted in subsequent years (Fitzhugh 2003, 2005). The site proved promising as it yielded detailed stratification alongside Neolithic remains. Radiocarbon dates from both the Neolithic and the Iron Age were obtained indicating an extended period of use. However, intensive investigation at the site was not undertaken as the project's attention was diverted to other sites bearing Bronze Age monumental architecture. Later,

the site was taken up by NOMAD Science who have conducted surveys and excavations there since (Clark 2015, Clark and Bayarsaikhan 2016, 2017, 2018). Other recent studies of the site include a ground-penetrating radar survey (Vella 2018) and a morphological study of the stone tool inventory (Gribble 2021). It is hoped that Soyo will provide a detailed chronology of material culture for the earlier periods of Mongolian archaeology and especially the Neolithic and Early Bronze Age. This will help understand the nature of timing of Mongolia's earliest economic and cultural transitions. The critical transition to pastoralism, thought to have occurred during the Early Bronze Age (Clark 2014, p. 52), is of particular interest for archaeological research in the Darkhad.

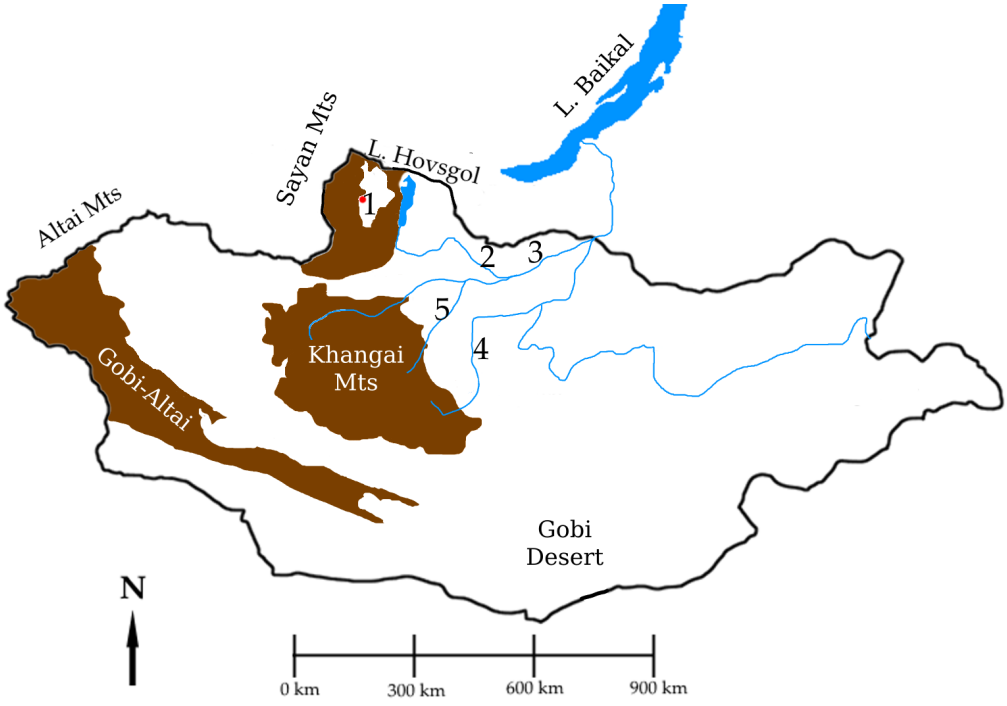

Figure 1.1: Geographic map of Mongolia showing the location of Soyo and important rivers and mountain ranges for Mongolian archaeology. 1. Soyo; 2. Egiin River; 3. Selenge River; 4. Orkhon River; 5. Khanuy River

In order to be able to date the stratigraphic layers at Soyo, it is essential that their morphology - including depth, thickness, extent - first be understood. Given the expansive size of Soyo, relying solely on test pits to determine this is not feasible. The variety in surface morphology (sand dunes, stable surfaces, boulder fields) also suggests an equally complex subsurface. Geophysical methods have had a long and extensive use in archaeology (Clark 1975, Gaffney 2008, Campana and Piro 2009, El-Qady and Metwaly, Mohamed 2019) for a variety of archaeological purposes including understanding site stratigraphy (Challis and Howard 2006, Carey *et al.* 2017, 2018). A ground-penetrating radar survey of part of Soyo has already been completed (Vella 2018) but it was highly localised to one part of the site. Without stratigraphic controls over a wider area, it is difficult extrapolate

geophysical information across an entire site. Furthermore, the radiocarbon dating was hindered by turbated stratigraphy. One stratigraphic unit contained samples that have been dated to over ten thousand years apart.

The use of multiple geophysical techniques can improve interpretability by targeting different physical properties of the subsurface. By using multiple methods over a wider area, a more complete picture of the sedimentary structure of Soyo will be obtained. Individual, local sedimentary layers, once correlated into site-wide units, can thus be dated to provide a chronological framework and give context to the archaeological remains.

1.2 Research Aims and Significance

This present research program was undertaken with three primary intentions.

- To use geophysical methods (primarily ground-penetrating radar and electrical resistivity tomography) to build a model for the stratigraphy of Soyo.
- To use dating techniques such as radiocarbon dating to give an age for each major sedimentary unit in the stratigraphic model and to provide chronological constraints for the site as a whole.
- To use existing palaeoclimate records to interpret the likely environmental context for the deposition of each stratigraphic unit.

In addition to these, three more specific, unresolved questions regarding Soyo are addressed.

- How do the dates acquired by Vella (2018) relate to the rest of Soyo and are there surviving, datable strata between 12,900 and 1250 years BP?
- What is the date of the material culture at Soyo and particularly the date of the transition in stone tool artefacts identified by Gribble (2021)?
- Is Soyo a good choice in site for research into the advent of pastoralism in Mongolia which is thought to have taken place in the Early Bronze Age?

The primary goal of this research is to build and date a model of the stratigraphy at Soyo. This will be achieved by using geophysics to trace stratigraphic layers beneath the earth using test pits and excavation units as stratigraphic controls. The geophysics will be supplemented with absolute dating of charcoal, wood and bone samples recovered from the excavations. These can be used to date the local stratigraphy and, by extension, the site-wide stratigraphy. By comparison to existing climate records from the region, the contemporary environments for each dated strata can be elucidated giving an environmental context to human occupation at Soyo. This is a critical step since environmental factors are a frequently cited cause or precipitating catalyst by archaeologists for various changes in past human behaviour.

Once a chronological framework for the sedimentology of Soyo has been established, it will be possible to answer the research questions presented. Whether any of the chronological gap in the dates provided by Vella (2018) can be filled will be easily seen with the new radiocarbon dates from elsewhere at Soyo. These may also extend the age range for the site's formation and occupation history. This is important because the standing difficulty in the chronological interpretation of the site prevents any attempt at answering questions pertinent to Mongolian archaeology at large. Specifically the apparent gap in stratigraphy incorporates the critical Neolithic and Early Bronze Age periods which are of particular interest in the field of Mongolian archaeology.

The dating of transitions in material culture will be a direct consequence of this research since previous studies (Gribble 2021) have had to rely on describing changes as a function of depth rather than in terms of stratigraphy. By comparing the depths at which artefacts were found to the new stratigraphic model, it will be possible to more accurately compare trends identified in different excavation units. This is a key outcome of the research at Soyo because understanding trends in material culture will shape our understanding of past human behaviours and processes. If changes in material culture can be dated to the Neolithic and Early Bronze Age, that will inform our understanding of past behaviours leading up to the nomadic Late Bronze Age populations of Mongolia.

Finally, and in connection to the last point, this research will provide greater insight into the suitability of Soyo for answering certain questions being asked in the wider field of Mongolian archaeology. This will be answered by looking for stratigraphic separation between layers of the appropriate time periods. For example, if Soyo is a suitable site for further research for identifying the shift to pastoralism thought to be concurrent with the Early Bronze Age, it should have separated strata before (Neolithic), during (Early Bronze Age) and after (Late Bronze Age). This would allow the identification of changes in the archaeological finds that may help explain the process behind the transition including how and why it occurred. If Soyo does prove to be a suitable site for investigating the origins of pastoralism, that would be highly significant to Mongolian archaeology at large since this is currently an open question. This research would provide direct answers on the areas with relevant preserved stratigraphy and the most effective places to excavate. On the other hand, if Soyo proves not to be suitable, this is also an important contribution to Mongolian archaeology since it would steer efforts away from unfruitful endeavours and provide insight on whether this approach to the question is likely to succeed elsewhere or not.

1.3 Chapter Outline

In Chapter 2 "Background," the archaeological literature is primarily discussed. It begins with an overview of archaeological time periods. A short summary of the Palaeolithic is

given before moving onto the Mesolithic-Neolithic along with an explanation of the terminology in Mongolia for the Stone Age of the Holocene. After that, the (Late) Bronze Age is discussed which finishes with the transition into the Iron Age. A special section is dedicated to the important topic of nomadic pastoralism and theories on the origins and motivations of the phenomenon including general trajectories and timelines for the emergence of pastoralism on the Eurasian steppe. A closer examination is made of the earliest pastoralism on the Mongolian steppe and its rise to prominence. The background chapter also comprehensively summarises the work that has taken place at Soyo so far including archaeological investigations by the Deer Stone Project 2002-2004 and NOMAD Science 2015-2018 including the pedestrian surveys that have been conducted in the wider landscape. A description of the geology and geomorphology of the landscape is also provided since it is of vital importance to the interpretation of the geology at Soyo. Every scientific date from specifically archaeological contexts in the Darkhad basin is also presented alongside the information from Soyo in order to give it chronological context. This forms the most complete summary of Soyo published as of this date. The chapter concludes with a summary of palaeoclimate records from the Darkhad, Lake Hovsgol, Lake Baikal and elsewhere in Mongolia. Detailed attention is given to the chronology of the rise and fall of the Darkhad palaeolake during the Holocene so that the model of Soyo's stratigraphy can be given its proper climatic and environmental context.

Chapter 3 "Methodology" is dedicated to exploring the background of the methods used in this research. The bulk of this chapter discusses the geophysical techniques of electrical resistivity tomography, ground-penetrating radar and magnetic methods. For each method, an explanation of the underlying physics is given first. The explanations are intended to be in-depth but intuitive with minimal mathematics. The desired outcome is explain *why* geophysics can be used in archaeology rather than merely stating *how* it can be. Secondly, a brief explanation is given of how each of the types of surveys is conducted followed by more explanation of the processing steps that can be performed on the raw data obtained. Thirdly, the range of uses for each method is explored including different archaeological targets that can be detected and different approaches to using geophysics in archaeology. Aside from the geophysics, the other methods used in this research are briefly explained as well. These include sediment analyses, radiocarbon dating and photogrammetry.

Chapter 4 "Methods" documents the actual steps taken for each method employed in this project. This includes both data collection in the field and processing steps taken afterwards for the geophysics, photogrammetry, stratigraphic pits and sediment analysis, geopositioning and GIS, and radiocarbon dating.

Chapter 5 "Results" presents the results obtained. It includes individual results from each method but not products obtained by comparison and interpretation of multiple methods.

Chapter 6 "Discussion" begins by synthesising all of the results from the previous chapter

into a unified model of Soyo. This involves correlating all of the stratigraphic information into one master stratigraphic scheme including the information gained from previous studies at the site. A model for the structure of Soyo along with an explanation on the likely depositional environments and site formation history is proposed. This section also elaborates on the age chronology of each master stratigraphic unit based on current and prior radiocarbon dating and compares it with the existing palaeoclimate records. Having elaborated on the structure and chronology of Soyo, the attention then turns to the archaeological record both at Soyo and in the surrounding landscape. Some conclusions are offered to explain the record and alternative interpretations are made where the assumed chronology in the literature does not match the dates from this work. Chapter 6 also considers the implications this research brings to both Mongolian archaeology as a whole and to similar geoarchaeological projects. In particular, the suitability of Soyo is assessed regarding the search for transitions between Mesolithic-Neolithic and Early Bronze Age cultures. The difficulties faced during the project and promising lines for future research are expounded on at the end.

Chapter 7 "Conclusion" summarises the work undertaken for this thesis and provides answers to the research questions posed above. Some major limitations and future recommendations specifically regarding the work at Soyo are reiterated.

1.4 Conventions Used

Throughout this thesis, a variety of specific terminology is used and it would do well to explain those here. First, the dating conventions used here are as follows. "BP" always refers to uncalibrated radiocarbon years before present (where "present" means AD 1950). This is only ever affixed to a radiocarbon date. Calibrated carbon dates are affixed with the customary "cal. BP" and are calibrated with the IntCal20 calibration curve (Reimer *et al*. 2020). Every carbon date acquired from the literature was recalibrated using IntCal20 with rcarbon (an R package). The acronym *kya* (in italics) is used as a general purpose way of expressing thousands of (calendar) years before the present. The present is again defined to be AD 1950. It does not have any particular technical meaning and is used to compare ages more generally and to discuss sequences of events.

Periodisation terms are rendered as acronyms where this is conventional to do so and the meaning is clear. For example, *EBA* for *Early Bronze Age*, *LBA* for *Late Bronze Age*, *EIA* for *Early Iron Age* and so on. Terms like *Bronze Age* and *Iron Age* are written in full because it may be less clear what *BA* and *IA* mean.

Toponyms are given in both their English and Mongolian (transliterated) forms. For example, the river that flows past Soyo can be referred to either as the River Hog or as the Hogiin Gol. To aid the reader, a table of common geographic features has been made which translates between the Mongolian and English (tab. 1.1). Like any language that is

English	Mongolian
River	Gol
Lake	Nuur
Hill	Tolgoi
Conifer forest	Taiga
Mountain	Uul

Table 1.1: Table of equivalent English and Mongolian toponyms.

not written in Latin script, Mongolian has multiple transliterations that are encountered in the archaeological literature. An attempt to consistently use one transliteration system was not made here. Instead, the spelling that was most commonly encountered was used. The most notable (and potentially confusing) difference in spelling is in the use of ”kh” or ”h” to render ”x” in Cyrillic. For example, *Darkhad* is also spelled *Darhad* (amongst other spellings) while *Hovsgol* may also be rendered as *Khuvsgul* (among others). Some care needs to be taken when reading to recognise different forms of the same place name.

Chapter 2

Background

2.1 Pre-Bronze Mongolia

The archaeology of Stone Age Mongolia is relatively unstudied. Only a limited number of sites have been found and even fewer are stratified. It is difficult, therefore, to construct a sequence of technological and behavioural changes for this time period so that it can be further classified into smaller subperiods. This makes existing work on periodisation invaluable for the archaeologist of this time period.

Of all the Stone Age periods of Mongolia, the one for which we have the most developed knowledge is the Upper Palaeolithic. This has been split into several subperiods based on changes in the types and frequencies of lithic artefacts which are the Initial, Early, Middle and Late Upper Palaeolithic periods. The Initial Upper Palaeolithic is thought to have begun between 50 and 46 *kya* (Khatsenovich *et al*. 2017, p. 90, Zwyns *et al*. 2019, p. 3) and introduced new blade technology at the transition from the Middle Palaeolithic which had been characterised by flakes (Zwyns *et al*. 2014, p. 64). Since most of the discovered Initial Upper Palaeolithic sites are from the Selenge River region, it has been hypothesised that this area was a major migration route into Mongolia during MIS3 (Zwyns *et al*. 2014, 2019, Wright 2021, p. 437). The Altai has also been suggested as a possible intermediary area through which IUP technology entered Mongolia since this location is traditionally considered to have had the oldest IUP assemblages (Rybin *et al*. 2016, p. 74, Khatsenovich *et al*. 2017, p. 91). More recent dating indicates that IUP appeared in northern Mongolia around the same time as in the Altai (Zwyns *et al*. 2019, p. 5) and that its appearance is probably linked to the dispersal of Homo *sapiens* throughout the region (Zwyns *et al*. 2019, pp. 6–7). The Middle Upper Palaeolithic (concurrent with the LGM) saw a sharp decrease in the number of sites across Mongolia (Rybin *et al*. 2016, p. 76) and in the number of blades (Gladyshev *et al*. 2010, p. 39, Rybin *et al*. 2016, p. 79) but the following Late Upper Palaeolithic saw the flourishing of a new microcore and blade industry (Gladyshev *et al*. 2010, p. 39, Rybin *et al*. 2016, pp. 79–80). Although the evidence for climatic impact on intensity of occupation in Mongolia is still in its infancy, it is considered that the rise of microblade technologies in the post-LGM period was an adaptation to the harsh climate

by mobile foraging groups (Yi *et al*. 2016, Takakura 2020, p. 1).

2.1.1 The Holocene Stone Age: A Note on Terminology

There is little known about the Mongolian Holocene; however, recent scholarship has made progress towards a greater understanding of it. Unfortunately, there is a fundamental problem that has not been clearly resolved which is the question of what to call the period that lies between the Upper Palaeolithic and the Bronze Age. The contenders - *Neolithic*, *Mesolithic* and *Epipalaeolithic* - are well known in the archaeology of Europe and the Near East. In particular, the Neolithic is typically understood to mean something to do with the domestication of animals and especially plants, sedentism and other major changes in human behaviour. The word itself was coined by Sir John Lubbock who made a twofold division in the pre-metallic age. The Neolithic was distinguished from the Palaeolithic on the basis of the presence of ground stone tools, pottery, architecture, domestication of plants and animals, and the absence of megafauna (Lubbock 1865, Clark 1980, pp. 1-2). However, it is V. Gordon Childe whose name is most attached to the concept of the Neolithic and its break from earlier times. Childe introduced the explicit concept of a "Neolithic revolution" which is to say he conceived of the Neolithic as the pivotal moment in human history. Even more so, the Neolithic revolution must have been a specific and localised event: localised to the Near East from whence it spread to the rest of the world (Childe 1929, pp. 1–3). However, a different definition of the Neolithic was adopted in areas that were dominated by the Soviets. There the Neolithic meant pottery (Chard 1958, Kuzmin 2010). It is important to keep this difference in terminology in mind while thinking about this period of time in different places around the world.

Following more archaeological study on Stone Age remains in Europe and the Near East, it became apparent that going from "Old" into "New" was not such a sharp boundary and that there were cultural assemblages that could not comfortably be placed in either. A prime example is the Natufian culture of the Levant whose members practised sedentism alongside intensive and specialised resource acquisition: a marked break from the mobile hunter-gatherers who had preceded them and echoing the Neolithic to come (Belfer-Cohen 1991, p. 173). The Natufian is commonly assigned to the Epipalaeolithic of the Levant which implies that it is the epilogue to the Palaeolithic even though scholarship for decades has focused on its being the prologue to the Neolithic. For a fascinating history on the terminology of the Natufian time period and the changing thinking about what the Natufian represents, the reader is directed to Boyd (2018) and Richter and Mayer (2013). In Europe a similar transitional period between the Palaeolithic and the Neolithic has become the focus of increasing scholarship. There the term Mesolithic, to signify the independent importance of this period, has achieved acceptance although not unreservedly (Clark 1980, pp. 1–7). The Mesolithic period in Europe has become to be seen as one of regionalisation but also continuity (Kozłowski 2009, p. 25). In both the European and Levantine cases, the hard distinction between Palaeolithic and Neolithic has long softened into a transitional period.

Soviet custom	″Neolithic″
Séfériadès (2004)	″Mesolithic″ and ″Neolithic″
Wright (2006)	″Mesolithic″
Derevianko *et al*. (2008)	″Neolithic″
Houle (2010)	″Epipalaeolithic″
Clark (2014)	″Epipalaeolithic″
Schneider *et al*. (2016)	″Neolithic″
Janz *et al*. (2017)	″Mesolithic,″ ″Neolithic″ and ″Oasis I/II″
Seitsonen *et al*. (2018)	″Epipalaeolithic″ and ″Neolithic″
Rosen *et al*. (2019)	″Epipalaeolithic,″ ″Neolithic″ and ″Oasis I/II″
Wright (2021)	″Holocene hunter-gatherers″

Table 2.1: Summary of various authors' terminology for the period between the Upper Palaeolithic and Bronze Age of Mongolia

In Mongolia the search for a transitional period has also been undertaken in recent years. In this case, however, the transition is not one towards agriculture but towards pastoral nomadism and associated monumental constructions. Furthermore, the transition is not towards the Neolithic but towards the Late Bronze Age (LBA) from the preceding periods. In Mongolia the time between the Epipalaeolithic and the LBA (particularly the Early Bronze Age (EBA)) is thought to be the critical transition period involving the beginnings of pastoralism (Clark 2014, p. 52). However, there is no consensus on what to call the pre-Bronze period of Mongolia. As an ex-Soviet country, the use of the Soviet definition of Neolithic is still dominant but the Near Eastern definition as well as terms like Mesolithic and other terminology are also seen (Séfériadès 2004, Wright 2006, Janz 2012, Zhao *et al*. 2021). The reader should beware this terminological mire and be mindful of which terminology each author is using. See table 2.1 for an overview of naming schemes by several authors. In this work, the (hopefully) neutral *Mesolithic-Neolithic* is used to describe the pre-Bronze Age and post-Palaeolithic period in Mongolia in the general case. This term is chosen to not make any claims about the character of the archaeological material and sites belonging to that time frame. The word *Epipalaeolithic* is avoided so as to not join this period to the Palaeolithic. However, when describing material and sites from the literature, the original word used in that reference may be used. The reader should understand that no attempt at periodisation of archaeological material is being made here.

2.1.2 Archaeology of the Mongolian Mesolithic-Neolithic

Only a handful of Mesolithic-Neolithic sites in Mongolia have been studied with chronological changes in mind which only increases the uncertainty around periodisation. Most of these are in the Gobi region. The most developed chronology for the Holocene Stone

Age in Mongolia accordingly then comes from the Gobi region. The archaeological remains there have been divided up by Lisa Janz (2012) (see also (Janz *et al*. 2017, 2021, p. 2)) into three periods on the basis of wetland use appropriately named Oasis I, Oasis II and Oasis III (table 2.2). Oasis I (13.5-8.0 *kya*) is characterised by the production of microblades with a variety of core types and some fine retouching. Populations are highly mobile and low-fired pottery with organic temper makes an appearance by 9.6 *kya*. The variety of lithics types expands during the Oasis II (8.0-5.0 *kya*) period which saw the emergence of large grinding stones and partially polished stone tools. Sand and other clastic debris is added to the temper of pottery which is now decorated with impressions and mouldings. Microblade technology continues alongside bifacial and unifacial points. The organisation of population at this time appears to have been clustered into longer term habitation around forageable wetlands. Finally during Oasis III (5.0-3.0 *kya*), the grindings stones reduce in size, axes and adzes become fully polished and endscrapers made from microblades become common. There is also a shift towards conical cores dominating. New high-fired red-ware ceramics appear with paint, geometric incisions, stamps, mouldings and impressions. Copper smelting is demonstrated by the presence of slag.

The main feature of the Oasis chronological model is the change in economy from the Late Upper Pleistocene to the beginning of the Bronze Age in the Gobi region. The general trajectory proposed is an increase in broad-spectrum foraging and localised land usage centred around oases during the beginning stage of the Holocene (Janz *et al*. 2017, p. 14). While direct evidence is lacking, the shift in site occupation towards lakes and wetlands leading into Oasis I is taken as evidence for broad-spectrum foraging as ancient people focused on exploiting the variety of wetland animals and plants over hunting bigger game on the steppe. This interpretation is bolstered by more direct evidence from neighbouring northern China where grinding stones, starch grains and the remains of small game attest to an expanded diet (Janz *et al*. 2017, pp. 21–3).

A clear example of the shifting subsistence strategies comes from the site of Zaraa Uul situated within a palaeolake basin in the Gobi region. This site saw three major periods of use: two occupational periods during the Early Upper Palaeolithic (34,100-27,700 *kya*) and Middle Holocene (8500-6400 *kya*), and a period of mortuary use during during the Bronze Age (post 3500 *kya*) (Janz *et al*. 2021, pp. 14–5). The cultural assemblages at Zaraa Uul during the Middle Holocene are consistent with Oasis II assemblages being dominated by microblades and microblade debris with some flakes, points, ceramics milling stones and adzes (Janz *et al*. 2021, p. 3). During the part of the Middle Holocene in question, it is argued that the climate was much wetter based on geomorphology, faunal remains and phytoliths. The presence of trees is shown in the phytoliths and also by the finds of chipped axe-adzes. The wetter climate would then have allowed a lake or wetland to form within the basin at Zaraa Uul and caused a separation of land into woodland and grassland areas (Janz *et al*. 2021, p. 24). This environmental situation is given as the explanation for a change in diet seen. Megafauna and other large mixed-feeding or grazing animals were the game of choice for the Pleistocene hunters. Oasis II hunters, on the other

	Lithics	Other Artefacts	Economy	Other
Epipalaeolithic 19.0-13.5 *kya*	flakes pressure-flaked microblade industry retouched points			
Oasis I 13.5-8.0 *kya*	highly developed microblade industry flexible core types	Pottery by 9.6 *kya* (2021)		Largely a continuation of Epipalaeolithic High mobility
Oasis II 8.0-5.0 *kya*	Grinding stones Microblades Polished stone Varied cores Points including bifaces	Hearths Textile-impressed, low-fired, greyware pottery with coarse sand and organic temper	Wetland foraging	Longer term habitation
Oasis III 5.0-3.0 *kya*	Large grindstones decline Microblades Endscrapers Drills Polished axes and adzes Large knives Bifacial points Shift to conical core dominance	Ceramics more common High-fired redware sometimes painted with sand or organic temper Geometric designs, stamps, moulded rims and impressed Copper smelting	Domesticated animals? (2021)	Increased East-West divide in Gobi sites Higher mobility with more temporary campsites Intensive occupation of wetlands and dunefields

Table 2.2: Chronological summary of Gobi sites during the Oasis economies from Janz 2012, Janz *et al*. 2017 and Janz *et al*. 2021.

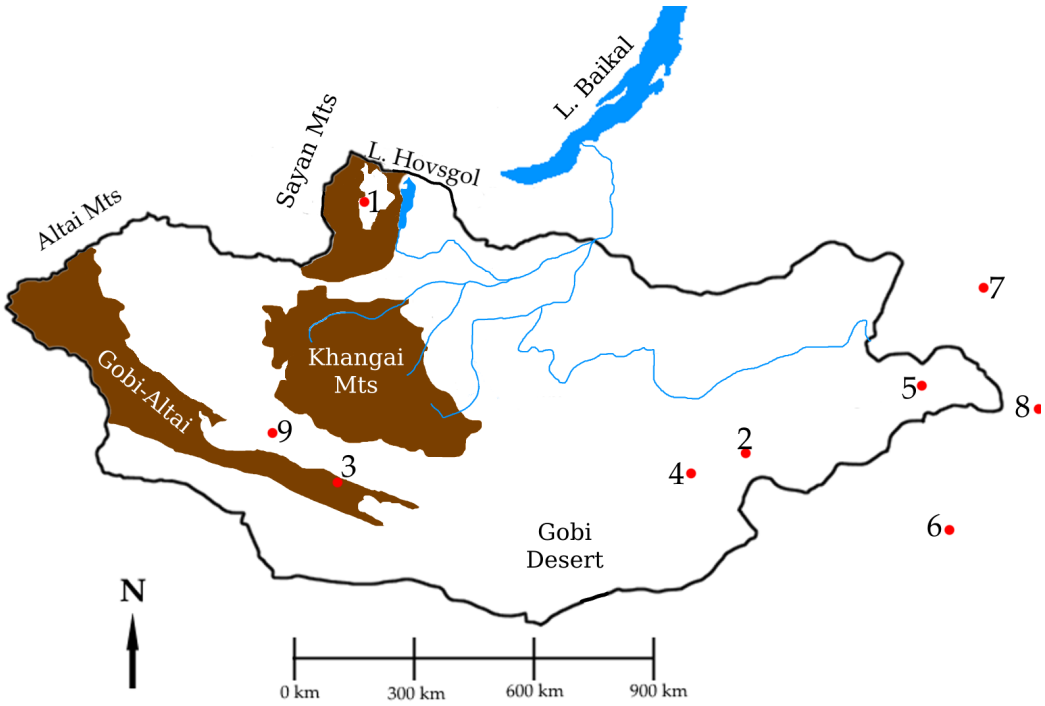

Figure 2.1: Map of Mesolithic-Neolithic sites and locations mentioned in this thesis. 1. Soyo; 2. Zaraa Uul; 3. Chikhen Agui; 4. Ikh Nartiin Chuulu; 5. Tamsagbulag; 6. Baiyinchanghan; 7. Hag; 8. Houtaomuga; 9. Gazar Agui-1

hand, preferred a mix of larger steppe grazers and small to medium forest feeders. From the Bronze Age, faunal assemblages consisted of domesticated sheep, horse, cattle and goat. The disappearance of megafauna and the formation of patchwork forest-and-steppe environments facilitated the emergence and hunting of specialised browsing herbivores of varying size (Janz *et al*. 2021, p. 23). The appearance of domesticated animals in the Bronze Age indicates potentially another subsistence adaption as the wetland environments that facilitated the Oasis II mixed economy dried out.

The rockshelter site of Chikhen Agui in the Gobi-Altai region covers a transitional period from the Pleistocene into the early Holocene ending some time in the ninth millennium cal. BP. There are three strata at Chikhen Agui. The lowest dates to the Upper Palaeolithic (Stratum 3) and the second from the initial Holocene (Stratum 2) (Derevianko *et al*. 2003, pp. 51–4). The lithic assemblage from Stratum 3 shows a preponderance of Levallois-like flakes with a sizeable fraction of blades. This would put Stratum 3 in the earliest stages of the Upper Palaeolithic (Derevianko *et al*. 2001, p. 33). However, the earliest dates reported from the site are significantly later than the IUP in northern Mongolia. The oldest was taken from a bone sample and likely (two sigma) postdates 35,800 cal. BP. The Holocene assemblage is heavily dominated in both tools and debitage by microblades and composite tools. Blades and points and their associated fragments are the next most common categories (Derevianko *et al*. 2003, p. 53). This site has been interpreted as a seasonal

hunting camp due to the low formality of the tool forms and proximity to a watering hole to which game would be attracted. The habitation interpretation is further supported by grass concentrations, which were interpreted as bedding, and the large number of hearths (Derevianko *et al*. 2003, pp. 54–5). Some more exotic artefacts found (nephrite pebble, serpentine pendant, ostrich shell beads) have encouraged a secondary interpretation of ritual activity at the cave (Derevianko *et al*. 2008). The time frame for this use of the cave ranges from 13,400 to approximately 9000-8000 cal. BP using the dates that are thought to be reliable (Derevianko *et al*. 2003, p. 51, 2008, p. 9). This would place it firmly within Janz' Oasis I period. The interpreted seasonal mobility, use of water environments and microblade industry all fit into the Oasis I pattern. It should be noted that, despite the rich finds at Chikhen Agui, caves do not appear to have been used extensively for occupation in prehistoric Altai. A survey of 24 caves in the Altai found only two caves bearing signs of prehistoric use. Both showed rock art but at only one (Gazar Agui 1) was found any artefacts (several microblades and an unidentified piece of bronze). The occupation of this cave was identified as "Neolithic" or "Bronze Age". It was hypothesised that cave habitation at this time was short and focused around the production of rock art (Vanwezer *et al*. 2021a, p. 84, 2021b, p. 7).

In the eastern Gobi hundreds of surface scatters have been identified particularly in Ikh Nartiin Chuulu Nature Reserve (Schneider *et al*. 2016, 2020). Approximately 900 "Neolithic" scatters were found comprising flaked tools, microblades, scrapers, point, ceramics and ground stone. One single date points to an age range that includes 4350 cal. BP for these assemblages (Schneider *et al*. 2016, p. 484). A salient feature here is the presence of ground-stone milling tools from which starch grains have been recovered (Schneider *et al.* 2016, pp. 484-90). This indicates at least some importance was given to plant processing and consumption in the eastern Gobi while the non-local material of these tools suggests the people using them maintained their mobility (Schneider *et al*. 2020, pp. 8–9).

The only Mongolian site that would comfortably fit into a Near Eastern or European style of Neolithic is Tamsagbulag which lies on the eastern border with China. This site was excavated by Okladnikov, Derevianko and Dorj and published mostly in Russian (Okladnikov and Derevianko 1970, Dorj 1971). A summary was published in English by Derevianko and Dorj (1992). A more recent expedition was made by the French Archaeological Mission in Mongolia which uncovered two more associated sites dating to the seventh millennium cal. BP (Séfériadès 2004). Further finds have been made from the late ninth to eighth millennium cal. BP (Zhao *et al*. 2021). Tamsagbulag was a sedentary village of semi-subterranean houses. The lithic assemblage was dominated by microliths and a variety of cores and core-tools, scrapers and knives. Bifacially flaked points, polished adzes (or axes) and pressure-flaked tools were also present (Derevianko and Dorj 1992, pp. 172–4, Séfériadès 2004, p. 143). Pottery was also found at the site which was a friable grey-ware with incised or impressed designs (Derevianko and Dorj 1992, p. 174, Séfériadès 2004, p. 143). Of particular interest is the presence of a mixed economy involving agriculture, pastoralism and hunter-gathering. Numerous grinding tools and hoes were found along

with cattle or auroch bones, fish bones and hunting equipment indicating a varied diet. Furthermore, there was some ritual use of bull remains at the site and at least one intramural burial with grave goods. (Derevianko and Dorj 1992, pp. 174–6). Tamsagbulag is a unique site in Mongolia but fits with other site in northeastern China and the Amur region. The nearby sites of Baiyinchanghan and Hag display similar uses of storage pits, burials (similarity only between Tamsagbulag and Hag), intensive plant processing, millet cultivation and sedentism. These sites were roughly contemporary with the earlier occupation at Tamsagbulag (Zhao *et al*. 2021, pp. 48, 52–3). It has been proposed that aurochs (previously thought to have died out during the Neolithic in this area) survived in significant enough numbers to have played a part in the Neolithic (6300-5000 cal. BP) economy of Houtaomuga in northeastern China (Cai *et al*. 2018). Due to the way the bones were cut and the age of death, it seems that these aurochs were used in feasting rituals but were unlikely to be domesticated (Cai *et al*. 2018, p. 78). It seems likely given the shared ritual use of bovines, mixed economies and construction of dwellings that Tamsagbulag fit more into the sphere of its neighbours to the East than with the rest of the Mongolian plateau. Sedentism and agriculture have a long history in that part of the world. Sedentism in particular has been shown to have arisen fairly rapidly around 7.9 *kya* in northeastern China with agriculture following over a longer period of time (Shelach-Lavi *et al*. 2019). In the Russian Far East, agriculture is known from 5467-5320 cal. BP (Kuzmin 2013) which means it was adopted by people already long familiar with pottery. The Russian Far East lays claim to some of the oldest pottery in the world appearing at least by c. 14 *kya* (according to direct dating on the ceramic sherds themselves) (Yanshina and Kovalenko 2022). Therefore, the ”Neolithisation” at Tamsagbulag is part of the trajectory of sedentism and agriculture ongoing in the River Amur region and northwestern China at that time and unrelated to the kind of ”Neolithic” that is under discussion throughout the rest of Mongolia.

2.2 Bronze Age

The Bronze Age of Mongolia is a period that is dominated (in the literature) by monuments (Wright 2021, p. 440 and see also Allard and Erdenebaatar 2005, Fitzhugh *et al*. 2010, Wright 2014, 2017, Honeychurch 2015, chap. 5, Ėnkhtör *et al*. 2018, Taylor *et al*. 2019). Although habitation and activity sites are known, their visibility in the landscape is low compared to monumental constructions (Honeychurch *et al*. 2007) and scholarship on them is limited. Therefore, the period has lost its original (Lubbockian) meaning of having bronzeworking technology and is considered as a period of widespread monument building and the social transformations (expressions of kinship, territoriality, ritual, etc.) that are variously hypothesised to go along with them (Houle 2016, p. 2). The Bronze Age is typically divided into an Early Bronze Age (EBA) and Late Bronze Age (LBA). The chronological boundaries of these periods, especially the beginning of the EBA, are currently nebulous. Since habitation sites of this time have been rarely studied and often contain few artefacts and secure dateable contexts, the chronology has historically been based mainly on monument transitions and pottery typologies (Honeychurch 2015, p. 132). The transi-

tion from EBA to LBA is placed during the late second millennium BC with the advent of widespread horse domestication (c. 1200 BC) given as a defining moment (Houle 2016, p. 2, Taylor *et al*. 2017, Wright 2021, p. 440). Sometimes a Terminal Bronze Age is grouped with the Early Iron Age period to categorise the time between the LBA and the Xiongnu polity (c. 800/700-400 BC) (Houle 2016, p. 2). However, sometimes the Terminal Bronze Age is incorporated as a subperiod of the LBA c. 1000-750 BC (Honeychurch 2015, p. 111).

Occupation sites of the Mongolian Bronze Age are not only difficult to distinguish from earlier periods because of their similar lithic tradition (Janz *et al*. 2017, p. 58, Wright 2021, p. 443) but also appear to be less frequent overall suggesting a change in way of life that affected the visibility of campsites in the present day landscape for archaeologists (Honeychurch 2015, p. 137). This (and the general lack of bronze items at occupation sites) may explain Maringer's (1963, p. 82) assertion that Mongolia largely had no Bronze Age at all. The changes in material culture in the Oasis II economies (Eneolithic/EBA) identified by Janz in the Gobi include increased beads, spindle whorls, copper slag and a distinctive tradition of high-fired, redware (compared the the earlier low-fired, sandy greyware) that is a diagnostic marker of the EBA (Janz *et al*. 2017, pp. 58–9). In the later EBA (c. 1550-1150 BC) of eastern Mongolia, the Ulaanzuukh culture produced similar occupation scatters of microblade industry remains and thin-walled, red ceramics (Wright *et al*. 2019, pp. 9–12). The bronze of the Bronze Age is far less commonly represented in assemblages. Most bronze objects are from the Terminal Bronze Age and EIA where they are included as grave goods (such as ornaments, bangles and knives) in slab graves. Few bronzes have been recovered the LBA deer stone and khirigsuur culture although they must have been familiar with the technology as seen from the carvings of bronze tools and weapons on their deer stones (see below) (Houle 2016, p. 9, Wright 2021, p. 550). A study has been done on the bronze objects from Baga Gazaryn Chuluu in the northern Gobi of eastern Mongolia which was described as a self-sufficient bronze-making site (Park *et al*. 2011, p. 816). Six out of the 54 sampled objects were reported as either LBA or LBA-EIA. The results of chemical analysis showed that there was a shift from pre-Xiongnu arsenical copper to tin-lead-bronzes of the Xiongnu period which was explained by increasing interaction with China where that alloy was common (Park *et al*. 2011, pp. 814–5).

The chronology of the change in subsistence patterns from Mesolithic-Neolithic hunter-gathering to nomadic pastoralism (or a mixed economy), as well as the processes involved in that change, is one of the major problems of the Bronze Age. This transition is assumed to have taken place during the EBA or that is at least where evidence is being sought (Clark 2014, p. 52). The earliest pastoralist culture is thought to be the Afanasievo culture in western Mongolia who have genetic links with steppe populations farther west (Jeong *et al*. 2018) and whose burials have been dated to c. 3000 BC (Taylor *et al*. 2019). From there the practice spread eastward and only reached the Gobi under the Ulaanzuukh-Tevsh culture c. 1450-1150 BC (Janz *et al*. 2017, p. 56). Another possible channel for the transmission of herding into Mongolia may have been reindeer herding from Siberia into northern Mongolia. This idea was one of the underpinning research questions of the Deer Stone Project

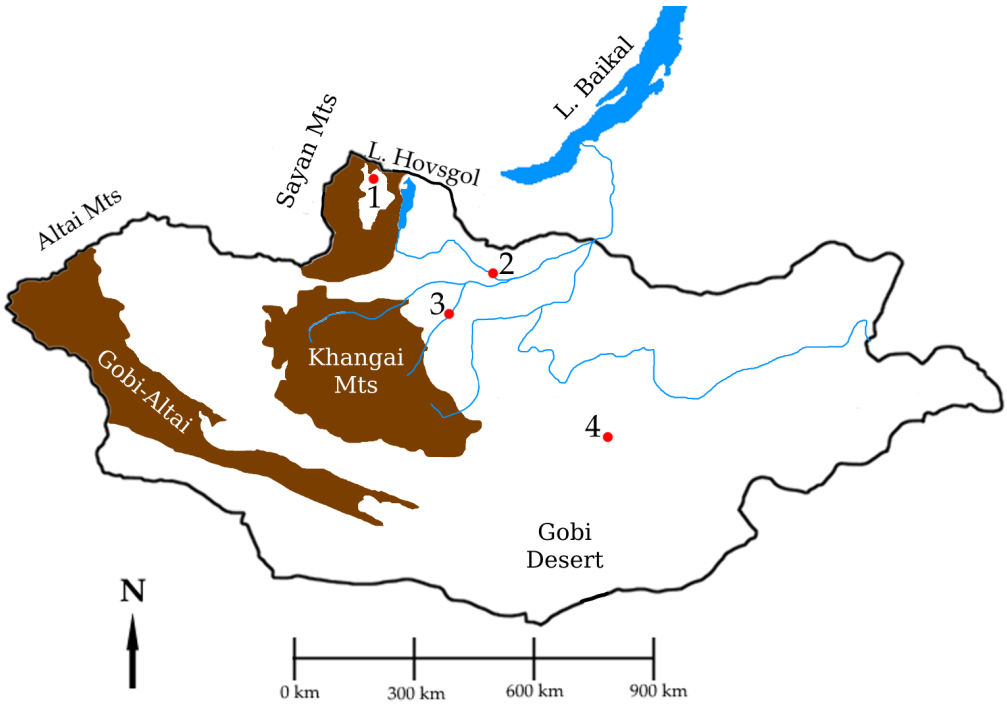

Figure 2.2: Map of Bronze Age sites and locations mentioned in this thesis. 1. Targan Nuur; 2. Egiin Gol valley; 3. Khanuy valley; 4. Urt Bulagyn

(Fitzhugh 2003, p. 14, 2005, p. 13) although it has not received much attention in the literature. The processes involved in the subsequent spread of pastoralism throughout Mongolia is an open question. Wright (2006, p. 298) has argued that the adoption of the nomadic pastoralist lifestyle was a voluntary procedure undertaken by hunter-gatherers who saw the prestige and power conveyed by individualised burials and other monuments and so took on the package of Bronze Age subsistence and monumental architecture. In the Darkhad there is EBA evidence for domesticated animals (within the context of a mixed economy) from burials (Clark 2014, p. 181) while gene flow from the western steppe did not reach the Hovsgol region until the LBA (Jeong *et al.* 2018, pp. 5–6) which further supports the idea that the spread of pastoralism happened through inter-group connections and exchanges rather than wholesale population migrations. The slow transmission of pastoralism throughout Mongolia, and the fact that these herders were not mounted until c. 1200 BC at least (Taylor *et al.* 2017), also speaks for a more complication series of interactions between groups rather than a rapid and sweeping transformation of the steppe economy by migrations of nomads. For further discussion on nomadic pastoralism in Mongolia, see Section 2.4.

The three major LBA settlement pattern studies in Mongolia are all in central and northern Mongolia and used the pattern of sites in the landscape to make inferences about social organisation. The Egiin Gol project in northern Mongolia (Honeychurch and Amartüvshin 2007, Honeychurch *et al.* 2007) was a milestone in such studies. A variety of surface sur-

vey intensities were used to map the sites by period. It was discovered that LBA and Early Iron Age (EIA) habitation and monument sites occupied primarily the tributary valleys of the river system leaving the main valley relatively unoccupied. Each valley yielded the same set of sites. This pattern was used to conclude that the LBA and EIA inhabitants formed networks of small, discrete units. The move of sites into the main valley during the subsequent Xiongnu period suggested a change in land use pattern and, therefore, the incorporation of the valley into a pre-existing, external political unit (Honeychurch *et al*. 2007, pp. 378–80). To the south of the Egiin Gol, the Khanuy Valley was surveyed to test the dependency hypothesis for the Mongolian case (the idea that nomadic pastoralist political complexity must be precipitated by a neighbouring sedentary civilisation - in this case China). Houle (2010, pp. 180, 183–4) argues for a restricted range of movement, surplus production, relatively higher population density and very slight social differentiation prior to Chinese contact all of which he levels against the dependency hypothesis as showing that social complexity pre-existed contact with sedentary neighbours to the South. Interestingly, the occupation sites in the Khanuy Valley show a bimodal clustering (following present day herders) with Winter camps in the sheltered valleys and Summer camps only a few kilometres away along the river. The territory between was filled with monuments (Houle 2010, p. 52). This pattern was not found along the Egiin Gol although it was noted that the river may have destroyed sites in the floodplain or hidden them by fluvial deposition (Honeychurch *et al*. 2007, p. 378). The final major survey of habitation sites took place near Targan Nuur in the Darkhad. There LBA sites were the most frequent followed by the Turkic period with Iron Age and Xiongnu sites virtually absent (Clark 2014, pp. 172–3). This perhaps speaks to a fragmentation of social connections following the LBA and Xiongnu culture having limited penetration into the Darkhad. The bimodal settlement pattern as found in the Khanuy Valley was not found in the Darkhad but this was very likely a result of the survey area boundaries. It may have been the case that the area only encompassed Summer camps (Clark 2014, p. 163). No clear spatial pattern was found to link LBA monuments with occupation areas with the biggest cluster of the former lying 5 km from the biggest cluster of the latter (Clark 2014, p. 171). The general picture that emerges from these studies is one of LBA peoples camping at certain places within the monumental landscape but that the choice of campsite is determined by factors other than proximity to those monuments (probably pragmatic factors related to herding). They may have moved short distances through the monumental landscape as in the Khanuy Valley or they may have moved longer distances. The meaning of the relation between monumental landscape and nomadic herding patterns to the people living at the time remains unclear.

Monuments are the most visible and studied Bronze Age remains. There are three main monuments that occur across the Mongolian landscape (although there are others that are more geographically limited): khirigsuurs, deer stones and slab graves. A khirigsuur has a complex structure. There is a central mound with is surrounded by a ”fence” of stones that is either square or circular. There may be a stone path leading from the central mound to the eastern or southeastern side of the fence. Outside, the larger mounds

have satellite mounds which are concentrated on the eastern and southern sides and rare on the western side. Surrounding the whole thing may be a field of stone circles. On the northern side there can be another stone path and a series of slab graves. The whole structure is typically oriented towards an East-West or Southeast-Northwest axis (Allard and Erdenebaatar 2005, p. 554, Frohlich *et al*. 2005, pp. 59–60). A prime example of a large khirigsuur showing the layout of features is Urt Bulagyn in the Khanuy Valley (Allard and Erdenebaatar 2005). Khirigsuurs are found across Mongolia but are more concentrated in the central, western and northern parts (Wright 2021, p. 447). In the Darkhad at least they tend to be located on the southern sides of hills (Frohlich *et al*. 2010, pp. 198–9). One big question about khirigsuurs is whether they were burials or not. Some have argued that khirigsuurs were not burials based on the inconsistent presence of human remains (Allard and Erdenebaatar 2005, p. 552, Wright 2006, pp. 203–4, 2014, p. 148). On the other hand, some areas (such as the Darkhad) yielded human remains in the central mounds of most khirigsuurs and there is a corresponding insistence that the monuments were burials (Fitzhugh and Leader 2006, p. 36, Frohlich *et al*. 2010, p. 196). It has been noted that inhumations are most common in western Mongolia while eastern khirigsuurs typically did not have them and suggested that this represents a change in practice as the monument form spread from West to East (Honeychurch 2015, pp. 114–5). Animal remains and artefacts are also uncommon at khirigsuurs and only occur in association with satellite features but include bronze objects, ceramics and notably horse remains (especially the head and hooves) and other fauna (Fitzhugh and Leader 2006, p. 36, Taylor *et al*. 2020a, Wright 2021, p. 447). Regardless of whether khirigsuurs were meant to be burials, they seem to also have been used for other purposes. Khirigsuurs were probably agglomerative structures that were built over time rather than in a single effort (Allard and Erdenebaatar 2005, p. 558, Wright 2006, p. 224). Therefore, there must have been some ongoing relationship between people and monument beyond simply a burial. Recent thinking on the matter has concluded that khirigsuurs were territorial markers for nomads occupying limited areas (Frohlich *et al*. 2010, pp. 205–6) or markers of social cohesion in a nomadic landscape that tended towards dispersion and fragmentation (Allard and Erdenebaatar 2005, p. 561, Houle 2010, pp. 187–90) or both (Wright 2014, p. 155). An analysis of the horse remains found under khirigsuur satellite features has revealed cut marks indicating the removal of meat, disarticulation of bones and a variety of killing methods. This suggests ongoing ritual and feasting activities were happening at khirigsuur sites which supports the hypothesis of a socially unifying function (Taylor *et al*. 2020a).

Deer stones are monolithic standing stones 1-3 m high that are named after their elaborate and stylised deer carvings. Deer stones have been categorised into four varieties: the "classic" Mongolian type, the Sayan-Tuva type, the Altai type and the Black Sea type. Only the Mongolian and Sayan-Tuva types actually regularly have zoomorphic imagery while the Altai type is a simpler style and the Black Sea type appears even less related (Jacobson-Tepfer 2001, p. 31). Examples of the Mongolian type are divided into three bands. At the top there are ring carvings on either side of the stone which have been suggested to be earrings or sun symbols. There is also sometimes an anthropomorphic face. The middle

Figure 2.3: A small Khirisgsuur. Note the circular ring of stones surrounding it. Photograph taken by the author at Ushkiin Uver.

panel contains the stylised deer with birds' beaks. The bottom displays a belt with bronze tools and weapons (Fitzhugh and Leader 2006, pp. 38–9). Deer stones are often associated with khirigsuur complexes giving rise to the notion of a deer stone-khirigsuur (DSK) complex and culture (Wright 2021, p. 449). The two forms are contemporaneous in the LBA (Taylor *et al*. 2019). Although slab graves can be found in association with khirigsuurs as well, these are thought to be later intrusions (Fitzhugh and Leader 2006, p. 37). The meaning of deer stones has been extensively hypothesised on (Jacobson-Tepfer 2001, Bayarsaikhan 2005, Fitzhugh and Leader 2006, pp. 37–9, Wright 2021, pp. 448–9). Notions of individual representation of a leader or ancestor or other tribal representation easily arise because of the anthropomorphic features of many stones, the belt of equipment in the bottom third and the similarity of the deer art with archaeologically known tattoos (Fitzhugh and Leader 2006, p. 39). Ideas of a widespread deer cult have been presented as well and deer stones have also been interpreted as cosmologies wherein the upper partition represents the heavens, the middle the earth and the lower the underworld (Jacobson-Tepfer 2001, pp. 34–8, 52).

The final major type of Bronze Age monument is the slab grave. This is a rectangular structure made of upright stone slabs which surround a shallow burial pit. The burial is overlain with a layer of smaller stones. Slab graves were most common in eastern Mon-

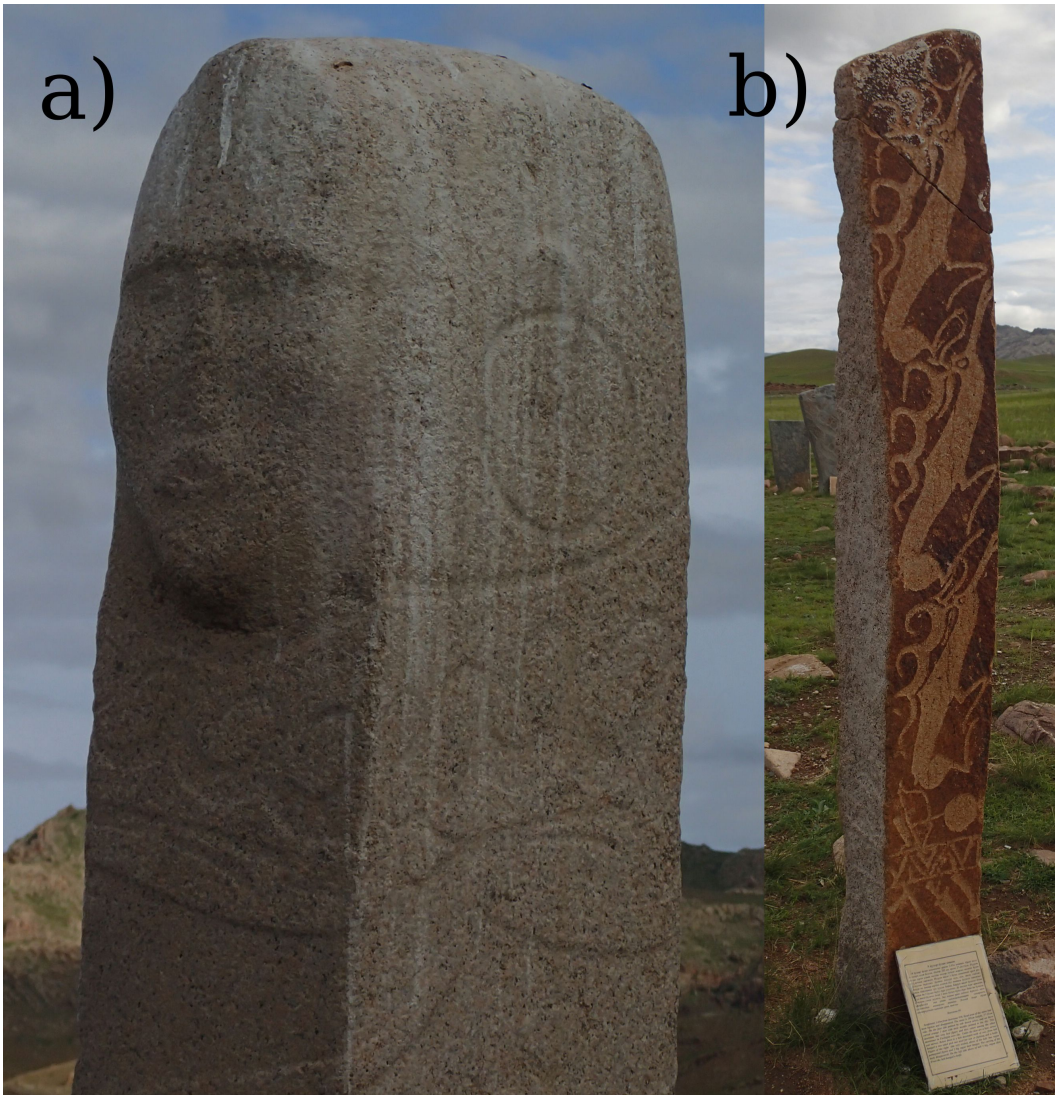

Figure 2.4: Two deer stones. a) Showing the upper third with anthropomorphic face and circular ″sun″ rings. b) Showing middle and lower thirds with stylised deer and bronze weaponry. Photographs taken by the author at Ushkiin Uver.

golia during the Terminal Bronze Age and EIA (10^{th} to 4^{th} centuries BC) (Wright 2021, pp. 449–50). Unlike khirigsuurs, these are unquestioned as burials. Slab graves have produced a vast amount and variety of grave goods compared to earlier burials which include faunal remains, bronze ornaments and tools, bone artefacts, stone artefacts, semi-precious stone and shell beads and ceramics. This array of material is suggested to show a more martial society, importance of animals in ritual and long distance contact (Allard and Erdenebaatar 2005, p. 548, Wright 2021, p. 550). The slab grave culture has roots in the earlier LBA (c. 1450-1150 BC) Ulaanzuukh culture which produced similar rectangular stone burial structures as well as ground-level alignments of stones and stone circles (Honeychurch 2015, p. 122, Wright *et al*. 2019). The Ulaanzuukh tradition was roughly contemporaneous with the DSK tradition with the former occupying the eastern parts of Mongolia and the latter occupying the western and central areas during the LBA (Honeychurch 2015, p. 122). Genetic research has suggested that the people of the slab grave culture had western steppe "Afanasievo-like" DNA admixture from the LBA which suggests some movement of people eastward at around the time of the domestication of the horse. The construction of slab graves then diffused back westward by adoption rather than migration (Rogers and Kaestle 2022). Previous research, however, had stated that the Ulaanzuukh-slab grave populations had no western admixture and that genetic mixing did not occur until the Xiongnu period (Jeong *et al*. 2020). Regardless, the slab grave form did expand westward and was often found in conjunction with DSK monumental sites. These are interpreted as intrusive elements on an earlier tradition (Fitzhugh and Leader 2006, p. 37) which may indicate a deliberate attachment or continuation to earlier monuments (Wright 2021, p. 550).

2.3 Soyo

The site of Soyo was discovered in 2002 by the American-Mongolian Deer Stone Project. A number of "Neolithic" artefacts were discovered from a buried cultural layer, including microblades and red-washed ceramics, but two hearths associated with the cultural layer were dated to the late first to early second millennium AD (Fitzhugh 2003, pp. 42–3). It was later discovered in 2003 that there were two culture-bearing layers very close to each other containing hearth stones, charcoal and bone. The lower of the two layers further contained cord-impressed pottery, microblades and wedge-shaped cores among other lithics. A hearth feature supposedly associated with this layer was dated at the time to 6510 - 5940 cal. BP (see figure 2.19 for comparison to the age of the Neolithic in the Gobi and Cis-Baikal). The artefact assemblage found was considered to be similar to other Neolithic assemblages from Mongolia and Siberia. The upper layer was associated with more hearths and animal remains as well as some disc-shaped fire-cracked stones (Fitzhugh 2005, pp. 17–8). A natural timber horizon was also discovered eroding into the river and was dated to 7161-6786 cal. BP (Fitzhugh 2003, p. 43). In 2004 further work was done at Soyo to uncover the Neolithic material there. Based on the limited excavations, a preliminary stratigraphy was developed consisting of four layers: an upper soil layer, dark brown

sand, yellow-red sand, and finally a light yellow sand. Artefacts were not found in this last layer which was as the base of the sequence. The notable examples consistent with other Neolithic finds around Mongolia include two arrowheads and a range of low-fired, sand-tempered ceramic fragments (Bayarsaikhan *et al*. 2005, p. 228). The Neolithic component of the pottery at Soyo is described as "a coarse sandy greyware" as opposed to the red-washed pottery which is likely Bronze Age although there is still a lot of research to be done on Mongolian pottery typology (Julia Clark pers. comm. 2023). The full catalogue of finds is dominated by microblades with some other pieces such as scrapers, points, ceramics and bone fragments (Bayarsaikhan *et al*. 2005, pp. 231–8). Further field seasons in the Darkhad by the Deer Stone Project did not work at the site of Soyo itself.

Regular archaeological study at Soyo did not resume until 2015 as the site had been used as a camping ground in the meantime by people undertaking expedient mining activity in the nearby Sayan Mountains. The fieldwork involved a mix of surface collection from the eroding cultural levels and excavations. The artefacts found were mostly Neolithic to Early Bronze Age lithics, ceramics and bones. There also appears to be evidence of either pottery firing or metallurgy in the form of vitreous slag (Clark 2015, pp. 3, 6). These excavations were dug over a wider area than in previous field seasons. The stratigraphy for the site was noted to consist of a sandy overburden followed by a dark soil and then orange-yellow silty sand both containing artefacts. In some excavation units such as Unit 1 there was also found a light coloured, archaeologically sterile sand beneath the culture-bearing layers (Clark 2015, pp. 3–4).

Having done an exploratory first season, the following season in 2016 took a focused approach using specialised methods. Aside from regional archaeological, botanical and ethnographic surveys, the bulk of that season involved intensive geological and geophysical surveys at the Soyo site itself in order to investigate its stratigraphy (Clark and Bayarsaikhan 2016). Nine new pits were excavated at both the eastern and western ends of the site. A ground-penetrating radar survey spanned 46,000 m^2 covering much of the studied area of Soyo south of the river (fig. 2.5). This was done with the intention of extending the stratigraphic information gleaned from excavations so far across as large an area as possible

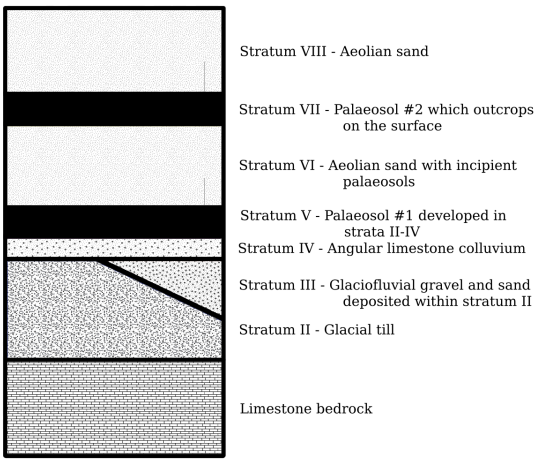

Figure 2.6: Diagram of earlier stratigraphic interpretation at Soyo (Putnam 2016). Figure is schematic only and not to scale.

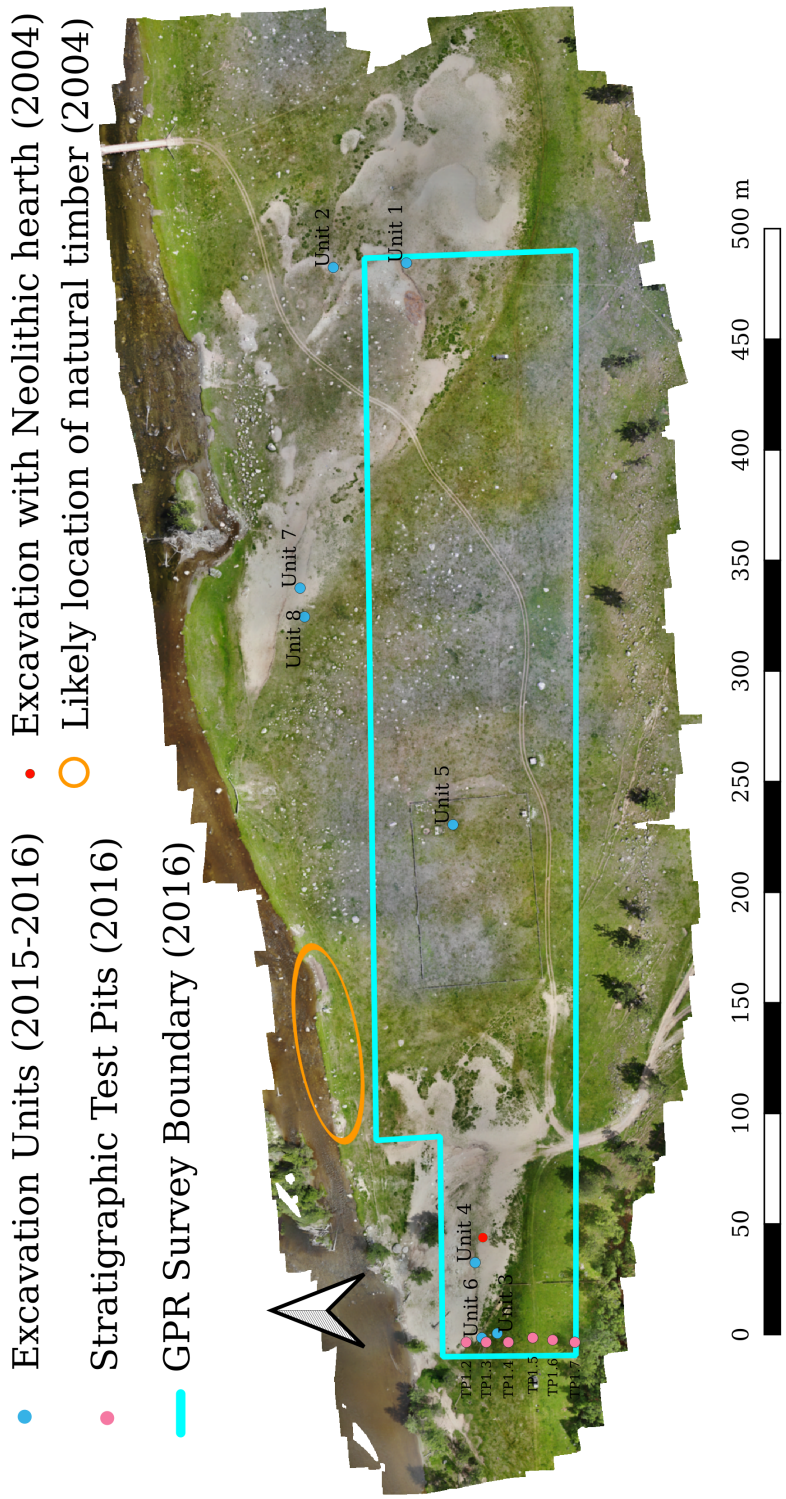

Figure 2.5: Map of excavations and surveys done at the site of Soyo up until 2016.

ANSTO Code	Stratigraphic Level	Calibrated Age BP (2σ)
OZV573	B	Modern
OZV574	B	Modern
OZV582	B	263-220; 144-24
OZV576	C	256-224; 139-32
OZV575	C	424-392; 318-285; 166-156
OZV581	D	907-864; 858-844; 833-734
OZV580	G	1242-1228; 1176-1061
OZV584	G	1242-1229; 1176-1060
OZV577	G	12892-12858; 12848-12747

Table 2.3: Carbon-14 dates from excavation unit 6 during the 2016 field season at Soyo (Vella 2018) calibrated using IntCal20 curve.

(Clark and Bayarsaikhan 2016, p. 4). This survey would be combined with several new test pits and excavations as well as a high resolution orthophoto and digital elevation model obtained through aerial photographs and photogrammetry. However, only a small part (6,000 m^2) of the total surveyed area was processed and interpreted resulting in a limited model for the site structure (Vella 2018, pp. 48–52). Nevertheless, the extents and depths of two palaeosols and the lodgement till surface were able to be mapped across the western end where much of the archaeological work done by the Deer Stone Project had taken place. Further to this, a geological interpretation was made of the test pit strata (fig. 2.6). The sequence started with the limestone bedrock on which glacial lodgement till sat. This till was surrounded by a possible glaciolacustrine sand and capped with limestone colluvium from the nearby Soyo Hill. A palaeosol also developed on top of this substrate. Overlying the palaeosol were aeolian sands, another palaeosol and then aeolian sand dunes (Putnam 2016). Finally, nine radiocarbon dates were obtained from one of the excavation pits (Unit 6) which are tabulated in figures 2.3 and 2.7 (Vella 2018, p. 54). These show that there was a great range in the chronology at this part of the site. Of particular concern was the gap between the single oldest sample (OZV577 10,900±40 BP) and the middle cluster of dates (OZV580 1205±25 and OZV584 1200±25). This discrepancy was one of the motivating problems behind the 2019 Soyo field season and the present research.

Over the course of 2015 to 2016, a total of 340 lithic artefacts were retrieved from excavated contexts. Ninety-six of these were selected for a study on the variability of lithics over time at Soyo (Gribble 2021, p. 69). The lack of grindstones was noted as a potential indication that no grass or seed processing was happening at the site and that the inhabitants practised a more mobile habitation strategy. While no points were found either, the practice of hunting was not ruled out on the basis that microblades were common throughout all stratigraphic levels (Gribble 2021, pp. 119–21). It should be noted that, while no points were contained in Gribble's sample, points are found in the finds catalogue from Soyo.

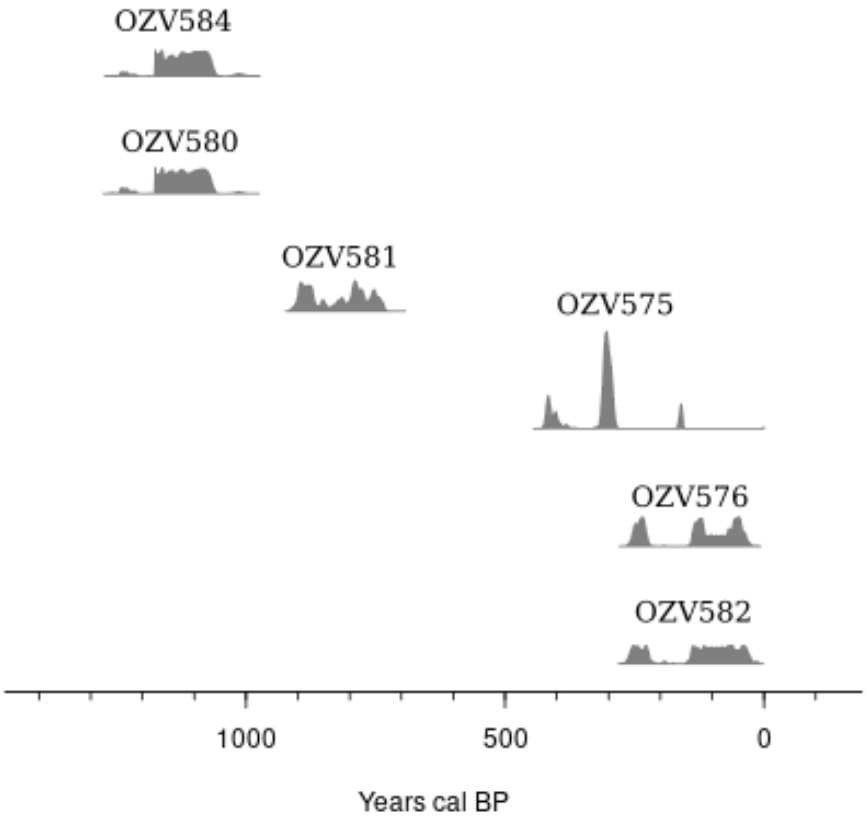

Figure 2.7: Non-modern carbon-14 dates from excavation unit 6 during the 2016 field season at Soyo (Vella 2018). Sample OZV577 has been omitted to increase the visibility of the other results.

It was found that a change occurred in the lithic record from using only chert to using a wider variety of materials such as quartzite. The chert (mostly black chert) is from an unknown provenance but pXRF analysis using a Bruker Tracer 5i instrument has suggested a single main source given the similarity between most samples in terms of aluminium, iron and titanium content (Gribble 2021, pp. 83–5). Quartzite is found in the region surrounding Soyo so it has been suggested that its use was caused by a change towards lower mobility in the Darkhad (Gribble 2021, pp. 127–9). While this transition has been tentatively hypothesised as being contemporaneous with the Mesolithic-Neolithic to Bronze Age transition in Mongolia on the basis of dating done at Soyo (Gribble 2021, p. 124), the contexts that produced the lithic artefacts are far from the test pits that currently have been carbon dated and it is not yet known how they correlate.

Figure 2.8: A sample of lithics from the 2016 field season at Soyo courtesy of Julia Clark.

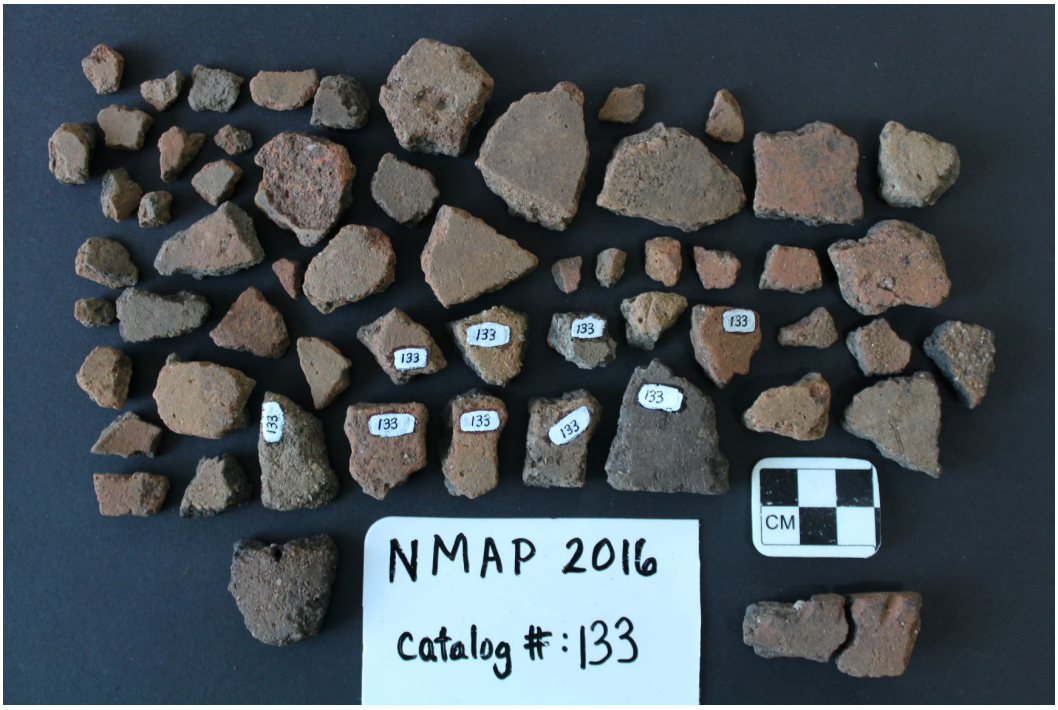

Figure 2.9: A sample of ceramic material from the 2016 field season at Soyo courtesy of Julia Clark.

The 2017 field season saw less work at the Soyo site itself than the previous year as other sites in the surrounding landscape were investigated (fig. 2.17). Two of the test pits from 2016 (T1.4 and T1.3) were reopened to provide further dating opportunities. It was stated that the previous interpretation of the stratigraphy had misidentified the limestone bedrock (at least in T1.4) as glacial till (Clark and Bayarsaikhan 2017, p. 5). However, the geological report in question clearly states that no limestone was found within the till which was, in fact, comprised mostly of granite boulders (Putnam 2016, p. 1). In the appendix to Vella's Master's thesis on the 2016 results, the lithology of the lowest unit in T1.4 was described as "Glacial fill made up of granite boulders, sub-angualr[sic] limestone rocks and smaller rounded river rocks" (Vella 2018, p. 107). On the northern side of the river at a site called Bayanii Am 1, more artefacts (N=360) were found exposed by erosion. A test pit turned up a further 1096 lithics, 17 charcoal fragments and 424 animal bones in the top layer of soil. The main categories of lithics found were (micro)bladelet fragments, flakes and debris fragments. Minor categories included points, cores and scrapers (Clark and Bayarsaikhan 2017, pp. 14–5). At Bayanii Am 3 to the Northwest, four pre-LGM lithic artefacts made of quartz were found on a terrace above the river (which must have been out of reach of the glacier - elevation 1715 m a.s.l.) which were two unipolar flake cores, one piece of debitage and a scraper fragment (Clark and Bayarsaikhan 2017, p. 16). Some of the other finds include three apparently undisturbed but unproductive burials as well

Figure 2.10: A sample of animal bone from the 2016 field season at Soyo courtesy of Julia Clark.

as two new deer stones, including one with an unusual spiral design (Clark and Bayarsaikhan 2017, p. 30), but the bulk of the work was done at the site of Bagsagiin Bulan downriver of Soyo. There an architectural structure was found with a central hearth surrounded by a ring of stones with two postholes found nearby (Clark and Bayarsaikhan 2017, p. 8). The small finds are comprised of a mix of ceramics, animal bone and lithics including microblades. A large amount of charcoal was also found as would be expected from the vicinity of a hearth. This site has been interpreted as a LBA habitation site based on the ceramics although the predominance of stone tools may indicate a much earlier date (Clark and Bayarsaikhan 2017, p. 11). A date of c. 4.5 *kya* (4056 ±15) from the hearth charcoal has been published (Taylor *et al*. 2020b). Unfortunately, the faunal remains selected for dating only yielded recent or modern dates so the authors were unable to make conclusions about the nature of contemporary subsistence strategies. The explanations given for this were that the context had become exposed or that later material had become mixed in through taphonomic processes (Taylor *et al*. 2020b). Despite this, the site is important for its demonstration of architecture and habitation site layout at that time.

The field season of 2018 continued the regional approach with attention being mainly given to two sub-areas at Bagsagiin Bulan downstream from Soyo which had been discovered in a pedestrian survey the previous year. The first area produced 30 orange-red ceramics with blackened interiors from the LBA. The other area produced only microblades and flakes indicative of Neolithic or EBA for a total of about 50 lithics (Clark and Bayarsaikhan 2018, p. 3). Since the two spatially separated areas produced two distinct

assemblages, it is hypothesised that the Mesolithic-Neolithic-EBA and LBA populations possessed different criteria for camp sites which may indicate a difference in subsistence (Clark and Bayarsaikhan 2018, p. 8).

2.3.1 The Geology and Geomorphology of the Area around Soyo

Soyo is located on the western side of the Darkhad basin which forms part of the Baikal Rift Zone (Orkhonselenge *et al*. 2022, p. 239). The Baikal Rift Zone was formed through a series of tectonic stages spanning the Late Cretaceous to Oligocene, Oligocene to Early Pliocene, and Late Pliocene to Quaternary periods (Mats and Perepelova 2011). The basin is bordered on the western and northern sides by the Sayan Mountains. The dominant geology is Proterozoic schist but there are also intrusions of Palaeozoic to Mesozoic granites and deposits of Late Neoproterozoic to Palaeozoic carbonates which are significant for understanding the geology of Soyo (Orkhonselenge *et al*. 2022, p. 236, Tsypukova *et al*. 2022, fig. 2). The Darkhad has held numerous palaeolakes during the Cenozoic Period (see Section 2.6) and this has left more than 210 m of lacustrine deposits in the basin (Ufland *et al*. 1971, Krivonogov *et al*. 2005, p. 83). This has resulted in topography of relatively flat plains above which isolated hills (former islands) rise.

Soyo sits on the banks of the Hogiin Gol where it exits the mountains (fig. 2.11). The valley the river runs through is a U-shaped glacial valley which terminates in a large terminal moraine a kilometre and a half west (upriver) of Soyo. Behind this terminal moraine are multiple recessional moraines formed as the glacier cycles between retreating and advancing. The river passes through a breach on the terminal moraine's northern side and enters a subsequent, smaller "Soyo" glacial valley which had been carved through the Darkhad lake sediments during previous glacial periods. This small valley is bounded by lateral moraines (fig. 2.12) consisting of granite and schist boulders. These were sourced from the schist and granites of the Sayan Mountains. There appear to be at least three generations of lateral moraines on the northern side of the river but only two on the southern side. A previous dating study has shown that high lateral moraines on the side of the breach pre-date the terminal moraine by several tens of thousands of years (Gillespie *et al*. 2008). Therefore, it is likely that there have been previous older generations of glaciation which extended beyond the mountains and produced the outer lateral moraines. The inmost lateral moraines were certainly produced after the large terminal moraine as the valley formed between them extends directly from the breach in the terminal moraine. There is evidence of a pro-glacial lake outburst flood in the form of channelled scour or ripple marks radiating from the breach in the terminal moraine. Furthermore, a kilometre west of Soyo there are possible ripple marks and gravel dunes (fig. 2.13) where the structural constraints on the outflowing water would have opened up. The archaeological impact of the glaciation at Soyo is that all previous material would have been scraped away. Therefore, no archaeological material prior to the glaciation that produced the smaller valley (which is interpreted to be concurrent or younger than the large terminal moraine) will be found at Soyo.

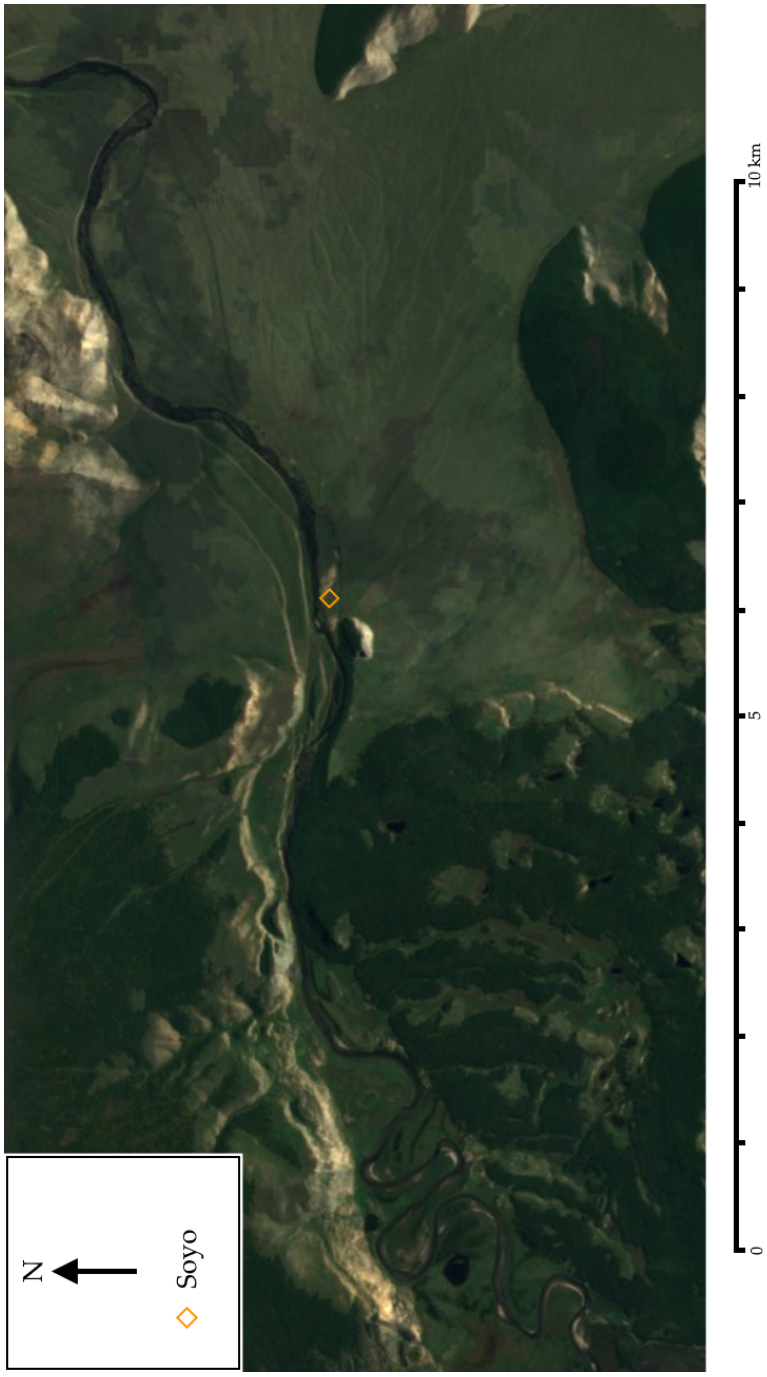

Figure 2.11: Satellite image (Copernicus Sentinel-2 data) of the area around Soyo which is shown by the orange diamond. The Soyo hill lies to its immediate southwest.

Figure 2.12: Photograph from Soyo looking across the river at multiple generations of lateral moraines.

The Hogiin Gol undergoes a change in morphology as it exits the mountains. A transition from braided river to meandering river is observed about 16 km west of the terminal moraine. However, the river returns to a braided stream as it exits through the moraine breach and continues that way for another 15 km or so. This section of river is filled with numerous channel bars (fig. 2.14) and alternate side bars (on one of which Soyo is located). A corresponding change is noted in the channel slope of the river seen in fig. 2.15. The channel slope changes from being near horizontal to having an appreciable slope of 0.4%. The reason for this is probably due to a combination of structural constraints imposed by the moraine-bounded "Soyo" valley and erosion-resistant material in the terminal moraine. The fact that the Hogiin Gol is forced through a former glacial valley constrains the river and prevents it from forming meanders as the boulders in the lateral moraines consolidate the banks to resist erosion. This forces the river to adopt a straighter channel. It is known from experimental work on river morphology that rivers with moderately sinuous thalwegs and alternate side bars are most stable at slopes of 0.2-1.3% (Schumm 1971). It is possible then that the forced reduction in sinuosity resulted in a change in channel slope. The total discharge of the river must remain the same which necessitates a shallower river. A lower depth to width ratio is one explanation proposed

Figure 2.13: Photograph from Soyo Tolgoi looking upstream at ripples and gravel bars potentially related to an outburst flood. Photograph courtesy of Zee.

for braiding in rivers (Easterbrook 1969, p. 125). The alternate hypothesis is that the choke point through the large terminal moraine provides serious resistance to erosion due to the presence of hard metamorphic and igneous boulders deposited there. This effectively results in an elevated local baselevel which is the level below which erosion cannot lower a landscape (Easterbrook 1969, p. 167). Structural morphology and local bedrock can prevent river response to baselevel changes from propagating upstream (Schumm 1993, pp. 281–2). Therefore, when the Darkhad-wide baselevel dropped (as happened with the draining of its palaeolakes), the effect of this may not have extended beyond the terminal moraine west of Soyo. This creates two separate sections of river. The upper section ends in a meandering fluvial plain before the baselevel lowering causes rejuvenation of downward erosion and the reformation of a braided river. The explanation for the change in river morphology is significant because it has implications for its role in the accumulation of sediment at Soyo.

The site of Soyo sits on one of the alternate sand bars along the southern side of the river. It also lies to the northeast of the limestone Soyo Hill which rises approximately 70 m off the plain of lake sediments. More limestone bedrock outcrops just north of the hill and marks the most western limit of the sand bar. This limestone outcrop is a few metres tall and probably somewhat shields the site from fluvial erosion. The topography of the site generally slopes down from west to east and a boulder field of schist and granite is exposed which are undoubtedly of the same glacial origin as the ones in the lateral moraines. The

Figure 2.14: Photograph of Hogiin Gol showing mid-channel bars.

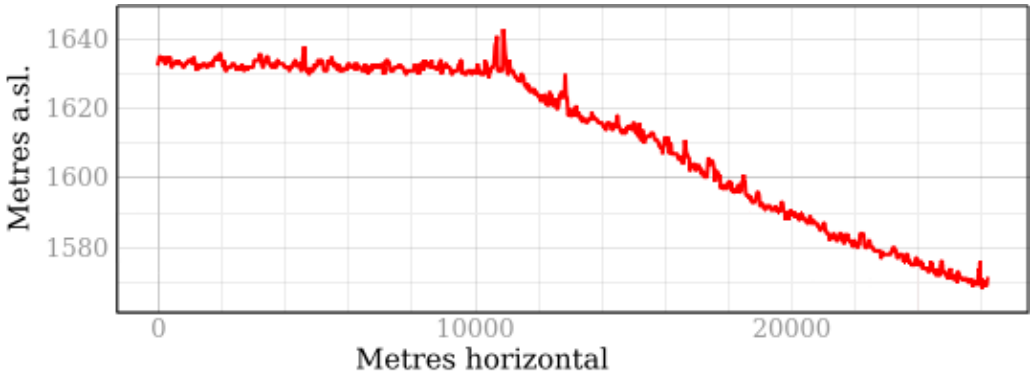

Figure 2.15: Profile of Hogiin Gol channel slope as obtained from a DEM of the area. Where the slope changes is where the river passes though the breach in the terminal moraine.

site also slopes towards the river and there is a natural ford in the west which is used even today despite the existence of a bridge just 500 m downstream. While most of the site is covered by grass, there are two areas of notable land surface instability and aeolian activity. One, which has an aeolian dune system and erosional slope, is towards the western end of the site while the other is a series of dune blowouts farther east. Both areas hold exposed palaeosols.

2.3.2 Regional Survey Surrounding Soyo

Over the course of 2015-2017, a survey of the region surrounding Soyo was conducted along a 12 km stretch of the Hogiin Gol (Clark 2015, Clark and Bayarsaikhan 2016, 2017). Many monuments were discovered including khirigsuurs, burials, deer stones and numerous "stone features." Artefact scatters were also recorded. The results of the survey can be seen in figure 2.17. The black outline indicates the extent of the intensive pedestrian survey as of 2017. The vast majority of monuments fall into the "stone feature" category which includes mounds and circles of stones. The distribution of monuments forms two clear clusters despite the intensive survey done in between. The upstream cluster contains

Figure 2.16: Photograph looking downstream of the limestone cliff marking the western end of Soyo. The hill is just to the right. Courtesy of Zee.

stone features over a 5 km stretch of river and two burials. It also encompasses the sites of Soyo and Bayanii Am 1/3. The downstream cluster also contains many stone features and two further burials but also a cluster of khirigsuurs. Bagsagiin Bulan is located on the western edge of this cluster along with a nearby deer stone and there is another deer stone located 1.5 km outside the survey area to the East. The downstream cluster is much tighter than the other. Possibly this is due to being located at a tight bend in the river so that the riverside area is spatially more compact and also because of the bounds of the survey area. There may be further monuments to this cluster that have yet to be surveyed. The presence of a DSK complex demonstrates LBA occupation in the area although it cannot be said whether the people who built it camped at Soyo. Given the clear evidence for LBA habitation at Bagsagiin Bulan (Clark and Bayarsaikhan 2017) 1.5 km away, it seems probable that it was related.

The evidence for occupation comes from surface scatters of artefacts and the four excavated sites of Soyo, Bagsagiin Bulan, Bayanii Am 1 and Bayanii Am 3. These have been detailed in Section 2.3. Apart from these, artefact scatters (either identified as such or groups of five or more where numbers were available) were found across the full length of intensively surveyed area. The majority of these were lithic scatters with some ceramic scatters as well. Assuming these represent some kind of occupation area (habitation, pro-

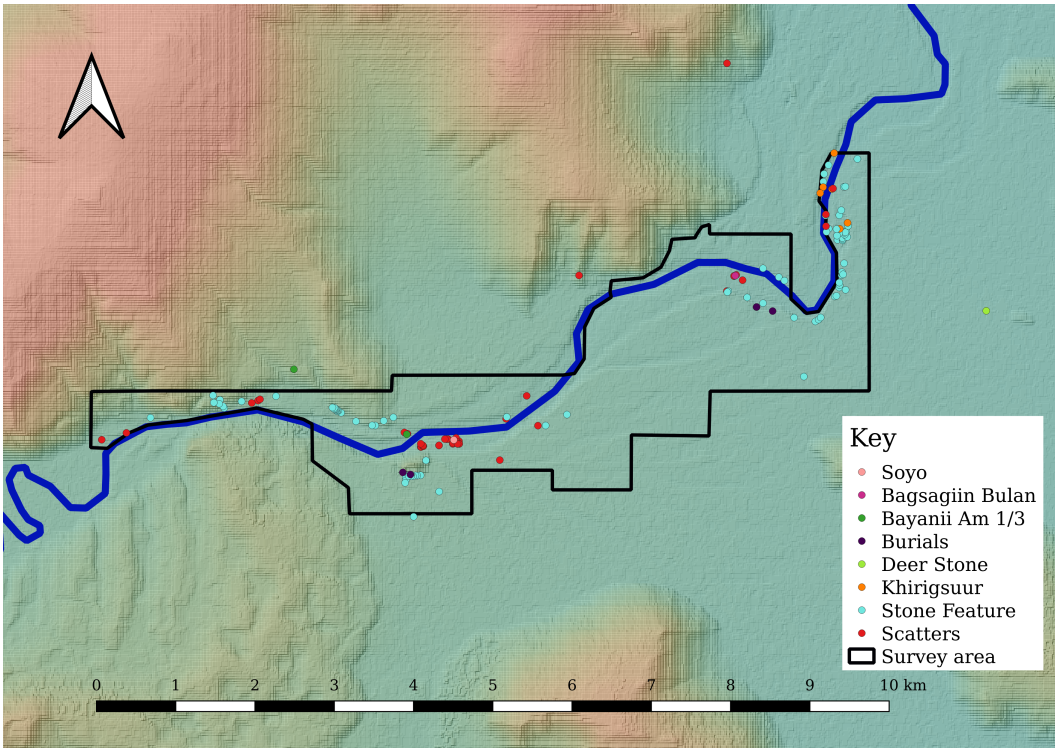

Figure 2.17: Map of the pedestrian survey carried out in the vicinity of Soyo as of 2018. Hillshade generated from JAXA ALOS 3D 30 metre DEM v3.2 (2021).

duction or some other kind of unspecified activity), the occupation of the area follows a similar clustering into two parts as the monumental landscape. The occupation areas show great correlation to monumental areas in contrast to Clark (2014). Some caution is called for in being too eager with an interpretation here since the survey extent is small. Further work also needs to be done on categorising the small finds by period. Most of the scatters were of lithic artefacts. Lithic technologies in the Mesolithic-Neolithic and EBA periods of the Gobi are similar because of the enduring microblade industry and thus assemblages can be difficult to differentiate (Janz 2012, p. 182). The occupation areas may be partly or largely contemporaneous, prior or posterior to the monuments they are near. In the upstream cluster, the majority of occupation areas are at Soyo or close to it. A few sites were also found in the more sheltered glacial valley further upstream. This may represent part of a possible seasonal migration route at some point. In the downstream cluster, occupation areas were found in association both with the site of Bagsagiin Bulan and the DSK complexes. If the spatial pattern at Soyo is interpreted according to the findings of Houle (2010), any Bronze Age occupation sites along the river would be considered Summer camps with the corresponding Winter camps being in the nearby sheltered valleys. This would put the Winter camps outside the survey area as of 2017 so the short range mobility hypothesis developed by Houle in the Khanuy Valley cannot yet be tested at Soyo. However, contemporary use of the area is as a Winter camp site which is supported by the higher concentration of artefacts found at Soyo compared to elsewhere nearby (Julia Clark

pers. comm. 2023). Therefore, the pattern found at Khanuy valley may not be applicable to Soyo.

A closer look at the patterning of monuments in the Soyo cluster is suggestive in light of the hypotheses about monuments being territorial markers (see Frohlich *et al*. (2010, pp. 205–6) and Wright (2014, p. 155) for this in the context of LBA monuments specifically). Although most of these monuments are stone features without a clear periodisation, the monuments are positioned in the pass through the large terminal moraine, on the southern side of Soyo Tolgoi and eastwards along the Hogiin Gol. These would place them in the path of any visitor to Soyo coming along the natural routes. It is interesting that most of the stone features in the Soyo cluster (and the two burials) are found on south-facing slopes which mimics the pattern often found in khirigsuurs in the Darkhad (Frohlich *et al*. 2010, p. 199). Although these are not khirigsuurs and there is no information to tell if they are even LBA, it is a curious similarity. This stands in contrast to the Bagsagiin Bulan cluster where all of the monuments (including the khirigsuurs) are located on more open terrain.

2.3.3 Darkhad Basin Chronology

Aside from the numerous carbon dates that have now been retrieved from the site of Soyo, there exist other dated material in the wider Darkhad region which will provide some chronological context for Soyo (figures 2.4 and 2.18). Virtually all of these come from Bronze Age monuments which is to be expected considering the research objectives that have predominated in Mongolian archaeology and the prominence of monuments compared to other types of sites. Three burial mounds near Soyo were dated to 3.2-2.5 *kya* (Fitzhugh and Leader 2006, p. 78). Unfortunately, the location of these in relation to Soyo is unspecified. Other dated mounds from the Darkhad include an EBA burial at Khogorgo-3 along the Shishkhid Gol 3831-3582 cal. BP (Fitzhugh *et al*. 2008, tbl. 1) and a khirigsuur from Renchinlkhumbe sum (administrative district) 3173-2992 cal. BP (Taylor *et al*. 2017, app. 1). A similar EBA burial to Khogorgo-3 was found approximately 12 km to its east in 2012 and dates to 3884-3638 cal. BP which is a remarkably similar age (Clark 2014, pp. 102–3). Very recently, three burials from Khorig - an hour's drive south of Soyo - were dated to the late twelfth to fourteenth centuries AD (Ventresca Miller *et al*. 2023). Some deer stones from the Darkhad have also been dated. Three of these were dated to 3180-2953 cal. BP (Bayarsaikhan *et al*. 2005, p. 244), 3342-3062 cal. BP (Fitzhugh and Leece 2007, tbl. 1) and 2966-2844 cal. BP (Taylor *et al*. 2017, app. 1). Another example from the northern and of the Darkhad basin at Hort Azur dated to 2879-2750 cal. BP (Fitzhugh *et al*. 2008, tbl. 1). Previously, the oldest deer stone was from the Evdt Valley tributary to the Shishkhid Gol at 3357-3079 cal. BP (Fitzhugh and Leece 2007, p. 7). However, a particularly old deer stone was found to date from 4152-3883 cal. BP although some doubts over the association between the charcoal sample and the deer stone were raised (Clark 2014, pp. 105–6). One final date came from a pit house deep in the mountains along the Shishkhid Gol almost as far as the Russian border which dated to 1312-1063 cal. BP (Fitzhugh 2003, pp. 38–40).

BP	cal. BP (2σ)	Context	Source
6090±70	7161-6755	Timber horizon	Fitzhugh (2003)
5480±80	6546-5938	Hearth	Fitzhugh (2005)
3697±54	4229-3883	Deer Stone	Clark (2014)
3489±45	3884-3638	Grave	Clark (2014)
3450±40	3831-3582	Burial	Fitzhugh *et al*. (2008)
3030±40	3357-3079	Deer Stone	Fitzhugh and Leece (2007)
3000±40	3342-3009	Deer Stone	Fitzhugh and Leece (2007)
2934±31	3204-2966	Khirigsuur	Taylor *et al*. (2017)
2920±40	3207-2953	Deer Stone	Fitzhugh (2005)
2900±50	3203-2880	Burial	Fitzhugh and Leader (2006)
2800±50	3057-2778	Burial	Fitzhugh and Leader (2006)
2800±31	2994-2788	Deer Stone	Taylor *et al*. (2017)
2710±40	2913-2750	Deer Stone	Fitzhugh *et al*. (2008)
2560±50	2761-2471	Burial	Fitzhugh and Leader (2006)
1300±70	1343-1063	Pit	Fitzhugh (2003)
1170±50	1244-958	Hearth	Fitzhugh (2003)
1020±50	1054-792	Hearth	Fitzhugh (2003)
826±29	782-681	Burial	Ventresca Miller *et al*. (2021)
698±29	680-563	Burial	Ventresca Miller *et al*. (2021)
638±29	663-555	Burial	Ventresca Miller *et al*. (2021)

Table 2.4: Carbon-14 dates reported in the literature from archaeological contexts in the Darkhad calibrated using IntCal20 curve.

The bulk of these dates lie in the range of 4.2-2.5 *kya* and represent a flourishing of Bronze Age monument activity (see figure 2.19 for age comparison to the Gobi and Cis-Baikal). The oldest deer stones might slightly predate the LBA (or even largely predate it if the 4152-3883 cal. BP date is secure) which may mean that the Darkhad was an early nucleus for the spread of deer stone culture. This prevalence of Bronze Age dates likely results from the research interests of those working in the region more than any trend in the frequency of occupation sites. Nevertheless, it is interesting that, aside from Soyo, there is an absence of dated archaeological sites from prior to the second millennium BC. The chronology of the Mesolithic-Neolithic of the Darkhad is virtually unknown as compared to elsewhere in Mongolia. A study (Clark 2014) of the northern Darkhad revealed very few pre-LBA sites compared to LBA so it may be that site density from that time really is low. However, the lack of earlier sites from the topographically lowest point in the basin is more likely the result of there being an elevated lake level during much of the Holocene which would have inundated the area (see Section 2.6 for further details). The search for earlier material should be done in parts of the basin above 1600 m a.s.l. for that reason.

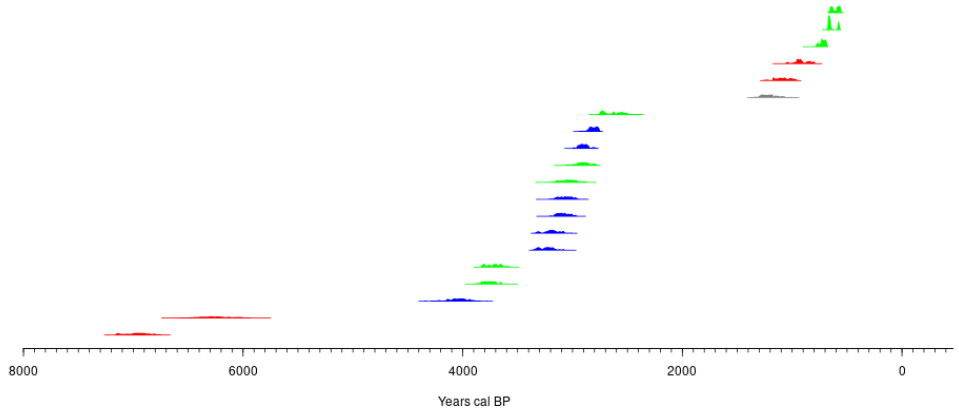

Figure 2.18: Plot of carbon dates obtained from archaeological contexts in the Darkhad. Red indicates the sample was taken from Soyo. Blue indicates either a deer stone or khirigsuur (DSK culture). Green indicates any other burial. Grey is the dated pit from Fitzhugh (2003).

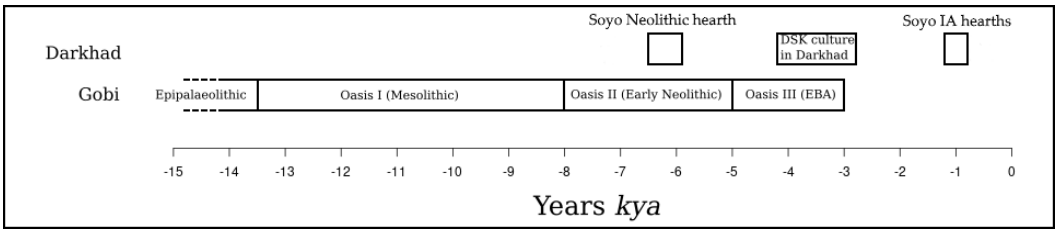

Figure 2.19: Comparison of the age of some of the Darkhad archaeology with the Gobi chronology. Note the Neolithic hearth is contemporary with Oasis II (Early Neolithic).

2.4 Nomadic Pastoralism

The origin of nomadic pastoralism occupies a central position among research questions in Central Asian archaeology. The importance of the nomad in many parts of the world has been appreciated and many attempts have been made to precisely characterise the lifestyle and explain its origins and the motivations that lay behind it. We must first ask what is a nomadic pastoralist. A sensible person would answer that it is a person who engages in herding animals and does not have a permanent place of residence. This is all very good but it has doubled the number of questions being asked. How much pastoralism must one do to be a pastoralist? How long can one stay in one place before ceasing to be a nomad? Even more confusion is brought in by the interchangeable usage of "nomadic pastoralist" and "nomad." More restrictive definitions of the term have been proposed. Khazanov (1994, pp. 15–6) has defined a nomads as groups who are nearly all engaged

in free range pastoralism and who undertake regular, cyclic migrations. Cribb (1991, pp. 17–20) defines pastoralism as mostly relying on herding for subsistence and nomadism as the regular movement of both people and their productive base within one ecological niche. A nomadic pastoralist would then encompass both of these. According to both Khazanov and Cribb, hunter-gatherers do not count as nomadic because both authors see the "food extraction" of hunter-gatherers and the "food production" of nomadic pastoralists as being too fundamentally different for the two groups to be associated under one word (Cribb 1991, pp. 20–2, Khazanov 1994, p. 15). Here the terms "nomad" and "nomadic pastoralist" are conflated to only include one particular group of mobile peoples to the exclusion of all others (as Cribb does when he says that nomads move within one ecological niche). Nomads seem to be defined as much by what they are not as what they are. This is a likely source of confusion since the common definition of nomadism pertains exclusively to mobility and not at all to any particular economic activity. In any case the problem can be sidestepped simply by referring to such peoples as "nomadic pastoralists" which is what will be done here.

The most predominant question in the archaeology of nomadic pastoralists has been how to explain their origins and there has been a large variety of candidate hypotheses put forth. Although the domestication of animals has a venerable history like that of plants, it was not until much later that specialised nomadic pastoralists appeared. One of the earliest explanations that was widespread before the twentieth century was that it developed directly out of hunting practices. Hunters following the seasonal migration routes of herbivores would in a certain way "adopt" a herd and the process of domestication would begin (Khazanov 1994, pp. 85–6). However, it became apparent that nomadic pastoralism was a later phenomenon than pastoralism itself. Lees and Bates (1974) provided a different sort of explanation for the Near East. Beginning from the fact that the areas that have suitable rainfall for agriculture also have the best pasture, they explain that mixed agropastoralism was the obvious and natural path for early subsistence since both could be easily practised in the same area. This allowed a mitigation of risk by having many productive activities. However, the advent of canal irrigation provided an alternative way to mitigate risk by protecting against disastrously poor rain and by allowing intensification of agriculture leading to greater surpluses and storage of food. As the practice of irrigated agriculture increased, there was pressure away from mixed economies due to competition over land and manpower between agriculturalists and pastoralists. Settlement patterns also changed to allow more people to live in dryer zones. These factors made it more difficult to practice both activities in terms of both allocation of labour and in terms of the increasing distance required to travel to reach suitable pasture. Furthermore, the intensification of agriculture led to diminishing returns pushing people into alternative specialisations. Therefore, nomadic pastoralism was one result. It is important to note that under this model, nomadic pastoralists were not considered self-sufficient and required regular access to settled communities and their agricultural products for trade or raid. The exact way nomadic pastoralists gained access to these products could vary depending on the particular circumstances (Lees and Bates 1974, p. 191).

A somewhat related model was put forth to explain the emergence of nomadic pastoralism in the Zagros Mountains by Gilbert (1983). According to this model the earliest herders would utilise the best pasture which is at high elevation and stable their animals at a lower elevation in Winter. Increasing herd sizes meant it was no longer feasible to stable the animals and it became necessary to travel much farther distances. At the same time an intensification of agriculture (and thus relative marginalisation of pastoralism) raised the price of animal products and made pastoralism more attractive as a specialist activity than a generalist one. With the establishment of longer transhumance routes and greater specialisation, it became possible for some groups to drift away from the defined routes and become fully nomadic. Attempts at centralised control by settled polities may have increased the divide between agriculturalist and nomadic pastoralists as the latter are more able to resist (Gilbert 1983, pp. 110–4). Even though the possibility of full nomadic pastoralism is unlocked, it was another matter entirely of actually embarking on that path. It is conceived not as a isolated kind of existence but as a choice that could be made as the situation warrants. Therefore, we may speak of tendencies towards or away from nomadic pastoralism (Gilbert 1983, pp. 114–5).

Both Lees and Bates and Gilbert place the origins of nomadic pastoralism as one effect of a larger restructuring of subsistence activities. This tie of fates is also seen in Sherratt's (1981) "Secondary Products Revolution" which posits that the secondary (non-fatal) uses of animals such as milk, traction and wool enabled pastoralists to move into more marginal areas and become less closely reliant on agriculturalists. This expansion of animal use is supposed to have allowed mixed economy groups to move into the Eurasian steppes and form a new cultural group that is associated with kurgan burial mounds (Sherratt 1981, pp. 295–6). What is interesting about the Secondary Products Revolution idea is that the way pastoralist developments affected agricultural settlements is given a prominent position. For example, the added mobility of nomadic pastoralists in previously unoccupied lands is theorised to have changed patterns of trade and led to new connections between distant lands (Sherratt 1981, p. 287). The introduction of the animal-drawn plough in combination with new animal fibres is proposed to have changed the male and female spheres of activity with women moving away from agricultural labour into spinning and weaving (Sherratt 1981, p. 297).

Some have questioned the concept of an origins for nomadic pastoralism at all. The phenomenon is seen as a subsistence specialisation that appears and disappears as the wider situation warrants instead of a fixed and irreversible process. The same group of people may go back and forth between subsistence strategies over time (Cribb 1991, pp. 12–14, 59–64). The idea is rather than there being a single original event or process of people becoming pastoral nomads we may instead speak of *motivations* for becoming so. These motivations could be any number of environmental or political conditions but at least involves some measure of political instability and the concentration of herds into the hands of fewer people. Under these conditions subsistence strategies crystallise into specialised

nomadic pastoralism and sedentary agriculture along kinship lines (Cribb 1991, p. 63). The reverse is also true. Greater political stability would lead to more mixed economies and more permeable tribal bounds (Cribb 1991, p. 62). The explicit link made between nomadisation and kinship is especially intriguing in the light of Joshua Wright's portrayal of the adoption of nomadic pastoralism in the Egiin Gol valley as a political and group statement (Wright 2006).

So far a range of explanations for the appearance of nomadic pastoralists has been examined in general but only in general. Historically speaking the study of nomadic pastoralism and its origins has centred around the Near East since that it historically where much archaeological work in general has been done. What has not been made adequately apparent in the preceding discussion is a sense of distinction between these groups: only between they and their settled neighbours. Nomadic pastoralism was practised differently in different parts of the world and the precise origins, composition of herds and relation to other peoples all serve to highlight regional distinctions and tangled trajectories between different groups (Honeychurch and Makarewicz 2016, p. 343). Even within geographical regions such as the Eurasian steppe, it has been revealed that there was substantial independence in regional development. The western steppe around the Black Sea was home to agro-pastoralists who kept a mix of animals around the fifth millennium BC. In the time leading up to the Bronze Age, these people living around the Black Sea intensified their subsistence activities while people living in the drier lands to the East around the Caspian Sea engaged in a distinct hunter-gatherer economy based around seasonal and more permanent settlements. The distinction between the two economic strategies blurred in the fourth millennium BC when hunter-gatherers began to directly borrow sheep and goat herding. In the Early Bronze Age (3200-2600 BC) fully specialised nomadic pastoralists emerged as the Yamnaya (pit grave) culture. These communities were engaged in cattle-based pastoralism in the areas around the Black Sea and mobile sheep and goat pastoralism around the Caspian Sea (Khazanov 1994, p. 91, Bendrey 2011, p. 7, Frachetti 2012, pp. 7–8). In the central steppe pastoralism did not appear until the middle of the fourth millennium BC with the Botai culture. Horses were dominant here and in fact at the type site of Botai, 99% of the faunal assemblage was horse. Furthermore, the Botai do not appear to have been particularly mobile or at least had year round settlements (Khazanov 1994, p. 91, Frachetti 2012, p. 9). In the third millennium BC the peoples of the central steppe appear to have switched to mixed herds of ungulates because of influence from the western and eastern steppes although the Iron Age sites still reportedly placed an emphasis on horse (Bendrey 2011, p. 7, Frachetti 2012, p. 9). Although there was a strong tradition of horse domestication in the central steppe from the fourth millennium, there is no evidence of riding paraphernalia but this does not mean they could not have ridden bareback (Khazanov 1994, pp. 91–2). Note that, very recently, it has been argued that the horse remains recovered from Botai from the fourth millennium BC were not from domesticated horses but a sister taxon of wild horse and that the domestication of the horse on the central steppe should be assigned to a later date (Taylor and Barrón-Ortiz 2021). On the eastern steppe nomadic pastoralism appeared around the same time with the Afanasievo culture

but was primarily based around sheep and goats and a vertical transhumance. Hunting and fishing also supplemented their subsistence. Afanasievo burials yield hunted animals as half of the remains, in contrast to 27% at settlement sites, so there may have been some social or ritual aspect around hunting among nomadic pastoralists even as herding became the dominant economic activity (Khazanov 1994, pp. 90–1, Frachetti 2012, pp. 10–1). The origins of the Afanasievo are an open question since the prior Neolithic populations of the Altai region show little continuity (Frachetti 2012, p. 10). The Afanasievo had been thought to be the result of Yamnaya migrations across the whole of the Eurasian steppe but, given the regionalism evident, Frachetti gives an alternative route through the "Inner Asian Mountain Corridor" which runs from the Iranian plateau to the Altai. He notes that the agro-pastoral groups along this mountain fringe kept sheep and goats in contrast the the cattle of the oasis and plains villages in southern Central Asia and the horses of the central steppe. This is borne out by recent findings of domesticated sheep at Obishir V in southern Kyrgyzstan from c. 6000 BC which is 3000 years earlier than previously thought (Taylor *et al*. 2021). Furthermore, the genetic lines of sheep show stronger affinity with those of the eastern steppe and of the Near East than with the western steppe (Frachetti 2012, pp. 13–14) although genetic ties between the actual Afanasievo and Yamnaya people still give room for an easterly migration (Jeong *et al*. 2018, 2020, Taylor *et al*. 2019, p. 2). The regionalisation seen in the favouring (but not complete replacement by) certain domesticates in the western, central and eastern steppe may simply be, as Bendrey has argued, due to environment factors. There is a precipitation gradient decrease West to East across the steppe. Since cattle do not weather drought well, we would expect to find them in the wetter western steppe. Sheep and goats would be more suited to the arid and mountain-adjacent eastern steppe while horses are apparently quite suited for the cold, snowy pastures of southern Russia (Bendrey 2011, pp. 10–2). It should be noted, however, that the environmental data for Bendrey (2011) is modern and it would be helpful to know if this situation were true at the time in question in order to test this idea. There may also be other, non-environmental factors that played a part in the regionalisation of pastoral strategies.

On the Mongolian plateau itself, the first pastoralism was brought in by Afanasievo populations from the Eurasian steppe (Volkov 1995, p. 320, Taylor *et al*. 2019, pp. 2–3). The timing has been a matter of discussion with the estimates falling in the third and second millennia BC between the hunter-gatherers of the pre-bronze periods and the widespread nomadic pastoralism of the Late Bronze Age (Clark 2014, pp. 50–2). Very recently new dating studies have been published which show that the earliest evidence of pastoralism in Mongolia come from Early Bronze Afanasievo burials c. 3300-2900 BC which are stone burial mounds and have produced cattle, sheep, goat and dog bones and carts (Taylor *et al*. 2019, pp. 2, 9–10, Wilkin *et al*. 2020). The presence of specific milk proteins in human dental calculus (Wilkin *et al*. 2020) shows that these animals were indeed used for subsistence and helps alleviate concerns over whether changes in animal bones in burials really correspond to changes in subsistence. The Afanasievo culture was followed by the Chemerchek culture which continued in the tradition of pastoralism. The concentration of

these early pastoralist sites in the western half of Mongolia and the shared burial patterns (such as flexed burials) support the hypothesis that pastoralism arrived in Mongolia from the Eurasian steppes further west. In the second half of the second millennium BC, there was a flowering of the number and types of pastoralist sites across Mongolia (Taylor *et al*. 2019, pp. 12–3). This was followed by the very important domestication of the horse and its rapid spread across Mongolia which is put at c. 1200 BC (Late Bronze Age) and associated with deer stone and khirigsuur sites although the advent of khirigsuurs may predate deer stones and the domestic horse by two centuries (Taylor *et al*. 2017, p. 52). Whereas the introduction of herding to Mongolia has been largely placed on the shoulders of the Afanasievo migrants, the explanation for this latter shift to horses and associated cultural changes is less certain. One of the earliest explanations for the cause of this transition from pastoralist to horse-mounted pastoralist was that the cultural frontier between Chinese and Mongolians became crystallised and led the latter to reject the Chinese way of life and embrace steppe nomadism (Lattimore 1940, pp. 56–9). Khazanov (1994, pp. 94–5) argued that the catalysing factors for embracing a fully nomadic, mounted pastoralism were aridification of the environment and the emergence of neighbouring settled civilisations. However, it is argued that the cause of this transition cannot be that mounted pastoralism arose due to aridification and resource scarcity because it occurred *after* an arid period during a time of climate amelioration (Taylor *et al*. 2017, p. 54). It may be that the success of the horse was at least partially due to the consumption of horse milk in its fermented form as a social activity (Wilkin *et al*. 2020, pp. 350–1). Furthermore, the role of neighbouring states in the rise of the steppe nomad mode of existence has, as it pertains to Mongolia, been called into question (Houle 2010). Other explanations have focused on the role of social interactions within Mongolian steppe peoples. For example, Wright (2006, pp. 296–8) suggests that nomadic pastoralism was adopted by existing populations out of a desire for both the status and power symbolised by the associated monuments and the economic and social security afforded by domesticated animals.

The difficulty of finding the remains of nomadic pastoralists in the archaeological record has been commonly lamented. The ephemerality and sparseness of sites have been stressed as well as the likelihood that such smaller site would be erased or hidden by taphonomic processes (Gilbert 1983, pp. 107–8, Houle 2010, p. 36, Clark 2014, p. 77, Honeychurch and Makarewicz 2016, p. 349). It is not that nomadic pastoralists leave no trace whatsoever but that the traces they do leave are difficult to distinguish from other assemblages (Cribb 1991, p. 69). Furthermore, the temporary habitation and lack of extensive construction means that most sites have shallow or no stratigraphy outside of hearths and middens (Cribb 1991, p. 80). Nevertheless, we ought to be able to draw some general conclusions about what a nomadic pastoralist site should look like. Cribb divides artefacts up according to three axes: fixtures - portables, durables - perishables, and valuables - expendables. The survivability and visibility of material culture is determined by where it falls on these three axes. Because of the high mobility of nomads, we ought to expect to find mostly fixtures and expendables (Cribb 1991, pp. 68–9). Putting it another way, if a site is high in relatively immovable fixtures and expendable items, it may be that the site was inhabited

by a mobile population. It has been suggested that a complex survey on multiple scales may be most suited to studying mobile populations at they move around the landscape (Honeychurch *et al*. 2007, Wright *et al*. 2009, Honeychurch and Makarewicz 2016, p. 349).

2.5 Climate

Mongolia is situated between three very different geographical regions: Siberia to the north, Central Asia to the west and East Asia to the southeast. The high Sayan and Altai mountain ranges bound the region to the north and west and limit the transport of precipitation into Mongolia leading to greater aridity in much of the area (Goulden *et al*. 2011, p. 91). Mongolia is broken up into five main environmental zones which increase in aridity southward. In the northern reaches lies the southern extension of the Siberian taiga. This is comprised of primarily pine and larch trees which are cold-resistant. Following this is a forest-and-steppe transitional zone and then the steppe proper which dominates the Mongolian landscape. On the southern side are the transitional desert-steppe and desert regions (Goulden *et al*. 2011, pp. 96–8). The Darkhad Basin (in which Soyo lies) is the westernmost in a series of rift basins extending northeast to Lake Baikal (Gillespie *et al*. 2008, p. 170).

Throughout the Late Pleistocene and Holocene, this area, along with wider Mongolia, has seen many climatic transitions which have impacted the environmental zones and human occupation. After the Last Glacial Maximum (LGM), the general trend was towards a warmer and wetter climate as glaciers receded in the mountains to the north and west of Mongolia. The timing of the end of the last glacial period around the Darkhad is approximately 17 *kya* (Gillespie *et al*. 2008, p. 183, Arzhannikov *et al*. 2012, p. 30) which is followed by a rise in temperatures and precipitation better seen at neighbouring Lake Hovsgol (Fedotov *et al*. 2004, p. 255, Prokopenko *et al*. 2007, p. 11, Murakami *et al*. 2010, p. 379). A similar climatic amelioration is also seen at Lake Baikal around 18-14 *kya* (Horiuchi *et al*. 2000, p. 106) and in the Mongolian Altai from 15.9 *kya* (Blyakharchuk *et al*. 2004, pp. 269–71). This trend is punctuated to varying degrees by a drier, colder period roughly corresponding to the Younger Dryas event. However, it is weakly represented or not represented at all in many Mongolian and Siberian records. A cold, dry event is recorded in the lake sediments of modern Dood Nuur in the Darkhad prior to 9.5 *kya* which is interpreted to correspond to the Younger Dryas event (Narantsetseg *et al*. 2013, p. 20). Lake Hovsgol contains the clearest and most consistent evidence of a warm and wet Bølling-Allerød period followed by a colder and dry Younger Dryas at 15-11.5 *kya* (Fedotov *et al*. 2004, p. 255). Choi *et al*. (2014, pp. 1146–7) determined using beryllium isotopes that the Younger Dryas event at Lake Hovsgol began at 12.7 *kya* and was preceded by a warmer period which is consistent with other studies. Prokopenko *et al*. (2007, p. 11) presented pollen records showing an increase in precipitation and forestation starting around 14 *kya*. A weak spike in steppe vegetation may indicate the Younger Dryas event but it is not easily distinguishable from the preceding or following periods. Pollen from Lake Baikal

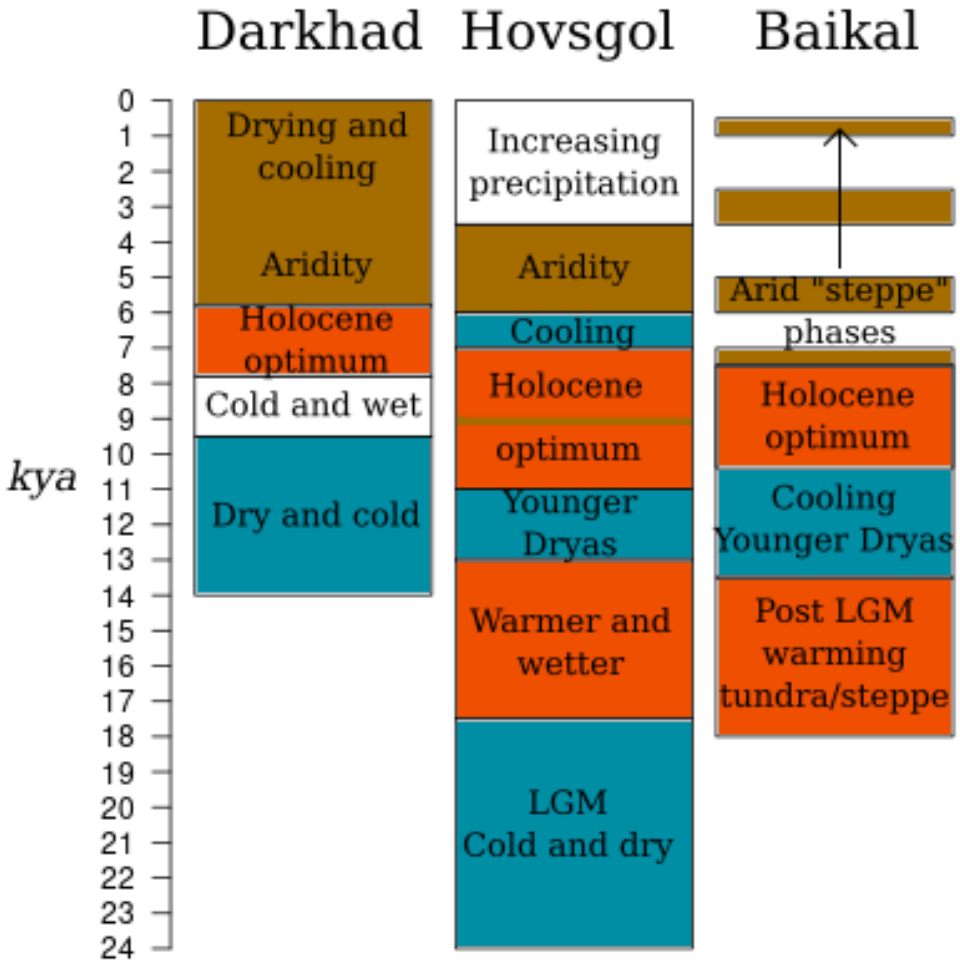

Figure 2.20: Summary of climate variation in the Darkhad, Hovsgol and Baikal basins. Blue is used to indicate colder and dryer periods, orange is used to indicate warmer and wetter periods, brown is used to indicate periods of greater aridity and steppe conditions.

suggests a climatically unstable period from 13.0-10.4 *kya* with fluctuating taiga and steppe coverage. Colder intervals occurred around 12.5 *kya* and 11.5-11.0 *kya* (Tarasov *et al*. 2007, pp. 448–9). Analysis of δ13C and carbon to nitrogen ratios suggest a fluctuation in surface productivity from 14-12 *kya* and a possible cooling although not necessarily identical to the Younger Dryas event (Horiuchi *et al*. 2000, pp. 104, 106). Elsewhere the situation varies. Cool and wet conditions are recorded in northern Kazakhstan from 15.5-11.5 *kya* but Altai region pollen records have not yet indicated the occurrence of a similar cooling period there (Blyakharchuk *et al*. 2004, pp. 271–2).

During the subsequent Holocene, the general climatic trend in Mongolia was increasing temperatures and moisture to a climatic optimum before a sharp arid event in the mid-Holocene. Following that was a return to more humid conditions (An *et al*. 2008, p. 288).

The Darkhad experienced climatic amelioration from 7.8 *kya* which was followed by increasing aridity and regression of Dood Nuur after 5.8 *kya* (Narantsetseg *et al*. 2013, p. 22). The trend towards climatic optimum began earlier at Lake Hovsgol around 11.0-10.5 *kya* (Prokopenko *et al*. 2007, p. 11) or even as early as 12.5 *kya* (Murakami *et al*. 2010, p. 379). Prokopenko *et al*. (2007, p. 11) note weak evidence for increased steppe pollen around 9.5 *kya* and for cooling between 7.0 *kya* and 5.5 *kya* while beryllium isotope analysis indicates a lengthier cold and dry period after 9.4 *kya* (Choi *et al*. 2014, p. 1145). As in the Darkhad, there is a phase of aridification variously dated between 6.0-3.5 *kya*, 5.5-4.0 *kya*, and centred around 5.5 *kya* and which is followed by an increasing precipitation to evaporation ratio after 3.5 *kya* as shown by sediment, diatom and pollen records (Fedotov *et al*. 2004, p. 256, Prokopenko *et al*. 2007, p. 11). At Lake Baikal the general warming is interrupted by four "steppe events" at 7.5 *kya*, 5.5 *kya*, 3.0 *kya* and 1.0-0.5 *kya* (Tarasov *et al*. 2007, p. 451), the second of which corresponds with a sharp decline in the southwestern Altai taiga at 5.7-4.5 *kya* (Blyakharchuk *et al*. 2004, p. 274). These periods of increased aridity (at least at Lake Baikal) are linked with periods of weakened monsoons (Tarasov *et al*. 2007, p. 452). These climatic trends and events are summarised in figure 2.20.

2.6 Darkhad Palaeolake

In the past, the Darkhad basin was filled by a series of palaeolakes of varying sizes. Soviet researchers found more than 210 m of lake sediment which they dated to two broad stages during the Pliocene/Early Pleistocene and Middle/Late Pleistocene on the basis of palynological results (Ufland *et al*. 1971, Krivonogov *et al*. 2005, p. 83). The latest lake stage was given as MIS3 (Krivonogov *et al*. 2005, p. 87). However, it has since been shown that a lake existed at various times throughout the post LGM and Holocene. It is these lakes that are most interesting from the archaeological perspective. Krivonogov *et al*. (2005) had proposed that the Darkhad only had a high level during MIS5 and that subsequent lakes, particularly during the Holocene, were very shallow (1545 m a.s.l.). This conclusion was made on the basis of a presumed lack of significant glaciation during MIS2 and, therefore, that such lakes could only have been dammed by alluvial fan deposits from the Tengis Gol tributary. Gillespie *et al*. (2008) undertook a basin-wide project to date the glaciation using beryllium, carbon and luminescence (IRSL) dating and found evidence for a significant period of glaciation from 19 *kya* to 17 *kya*. They proposed that the Shishkhid Gol outflow from the Darkhad basin was blocked by the Tengis glacier at this time and gave rise to a deep palaeolake (1670-1679 m a.s.l.). This lake lasted until 14 *kya* (according to a beach sand luminescence date) at which most or all of the water was discharged (Batbaatar and Gillespie 2016b, pp. 1761, 1771). Recently, it has been suggested that another ice dam downstream of the Tengis tributary was responsible for the deepest Darkhad palaeolakes since the 1713 m a.s.l. shorelines from an earlier stage of inundation (MIS3 or earlier in MIS2) continue into the Shishkhid Gol valley beyond the Tengis-Shishkhid confluence (Komatsu *et al*. 2009, p. 152, Arzhannikov *et al*. 2023, p. 16). The damming mechanism may have been even more complex than thought which would have implications on the

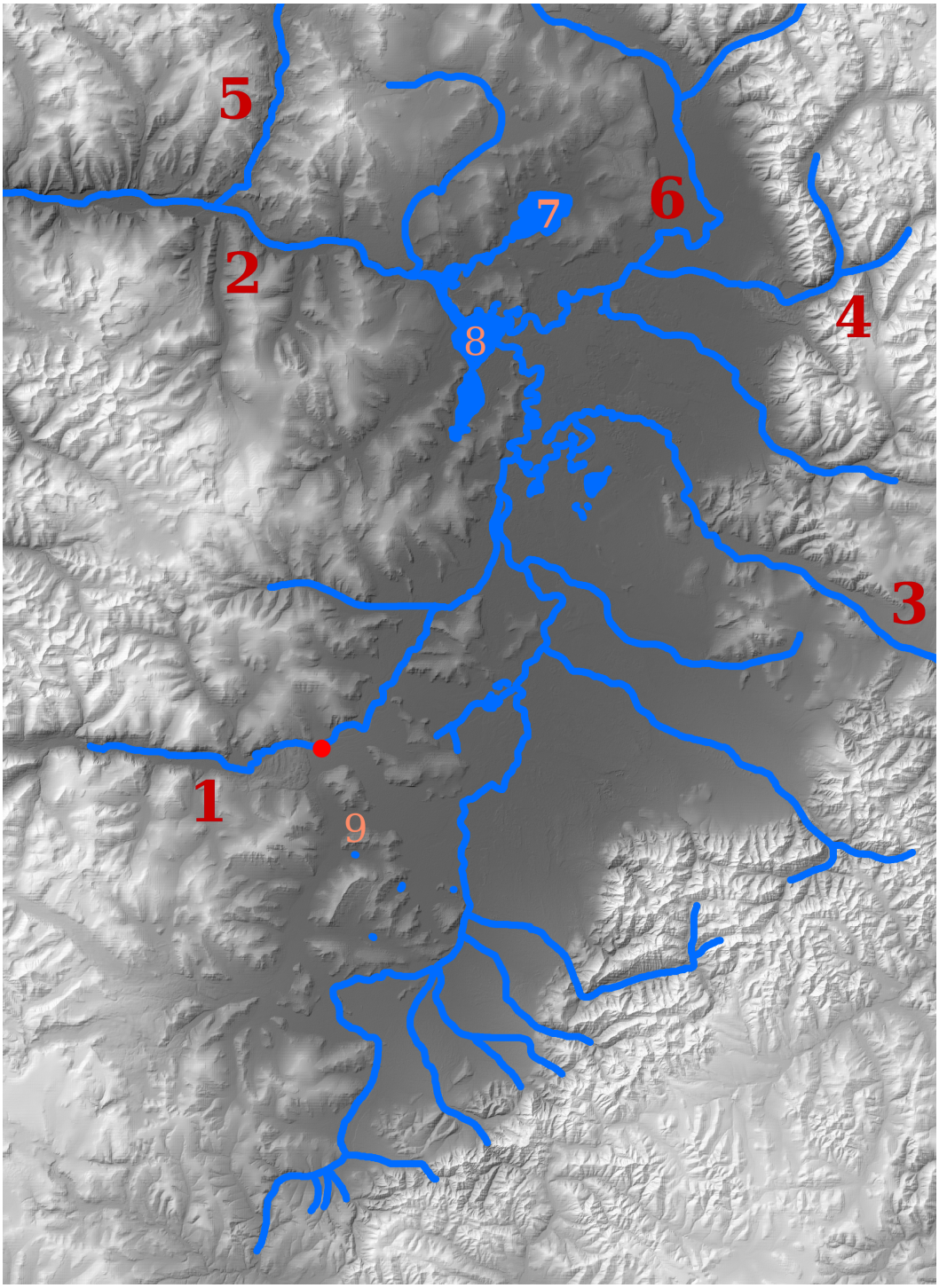

Figure 2.21: Topographic map of the Darkhad basin showing major rivers (red labels) and lakes (pink labels). Soyo is shown by the red dot. 1. Hogiin Gol; 2. Shishkhid Gol; 3. Arsain Gol; 4. Jarai Gol; 5. Tengis Gol; 6. Shargyn Gol; 7. Targan Nuur; 8. Dood Nuur; 9. Zayaday Nuur. DEM is JAXA ALOS 3D 30 metre DEM v3.2 (2021).

dating of the palaeolake since much of the chronology so far is based on beryllium dating of glacial moraines.

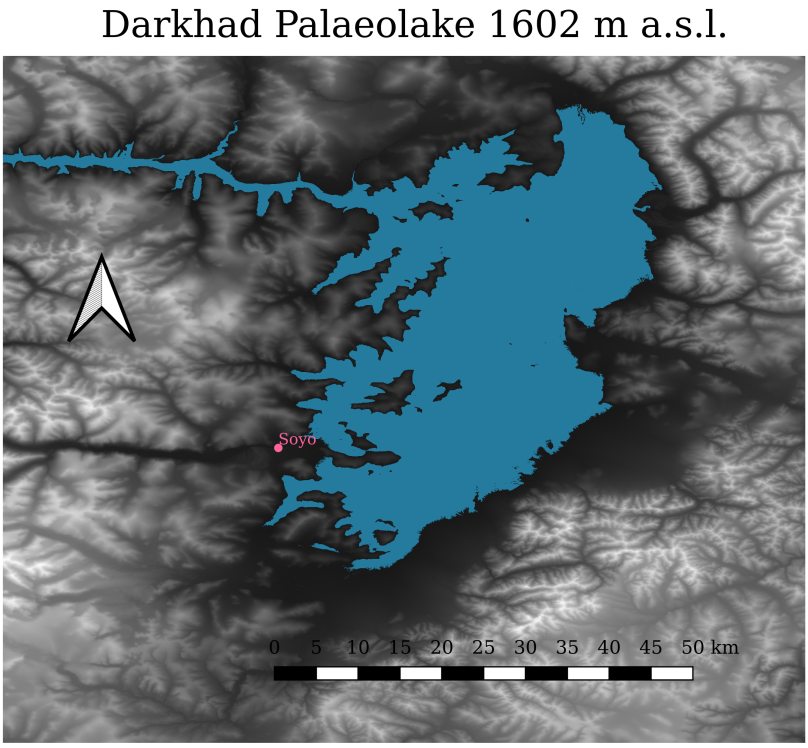

Figure 2.22: Extent of a lake filling the Darkhad basin up to 1602 m a.s.l. Soyo is shown in pink. DEM is JAXA ALOS 3D 30 metre DEM v3.2 (2021).

Following the decline of the Darkhad lake at 14 *kya*, there are conflicting ideas about the state of the basin for the subsequent five thousand years or so. According to diatom and other sedimentary records from the area of the modern Lake Dood and Hodon outcrop, there was a (near) total absence of the lake during 14-9.5 *kya* (Krivonogov *et al*. 2012, Narantsetseg *et al*. 2013). However, shorelines at 1602 m a.s.l. and dated near-shore lake sediments from the same elevation point to the existence of a lake at this time (fig. 2.22). In particular, mollusc shells (14-12 *kya*) from across the basin (including two from Zayaday Nuur about 10 km SSE of Soyo demonstrating its spatial relation to this lake), IRSL on a silt sample (12.6 *kya*), and charcoal (10-11 *kya*) were used to date this shoreline. A date between 10-11 *kya* was chosen on the basis of possible reservoir effects. The culprit for damming this lake was proposed to be the alluvial outwash fan at the Tengis-Shishkhid confluence (Gillespie *et al*. 2008, pp. 172, 180). A suggestion made for a resolution to this conflict has been a rapid drainage of the lake combined with uncertainties in the dating such that there was a sufficiently lengthy period with no lake prior to 9.5 *kya* for those sediments around Lake Dood to form. Alternatively, it has been suggested that the 14-9.5 *kya* segment of sediments in question were existing sediments eroded from upstream and redeposited around Lake Dood. Therefore, the dates obtained from that section would not

represent the period of final deposition (Batbaatar and Gillespie 2016a, p. 1741).

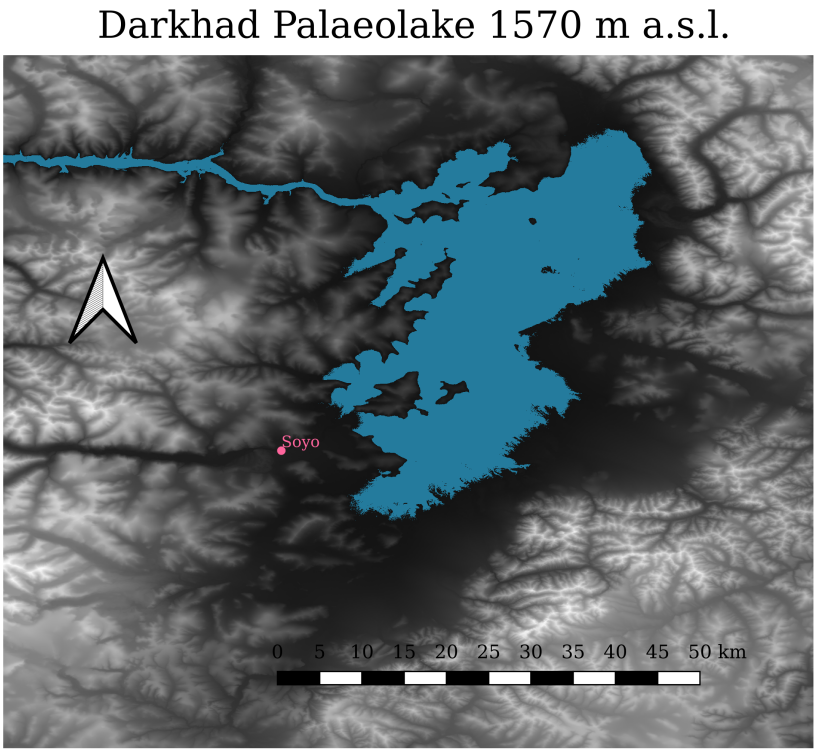

Figure 2.23: Extent of a lake filling the Darkhad basin up to 1570 m a.s.l. Soyo is shown in pink. DEM is JAXA ALOS 3D 30 metre DEM v3.2 (2021).

In any case, there appears to have been a partial replenishment of the lake following 9.5 *kya*. Krivonogov *et al*. (2012) propose fluctuating lake levels between 9.6-4.5 *kya* followed by a retreat of the lake to modern levels by 3.9 *kya*. Narantsetseg *et al*. (2013) suggest that the lake at this time was low because of the low amounts of deep water diatoms with lake level reduction occurring around 5.8 *kya*. A chironomid study on sediments from the Hodon outcrop demonstrates a rising lake at 9 *kya* due to a change from littoral to sublittoral and profundal taxa lasting until 4.5 *kya* (Ni *et al*. 2022). This final stage of the palaeolake was likely dammed by alluvial outwash which forms a series of cones 2-50 m high. This would have allowed only fairly low lake levels 1540-1570 m a.s.l. (fig. 2.23) (Krivonogov *et al*. 2012, pp. 147–8). Substantial decline in the palaeolake (to below 1560 m a.s.l.) by 3.5 *kya* is shown by the dated palaeosol in the post-lake loess at Shargyn Gol cutbank (Gillespie *et al*. 2008). The different models for the filling and emptying of the Darkhad palaeolake are summarised in figure 2.24.

Aside from its implications in constraining human occupation of the Darkhad, one of the primary points of interest in studying the palaeolake is that it was the major source of water for one of the largest known outburst floods. This deluge travelled down the River

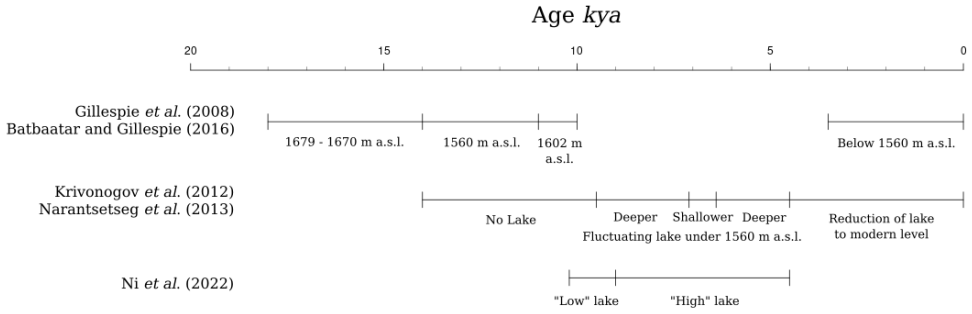

Figure 2.24: Summary and comparison of the two major theories regarding the chronology of the Darkhad palaeolake after the LGM.

Yenisei dramatically changing the landscape and exiting into the Arctic Ocean (Komatsu *et al*. 2009). See Komatsu *et al*. (2016) for an historical summary of the literature on Pleistocene Siberian flooding. Unfortunately, there has yet to be a comprehensive dating project on the flood deposits themselves (but see (Arzhannikova *et al*. 2014) for a study on their geology) so the timing of outburst floods has been inferred from the timing of the rises and falls of the Darkhad palaeolake (Arzhannikov *et al*. 2023, p. 2). Therefore, the timing of flooding cannot be used to provide a definite end date to periods of high palaeolake levels. Nevertheless, we know that they did occur and have probably had an impact on the Darkhad basin itself as much as on the basins and valleys downstream. The ability of even relatively smaller flooding events to scour away metres of rock and sediment is well documented from contemporary events (Breien *et al*. 2008, Lamb and Fonstad 2010). It stands to reason, therefore, that even larger flooding events could have scoured away parts of the lake floor in the Darkhad basin and that has been given as an explanation for the lack of MIS2 lake sediments in some stratigraphic sections (Batbaatar and Gillespie 2016a, p. 1748).

Chapter 3

Methodology

3.1 Geophysics

One of the problems faced by the archaeologist is the time consuming and expensive nature of excavation. Geophysical techniques can be used to reduce this through pre-excavation exploratory mapping and stratigraphic investigations. Suitable places for excavation, such as the deepest stratigraphy in a rockshelter or proximity to potential archaeological features, can be found using geophysics. Known features can be mapped beyond the confines of the excavation. A second advantage to the use of geophysics on archaeological sites is the fact that they reduce the need to disturb the site. The preserves more of the site intact for future research inquiries. There is a large range of techniques that can be used for archaeological purposes depending on the properties of the target material and the research design. Some of the most commonly used include resistivity in the form of both fixed-probe array and as electrical resistivity tomography (ERT), ground-penetrating radar (GPR), magnetometry, magnetic susceptibility which are explained in this chapter. Other methods such as electromagnetic induction (EMI) are also frequently used and seismic and induced polarisation are used occasionally. In the field of Mongolian archaeology, a range of geophysical techniques has been used. Methods used have included magnetometry, GPR, electrical resistivity and EMI for the purposes of determining urban layouts (Grützner *et al*. 2012, Linzen *et al*. 2019, Miller *et al*. 2019, Bemmann *et al*. 2022, Reichert *et al*. 2022), investigating buried structures such as tombs and walls (Ates 2002a, Batmunkh *et al*. 2004, Khuut and Sato 2009, Khuut *et al*. 2015a, 2018, 2019), investigating both natural and artificial stratigraphic layers (Grützner *et al*. 2012, Vella 2018), investigating graves (Ates 2002b, Khuut *et al*. 2015b), and general archaeological prospection (Bemmann *et al*. 2011, Lin *et al*. 2011).

While the use of geophysics has had a long history in archaeology, many archaeologists are unfamiliar with how the techniques work and thus are also unfamiliar with methods of collecting and interpreting geophysical data. It is possible to train someone to operate the equipment and process the results into a usable product. However, an understanding of how those results came about on the fundamental level enables much more rigorous

and confident interpretations and can help someone come up with alternative hypotheses when data defies more common explanations. Furthermore, a greater understanding of geophysics should promote greater adoption of the methods as the archaeologist becomes more aware of the usefulness and drawbacks of each method. Therefore, an explanation of some physics is required. There are many helpful books on the subject of geophysics including ones written for archaeologists. Unfortunately, these can largely be divided into two camps: simple explanations that teach only the basics and complex, in depth explanations involving pages of mathematics. What is needed is an account of geophysical methods for the archaeologist who wishes to go beyond the basics but is lost in literature for the specialist - an intuitive explanation of *why* geophysics works by linking the physics with the application rather than just *that* it works. This is what is attempted here.

Geophysics is the study of the earth by exploiting differences in the physical properties of different geological materials. Every material has a particular electrical resistivity value and a particular magnetic susceptibility and various other properties inherent to that material. By remotely sensing these properties (without having to excavate), it is possible to understand the structure of geological strata beneath the earth. Since archaeology is typically found within (and is therefore presumed to be associated with) sedimentary layers, the application of geophysics to archaeology is self-evident. Some geophysical techniques can also directly detect the archaeology itself if it is made of certain materials (especially magnetometry).

Geophysical methods can be divided into two broad categories: methods which produce a plan view of a site and methods that produce a profile view of the subsurface. This is the first and primary practical distinction and the choice of method at a site will partially depend on whether the research questions relate to horizontal or vertical distinctions. Plan view methods include magnetometry, resistivity surveys and magnetic susceptibility. Profile methods include GPR and ERT. Aside from this, it is also important to know the kinds of materials being targeted by the research question as well as their approximate size and depth of burial so the most appropriate choice in method can be made.

3.1.1 Basics of Electricity

An electric current is defined as the transport of electrical charge. This charge is a property of certain subatomic particles (notably electrons and protons) and, therefore, any material may conduct electricity inasmuch as it allows for the movement of charged particles. Common electrical conductors include metals, whose structures allow electrons to flow relatively freely through a "sea" of electrons, and solutions containing charged ions which can, of course, move freely as they are not bound. Like charges repel while opposite charges attract so normally free charged particles are mixed evenly such that the total charge of any local region is zero. The presence of a sufficiently strong external charge changes this. Such a charge exerts an electric field which attracts oppositely charged particles and repels like charged particles. The resulting motion of charge is electric current.

Unlike magnetic fields, electric fields can be bipolar or unipolar meaning they may be the result of a positive and negative source working in tandem or just one of the two (fig. 3.1). A free charged particle in an electric field is said to have electric potential which is analogous to gravitational potential. The electric potential (E_p) is related to the strength of the electric field (E).

$$E = -\nabla E_p$$

Because it's only meaningful to talk about a difference in potential, we usually compare a single potential with an arbitrary zero reference point. Difference in electric potential is called voltage. As a free charge moves due to the force exerted by an electric field, it loses electric potential. The amount of potential lost as the charge moves from point A to point B is known as the voltage drop across that distance.

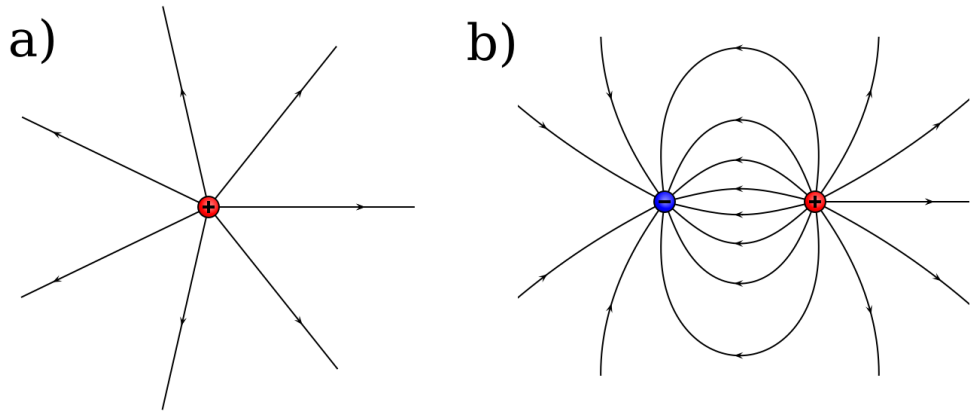

Figure 3.1: Diagram of electric field lines showing monopole (a) and dipole (b) arrangements. Diagram produced using VectorFieldPlot.

Moving from free charges in three dimensional space to series circuits, the concept is the same except the current flows as electrons through a wire. The battery, or other power source, provides a voltage drop across the entire length of the circuit. As current flows, the electrons lose exactly that much electric potential as they travel from the negative electrode of the battery to the positive. If one measures the voltage over only a part of the circuit, the measurement will be lower than for the entire circuit. Arbitrarily partitioning the circuit into non-overlapping sections will result in a series of voltages that add up to the total voltage of the circuit (fig. 3.2). Electric currents in a circuit obey what is known as Ohm's law which states that the voltage applied to a circuit (measured in volts) is equal to the current (in amperes) times the resistance (in ohms).

$$V = IR$$

The current is how much electric charge flows past a point per second and is the same at any point along the circuit. Electrical resistance is the property of an object or region

of physical matter that is how much it resists an electric current. Every object has such a value whether it be very low (a metal wire) or very high (a volume of air). In a circuit the voltage is determined by the power supply so raising the resistance will lower the current and *vice versa*. If the resistance of a component is changed, the total voltage across the circuit is unchanged but the gradient of electric potential drop across that component is changed. Ohm's law applies not just to the whole circuit but to any arbitrary portion of the circuit. Therefore, if a component with high resistance (called a resistor) is added at one location, the voltage (decrease in electric potential) across that component will be higher than the voltage across a component with low resistance. This is because the current must remain the same around the circuit. Intuitively, the drop in electric potential across the circuit is weighted towards areas of higher resistance.

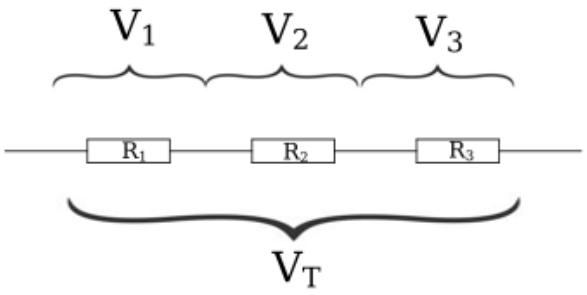

$$V_T = V_1 + V_2 + V_3$$
$$R_T = R_1 + R_2 + R_3$$

Figure 3.2: Diagram of a section of a series circuit. The resistances of and voltages across each component are added together to determine the total resistance and voltage drop. Current must be the same at all three components.

In a parallel circuit the voltage across all branches is the same but the current is divided according to the resistance of each branch. More current flows through branches with lower resistance (fig. 3.3). The resistances along a series circuit can be simply added together to obtain the total resistance. However, adding an alternative path in a parallel circuit serves to lower the total resistance even if the resistance along that particular path is high. The total resistance of a branched section is given as follows.

$$\frac{1}{R_T} = \frac{1}{R_1} + \frac{1}{R_2} + \frac{1}{R_3} + \cdots$$

A branched parallel section may be a single component in a larger series circuit.

Extending the concepts developed thus far to current flow in three dimensions requires different but related quantities to express what is happening. Ohm's law allows us to

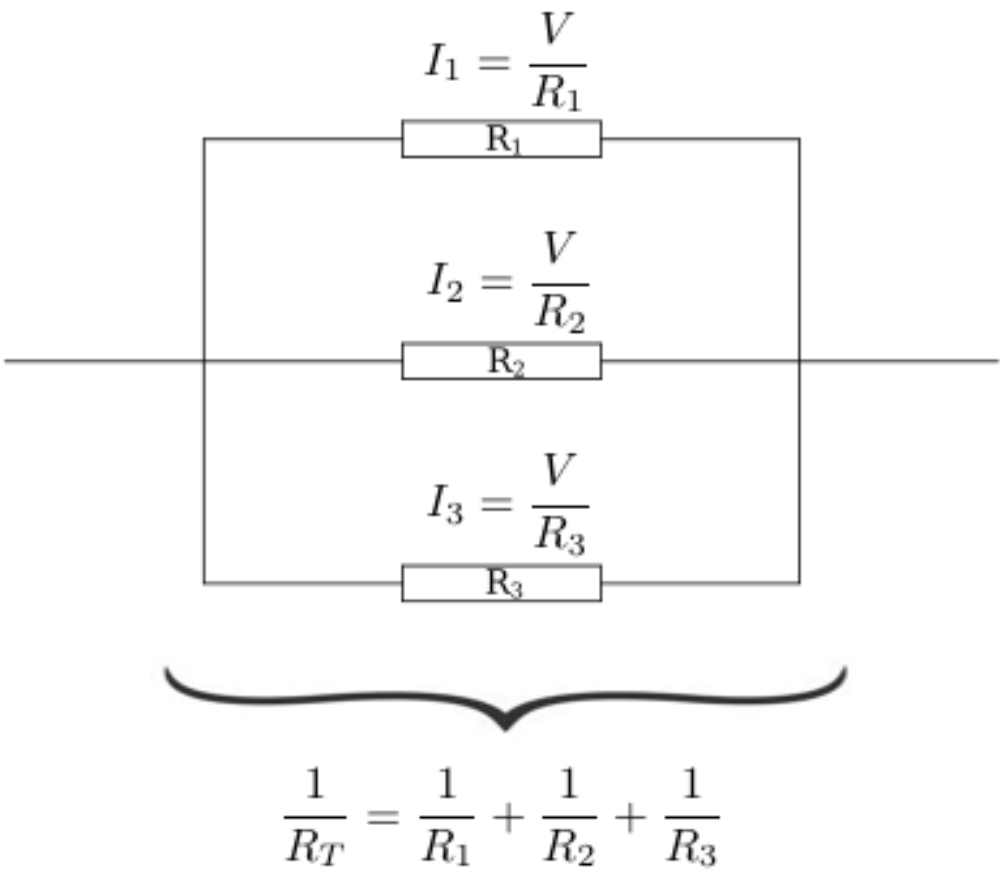

Figure 3.3: Diagram of a section of a parallel circuit. The total resistance of the section is *not* the sum of individual resistances. Voltage is equal across all three branches so the current differs according to the resistance of each branch.

easily calculate the resistance of an object given known or measured voltage and current. However, the resistance of an object is not just related to the material but also to its size and shape. The longer an object in the direction of current, the more it resists that current. The greater the cross-sectional area of an object, the less it resists the current. Resistance is related to geometry in the following way.

$$R = \rho \frac{L}{A}$$

The coefficient ρ (Greek letter rho) is the intrinsic property of a particular material called resistivity (measured in ohm-metres) that determines how much an object resists electricity independent of its geometry. The difference between resistance and resistivity can also be understood in this way: Resistance is an aggregate value that applies to an entire three dimensional volume while resistivity is the limit of that value as the volume contracts to a point. This distinction is important because it allows us to describe the electrical properties of the subsurface in terms of values at particular points and to therefore be able to

map this information (Grant and West 1965, p. 390). We are now able to rewrite Ohm's law as a vector equation where E is the (vector) electric field, ρ is the (scalar) resistivity, and j is the (vector) current density which is the amount of current passing through a unit area (fig. 3.4).

$$E = \rho j$$

What this equation says is that the current vector at any point points in the same direction as the electric field and that the strength of the current is in proportion to the strength of the electric field and inversely proportional to the resistivity at that point. We know by the first equation of this chapter that both of these quantities point in the opposite direction to the steepest gradient of electric potential. Therefore, we can easily describe the contour surfaces of equal potential. If we set the directional derivative of the electric potential with respect to some unit vector u, we get the following.

$$\nabla E_p \cdot u = 0$$

$$E \cdot u = 0$$

By the properties of the dot product, this means the direction of no change in potential is orthogonal to the electric field and thus to the direction of current. The contour surfaces are locally orthogonal to the direction of current everywhere (fig. 3.5). In the simplest case of a field emanating from a single point, the contour surfaces form concentric spheres around the charged point.

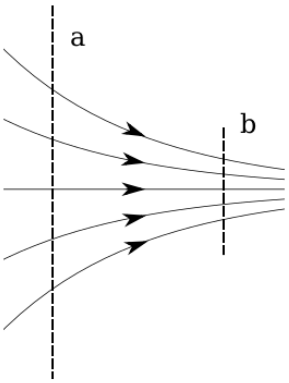

Figure 3.4: The arrows represent electric current. The density of current through (a) is less than the density of current through (b).

3.1.2 The Electrical Resistivity Tomography Survey

An electrical resistivity survey is a relatively simple affair. The measuring instrument itself usually comes contained in a box to which it is necessary to supply a power source. A line

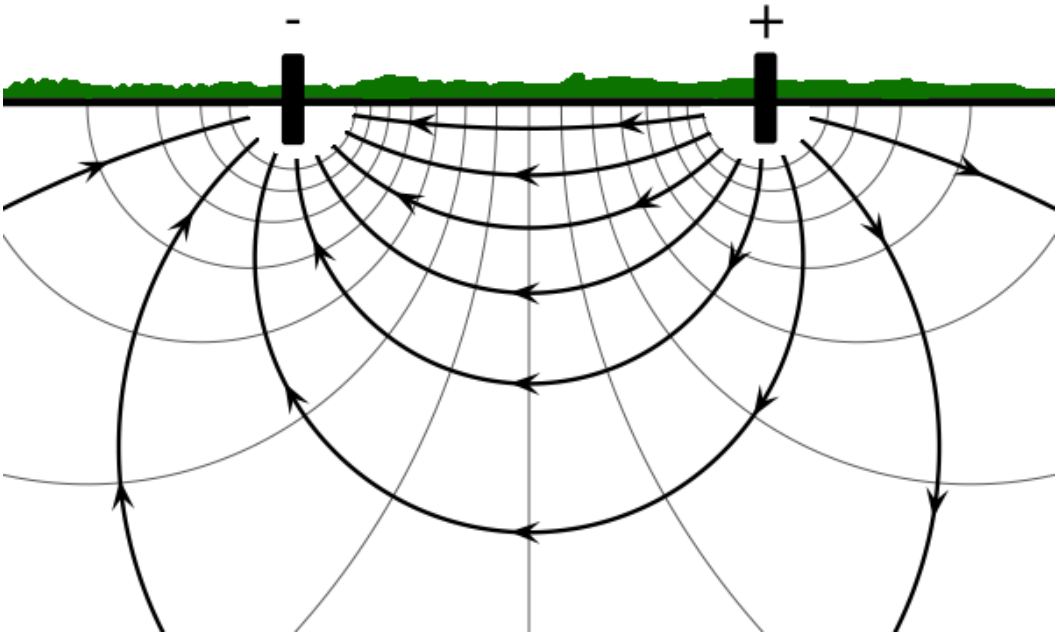

Figure 3.5: Diagram of the isopotential contours (light grey) and current field lines (black with arrows) resulting from a configuration of one positive electrode and one negative electrode placed into the ground. Note that the two are everywhere orthogonal. Diagram produced using VectorFieldPlot).

of special metal electrodes are hammered into the ground at equal spacing and are connected to the instrument with a cable that runs the entire length of the survey line (fig. 3.6). Usually it is required to pour salt water over the electrodes to reduce contact resistance. This is extra, unwanted resistance caused by a number of factors including poor interfacing between the metal and soil and corroded metal contacts. Scrubbing the contacts clean may also help the latter. Upon selecting the appropriate settings for the survey, the instrument will take many data points using different combinations of electrodes. ERT surveys are usually taken as 2D profiles which can be interpreted individually or combined in tight formation to create a pseudo-3D model. It is also possible to take fully 3D ERT surveys using a 2D array of surface electrodes.

While ERT specifically refers to the setup described above taking hundreds of measurements using dozens of electrodes in one straight line, a simpler-to-understand way of testing the resistivity of the ground is taking individual measurements as either a 1D sounding to probe depth or in a grid pattern on the surface of the ground to obtain a plan view of the site. These are called vertical and horizontal exploration respectively (Grant and West 1965, pp. 386–7). Each measurement is taken by first setting a number of electrodes into the ground (usually two current electrodes and two potential electrodes). The spatial configuration of these electrodes is called the array of which there are many types. A common example is the Wenner array which has four electrodes equally spaced apart in the order

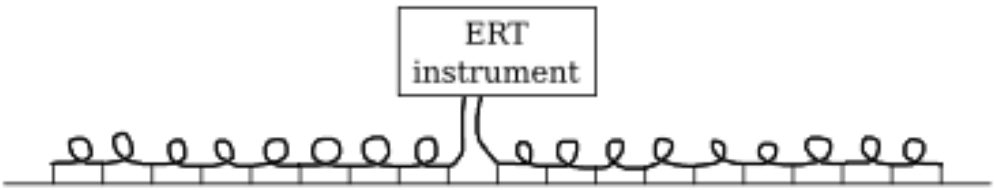

Figure 3.6: Diagram of an ERT setup. Each metal electrode in the ground is connected to the instrument by one or two long cables.

current, potential, potential, current (fig. 3.7). An electric current is passed through the ground via the current electrodes and the voltage is measured between the potential electrodes. At the same time the current is also measured which gives us, by Ohm's law, the resistance of a volume of earth between the potential electrodes. The resistance can be used to calculate a value called the apparent resistivity (ρ_a) which is assigned to a point in the ground using a geometric factor determined by the particular array used (Grant and West 1965, p. 388). Since the arrangement of current and potential electrodes is different for each array, it follows that a different part of the ground relative to the current electrodes is measured for each and hence it is necessary to make a correction to make them comparable. It is important to keep in mind that the apparent resistivity is not the true resistivity at any point but is the value it would take if the ground were completely homogeneous. In a real situation it represents an aggregate value for the surrounding earth (Schmidt 2013, pp. 50–1). The apparent resistivity is assigned to a single point beneath the ground which is considered to be the average or central point for that measurement. This point lies half way between the potential electrodes and at what is known as the depth of investigation. The depth of investigation is often given as either the depth of maximum sensitivity (the point that contributes most to the measurement) or as the depth of median sensitivity (the point at which the overlying and underlying regions of earth each contribute equally to the measurement) (Loke 2004, p. 25). In the ERT survey, many individual measurements are made with each producing an apparent resistivity at a particular depth and position along the line. This is known as a pseudosection and is used as the basis for the later processing stages.

The question of the depth that can be seen depends mainly on the spacing of electrodes (and therefore total length of the array) but also the type of array being used and the magnitude of contrast between resistivity in the ground (Loke 2004, pp. 25–7, Schmidt 2013, pp. 79–80). Of these the total length of the array is the most important since it can be chosen by the operator and has much greater effect than the type of array used. Depth is given as a ratio with the length of the array (depth:length). The theoretical median sensitivity value for the Wenner array is 0.173 while the values for the dipole-dipole array start at 0.139 and increase from there as the n factor increases (Edwards 1977, p. 1033).

A natural question that now arises is how can the potential electrodes, which are shal-

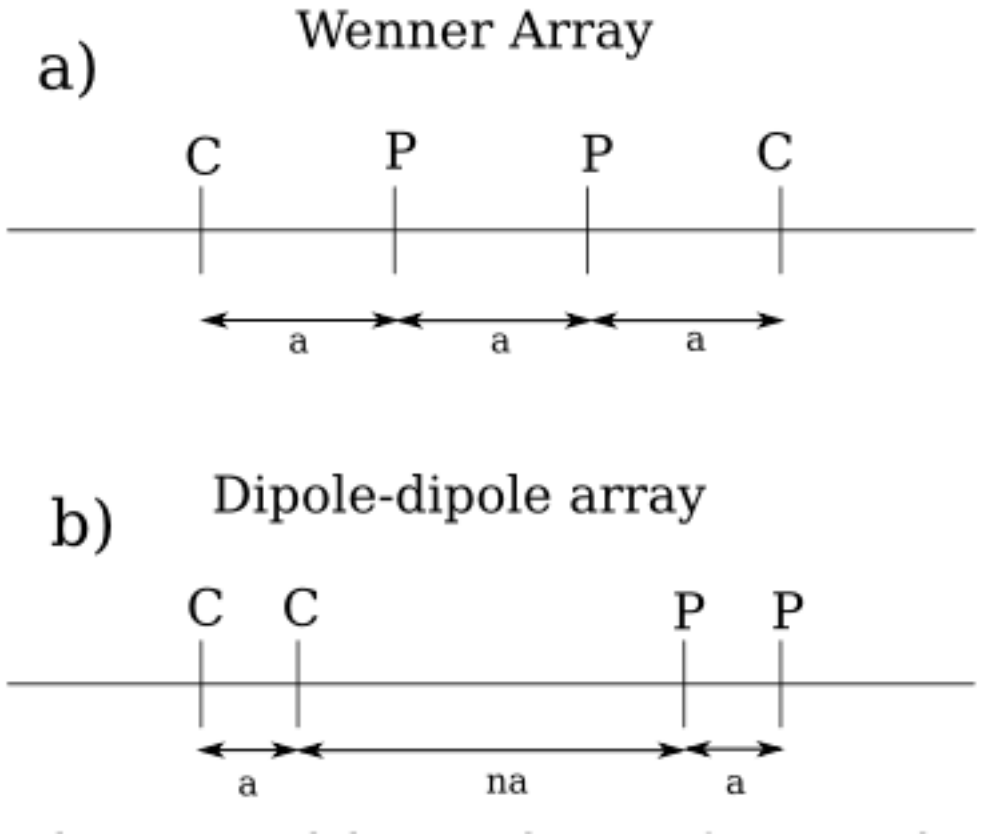

Figure 3.7: Diagram of the configuration of electrodes for the Wenner (a) and dipole-dipole arrays (b). a) All three intervals marked by a must be equal. b) The two intervals (a) between the pairs of current and potential electrodes must be equal distance. The interval in between those pairs of electrodes must be an integer multiple of a.

lowly hammered into the surface, provide any information about the state of the earth much deeper down? Since we are only able to take measurements of voltage across the surface, it would seem reasonable to suppose that only the resistivities of the shallow subsurface could be obtained. However, changes in resistivity at depth do affect the flow of current at the surface. Suppose there is an object at depth with a significantly different resistivity to its surrounding matrix. In the case the body is of a high resistivity so the current is forced to flow more around it than it otherwise would (the extreme case being a perfect insulator which would force all current to flow around it). In the case of a low resistivity object, the current flows more through the object. In this way, the current density at a particular point is related to the resistivity at that point. If the current is changed in one area, it has an outwardly radiating effect as the current in neighbouring regions redistributes itself to accommodate this new change. These distortions in the path of current also distort the contour lines of equal electric potential because they must always be oriented orthogonally to the direction of current. This creates an alteration in the gradient of electric potential across the surface from one current electrode to the other (see fig. 3.8). It is this alteration from what would be expected for a homogeneous ground that is detected

Array Type	Ratio of Median Depth to Total Length
Wenner	0.173
Dipole-dipole	
n=1	0.139
n=4	0.203
n=8	0.224

Table 3.1: Theoretical depths of investigation for Wenner and dipole-dipole arrays. Values taken from Edwards (1977).

with resistivity methods and allows for inferences about depth to be made from surface observations (Schmidt 2013, pp. 52–4). One of the assumptions then that is made in a survey is that the ground to either side is equivalent. That is that one side of the ERT line is not substantially different from the other. The same reason why it is possible to detect objects at depth also applies to laterally placed objects and, therefore, some care and attention should be paid to this fact when setting up a survey and when interpreting results.

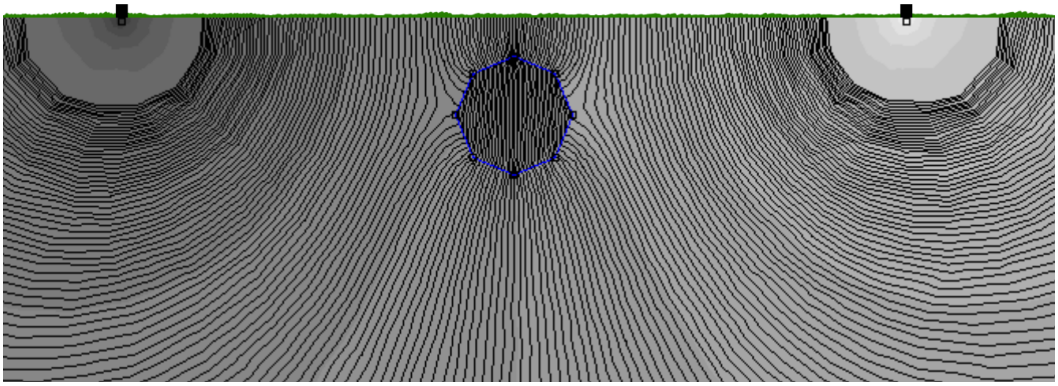

Figure 3.8: Diagram showing the isopotential contour lines distorting around a resistive object. This causes the gradient of electric potential drop (voltage) at the surface to be altered which is measured by the ERT instrument. Diagram produced using Finite Element Method Magnetics.

3.1.3 Inversion

Electrical resistivity tomography involves a difficult mathematical problem to overcome which is that the outcome (the measurements taken) is known but the inputs (the physical reality of the subsurface) are not. Given a particular section of earth where the resistivities are known at every point, the results of an ERT survey could be easily calculated without even taking it. This is known as the *forward problem*. Doing the reverse (which is what is attempted with ERT) is known as the *inverse problem* and is much more difficult. Unfortunately, insufficient information is obtained from an ERT survey for a unique solution

to the inverse problem meaning the inverse problem is what is known as *mathematically ill-posed* (Günther 2004, p. 14, Schmidt 2013, p. 50). In order to have enough information it would be necessary to take measurements across the entire boundary of a closed region of earth. This would require excavating the site which would defeat the purpose of doing a geophysical survey in the first place.

Originally, resistivity profiles were obtained by taking vertical (increasing electrode spacing over a central point) and horizontal (moving the four probe array laterally) surveys and combining the resulting apparent resistivities into 2D profiles. This was done as a pseudosection with points plotted at intersecting 45° angles from the midpoints of the two pairs of electrodes in the case of the dipole-dipole array (Hallof 1957, pp.25-6). This was the method used to plot combined surveys as a matter of convention although not without the understanding that the "depth" so achieved was not true depth. More accurate placement of points in a pseudosection was obtained by recognising that depth was largely a function of the length of the array and working out the ratios between length and depth for each array empirically (Edwards 1977). This modified pseudosection allowed relatively accurate estimates of depth to the top interface of interesting features. More recently numerical methods required to tackle this problem have since been developed which allow even more accurate reconstructions of resistivity profiles (Noel and Xu 1991, p. 95, Loke *et al*. 2013).

The inversion process first generates a mesh to divide the earth into discrete cells. Each of these cells is given a single value of resistivity. The values for the initial model are usually taken from the pseudosection of apparent resistivities. After this an iterative numerical method is applied to the model such as the Gauss-Newton method or another approach (Mufti 1976, Loke and Dahlin 2002, Günther 2004, pp. 8–14, Loke *et al*. 2013, p. 138). These methods parameterise the model as a vector **m**. This vector can be thought of as a collection of all the resistivities for each cell in the mesh for the current model. In each iteration of the inversion process the algorithm calculates the vector of the expected survey results if the model is true **f**(**m**) and compares them with the vector of actual measured results **y**. The discrepancy vector **g** = **y** - **f** is then how much the calculated results (according to the model) are different from the actual measurements. The Jacobian matrix of the discrepancy vector is used to estimate how much to alter the model for the next iteration in order to minimise the difference between the calculated model response and the actual survey results (Günther 2004, pp. 8–9, Loke 2004, p. 12). Schematically, the process looks like figure 3.9. This difference can be calculated using different norms (the length of a vector). The two common norms for resistivity inversion are the L^2 and L^1 norms. The L^2 norm is the intuitive, "normal" length which is calculated as follows.

$$\|\mathbf{g}\|^2 = \sum_i {g_i}^2$$

Using this norm penalises large errors meaning models with moderate overall errors are preferred over models with a few large errors. The L^1 norm takes this form.

$$\|\mathbf{g}\| = \sum_i |g_i|$$

Using the L^1 norm only minimises the absolute error which means that the algorithm will prefer a model with a lower overall error regardless of how unevenly that error is distributed. The L^1 norm is a better choice if there is an extreme range in resistivity outliers or if the desired model is thought to have bodies of internally consistent resistivity with sharp boundaries. This will create a model that is often described as "blocky" but with the potential for decreased resolution (Günther 2004, p. 9, Loke 2004, pp. 13–4, Günther and Rücker 2019, pp. 10–1). Due to the non-uniqueness of the solution, it is necessary to apply additional constraints called regularisation. Regularisation is used to find the solution to the inversion problem that most exemplifies a particular property. This can be done on each iteration to dampen the model update vector or it can be applied to the model itself to constrain its general character by keeping it in the neighbourhood of an *a priori* model (Günther 2004, pp. 15–6). One common form of regularisation is called Occam's inversion which attempts to smooth the model (Constable *et al*. 1987). The rationale behind this approach is that by removing any features in the model that aren't necessary to explain the data, spurious features may be minimised and we can be more confident that every feature corresponds to something real in the ground (Constable *et al*. 1987, p. 290). The obvious drawback to this is that it is easy to erase real features so smoothing should be applied judiciously. A regularising parameter is used to determine how much importance is to be given to the form of regularisation. The choice of parameter is a trade off between a noisy model that better fits the data and a smooth model with worse fit (Rücker 2010, p. 66). A rigorous way of determining this is by means of an L-curve plotting data fit against model roughness for different values of the regularising parameter. The optimum value is taken to be the one at maximum curvature of the plot (Günther *et al*. 2006, p. 509).

As the inversion process is not "calculating" the answer in the normal sense (analytic solution) but converging to the answer in a series of steps (numerical solution), the program needs to be given a condition to know when to stop. The condition should be chosen so that the results are "close enough." As the inversion process continues, the difference between one model and the next in the series becomes smaller but the processing time is the same. Therefore, it is expedient to end the process when the change in model is too small to be worth the time to compute. The convergence criterion used by the inversion program usually takes the form of estimating these diminishing returns of minimising the objective function which is the sum of the L^p norms of the difference between the data (d) and model response (f) divided by the voltage error (ε) (Günther *et al*. 2006, p. 508).

$$\Phi = \sum_i^N \left\| \frac{d_i - f_i}{\varepsilon_i} \right\|^p$$

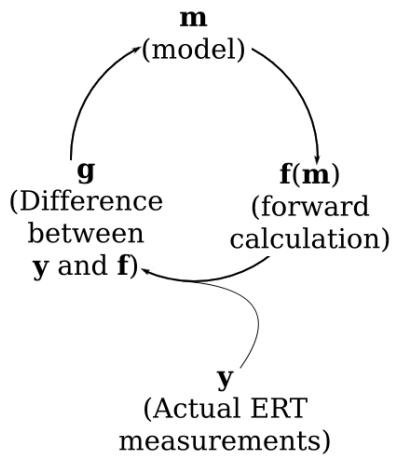

Figure 3.9: Schematic flowchart of the iterative inversion process.

One way is to calculate the change in Φ between each iteration and terminate the inversion when that change becomes suitably small. Another way is to calculate how well the model response fits within the assumed error of the data and terminate when χ^2 ¡ 1 (Günther and Rücker 2019, p. 8).

$$\chi^2 = \frac{\Phi}{N}$$

Essentially what this criterion says is that on average the difference between the model response and the data should be less than the error term associated with the voltage measurement. This makes sense because there is no point in continuing to refine the model beyond the accuracy of the measured data. Setting a maximum limit for the root mean square error of the model, or else a threshold on the change in such between iterations, is another way of determining when to end inversion (Geotomo Software 2019, p. 67).

$$rms = \sqrt{d_1 - f_i}$$

3.1.4 The Use of Electrical Resistivity Tomography in Archaeology

Resistivity surveys have been valued for their ability to detect a variety of archaeological features including ditches, pits, walls, foundations and roads (Atkinson 1952, pp. 68–9, Clark 1986, p. 1404). More specifically it is primarily changes in water content that is detectable (Grant and West 1965, p. 393). This is because it is the charged ions in water that carry electric current in the ground. Walls and other less porous features hold less water and so usually give a higher resistivity reading. Disturbed soil is generally less tightly packed than undisturbed soil and so can hold more water and sometimes give a lower resistivity reading than the surrounding soil (Clark 1996, p. 37). It is known experimentally that non-conductive (especially not containing clay), isotropic clastic rocks and sediments that, when fully saturated, their conductivity follows Archie's law where

ϱ_t is the bulk resistivity of the sample, ϱ_w is the resistivity of the fluid (water and dissolved ions), $\vartheta$is the porosity of the rock or sediment, and a and m are experimentally derived parameters (Keller 1971, p. 35).

$$\rho_t = a\rho_w\theta^{-m}$$

For unsaturated rocks and sediments in the vadose zone where the grains still have a continuous coating of water, another law applies.

$$\frac{\rho_t}{\rho_{100}} = S_w^{-n}$$

Where S_w is the fraction of pore space filled with water and ϱ_{100} is the bulk resistivity of the rock or sediment when fully saturated. This can be combined with Archie's law and simplified using typical values of 2 for m and n to the following equation (Keller 1971, pp. 39–40).

$$\rho_t = \frac{\rho_w}{W^2}$$

Where W is the water content per volume of rock or sediment. This is only a rough guide but it shows the importance of the water content in non-conductive sediments as the resistivity is proportional to the inverse square of the water content. The actual resistivity value of a sediment may vary significantly from what is predicted by this relationship depending on its mineralogy and grain size and packing.

The first resistivity survey used in archaeology involved taking a collection of resistivity measurements at a Neolithic site at Dorchester-on-Thames in 1946 where three circular ditches and a number of pits were able to be located prior to the excavation (Atkinson 1952, pp. 59, 68, Clark 1996, p. 12). In this case, the technique used was not ERT but a horizontal resistivity survey using a four-pronged probe. This creates a plan view of the site's electrical resistance at constant depth. Another related technique (iso-potential survey) was employed in 1938 at Williamsburg in the USA but this did not involve the calculation of resistance or resistivity (Bevan 2000). It soon became apparent from early field trials that the relative moisture content (and thus resistivity) of a soil depends not only on its porosity but also on the time of year due to differing rainfall between seasons. A porous ditch may hold more water after rain but it also loses water more easily to evaporation during a dry season. Therefore, the same ditch may give a high or low reading depending on recent weather (Clark 1975, pp. 300–2, Schmidt 2013, pp. 123–5). Ditches and other features containing disturbed sediment remain a primary target for investigation by resistivity. Three dimensional and pseudo-3D ERT surveys have been used to investigate the depth and structure of ditches (Nowaczinski *et al*. 2012) as well as characterise pits according to their morphology (Nowaczinski *et al*. 2015). ERT is especially good for the detection of air-filled voids such as tombs (Tonkov and Loke 2006) and in karst landscapes (Bermejo *et al*. 2017) because of the contrast between the extremely high resistivity of air and the host matrix of sediment and has also been used to detect archaeological voids prior to construction projects (Ungureanu *et al*. 2017).

The detection of stone walls is of particular interest to archaeologists working in ancient settlement contexts. ERT is well suited to the detection of stone because of its much lower moisture content compared to sediment and has been used to delineate buried walls at a number of sites (Simyrdanis *et al*. 2016, Al-Saadi *et al*. 2018, De Giorgi and Leucci 2018, Moník *et al*. 2018). At all of these sites, ERT was collected as multiple overlapping lines. The data was interpolated into a pseudo-3D model and depth slices were taken to show a plan view of the sites at multiple depths. This approach has the advantage of familiarity to those accustomed to plan view surveys and it is appropriate in the case of target features with high horizontality and low verticality such as walls. However, it also has a disadvantage in that the targeted feature may not be horizontal and may appear across different depth levels. It also requires that the same feature have close to the same resistivity throughout the site. This may not always be the case due to variance in groundwater and structural homogeneity (bigger gaps between stones). Finally, this approach is best done with small line spacings (comparable to the electrode spacings) to maintain an appropriate resolution for the target which would be time consuming to cover a large area.

One very important aspect of an archaeological site is the sedimentary depositional environment it was formed in as well as the stratigraphy of the site itself and the conjunction of its artificial and natural deposits. ERT can be used to study this structure and provide a broader stratigraphic context context to a site. This relies on different stratigraphic units having different electrical resistance which usually means differing porosities for ion-bearing water to percolate through although the clay content will also have a marked effect. ERT has been used to investigate archaeological occupation layers (Berge and Drahor 2011, Al-Khersan *et al*. 2016) and built earthen constructions such as ramparts (Grützner *et al*. 2012, Klanica *et al*. 2022), In these cases, the focus is still very much on features and strata that were directly or indirectly derived from human activity. However, the focus can also be placed primarily on the environmental context by reconstructing ancient landscapes in which human occupation or activity took place (Similox-Tohon *et al*. 2004, Papadopoulos *et al*. 2014, De Giorgi and Leucci 2018, Kowlessar *et al*. 2023) and delimiting between natural and artificial layers (Nowaczinski *et al*. 2012, Papadopoulos *et al*. 2014, Gaber *et al*. 2021). Here the archaeological remains are situated in their broader spatial context and both they and natural features are treated as a unified complex to be investigated. Being able to reconstruct past landscapes is a critical first step for understanding how people used and interacted with them. ERT tends to perform well for these larger scale stratigraphic investigations as its limitations with resolution become less of a problem and high depth penetration becomes desirable. The boundary between unconsolidated sediment and rock also shows up well which improves its usefulness.

A very similar approach to landscape reconstruction is to reconstruct the entire stratigraphic sequence by mapping the depths and thicknesses of strata across a site. This is often called deposit modelling (Carey *et al*. 2018). Due to the importance of this approach to this study, it will be dealt with separately (Section 3.1.8). Both landscape reconstruction and stratigraphic modelling can be performed at almost any scale from large valleys

and basins to individual stream channels. The choice of scale is dependent largely on the archaeological project questions; however, a larger scale survey will mean lower density of information (resolution) for the same amount of time. In that sense it shares the same limitations in scalability as archaeological pedestrian surveys.

3.1.5 Wave Mechanics and Ground-Penetrating Radar

Ground penetrating radar (GPR) is a method based on the reflection of electromagnetic waves. It works by transmitting a series of radar pulses into the ground and listening for any incoming waves. As the pulses reach boundaries within the ground, some energy is reflected back to the receiver. The resulting reflections make up a waveform. As the GPR unit receives this waveform, it measures how long it has been since the initial pulse was transmitted in two-way travel time and also the amplitude of the reflection. Many recordings are made as the GPR is moved along the surface so that a profile image can be produced.

Radar uses a specific band of wavelengths (λ) in the electromagnetic (EM) spectrum called radio waves. Specifically, radio wavelengths lie between 1 mm and 100 km. For GPR purposes the radio wave is usually characterised by its frequency rather than its wavelength. These are related according to this formula where v is the velocity of the wave.

$$f = \frac{v}{\lambda}$$

GPR usually only operates over a portion of the radio spectrum at frequencies from 10 MHz to 1.5 GHz (Conyers 2013, p. 26). This is because of the competing needs for depth and resolution.

An EM wave travels through a medium at a velocity that is dependent on the properties of the material. The ratio of c (the speed of light in a vacuum) to v (the velocity in a particular medium) is called the refractive index and denoted by n. When a wave hits a boundary between two values of n, some of the energy is transmitted through the boundary and some is reflected back (fig. 3.10). When the angle of incidence is 0° (not always true for GPR), the amplitude reflected back is proportional to the reflectance R which is easily simplified from Fresnel's equations (Witten 2006, p. 216).

$$R = \frac{n_2 - n_1}{n_2 + n_1}$$

The amplitude transmitted is proportional to $1–R$. Therefore, changes in the refractive index of the sediments beneath the ground will result in reflections that can be recorded. Moreover, the magnitude of the amplitude received back is dependent on the difference between the two indices and can thus can qualitatively help narrow down of the kinds of materials being detected.

As stated, the refractive index of a medium is related to the velocity of an EM wave passing

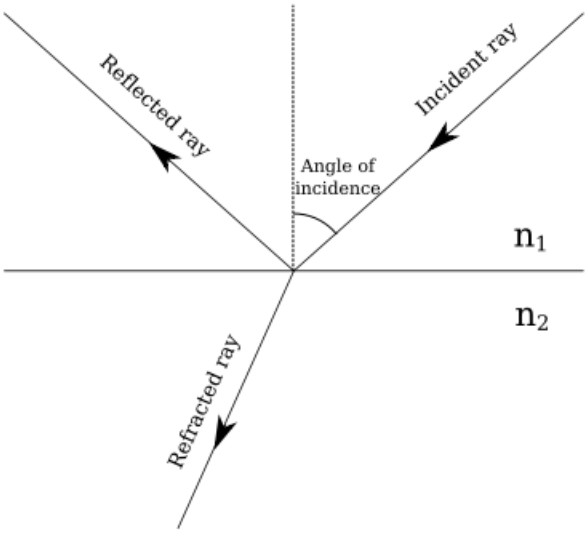

Figure 3.10: Diagram showing the refraction and reflection of a wave as it hits a boundary between two materials.

through it. Every material has a relative dielectric permittivity property which is roughly speaking a measure of how well it can electrically polarise in response to an electromagnetic pulse (Cassidy 2009a, p. 45). The velocity of an EM wave is dependent on a number of quantities including the relative dielectric permittivity (ε_r), relative magnetic permeability (μ_r) and a term of $(\sigma/2\pi f\varepsilon)^2$ (Cassidy 2009a, p. 58). In the case of GPR where the frequencies are in hundreds of millions of Hertz, the squared term effectively disappears and the velocity can be approximated in a simple form (Annan 2005, pp. 370–1).

$$v \approx \frac{c}{\sqrt{\varepsilon_r \mu_r}}$$

In a non-magnetic material, $\mu_r = 1$ and so the velocity is only dependent on the inverse square root of the relative dielectric permittivity. This means that the refractive indices above can be rewritten as $\sqrt{\varepsilon_r \mu_r}$. The usefulness of this result lies in its explanation that what causes radar reflections are differences between two materials in their polarisability in response to the electric field of an EM wave and also its magnetic permeability (which is related to susceptibility).

Relative dielectric permittivity is the ratio between the dielectric permittivities of the material to that of a vacuum. For radar it ranges between values of 1 for air and 80 for water. Dry geological materials have generally quite low permittivities (table 3.2) and so the predominant factor causing reflections in GPR is the amount of water contained withing a geological unit (Davis and Annan 1989, p. 536, Everett 2013, p. 242). The reason behind differences in permittivity is related to how EM waves propagate. EM waves are composed of an oscillating electric field and an orthogonal oscillating magnetic field. When the wave passes through a material, the electric field (E) causes positive and negative charges

Material	RDP
Air	1
Ice	3-4
Dry sand	3-5
Granite	4-6
Limestone	4-8
Wet sand	20-30
Clay	5-40
Water	80

Table 3.2: Relative dielectric permittivities for some common materials. Taken from Davis and Annan (1989).

in the material to separate slightly resulting in some polarisation (fig. 3.11). Excess electric potential energy is stored in the material at this point if there is a structure to the material that opposes this separation (for example an ionic lattice or molecular structure as opposed to free particles). The charges move back to their normal state which releases the energy and propagates the wave. However, this process is slower than the speed of light in a vacuum and so the velocity of the EM wave is slowed. The dielectric permittivity is related to the density of charge separation as $D = \varepsilon E$ (Cassidy 2009a, pp. 45–6). There are a range of different mechanisms for this process which involve different types of bound and free charges. These include the dipoles of polar molecules, bonded atoms or ions and electron clouds. Each of these mechanisms increases the dielectric permittivity of a material but each also has a maximum frequency to occur. It takes time for the charges to be polarised and then relaxed so as the frequency of the EM wave increases, the charges spend more time in motion. After a certain frequency, the charges can no longer keep up with the alternating electric field and so that mechanism no longer occurs. GPR uses the range of frequencies for which the dominant mechanism is the polarisation and relaxation of molecular dipoles. By far the most common and important polar molecule is water (fig. 3.12). In its absence, the dielectric permittivity is largely determined by atomic and electronic polarisation which gives rise to much smaller values for permittivity. Therefore, water plays the dominant role in the determination of dielectric permittivity at GPR frequencies (Cassidy 2009a, pp. 47–9).

A secondary effect on the velocity of an EM wave and its reflectance is due to the relative magnetic permeability (μ_r) of the medium. Relative magnetic permeability is related to volume specific magnetic susceptibility by $\kappa = \mu_r - 1$ (Chikazumi 1964, p. 6). The majority of geological materials have a magnetic susceptibility less than $\kappa = 10^{-2}$ and so a relative permeability of very close to $\mu_r = 1$ (Hanson *et al*. 2005, p. 157). Therefore, this effect can usually be discounted in GPR surveys except in the case of highly magnetic objects such as iron. These are very strong reflectors of EM waves and will obscure anything else beneath them by a stack of high amplitude reflections (Cassidy 2009a, pp. 55–6, Conyers

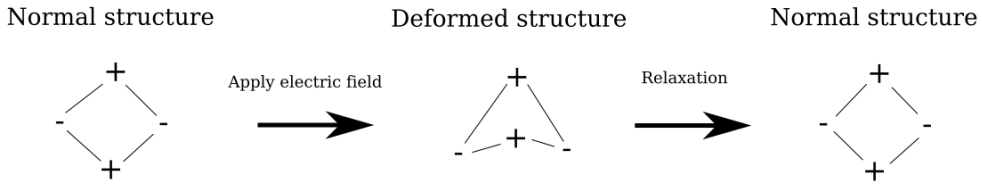

Figure 3.11: Diagram showing the separation of charge in a bound structure as it deforms under an electric field and then relaxes.

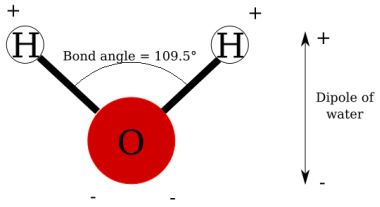

Figure 3.12: The structure of the water molecule. Its bent shape means there is a net separation (dipole) between the positively charged hydrogen atoms and negatively charged oxygen atom. Under an electric field, these dipoles with align to the direction of field.

2013, p. 57). This potential interference can range from irrelevant to highly troublesome depending on the nature of the site.

The situation so far described shows how radio waves are able to propagate in the ground and reflect off boundaries but no physical interaction can occur without some kind of energy loss. This loss is called attenuation. Ground penetrating radar is constrained by two different kinds of attenuation. The first is related to the polarisation and relaxation of electrical charge as the wave propagates. Every time this happens there is an associated loss of energy as heat due to the motion of particles. The higher the GPR frequency the more time these particles are in kept in motion and the more energy is lost through heat. This results in a spike in energy attenuation at frequencies higher than a few gigahertz (Annan 2005, p. 369, Cassidy 2009a, pp. 47–8). GPR antennas do not generally emit such high frequencies but the use of a higher frequency used will still increase how quickly energy is lost and reduce the depth reached. The second kind of attenuation caused by high conductivity is of serious practical concern. The wave propagation mechanism relies on the storage and subsequent release of energy under an alternating electric field. It is important that the separation of positive and negative charges be relaxed which generally happens as the system restores itself. However, if there are free charged particle in the medium (for example ions in solution), these are separated due to the electric field and there is no opposing, restorative force from this to propagate the electromagnetic wave as there is with the separation of bound charges. The charges are simply conducted away with the energy dispersing as heat. This causes a diminishment in the electric field very quickly and it is

consequently well known that GPR has poor depth penetration in conductive sediments (Cassidy 2009a, pp. 54–5, Conyers 2013, p. 53).

Two reflection events will only be distinguishable if they are separated by enough time that they do not significantly overlap. The required separation depends on the frequency and bandwidth of the antenna. Higher values of both increase resolution so there is a trade off between resolution and depth (Davis and Annan 1989, pp. 539–40). In the case of a thinly layered ground, the successive reflections might be so frequent that destructive interference results in the elimination or muting of reflections. Sometimes only the first layer interface may be visible (Conyers 2013, pp. 67–8).

3.1.6 Ground-Penetrating Radar Processing

In a GPR survey, pulses are transmitted and reflections are received as the instrument is rolled or dragged over the ground. Each time window, over which reflections are recorded, forms a trace which is a reflection waveform. Often multiple measurements are taken in the same location with the incoming waveform being sampled at different times. In this way, a full trace is built up. This is done to obtain a higher data density than would otherwise be possible (Annan 2005, p. 388). Many traces are collected at a fixed interval, either by time or by distance, which builds up a two dimensional profile of results. A raw GPR profile is scarcely interpretable except where the targeted features are very reflective and shallow. A range of processing filters are necessary in order to bring out the information within. However, it is not wise to unthinkingly apply a generalised list of processing steps to every set of GPR data. Processing steps should be applied with a reason in mind and with the understanding that the raw data is being modified in some way (Cassidy 2009b, pp. 141–2, Conyers 2013, p. 130). Therefore, an understanding of what each type of processing does is in order.

Ground penetrating radar works by sending out EM pulses using a transmitting antenna and then recording incoming pulses over a set time window using a receiving antenna. So that no potential information is lost, the receiving antenna begins listening slightly before any pulses are transmitted. This means that every recorded reflection is slightly delayed and the traces must be corrected. This is done with a time zero correction which subtracts a certain amount of time across the entire profile. Usually this is done so that the direct wave (the pulse transmitted through the air directly from transmitter to receiver) is at the top of the profile (Cassidy 2009b, p. 150, Everett 2013, p. 253). There are several different points within the direct wave that can be chosen. Typical choices are somewhere between the first negative peak and the first positive peak (which is easy to distinguish). It has been suggested that an earlier point around the negative peak of point of zero amplitude between them is better for making depth determinations (Yelf and Yelf 2004).

In the received GPR waveform there will be long term trends in the baseline of the amplitude. This is due to low frequency emissions called wow from the antenna. A de-wow

filter reduces the base amplitude to zero so that the waveform is consistent throughout the trace (Cassidy 2009b, p. 150, Everett 2013, pp. 253–4).

Because of the attenuation that is present in all media, the received signal is considerably damped over the course of the receiving time window. Therefore, it is the case that later reflections are minuscule in amplitude compared to earlier reflections (but importantly still present in the raw data). For the default colour scale (or however the amplitude is represented) of the viewing software this will usually make these reflections indiscernible. A constant scaling factor applied to the amplitude of every trace would make later reflections visible but at the cost of excessive contrast in the earlier reflections. To achieve a consistent level of contrast between positive and negative peaks throughout the profile, a gain function is applied to every trace. This increases the amplitude of specific regions along the trace in a way that is dependant on the time axis. Thus later reflections can be increased more than earlier reflections (Goodman and Piro 2013, pp. 37–40). The gain function can be adjusted to match how quickly the signal attenuates in a particular ground. Gain can be applied using an automatic gain function that adjusts each time window according to its mean amplitude. Alternatively, the gain function can be set manually using a class of function (for example exponential) and adjusting the parameters until the user is satisfied (Cassidy 2009b, p. 162).

Antennas for GPR are specified by a particular frequency but in actuality they transmit across a broad range of frequencies. The listed frequency is called the central frequency of the antenna (Conyers 2013, pp. 42–3). This can lead to low and high frequency noise cluttering the image. Low frequency noise is characterised by long term trends in the amplitude while high frequency noise results in erratic "static" obscuring more important details. Unwanted frequencies can be removed from the trace waveforms through a bandpass filter. This shifts the waveform into the frequency domain using a Fourier transform and removes all frequencies except those in a specified "pass" band before shifting back to the time domain (Goodman and Piro 2013, p. 40). One common type of bandpass filter is the Butterworth filter which preserves relative amplitudes between frequencies. The downside is the potential to introduce artificial ringing responses in the data which must be taken into account during interpretation (Cassidy 2009b, p. 155).

When the receiving antenna of the GPR instrument records incoming EM pulses, it has no way of distinguishing between actual reflections from the transmitted pulse and outside waves that did not originate from the instrument. Furthermore, there will always be ringing from the antenna as it transmits the pulse because of the limitations of antenna design (Conyers 2013, p. 43). Both of these sources of systematic noise produce horizontal bands in the reflection profile which can be removed using a background removal process. This step takes the average of all the traces along a specified distance and subtracts that average from each relevant trace leaving only the deviation from the background average (Goodman and Piro 2013, pp. 46–8). Since the process is applied to a specified horizontal distance, the processor can determine how aggressive the filter is. A smaller distance re-

sults in a more aggressive filter since a feature needs to be constant over a smaller distance to be removed. To understand this, consider the case where background removal is applied to each individual trace. The average of one thing is the thing itself and so applying background removal in this way would remove all of the data. One should be very careful when selecting this parameter since it is possible for reflections from flat, horizontal layers to be removed accidentally (Goodman and Piro 2013, p. 47).

In order to make good use of GPR in archaeology, it is necessary to think about what kinds of objects and features at a particular site will reflect radar and in what kinds of patterns these reflections will appear. There are two main types: planar reflections and hyperbolic reflections. Planar reflections occur as waves bounce off horizontal boundaries in the ground. They appear as continuous and relatively smooth reflections in the GPR profile (Conyers 2013, p. 59). Hyperbolae appear as discrete reflections in the shape of an upside down "U" or "V." They indicate the presence of a fairly small and round feature. Hyperbolae are formed because radio waves are not only transmitted straight down but also outwards in a conical shape. If an object is relatively small and roundish, it will be able to reflect waves back at the GPR instrument when it is anywhere in the cone. However, the instrument has no way of knowing which direction an incoming pulse came from and records everything as being directly beneath. Because it takes longer for a wave to reflect off such an object as the GPR moves laterally away from it, the apparent reflections become deeper also (fig. 3.13) (Conyers 2013, pp. 59–60). If the object is given the coordinates (0, -d), a little trigonometry shows that the resulting reflection is given by this equation which is a form of the general hyperbola.

$$h(x) = -\sqrt{x^2 + d^2}$$

The deeper the object is, the less curvature the hyperbola has. This can be very useful in interpreting GPR since they can be used to estimate the velocity of the radio wave through the ground and hence convert the two way time axis to a proper depth axis (Conyers 2013, pp. 125–7).

3.1.7 The Use of Ground-Penetrating Radar in Archaeology

Ground penetrating radar was first used for archaeology during the 1970s with a slew of successes but saw limited adoption in places such as Britain due to the sodden, clay soils limiting the penetration of radio waves (Clark 1996, p. 118, Conyers 2013, pp. 19–20). Many GPR surveys in archaeology were interpreted under a scheme of anomalous reflections against a blank matrix. This is to say that all reflections must be (archaeologically) interesting. The inevitable disappointment that befell those with this kind of thinking led to GPR being seen as unreliable (Conyers 2013, p. 20). Of course GPR will pick up any subsurface heterogeneity, whether geological or anthropological in origin, including features that are irrelevant to current research questions. More important to understand is that

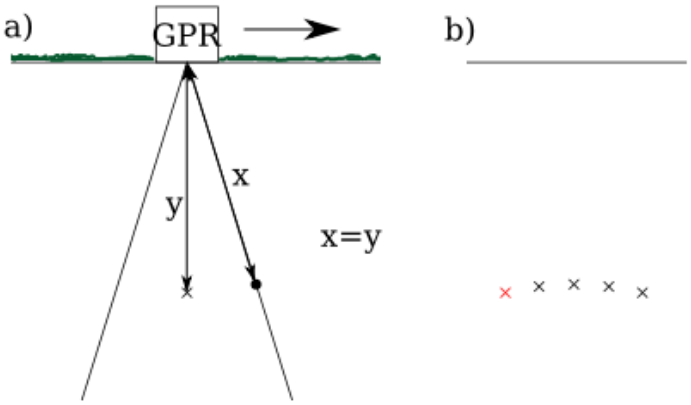

Figure 3.13: How hyperbolae are formed. a) The round object to the right side of the radar cone is plotted on the GPR profile as if it were located at the x directly beneath. Two-way times x and y are equal. b) Hypothetical GPR profile showing five points along the hyperbola. The measurement from (a) is highlighted in red.

sought-after archaeological features may not show up at all if their physical properties do not significantly differ from the surrounding sediments. Caution is justified in making any interpretation based on the absence of reflections.

The use of GPR in archaeology falls into two broad camps. The first is to use GPR to identify and investigate strictly archaeological features. Usually these are architectural remains such as buildings floors and walls (Imai *et al*. 1987, Urban *et al*. 2016, Correia 2019), monumental town constructions (Grützner *et al*. 2012, Ristić *et al*. 2020) and stone tombs (Orlando 2013). Depending on the construction and material of these remains, very clear and interpretable images can be produced. It is common in GPR surveys to collate a grid of profiles into a rectangular prism and then slice it horizontally to produced plan view maps of different depths. This is convenient for the presentation of spatial information but it has the drawback of obscuring vertical relations between complex objects buried in the ground (Kelly *et al*. 2021, p. 6).

The second main use of GPR is to investigate the sediments within which the archaeological remains sit. The study of the sediments holding archaeological objects is as important as the study of the objects themselves and can reveal a lot about the formation and modification of a site. GPR has been used, among other things, to identify human modifications of the landscape such as trenches (Al-Khersan *et al*. 2016) as well as the structure of sites and the topography of ancient land surfaces (Corradini *et al*. 2020). The investigation of stratigraphy in rock shelters (Miller *et al*. 2016, Papadimitrios *et al*. 2019, Armstrong *et al*. 2021) is a key use of the technique as research questions typically revolve around mapping the depth to bedrock which GPR is able to easily accomplish. GPR also has an advantage over some other geophysical techniques (such as ERT and seismic) in a cramped cave environment since the transmitted wave is mostly sent straight down and up. In contrast to

ERT where depth is achieved through a space-consuming row of electrodes, GPR is able to achieve its maximum depth right up to the cave wall. One other very important use of GPR is the detection of unmarked graves (Bevan 1991, Moffat 2015, Berezowski *et al*. 2021). The primary way graves can be detected with GPR is by looking for breaks in the stratigraphy of an appropriate size and shape (Moffat 2015, p. 47). These can be mapped using GIS and classified as probable or possible graves according to how closely the features match the expected length, width and depth for a grave of the target time period and culture (Moffat *et al*. 2020). It is also sometimes possible to detect certain objects that might be associated with the burials such as coffins if the contrast between dielectric permittivity is high enough (especially in the case of large metal fittings). This can be used in conjunction with the stratigraphic approach to increase the confidence of interpretation (King *et al*. 1993, Polymenakos 2019).

3.1.8 Stratigraphic Modelling

Given the integral role the use of geophysics (in particular ERT and GPR) has in modelling stratigraphy in this study, it would be beneficial to take a very close look at similar studies in the literature. These have been limited to those involving the use of ERT or GPR and an emphasis has been placed on the detection of palaeosols with GPR. Stratigraphic modelling has been reviewed recently by Carey *et al*. (2018) who define its aims as "to characterize subsurface sediment stratigraphy to understand geomorphological landscape evolution and to elucidate archaeological sites and their records" and to allow "an inference to be made about archaeological potential" (Carey *et al*. 2018, p. 496). Both GPR (Bristow and Jol 2003) and ERT (Smith and Sjogren 2006, Crook *et al*. 2008, Bellmunt *et al*. 2022) have been extensively used for similar stratigraphic modelling in geological applications as well.

Carey *et al*. (2006) used GPR to investigate the alluvial deposits in Trent Valley in England. The aim was to identify areas of high archaeological potential for future research. The GPR profiles were able to distinguish between major strata of gravel terraces and alluvium, minor bedding within the alluvium and a palaeochannel. Importantly, they were able to show that the difference in surface archaeology distribution between the terraces may be misleading and that the apparently less occupied one had far deeper alluvial deposits which may hide archaeological material. A major problem they faced using GPR was the attenuation in the clay-filled palaeochannel. A follow up study (Howard *et al*. 2008) was able to use ERT to reveal some internal structure in the channel. Specifically, the ERT was able to reveal the base of the palaeochannel but also had difficulty distinguishing the strata known through coring.

Another study (Chapman *et al*. 2009) was aimed at mapping the Bronze and Iron Age palaeosols in Scottish aeolian coastal dunes. The strong weather in the region threatens to expose and destroy the archaeological remains there so GPR was used to identify areas of highest risk (meaning areas with the thinnest dune overburden). The GPR data was

complemented with the use of boreholes for direct stratigraphic information.
Conyers *et al*. (2013) conducted a GPR survey over sand dunes which cover Jurassic bedrock in Portugal. Upper Pleistocene stone tools have been found just above this bedrock so it is thought to be the associated palaeosurface. The GPR was intended to map the topography of this palaeosurface. It was found that there were two gullies (part of a drainage system) incised into the bedrock. The stone tools were revealed to be concentrated in an area that would have been concealed from game animals on the floodplain and close to water which allowed the researchers to infer past behaviours of the users of the tools.
Schneider *et al*. (2017) used GPR to investigate a dune field in Germany with the aim of understanding the palaeotopography associated with two Mesolithic sites there. The landscape is originally glacio-fluvial and reworked by wind transport. GPR was used to map the depth of palaeosols and correlate between excavation units. It was able to be shown that the two Mesolithic sites were originally in prominent locations in the landscape even though they are nestled in low lying areas in modern times. It was reported that the GPR was able to penetrate several metres because of the favourable sandy dunes but the accuracy of the palaeotopographic DEM was hampered due to the irregular spacing of surveys.

Carey *et al*. (2017) used ERT to map floodplain deposits and palaeochannels in a fluvial valley in Wales. The deposits there included clays, sands and gravel terraces. Based on the differences in resistivity between these deposits, they were able to identify a system of palaeochannels and therefore estimate which areas had better potential for the preservation of archaeological remains. Furthermore, they used radiocarbon dating to aid with reconstructing the site's formation history and compare with climate records.

The final study presented here took place in northern Germany at the location of a former palaeolake (Corradini *et al*. 2020). GPR was used alongside coring to detect and map five buried islands that may hold Mesolithic settlement. It is intriguing that the islands (sand) showed up clearly even to a depth of two metres below the peat, gyttja and clay infill. It might be expected that the GPR signal would experience too much attenuation to be used in this environment. The reason for the project's success in spite of this is not speculated on. Nevertheless, the GPR-derived palaeolandform model was used with the dated archaeological remains to propose a sequence of lake-level lowering during the Holocene by which the number of emerged islands and intensity of occupation increased.

Many of these projects were on archaeological sites in river valleys and the use of a variety of remote sensing in such valleys to model deposits is not new (Challis and Howard 2006). Doubtlessly, this is because the aggradational nature of the landscape results in thick sequences of material which can bury archaeological sites and reshape the land topography into unrecognisable forms. In particular, former glacial landscapes with riverine and aeolian reworking appear to be prime locations for this type of approach (Carey *et al*. 2006, 2017, Howard *et al*. 2008, Schneider *et al*. 2017) This makes other similar sites (such as Soyo) attractive targets for this kind of modelling. Most of them had the identification of areas likely to hold (or still hold) archaeological material as one of their primary objectives

(Carey *et al*. 2006, 2017, Howard *et al*. 2008, Chapman *et al*. 2009, Corradini *et al*. 2020). It is necessary to have a sense of the buried landforms to steer excavation and management decisions in any archaeological project and these studies provide good examples of how to achieve this.

All of the above projects share the following common themes: the use of geophysical techniques to acquire the depths of targeted stratigraphy, the generation of a DEM to provide elevation correction to the geophysical data, the use of some kind of ground-truthing (cores, trenches *etc*.) to interpret geophysical facies, and the production of either palaeolandsurface DEMs using corrected elevation data or depths to targeted deposits and their thicknesses depending on the research question.

The use of GPR *versus* ERT ties into the research question. Studies that have investigated palaeochannels (Howard *et al*. 2008, Carey *et al*. 2017) found success using ERT where GPR may be ineffective due to conductive clay infill (Carey *et al*. 2006, p. 248). Studies that revolved around mapping the depth to palaeosols (Chapman *et al*. 2009, Schneider *et al*. 2017) or bedrock (Conyers *et al*. 2013) invariably used GPR as the method of choice. This is important because it shows what is likely to be findable using each method in these kinds of landscapes. Both ERT and GPR are complementary in their ability to target different landforms and can be used together to give a more complete picture of the subsurface. What is apparent from the literature is that the geophysics, while often the featured data set of articles, is not sufficient by itself and must be supported with positioning, a DEM and either cores or excavations. The geophysical surveys interpolate or extrapolate beyond the limited information available from archaeological excavation and allow large scale models of ancient landscapes and landscape-as-site formation histories to be formed.

3.1.9 Magnetometry

Magnetometry is one of the most frequently used geophysical methods in archaeology (Gaffney 2008, p. 316). It measures the local magnetic field strength to show areas where there is enhanced magnetism. A magnet is any object with a magnetic moment which is a vector quantity whose size is the strength of magnetisation and whose direction points from the magnet's south pole to north pole. The magnetic moment produces a magnetic field which interacts with other magnets. Magnetometry works because one magnet (in this case the Earth) will induce a magnetic field in any object within its own field. The strength of the induced field (M) is equal to the strength of the applied field (H) times the object's magnetic susceptibility (k).

$$M = kH$$

The induced field is always (except in the archaeologically unimportant case of diamagnetism) aligned in the same direction as the applied field meaning that the presence of material with significant magnetic susceptibility will initially and locally enhance the Earth's magnetic field. Objects that carry permanent (remnant) magnetism may be oriented in any direction as it is moved after having acquired its magnetism. In that case, the direc-

tion of magnetism can change to oppose the direction of Earth's magnetic field and there can, therefore, be destructive interference which locally weakens the Earth's magnetic field strength.

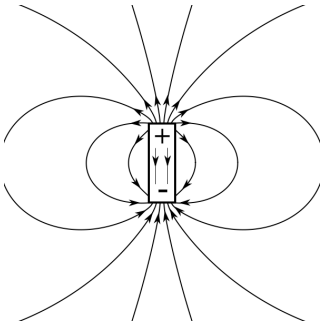

Figure 3.14: A magnet with its field lines.

What kind of materials are practicably detected by magnetometry depends on their magnetic susceptibility which is a property that depends on the material's inherent susceptibility as well as the object in question's shape and volume. The material itself has a volume-specific magnetic susceptibility μ but the induced magnetisation in an object is not only dependent on this. This is because there is an opposing demagnetisation within the magnetised object. This demagnetisation arises from the fact that there is a separation of magnetic poles within the object due to the external magnetic field. The magnetic field lines point from the north pole to the south pole both outside and inside the induced magnet (fig. 3.14). Therefore, the induced field lines will travel "backwards" inside the induced magnet from north pole to south pole in opposition to the external magnetic field (Chikazumi 1964, pp. 19–20). This effect is highly dependant on the shape of the object and the orientation of that shape within the external field. Long, narrow objects oriented in the direction of the external field have an effective susceptibility k that is almost equal to the volume susceptibility μ. Conversely, flat, sheetlike objects oriented such that the external field lines pass orthogonally through the plane have an effective susceptibility k that is almost independent of the volume susceptibility μ. The relationship between k and μ can be expressed in the following equation where V is the volume and N is the demagnetising factor (Witten 2006, p. 80).

$$k = \frac{\mu V}{1 + N\mu}$$

The cause of magnetism is an important topic because it gives rise to different kinds of magnetism and magnetic minerals. According to classical mechanics, we may envisage a magnetic moment arising from both the orbital motion of electrons (angular momentum) as well as their rotation (*i.e.* spin which can take values of $+\frac{1}{2}$ and $-\frac{1}{2}$ indicating opposing magnetic moment directions) (Chikazumi 1964, pp. 39–40). The exact details (quantum mechanics) are less important than the knowledge that it is the electrons that produce magnetism and that an intrinsic property called spin causes the resulting magnetic moment to be in one of two opposing directions. As electrons fill an atom's orbitals, they must obey the Pauli exclusion principle which states that no two particles may occupy the same set of quantum numbers. What this means for this discussion is that each atomic orbital may contain no more than one positive spin electron and no more than one negative spin electron. Furthermore, Hund's rule states that electrons will half fill every

orbital of the same energy level before pairing electrons up and that the unpaired electrons will align in spin direction (Chikazumi 1964, pp. 52–7, Morrish 1965, pp. 32–7). Atoms and ions with unpaired electrons have an extra spin-derived magnetic component which results in higher magnetic susceptibility.

In a system where the electron-produced magnetic moments are free to orient in random directions, thermal agitation will ensure that they do so. In the presence of an external magnetic field of sufficient strength to overcome the thermal agitation, the magnetic moments will align in the direction of the external field and so an induced net magnetic moment is created along with its associated magnetic field. When the external field disappears, so does the induced field and thermal agitation disorders the orientation (fig. 3.15). This property is called paramagnetism and is a relatively weak effect (Chikazumi 1964, p. 8).

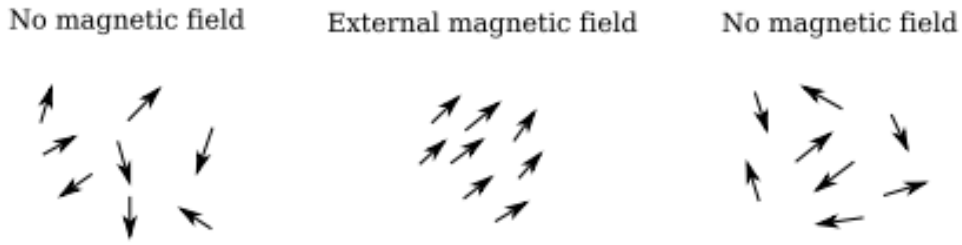

Figure 3.15: A diagram of paramagnetic moments. When a magnetic field is applied, they align to the direction of that field. When the external field is removed, the moment become randomly oriented again.

In some materials, the atomic magnetic moments are not free to orient in random directions but experience a strong tendency to locally conform in alignment because the crystal structure affects the orientation of the atomic orbitals. Above a certain temperature (the Curie point of a substance), thermal agitation will overcome this and the material will behave as a paramagnet. Below the Curie point, a spontaneous alignment will take place according to the ambient magnetic field which will last until the material is reheated above that temperature. This is known as ferromagnetism (Grant and West 1965, p. 356). Although there is a spontaneous magnetism in ferromagnetic minerals, there is not a net magnetic dipole under ordinary circumstances. This is because the mineral is broken up into different internal regions called magnetic domains. Within each domain there is a net moment due to alignment of electron spins but the domains are not aligned to each other. This results in no overall magnetic moment and so there is no magnetic field. All ferromagnetic grains above a certain size (in the order of micrometres) are multidomain grains. Under an external magnetic field, the domains will become aligned and a magnetisation will be induced in the ferromagnetic object. However, when the external field is removed, there is resistance to the reversion of the internal structure because of the energy required to change the domain walls. Therefore, the magnetisation is said to be permanent. It takes

a large external field in the opposite direction to completely demagnetise the object. In this way, a ferromagnetic object inside an alternating magnetic field (**H**) has an induced field (**M**) that lags behind. In a plot of **M** against **H**, this traces out a loop called a hysteresis loop (Grant and West 1965, pp. 357–60, Morrish 1965, pp. 332–3). The important implication for this is that some objects will retain a palaeomagnetism even after they have been moved or rotated compared to the Earth's magnetic field (or after the Earth's magnetic field has shifted). This remnant magnetisation will usually persist until the object becomes heated past its Curie point at which point thermal agitation will overcome the tendency of electron spins to align in a ferromagnetic material. This has important consequences for archaeology because of human use of fire which will be discussed later. Not all minerals that have electron spin interactions are ferromagnetic. It is also possible that the electron spins are anti-aligned in which case the magnetic moments cancel and there is no overall magnetisation. This is called antiferromagnetism. Sometimes these anti-aligned magnetic moments have a slight deviation from a common axis in which case there is a small magnetisation roughly orthogonal to the axis of anti-aligned magnetic moments (called canted antiferromagnetism). The most important case for the archaeologist is the case between ferromagnetism (complete alignment) and antiferromagnetism (complete anti-alignment) which is where the electron spin magnetic moments are unequally anti-aligned (ferrimagnetism) (fig. 3.16) (Evans and Heller 2003, pp. 8–9). The concepts of magnetic domains and hysteresis for ferromagnetism also apply to ferrimagnetism. The classic example of ferrimagnetism is in the ferrite minerals which are metal oxides of the form XFe_2O_4 where X is a metal (II) ion and have the spinel crystal structure.

The last main kind of magnetism is diamagnetism which produces a negative susceptibility. In a diamagnetic material. the induced magnetic field is in the opposite direction to the external magnetic field. This is due to the Larmor precession of electrons around an axis of magnetic flux. All materials have the property of diamagnetism but the effect is so exceedingly weak that it is unlikely to be significant to the archaeologist (Evans and Heller 2003, p. 7). Superparamagnetism is another kind of magnetism of ferromagnetic or ferrimagnetic grains that are so small that they behave as paramagnets (but with susceptibilities in the order of magnitudes that ferromagnets have). This will be explained in more detail with the magnetic susceptibility method (Section 3.2.1).

There are many kinds of magnetic materials of interest to archaeologists and it depends greatly on the specifics of the site in question. Many artefacts have a sizeable magnetisation (especially iron artefacts) which can be easily detected through magnetic means. This also applies to modern objects as well so the archaeologist must be careful when interpreting the results of magnetic surveys. Geological materials can also have measurable magnetisation so knowledge of the site's geology is important to be confident in the interpretation of a magnetometry survey. Apart from metals, the most archaeologically important magnetic minerals are a series of iron oxides: haematite, magnetite and maghaemite. Haematite (αFe_2O_3) is a canted antiferromagnetic mineral meaning it is slightly magnetic.

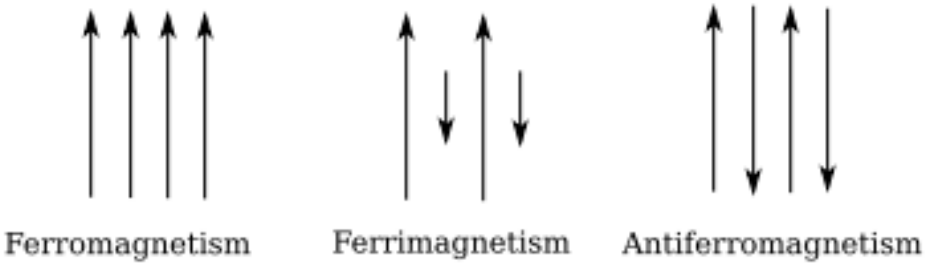

Figure 3.16: Diagram showing the difference between ferromagnetism, ferrimagnetism and antiferromagnetism. Note that the opposing magnetic moments in a ferrimagnetic material are not equal and so there is a net moment.

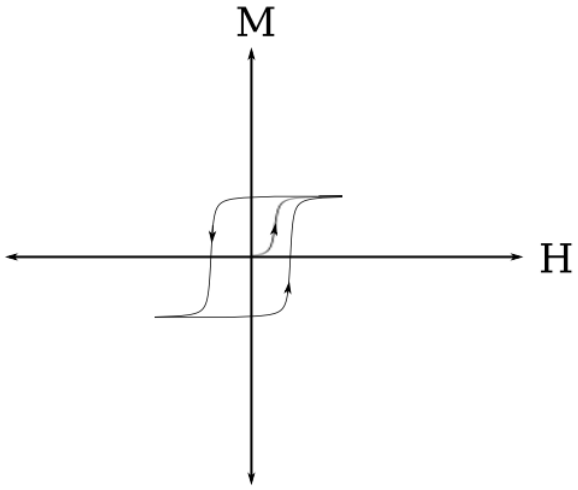

Figure 3.17: Plot of how the induced magnetic field **M** of a ferromagnet or ferrimagnet changes in accordance with an external magnetic field **H**.

Haematite is a very common mineral and provides a weak magnetism in many rocks and sediments but its susceptibility is relatively low by comparison to some other iron oxides (Evans and Heller 2003, p. 38). Magnetite is a reduced iron oxide (Fe_3O_4) which takes the spinel crystal structure. Magnetite is ferrimagnetic because the magnetism of one Fe (III) ion in each crystal unit is opposed by the magnetism of an Fe (III) ion and an Fe (II) ion combined. Magnetite has a Curie point of 580 °C (Evans and Heller 2003, p. 33). Maghaemite (γFe_2O_3) has the same spinel structure as magnetite and is also ferrimagnetic but all of the iron ions are in the more oxidised Fe (III) state. To maintain charge neutrality, one ninth of the iron sites are vacant as compared to magnetite. The Curie point of maghaemite is difficult to measure because the mineral is less stable at higher temperatures but it is estimated to be over 600 °C (Evans and Heller 2003, p. 40).

It is not just archaeological features and soil minerals that may be detected by magnetometry. Many rocks can be magnetic enough to show up in a survey. Rocks of a particular type vary widely from place to place. For example, a granite in one location is not the same as a granite in another location and this is true for their magnetic properties as it is for their other properties. Nevertheless, it is possible to make some broad statements. There have been suggestions made in the literature that igneous rocks are about an order of magnitude on average more magnetically susceptible than sedimentary rocks and unconsolidated sediment (Grant and West 1965, p. 366, Hanson *et al*. 2005, p. 157, Witten 2006, p. 84). This would suggest that igneous and metamorphic rocks might magnetically stand out against a sedimentary background on the basis of their induced magnetic fields alone. However, there is a more important consideration. Igneous rocks have cooled from magma or lava which is far beyond the Curie temperatures of the magnetic minerals discussed. These rocks, therefore, take on a permanent thermoremanent magnetisation in the direction of the Earth's magnetic field at the time (Grant and West 1965, pp. 369–70). This permanent magnetisation is much stronger than its induced magnetisation and makes igneous rocks much more magnetic than most sediments and sedimentary rocks (Hanson *et al*. 2005, p. 157, Witten 2006, p. 85). Apart from the mapping of natural features, if archaeological structures are made of strongly magnetic materials (such as granite) or weakly magnetic materials (such as limestone), they may show a magnetic contrast to the surrounding landscape. As an example, magnetometry was used to uncover buried megalithic tombs constructed of highly magnetically susceptible granite in Sri Lanka (Fassbinder and Becker 1999).

There are other magnetic minerals that may be of interest to archaeologists depending on the local site situation. The iron oxides discussed form one part of a whole complex of iron-titanium oxides which often occur in conjunction. Adding titanium to magnetite produces the titanomagnetite series whose extreme endmember is called ulvöspinel (Fe_2TiO_4). Adding titanium to haematite produces the titanohaematite series whose extreme endmember is called ilmenite ($FeTiO_3$) (Grant and West 1965, pp. 361–2). Increasing the titanium content along these series decreases the overall spontaneous magnetism (Ti^{4+} has no unpaired electrons and requires the reduction of an Fe3+ to Fe2+ which has one fewer unpaired electrons) and it also lowers the Curie temperature of these minerals. It turns out that at the higher titanium endmembers, the Curie temperature is below room temperature and so there is no spontaneous magnetism at all. This all makes the titanium enriched iron oxides less important for magnetic surveys at archaeological sites (Evans and Heller 2003, pp. 33–9). Other minerals of potential interest include iron hydroxides, iron sulphides and iron carbonates some of which are weakly magnetic in their own right and some of which may become oxidised to magnetic minerals. In particular, hydroxides such as goethite ($\alpha FeOOH$), lepidocrocite ($\gamma FeOOH$) and ferrihydrite ($5Fe_2O_3.9H_2O$) may be a significant factor in wetter environments (Grant and West 1965, p. 363, Clark 1996, p. 100, Evans and Heller 2003, pp. 41–3).

Iron is the most familiar magnetic material and it produces the strongest response of any-

thing that is likely to be found at an archaeological site with a magnetic susceptibility that is orders of magnitude above other common materials (Conyers 2018, p. 30). Iron is also ferromagnetic and can have its own permanent magnetism. Iron objects produce strong dipole readings which can completely obscure anything else in the immediate area. It is important to take into account the presence of modern iron on the surface (scrap metal, iron railings *etc*.) as well as the possibility of modern iron being buried just below the surface out of sight.

The magnetic minerals discussed above accumulate where they are deposited as sediment which gives those sediments their magnetism. The process of soil formation can enhance this magnetism as parent material weathers due to cycles of wetting and drying. Bacteria have also been identified as producers of single domain magnetite particles in soils (Fassbinder *et al*. 1990). Le Borne (1955) originally proposed a "fermentation" mechanism whereby alternating periods of oxidising and reducing conditions causing haematite to be converted into magnetite and then on to maghaemite. Subsequent proposals for the exact mechanism by which weakly- or non-magnetic iron minerals such as haematite are converted to highly magnetic minerals in soils are summarised in Dearing *et al*. (1996). After studying the magnetism of English soils they proposed that soluble Fe^{2+} ions are weathered from iron minerals and precipitate out as ferrihydrite. Ferrihydrite is easily reduced by bacteria to release excess Fe^{2+} ions. The excess Fe^{2+} cause ferrihydrite to dehydrate and oxidise to magnetite (fig. 3.18) (Dearing *et al*. 1996, p. 730). Naturally, the local climate (especially precipitation) will play a big role in supplying suitable conditions for this pathway to occur so a consideration of current and past climates will help interpretation. The magnetic enhancement of soils has some important implications for the magnetic signatures found at an archaeological site. Magnetometry can successfully detect archaeological earth disturbances such as ditches and pits in cases where the infilling material has a different magnetic susceptibility to the host matrix because a detectable magnetic feature is produced (Clark 1986, pp. 1407–8, Becker and Fassbinder 1999, Nowaczinski *et al*. 2015).

Areas of burning are a common archaeological feature searched for with magnetometry since it is well known that fires, especially hotter, anthropogenic fires, produce an appreciable magnetism in the surrounding soil (Linford and Canti 2001). The reason for this is due to the role of heat in the formation processes of the more strongly magnetic minerals magnetite and maghaemite. Magnetite is produced from a number of precursor iron-bearing minerals. It has been commonly said that haematite is the primary precursor which is heated in a reducing environment to form magnetite which is in turn heated in an oxidising environment to form maghaemite (Gaffney and Gater 2003, p. 38, Aspinall *et al*. 2008, pp. 23–4, Conyers 2018, p. 30). However, it has been argued that there is insufficient evidence that haematite is reduced to magnetite under the temperatures from wild fires in normal field conditions but that other minerals, particularly goethite, lepidocrocite and siderite ($FeCO_3$), are chemically altered into magnetite and maghaemite (Fassbinder 2015, p. 86). Regardless, magnetometry is an important tool for locating the remains and spatial distribution of ancient hearths and other burned features (Urban *et al*. 2019, Welc

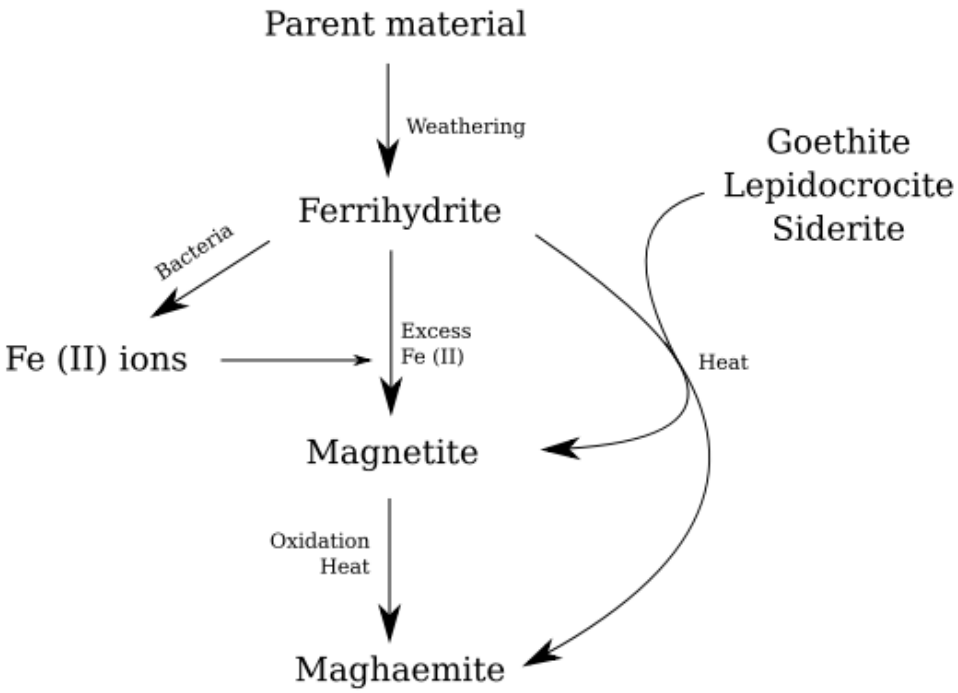

Figure 3.18: Diagram of the enhancement of magnetism in soils by converting iron-bearing minerals into more magnetic forms.

and Bobrowski 2020).

One of the most suitable archaeological materials to detect with magnetometry is fired clay. In fact, the prospection of buried kilns appears to have been its first ever use within archaeology (Clark 1996, pp. 16–7). Fired ceramic is visible in a magnetic survey partly because of the burning and conversion of iron-bearing minerals as discussed but also because of the thermoremanence of ferrimagnetic grains within the clay matrix. During the firing process, the clay is heated beyond the Curie point of magnetite and maghaemite which causes the electron spins to become unaligned due to thermal agitation. As the clay cools, the spins become realigned to the Earth's magnetic field in newly formed magnetic domains. If the ceramic objects are later moved, their magnetic moments become no longer aligned with the Earth's field which can reduce the overall magnetic signature in the case of a mass of bricks or pottery; however, if the ceramic is reheated sufficiently (a brick house burning down for instance), it will take on a new thermoremanent magnetisation direction (Aspinall *et al*. 2008, pp. 21–2). Magnetometry is a good option in cases where pottery or other ceramics are expected to be widely present and are the target of archaeological interest and it has been used at many sites for this purpose (Frederick and Abbott 1992, Aspinall *et al*. 2008, pp. 155–9, Moffat *et al*. 2011).

3.1.10 Using and Interpreting Geophysics in Spatial Archaeology

One of the primary data sets for any archaeological site is the topography in which it lies and the spatial arrangement of remains therein. This forms the basis for such subdisciplines as environmental archaeology and landscape archaeology where the topography is linked to the environment and man's perception of it. Environmental archaeology is particularly concerned (among other things) with topography since it is shaped by and influences the environment. The spatial distribution of archaeological remains with regard to the topography can yield interesting conclusions about past behaviours and use of geographic space (Evans 1978, pp. 5–6). This information is equally vital to those working under the heading of landscape archaeology. The topography and spatial arrangement of natural and cultural features combine to inform the mental overlays or perceptions of the composite landscape (David and Thomas 2008, p. 38). However, many ancient landscapes that represent long lived surfaces with accumulations of environmental and cultural modifications lie buried under subsequently deposited sediments (Evans 1978, p. 81, Stern 2008, p. 365). Geophysical methods can help uncover these ancient surfaces for further analysis. Moreover, they can do so quickly over a large area and at an appropriate resolution for archaeological purposes which has greatly improved the ability to study landscapes over broader areas and in greater detail (Cheetham 2008, p. 572). Exactly how and for what purpose they are used can vary between projects but fall into three main schemes: geophysics for prospection, for extrapolation and for hypothesis testing.

Geophysical methods have been used for many decades to map archaeological features across sites. Their most common use has been as prospecting tools to find areas of po-

tential interest (Gaffney and Gater 2003, pp. 13–18). A cursory reading of compendiums and handbooks of geophysics as applied to archaeology reveals a heavy use of the word "anomaly" and a corresponding emphasis on the discovery aspect of the methods (Clark 1975, 1996, Gaffney and Gater 2003). This is also seen in the title of one of the major early journals for publishing these surveys *Prospezioni Archeologiche* and the current *Archaeological Prospection*. Data is first collected and plotted. Readings in the data are then assigned an interpretation by reference to a set of known or suspected archaeological features. This set is the archaeologist's guess at what should be found at a particular site based on existing knowledge. Under this scheme, a map of potential archaeological features is obtained. Typically this type of geophysical survey is one of the first things done at a site before excavations. It soon became apparent among pioneers of archaeological geophysics that not all such mapped features are archaeologically interesting. Some of the problem is due to an incomplete reference set which overlooks geological features. Both the archaeology and the geology of a site should be kept in mind when interpreting geophysics in order to get the most reliable results. The form of geophysical readings is often taken as an interpretive clue since orderly rectangular and circular features are more likely to be man made. For example, linear features orthogonal to one another can be interpreted as walls where walls are an expected feature of the archaeology (Simyrdanis *et al*. 2016, pp. 11–3, Moník *et al*. 2018, Miller *et al*. 2019, p. 272).

A related way of using geophysics in archaeology is for the extrapolation of known features in the ground. Unlike with pure prospecting, only features that are known through excavation are mapped. First a geophysical survey is performed. Then excavations or auguring are done in key locations in order to correlate geophysical readings in those parts of the site with real changes in the subsurface. Because certain responses in the geophysical data are anchored to known features, it can be inferred that similar responses (to an appropriate extent) also indicate that feature or another of its type. Although this scheme for using geophysics could be characterised as informed prospecting, it differs from prospecting in the sense that its goals are different. The purpose of prospecting is to find out what exists whereas the purpose of extrapolation is to extend existing knowledge over a wider area. Some advantages of this scheme are that greater confidence can be had in the interpretation of a geophysical response if it can be spatially matched to a real object in the ground and effectively extending knowledge gained from limited excavations across a broader area meaning that more information can be obtained from less digging (Slater *et al*. 2000, p. 36, Keay *et al*. 2009, p. 162, Correia 2019, pp. 106–8).

The third use of geophysics is to test specific hypotheses and it is here that archaeological science becomes scientific archaeology. Based on prior work at a site (which may or may not itself be geophysical), ideas about its nature and extent may be developed. Geophysical methods, being relatively quick and inexpensive to use, may provide a suitable way to test these ideas. The results are said to either be consistent or inconsistent with the hypothesis (rather than prove or disprove). This is because it is usually difficult or outright impossible to say that something does not exist based on geophysical results.

Furthermore, a result that is consistent with one hypothesis may be also consistent with another. Hypothesis testing can be used to follow one of the previous schemes. By utilising additional geophysical methods to test the hypotheses developed from previous surveys, greater confidence in an interpretation is often achieved. Alternatively, surveying with multiple techniques from the outset can achieve the same result. Because hypothesis testing is an incrementally iterative process building towards a model, it is likely that there are more examples of it than can be discerned from the literature. However, one the earliest geophysical surveys provides a good example where the presence of a stone vault buried under a church in Williamsburg, USA was suspected from historical records. In 1938 an electric equipotential method was chosen to test for the presence of such a highly resistive object. The results were consistent with the hypothesis although it was later found that this was due to changes in the porosity of the soil (Bevan 2000). This demonstrates how results that are consistent with hypotheses do not prove them.

In practice these three schemes (summarised in fig. 3.19) for using geophysical methods in archaeology are often mixed and it may not be always clear how their use fits into the broader archaeological methods within the researcher's mind. Thinking carefully about how geophysics is to be used in a study can help produce more rigorous thinking about the nature of the results. It may also temper unrealistic expectations about the conclusiveness of any findings. For example, if a geophysical survey is done as a preliminary prospecting step before any excavation, the results should be understood as preliminary and there should not be any expectation that they will reveal very much other than the locations of features of *potential* interest.

3.2 Sediment Analysis

3.2.1 Magnetic Susceptibility

Magnetic susceptibility is a physical property of materials that governs how strongly a material develops its own magnetic field in response to an external magnetic field. The definition for magnetic susceptibility of an object is the ratio between its induced magnetic field (**M**) and the applied magnetic field (**H**).

$$\kappa = \frac{M}{H}$$

This is known as the volume susceptibility which is a dimensionless quantity. Magnetic susceptibility is often given as mass susceptibility (denoted by χ) which is derived by dividing this by the density of the material resulting in units of $m^3\ kg^{-1}$ (in SI units). The difference between magnetometry and magnetic susceptibility is that the former measures **M** (induced by Earth's magnetic field - no other field is applied by the user) while the latter measures **M** and compares it to the known applied **H**. This makes magnetic susceptibility more inherent to the material being studied (Clark 1996, pp. 99–100, Evans and Heller

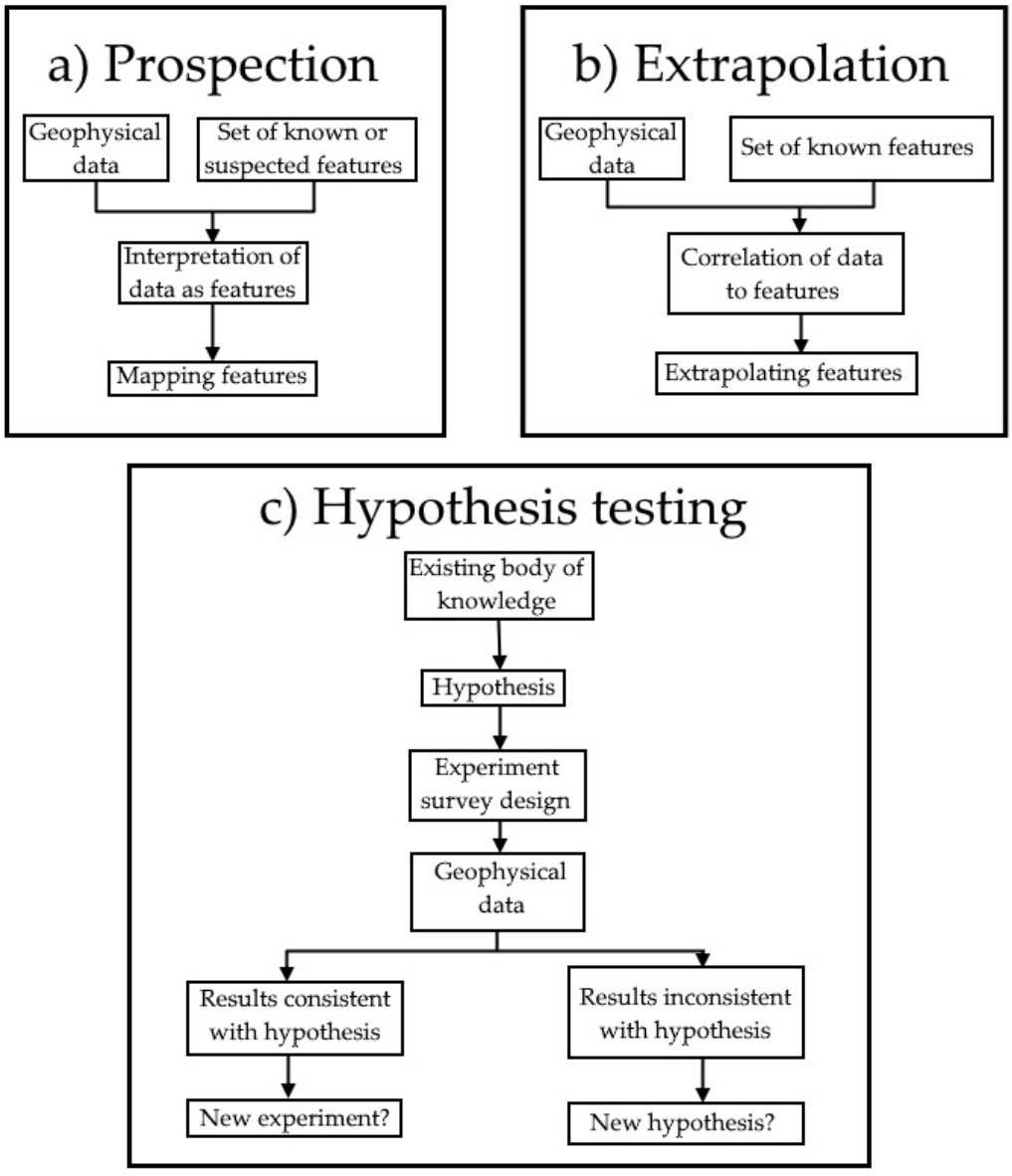

Figure 3.19: Flowcharts describing the processes of prospection (a), extrapolation (b) and hypothesis testing (c) as applied to the use of geophysics in archaeology.

2003, p. 9, Witten 2006, pp. 79–81).

Magnetic susceptibility can be measured via an alternating magnetic field with a particular frequency. When a sample is place within the field, an induced magnetism is generated which combines with the applied field such that the variation of the resulting magnetic field **B** over time is different in amplitude and frequency than the applied field **H** (Clark 1996, p. 102). These quantities are related in the following way where the constant μ_0 is the magnetic permeability of free space.

$$B = \mu_0(M + H)$$

This allows for the measurement of magnetic susceptibility which, as previously stated, is the ratio between **M** and **H**. When the applied field is alternating in direction, the magnetism induced in the sample will decay as thermal agitation causes magnetic moments to become anti-aligned (Evans and Heller 2003, pp. 16–7). For single-domained magnetic grains, the time this takes(τ) can be modelled as follows where V is volume, T is temperature, K is a mineral-specific constant of magnetic anisotropy, and k is the Boltzmann constant. This is called the relaxation time. Most importantly, it depends on the size of the grain such that a larger grain size requires a longer relaxation time (Morrish 1965, pp. 360–1, Worm and Jackson 1999, p. 416).

$$\tau = \tau_0 e^{\frac{KV}{kT}}$$

If the oscillation period of the applied magnetic field is faster than the relaxation time of the grain, it produces an out-of-phase signal to the applied field. This is known as hysteresis. If the oscillation period of the applied field is slower than the relaxation time of the grain, the induced magnetic field for that grain is in-phase with the applied field. For single-domain grains, there is a critical size (for a given frequency, temperature and mineralogy) under which they behave in a way similar to paramagnetism meaning they do not have a remanent magnetic field when **H** = 0 (fig. 3.20). However, their magnetic moments are much larger than those of paramagnetic materials. This property is called superparamagnetism. The implication is that, for magnetic grains near the superparamagnetic boundary, changes in the frequency of the applied field will result in changes in measured susceptibility (Grant and West 1965, pp. 360–1, Evans and Heller 2003, pp. 52–53). This leads to the concept of frequency dependence which captures the difference between induced magnetic fields from low frequency and high frequency applied fields (Clark 1996, pp. 103–4).

$$fd = \frac{\chi_{LF} - \chi_{HF}}{\chi_{LF}} \times 100$$

Frequency dependence shows how much of the magnetic material in a sample is made of these tiny, superparamagnetic grains.

Magnetic susceptibility can be used for both horizontal and vertical investigations of the sediments at archaeological sites. Although magnetic susceptibility is not used as fre-

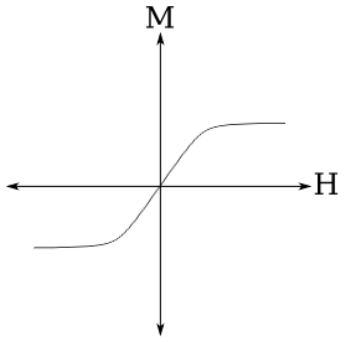

Figure 3.20: Plot of how the induced magnetic field **M** of a paramagnetic material responds to changes in an external magnetic field **H**.

quently for landscape studies as magnetometry, it does have the benefit of being able to detect magnetic features (such as might be produced from burning) in the immediate surface while buried features remain undetected because of the instrument's poor depth penetration as compared to total field magnetometers (Clark 1996, p. 99, Gaffney and Gater 2003, p. 120). Studies have shown that magnetic susceptibility and frequency dependence measurements are capable of detecting areas of intensive human occupation (Marmet *et al*. 1999) and of determining the distribution of burning with a landscape setting for more sparse occupation (Linford and Canti 2001). The magnetic susceptibility down stratigraphic columns is frequently measured as part of a suite of sediment analyses. Changes in magnetic susceptibility or frequency dependence can be used in conjunction with other methods to delimit stratigraphic facies (Narantsetseg *et al*. 2013), to detect pedogenesis and infer palaeoclimate (Evans and Heller 2003, pp. 136–44, Kravchinsky *et al*. 2008), to date loess-palaeosol sequences (Heller and Tungsheng 1984, Maher 2011, pp. 121–3) or to detect changes in human burning activity through sedimentary strata (Jones *et al*. 2022).

3.2.2 Grain Size

The size of sedimentary grains is a basic property of sedimentary rocks and unconsolidated sediments. The standard way of classifying grain size is with Wentworth size classes. Each size class differs from adjacent classes by a factor of two. The common categories include very coarse sand (1.0-2.0 mm), coarse sand (0.5-1.0 mm), medium sand (0.25-0.5 mm), fine sand (0.125-0.25 mm), very fine sand (0.0625-0.125 mm), silt (1/256 - 1/16 mm) and clay (sub 1/156 mm). These are summarised in table 3.3. Sizes above sand are called gravels and can be divided into granules (2-4 mm), pebbles (4-64 mm), cobbles (64-256 mm) or boulders (greater than 256 mm). Another way of reporting these sizes is with the phi scale which is calculated as the negative base two logarithm of the grain size in millimetres (Boggs 1995, pp. 79–81).

$$\phi = -log_2 d$$

Diameter (mm)	Wentworth Class
Above 2	Gravels
1-2	Very coarse sand
0.5-1	Coarse sand
0.25-0.5	Medium sand
0.125-0.25	Fine sand
0.0625-0.125	Very fine sand
Below 0.0625	Silts and clays

Table 3.3: Table of Wentworth classes for sands and their corresponding diameters in millimetres.

The size of a clast plays a major role in the velocity of the transporting medium (along with other factors such as depth in the case of rivers) that is required to pick up and deposit that clast. Therefore, the size of clasts deposited can inform us about the transport regime (Prothero and Schwab 2013, pp. 36–40). However, the applicability of sedimentary grain size studies to the understanding of both ancient and modern depositional environments and processes is not always straightforward and there can be considerable variability within the same depositional system due to factors such as differential sediment supply and local variations in the energy of a transport system (Boggs 1995, pp. 91–3). Nevertheless, it is frequently used in combination with other records in order to delimit stratigraphic units and to ascertain the depositional processes at sites of interest (Horiuchi *et al*. 2000, Ma *et al*. 2013, Narantsetseg *et al*. 2013).

3.2.3 X-Ray Fluorescence

X-ray fluorescence is a technique that provides a measure of the elemental composition of a sample. It works by bombarding the samples with photons (light). Sometimes the photon will impart enough energy for one of the non-valence electrons to escape its orbital and become a free electron. This leaves the newly created ion in an unstable state and an electron from a higher energy orbital will move to fill the vacancy in the lower energy orbital. The difference in energy between the two orbitals is then released as an x-ray (fig. 3.21). There are multiple allowable (according to quantum mechanics) energy changes within most atoms depending on which orbitals the ejected electron and in-filling electron came from but each element has a different signature of ejected x-rays. Therefore, the relative abundance of different elements in a sample can be known from measuring these x-rays (Margui and Van Grieken 2013, pp. 1–4). The release of energy from an electron dropping to a lower orbital can result in an emitted x-ray as described but it may also be absorbed by another electron which is then ejected from the atom as well (Auger effect). Most of the energy is released as x-rays in larger atoms but for smaller atoms the Auger effect is dominant. This makes XRF unsuitable for detecting the light elements (Margui and Van Grieken 2013, p. 1). X-ray fluorescence (and other techniques for determining

elemental composition) have a wide range of applications in archaeology for studying pigments, ceramics, obsidian and other artefacts. The technique is especially popular in provenance and manufacturing studies on artefactual objects (Shackley 2011, Donais and George 2018). In sedimentological studies, elemental compositions derived from XRF and other methods are used as proxies for environmental and climatic conditions. Different proportions and ratios for elements (especially between calcium, iron, titanium, silicon and aluminium) have been used to make inferences about environmental conditions and climatic events (Fedotov *et al*. 2004, Murakami *et al*. 2010, Choi *et al*. 2014, Pennington *et al*. 2019).

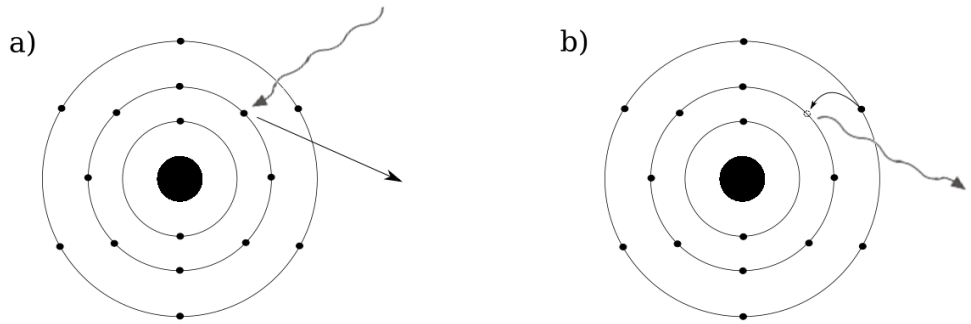

Figure 3.21: Diagram of x-ray fluorescence. a) The incident photon imparts enough energy to a non-valence electron that it can escape the electron shell and be emitted. b) An outer electron fills the inner vacancy left behind and the difference in energy levels between the two orbitals is emitted as electromagnetic energy.

3.2.4 Loss on Ignition

Loss on ignition is a method used to calculate the amount of organic matter and carbonates that a sediment or rock holds. It does so by heating the sample in a muffle furnace to a temperature where a chemical reaction produces carbon dioxide. This gas is released which reduces the mass of the sample. The procedure is divided into three stages (Dean 1974). First the samples are heated to at least 100 °C to drive off any unbound water and leave them dry. Then the samples are heated to 550 °C which combusts any contained organic material. Finally the samples are heated to 1000 °C which causes carbonates to break down into oxides and release carbon dioxide gas according to the following equation (using calcium carbonate as an example).

$$CaCO_3 \xrightarrow{\text{Heat}} CaO + CO_2$$

The proportion of mass lost at the second two steps can be easily calculated from the raw mass lost at that step over the mass of the dry sample (after heating to over 100 °C). Since samples are weighed in their crucibles at each step, the mass of the crucible also needs to be

subtracted from each mass measurement. The weight percentage of the organic material in the original dry sample is difficult to determine since the chemistry of it is generally unknown. The weight percentage of carbonates can be determined by multiplying the mass lost in the third step (heating to 1000 °C) by the molar mass of carbonate ions (60 g mol^{-1}) and dividing by the mass of the dry sample and the molar mass of carbon dioxide (44 g mol^{-1}) (Heiri *et al*. 2001, p. 102).

$$\text{wt\%(carbonate)} = \frac{(m(S_{1000}) - m(S_{550}))M(CO_3^{2-})}{m(S_{100})M(CO_2)}$$

One major potential problem that is likely to occur in most situations is that clays contain electrostatically bound water within their lattices that is also lost during the 1000 °C heating stage. This can cause significant error in samples that are rich in clay minerals and poor in carbonates (Dean 1974, p. 243). Other sources of error variability include position in the furnace, time spent under maximum temperature and the mass of the sample. The effect of these can be made negligible by rotating sample positions, heating for at least four hours at 550 °C and two hours at 1000 °C, and reducing variability in sample size (Heiri *et al*. 2001). The organic carbon content and carbonate content of sediments (whether measured through loss on ignition or in some other way) has been used to estimate the abundance of plant life (and hence palaeoenvironment and palaeoclimate) and make inferences about the changing sources and rate of sediment transport respectively (Horiuchi *et al*. 2000, Fedotov *et al*. 2004, Murakami *et al*. 2010, Narantsetseg *et al*. 2013).

3.3 Radioarbon Dating

As cosmic radiation hits Earth's atmosphere, it causes a cascade of reactions. One of these is the formation of ^{14}C nuclei from nitrogen. These nuclei are mixed throughout the atmosphere and eventually are taken up by plants and animals. While the organism is still alive, the ratio of ^{14}C to ^{12}C remains in equilibrium with the atmosphere because the decay of ^{14}C back to ^{14}N is balanced by the intake of new ^{14}C. However, once the organism dies, it no longer takes in any new ^{14}C and what is left decays at a predictable rate (Gillespie 1986, p. 1, Taylor 1987, p. 2). Carbon dating measures the proportion of ^{14}C remaining in organic remains and calculates when that organism died. Conventionally this was done by counting the number of decay events recorded in a given time which required comparatively large samples. With the advent of accelerator mass spectrometry (AMS) dating which differentiates between isotopes based on their masses the sample size required is much smaller (Gowlett 1987, pp. 129, 132, Taylor 1987, p. 73).

When collecting samples for dating, care must be taken to account for any possible contamination. This can include modern roots intruding on a layer of interest and carbonates in water systems. These contaminants can alter the amount of ^{14}C in the sample and should be removed if possible (Gillespie 1986, p. 7). Wood samples can also pose further difficulties because the tree to which it belonged may have been centuries old when it

died. This can inflate the age of such samples if they were cut off from equilibrium with the atmosphere significantly before the death of the tree (Gillespie 1986, p. 25, Taylor 1987, p. 45). Finally one must account for the fact that the rate of ^{14}C production has not been constant throughout time and so its proportion of total atmospheric carbon has not been constant either. A calibration curve must be used to correct the calculated age (Gillespie 1986, p. 28).

3.4 Photogrammetry

Photogrammetry is a process whereby a collection of photographs can be used to create a three dimensional model of an object. The process involves importing many photographs taken from a variety of angles and finds tie points that it can identify across multiple images. It then stitches the images together using distortions in the two-dimensional spatial arrangement of these tie points to infer how they, as well as the camera positions, sit in three dimensions. This process is known as structure-from-motion (Westoby *et al*. 2012). Positioning co-ordinates can be input by putting down flags in the field at known positions before taking the photographs and then marking them as special key points in the software during processing. The tie points are used as a base structure to fill in a denser point cloud representing the surface which can in turn be used to generate a mesh model and other georeferenced models. See Agisoft (2021) for a description of the general workflow for generating and georeferencing photogrammetry models.

Chapter 4

Methods

The data used in this thesis was obtained from Soyo, Mongolia over two field seasons. Ground penetrating radar data were collected in 2016 and seven stratigraphic test pits were dug at the western end of the site. These pits provided direct stratigraphic information and sediment samples for later analyses. Positioning for the GPR survey and stratigraphic test pits was provided by a static GPS. In 2019 the same area was covered by electrical resistivity tomography and magnetometry surveys. A further seven stratigraphic test pits were dug and more sediment samples were taken. The aerial photographs were retaken with a drone for more consistent quality. Positioning was done using a total station and real time kinematic system (RTK). In both seasons charcoal samples were collected for radiocarbon dating. The extent of the geophysical surveys and locations of test pits can be seen in fig. 4.1.

4.1 Geophysics

4.1.1 Electrical Resistivity Tomography

One of the primary goals in the 2019 field season was to conduct an ERT survey over the area previously covered by the GPR survey in 2016 (fig. 4.1). Due to the need to cover a large area in a relatively short two weeks, some sacrifices had to be made. An electrode spacing of one metre for each line (the largest distance allowed by our specialised cables) meant that the resolution of data was not sufficient to resolve thin layers in the sediments such as particularly palaeosols which were typically less than 20 cm thick at the site. It is not expected that one metre electrode spacing is sufficient to resolve features on that scale. One the other hand, it gives us good depth coverage down to several metres in order to detect the broader glacial deposits, bedrock and permafrost. The spacing between lines was set at a consistent 20 m.

The equipment used for the survey was a ZZ Flash-Res 64 channel resistivity meter (fig. 4.2). This immediately presented a problem since most of the GPR grids were 90 m long while 64 electrodes at one metre spacing cover only 63 m. To solve this a single roll-along

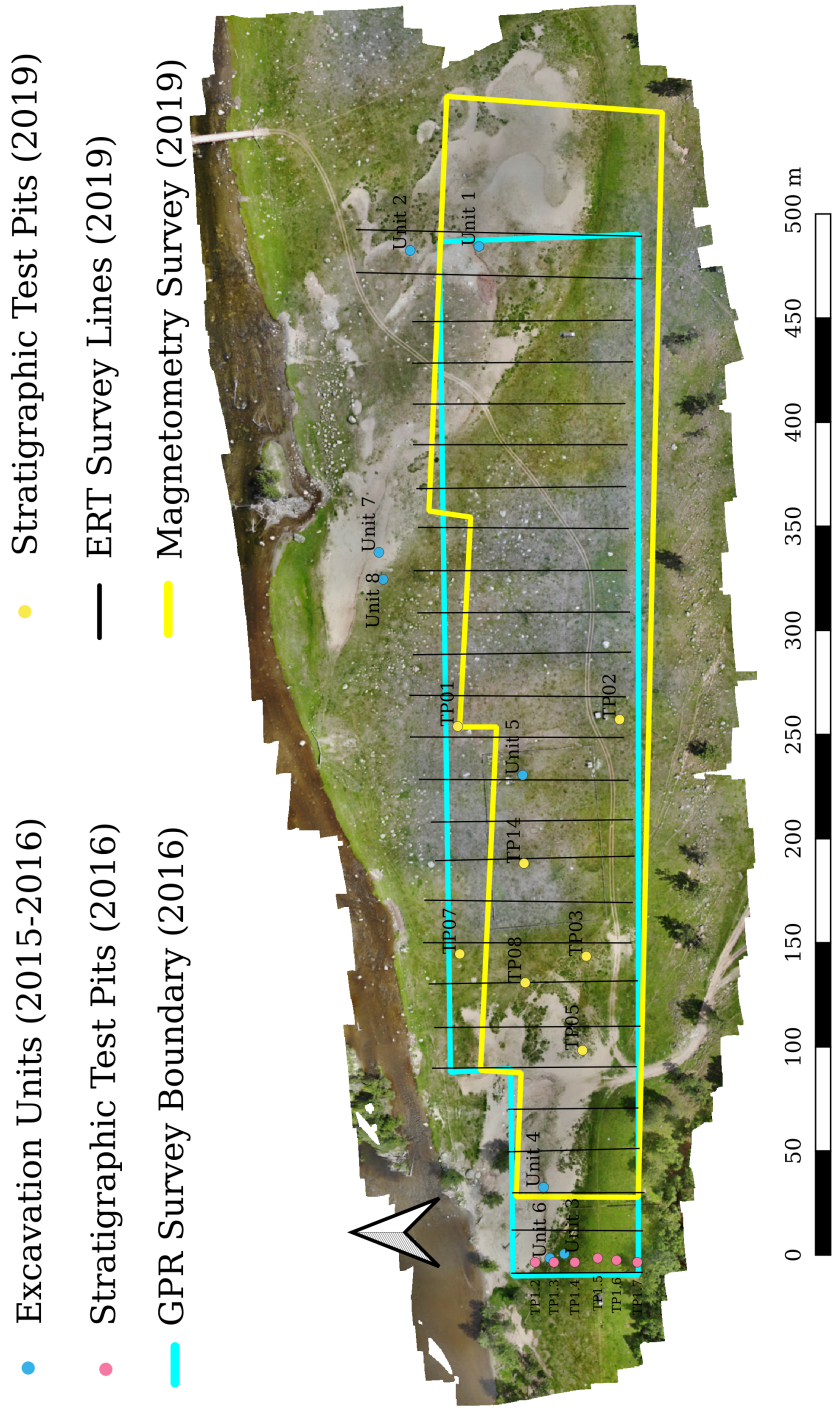

Figure 4.1: Map of Soyo showing extent of geophysical surveys and locations of test pits.

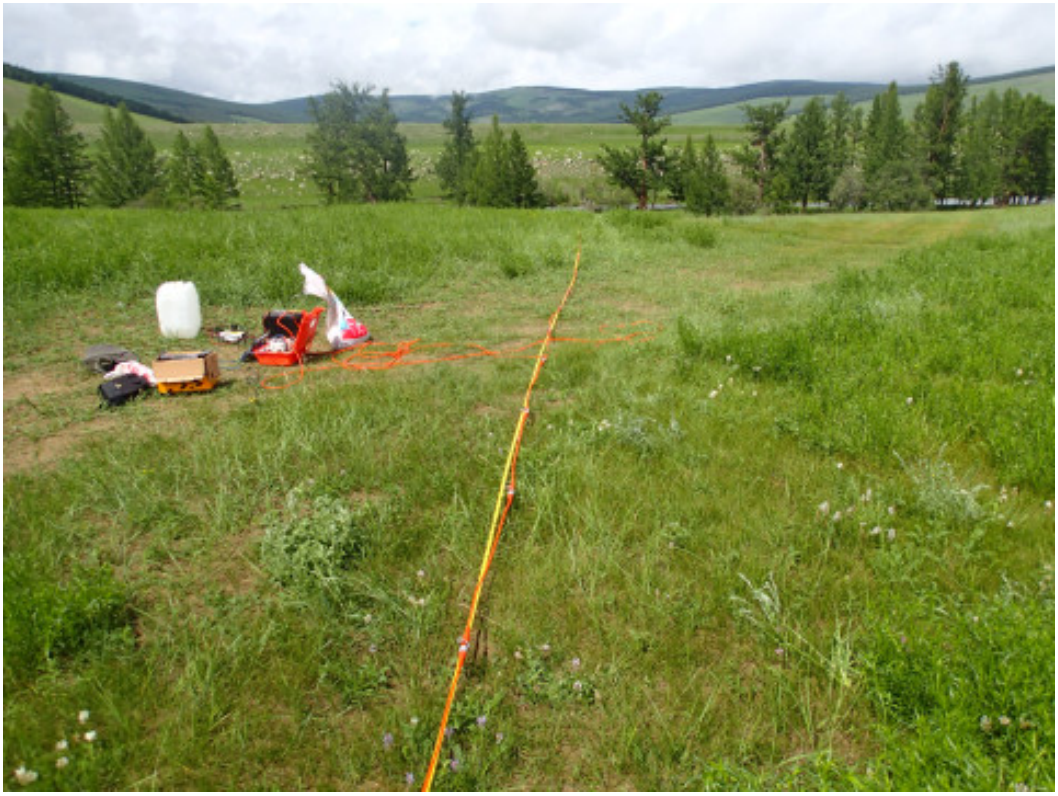

Figure 4.2: Photograph of ERT line.

was done where needed. A second ERT line was done starting at the 37 m mark of the first line and the two output files were later combined. This extended each line to 100 m with a 41% overlap between the two component lines. In two cases a third extension was done for a total of 137 m. Every ERT line was collected from South to North. The arrays used were the Wenner and dipole-dipole arrays. These were chosen as complementary methods since the Wenner array is better at horizontal resolution while the dipole-dipole has better vertical resolution (Loke 2004, pp. 29–30). While the primary goal is to determine the stratigraphic (generally horizontal) nature of Soyo, the high number of boulders on and under the surface (Putnam 2016, pp. 1–2) calls for good resolution of vertical boundaries as well. The relatively small electrode spacing for ERT surveys meant that a lower voltage was necessary to avoid blowing the fuse on the instrument. This is because closer electrodes results in a lower resistance between adjacent electrodes and thus a higher current drawn from the power supply. Therefore, the moderate option of 120 V was chosen. Contact resistances were typically in the range of 500-2000 Ω depending on the ground conditions. Average current per measurement was typically around 0.8-2.3 A. Currents below 0.006 A were filtered. Each measurement was taken over one second to ensure a stable reading and provide a measure of quality for the data. The measurements were accordingly taken as the average reading over that period. The Wenner arrays were taken with parameter $k = 15$ (see fig. 4.3 for how k and L determine array length) meaning the maximum electrode spacing allowed was 15 times the smallest spacing. Since the small-

est spacing is one metre, the maximum array length allowed was just 45 m. This would correspond to a theoretical maximum depth of about 8 m using the median sensitivity depth. The dipole-dipole arrays were taken using parameters $k = 10$, $L = 5$ meaning the maximum multiplier for electrode spacing was 10 but the distance between the current and potential pairs could be multiplied by a further factor of up to five. This put the theoretical maximum array length at 70 m which is longer than the actual physical length of the survey line. Therefore, the maximum depth was constrained by the physical length of the cables rather than by survey parameters and theoretically comes to around 13 m. Increasing both k and L together also increases the number of data points for dipole-dipole surveys. However, increasing k too much lowers the signal which can reduce the quality of results. This is especially the case with the dipole-dipole array because of the lower overall current. Increasing L slightly increases the depth of investigation but less than increasing k. Therefore, the density and resolution of data is increased by increasing L since the gap in depth between using $k = n$ and $k = n + 1$ is filled in.

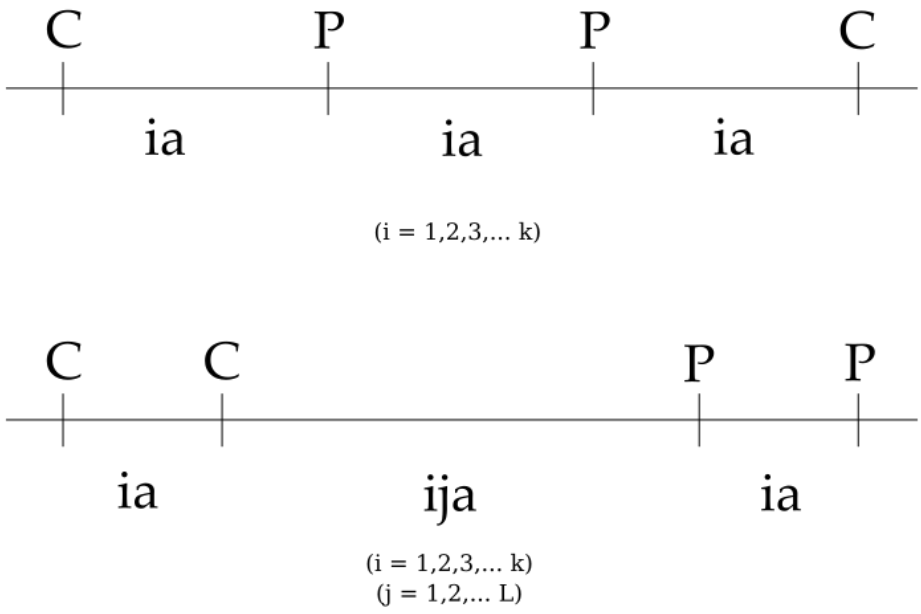

Figure 4.3: Diagram of Wenner(above) and dipole-dipole (below) arrays showing how parameters k and L affect array length. $i \in [1, k]$, $j \in [1, L]$ both natural numbers. By increasing these parameters, you increase the maximum possible length, and therefore depth, of the array.

The ERT data were processed using Boundless ERT (BERT) which is free/libre resistivity software. Lines were processed with the topography obtained from the survey positions obtained for every electrode using RTK GPS and a total station. These elevations were pasted into the correct data files (*.dat) generated by the configuration setup. Inversion of ERT data is highly dependant on geometry. Artefacts due to any deviation from flat

topography will be introduced into the results if it is not taken into account during inversion (Schmidt 2013, pp. 90–1). Because the ZZ acquisition software does not output the data in a format that is recognisable by third party inversion software, a python file had to be used to convert them into the format defined by Geotomo for their software Res2DInv which could be read (Geotomo Software 2019, pp. 13–8). The files were also manually expunged of outlier data points. As for the inversion process, most parameters were left as the default. In particular, the ratio of mesh discretisation size to electrode spacing at the surface was kept at 0.3 so that resistivity could be more smoothly modelled around the electrodes. For the modelling method, two approaches were taken. The first was to use the default L^2 norm and the default regularisation ($\lambda = 20$) in order to get a baseline smoothed image of the subsurface. The second approach was to use the L^1 norm by setting the parameters ROBUSTDATA and BLOCKYMODEL in the configuration file. This allows larger resistivity contrasts which should better model the boundaries between materials of very different electrical properties. The regularisation parameter was chosen by means of the L-curve which aims for an optimal compromise between model simplicity and fit (Günther 2004, pp. 21–23, Günther *et al*. 2006, p. 509). As indicated by Vogel (1996), some of the inversion models converged very slowly using the optimised regularisation parameter, taking well over a dozen iterations to reach the convergence criterion of $\chi^2 < 1$. The term χ^2, which estimates the fit of the model within the measurement errors, decreases each iteration and $\chi^2 = 1$ indicates a best fit within the input error level (3%) and input voltage error (100 µV) assumed by the program (Günther and Rücker 2019, p. 8). Under both inversion settings, the Jacobian matrix was recalculated in each iteration. This greatly increases the processing time but it is necessary for best results. One important parameter that was not used was z-weighting which controls the assumed vertical anisotropy of the model (useful for layered media) (Günther and Rücker 2019, p. 11). However, it wasn't clear how to choose an appropriate value without prejudicing the results and introducing artificial layers where there were none in the ground. Therefore, it was decided not to use this parameter. Finally, images of the completed results were saved for interpretation and comparison to other results. The colour scale used was "viridis" which is a perceptually uniform and continuous colour scale. This is important because discrete colour scales hide the true variation in the data and give dangerously false impressions of sharp boundaries where there may be none. Even in cases where there should be sharp boundaries, it is not known if they overlap with the boundaries generated by the colour scale unless a clever choice in cutoffs is chosen by analysing and clustering the data beforehand. Furthermore, most continuous maps are not perceptually uniform which means they have "plateaus" that group a large range under a perceptually indistinguishable colour and steep gradients where a lot of perceived change happens over a comparatively small range in the data (Bergman *et al*. 1995, Kovesi 2015). A perceptually uniform colour map solves this problem by plotting data as lightness rather than hue which is easier to interpret in data with high spatial frequency (Kovesi 2015, p. 5).

4.1.2 Ground-Penetrating Radar

During the 2016 field season to Soyo, an extensive GPR survey covering 42,000 m^2 (fig. 4.1) was done as part of Anthea Vella's masters thesis (Vella 2018). The survey was separated into several grids labelled A to F (fig. 4.5) beginning with grid A at the western end of the site where there is known to be archaeological material. The survey from there proceeded eastward until it reached a sand blowout. The lines in each grid were collected in a zigzag fashion whereby the first line was collected heading north, the second heading south, and so on. A 500 MHz Mala X3M antenna collected data with a 1.9 cm trace increment and 1024 samples per trace over a 75 ns two-way time window. Half a metre separated the individual parallel lines in every grid (Vella 2018, pp. 35–6). The use of a higher frequency antenna limits depth penetration but allows for higher resolution (Conyers 2013, p. 25) which was important for targeting thinner strata, especially any palaeosols.

Although several grids of GPR data were collected, only grid A had been previously processed and interpreted. With this thesis all grids have now been processed. Before importing the GPR profiles into Reflex, it was necessary to obtain topographic profiles to match each one. To do this, the DEM of the site was loaded into QGIS where a custom plugin was used to generate a grid of utm files by sampling elevation at the correct line spacing, trace increment and orientation. Only the four corners of each grid and the DEM raster layer itself needed to be provided. The output files were tab-delimited text files with the following fields: trace increment, northing, easting, elevation, utm zone. This format could be imported alongside the data files in Reflex using the WKSTRANS option. Further batch processing scripts (written in Python) were used to correct the orientation and numbering of lines where the acquisition or naming has been inconsistent (for example two adjacent lines collected in the same orientation).

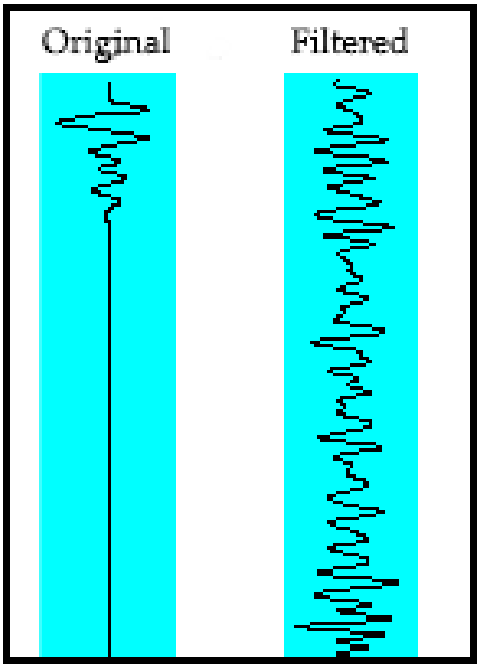

Figure 4.4: Example trace showing original versus after energy decay gain step.

The GPR profiles were processed in Reflex using time correction, dewow, gain function, bandpass filter and background removal steps. The same settings were used in each step for all profiles across the site to facilitate ease of processing. The values for parameters were chosen based on looking at many profiles in different parts of the site to determine the best choices overall. Although a careful approach of tailoring the processing steps to

Figure 4.5: Map of labelled GPR grids.

each line would naturally give better results, it was infeasible to do this over hundreds of lines. It was also unnecessary as the interest is in the broad stratigraphic trends rather than local stratigraphic variations. An average soil velocity of 0.12 m ns^{-1} was applied as a general value which was obtained by hyperbola fitting on many lines from different parts of the site. Doing a time correction is important in order to get accurate depths for features since the receiving antenna opens before the transmitting antenna. A point around where the ground wave first breaks was chosen as time zero because it was easy to identify by sight. This meant that 2.4 ns of time was taken off the beginning of every trace which, at a soil velocity of 0.12 m ns^{-1}, equates to approximately 14 cm of depth. Leaving this extra depth in could have made it more difficult to align the radar and stratigraphic profiles. The dewow step was done with a 2 ns time window in order to remove drift in the signal. Gain was achieved via an energy decay curve which is automatically calculated from a mean of every trace in the profile (Sandmeier 2020, p. 337). The amplitudes are then multiplied by a scaling factor which was chosen as 0.1 so that the maximum amplitudes all down the traces are contained within the possible integer range of the profile. The energy decay curve was chosen over other gain functions because it resulted in the most even amplitudes across the profile (see fig. 4.4). This made it so that reflections would not disappear and reappear and could be followed more easily. The relative amplitudes of reflections mattered less than being able to identify their extents. A Butterworth bandpass filter was applied to remove low and high frequency noise which would make it more difficult to interpret the profiles. The high and low cutoffs of 750 MHz and 200 Mhz were chosen such that the bulk of the main peak of the spectrum was included (fig. 4.6). The last processing step to be done was a background removal which was done in order to remove background noise. The average trace to be subtracted was taken over the entire profile so that only consistently horizontal banding would be removed and not any important reflections that happened to be locally horizontal.

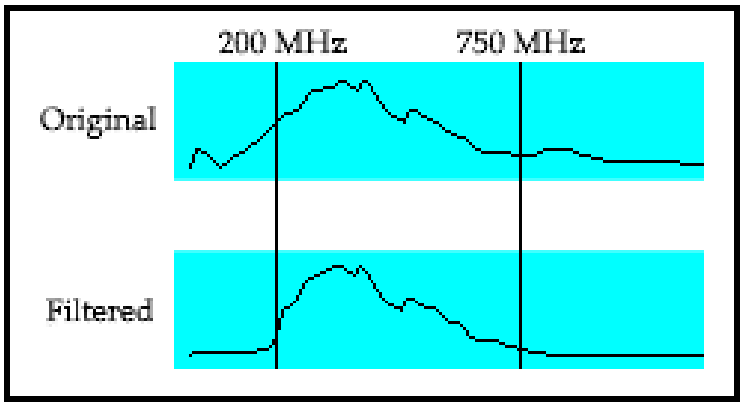

Figure 4.6: Example of fequency spectrum showing before and after a bandpass filter. 200 MHz and 750 MHz are shown in vertical lines.

After being processed, the profiles were "picked" which means identifiable boundaries as indicated by radar reflections were drawn over in Reflex. These picks were given different

codes according to their interpretation. They could then be exported as xyz data files and recombined into files that contained all xyz points in a grid for one pick code to give elevation models for each identified surface. However, only every fifth profile was included for picking due to the large scale of the survey and time consuming nature of the process. It was deemed unnecessary to have horizontal resolution of half a metre for a study of the broad stratigraphy across such a large area.

4.1.3 Magnetometry

A Bartington Grad 601 gradiometer was used in 2019 to map the magnetic landscape of Soyo. The survey was done as a series of 20 m ×20 m grids. The purpose of collecting these grids was to map areas where the magnetically enhanced soil layers were near the surface or outcropped and also to map potential areas of human occupation by identifying areas of burning. A recently built fence had cut off the western extremity of the site from easy surveying so the initial grids were placed on the east side of that fence about 40 m from the western edge of the GPR grids. From there, more were adjoined heading eastward until the last day of the trip whereupon they had extended 60 m beyond the last ERT and GPR lines, covering more of the sandy dune-blowout area (fig. 4.1). Within each grid the data was taken in a north-south zigzag fashion with 0.5 m between each transect and eight samples taken per metre. For the first three grids, a range of 1000 nT was used for the instrument but this was lowered to 100 nT for subsequent grids. The magnetic data was imported into the software program Snuffler for processing and exported as images in blocks of contiguous grids. Vertical and horizontal destripe filters as well as interpolation was used. These images were loaded into QGIS and georectified.

4.2 Photogrammetry

Although aerial photographs were taken by kite in 2016, many of these proved to be of poor quality or out of focus resulting in an inaccurate elevation model for parts of the site. Aerial photographs were retaken using a DJI Mavic Air drone in 2019 and combined into a 3D model using Agisoft's Metashape. Global positioning was incorporated from five known co-ordinates that were marked on the ground before taking the photographs. The photographs were first pruned of unfocused and poor quality images before being aligned into a sparse cloud which was then georeferenced using the five aforementioned known positions. High accuracy and no preselection options were used in order to increase the accuracy of the fit at the expense of time taken. The dense cloud was generated with the medium quality setting. Mild depth filtering was used as Soyo is a mostly open site with only a few scattered trees and, therefore, there is little in the way of abrupt elevation changes. Metashape allows for points in a dense cloud to be classified into user-defined categories. Two additional categories were created in order to classify river points and tree foliage points. These categories were taken out when creating the DEM as we are only interested in the land surface. The dense cloud (with all categories) was also used to make a 2.5D mesh and orthophoto. Both the DEM and orthophoto were exported as geoTIFFs

which preserved the global positioning information so that they could be combined with other survey data in a geographic information system (GIS). The orthophoto shows a rectified view of the surface which removes parallax so that the view is directly top down at every point. The effect is similar to a satellite image but at greatly enhanced resolution. Such a high resolution image of the site was necessary for identifying and tracing fine surface details such as outcropping of palaeosols and obstructions such as boulders and fences. The digital elevation model provides a topographic view of the site and was used for extracting elevation data for processing the geophysical surveys.

4.3 Stratigraphic Pits

Six stratigraphic pits and three excavation pits were dug in 2016 most of which were clustered at the western end of Soyo. The six stratigraphic pits combined with excavation unit six, were linearly aligned such that they lay along the length of one GPR profile (line 13 of grid A). This was so that the interpretation of the GPR in that location could be tightly constrained by observed geology. This interpretation would then be extended by correlating reflections between GPR lines (Clark and Bayarsaikhan 2016, Vella 2018, p. 38). To augment these, seven more stratigraphic pits were opened in 2019 to extend direct stratigraphic control over a larger portion of the site. Primarily these were in the sandy dune area west of a fenced enclosure comprising GPR grid B (fig. 4.1). Their locations were determined from a preliminary review of the GPR data and it was hoped that these pits would resolve some of the confusing reflections seen. A summary of the test pits is presented in table 4.1. In general the pits were one metre wide and one to three metres long. Depth also varied between 1.0-1.8 m. Three pits (TP01, TP02 and TP08) were excavated down until they hit a buried boulder. The other four (TP03, TP05, TP07 and TP14) were terminated either because the depth of the pit caused risk to the excavator or because of time constraints. Like in previous seasons each of the seven pits was logged. Stratigraphic units were identified based on visual appearance and their properties were recorded (grain size, sorting, angularity, colour and any other notable features). The depths of boundaries between each unit were measured from the top of the pit and all four walls were drawn to scale. At the end of the season, all of the pits were backfilled.

4.4 Sediment Analysis

In addition to the stratigraphic information obtained from the test pits, sediment samples were taken of each identified stratigraphic unit for a suite of sediment analyses. The purpose of these analyses was to increase the ability to correlate strata across different test pits and also to determine the environmental and depositional history of Soyo. The order of each analysis was performed was chosen to preserve the samples for as long as possible by doing non-destructive analyses before destructive ones.

Pit	GPR Grid	Depth (cm)	Area (m x m)
T1.2	A	150	0.5 x 0.5
T1.3	A	93	0.5 x 0.5
T1.4	A	86	0.5 x 0.5
T1.5	A	85	0.5 x 0.5
T1.6	A	83	0.5 x 0.5
T1.7	A	123	0.5 x 0.5
Unit 6	A	165	2.0 x 2.0
Unit 7	F	150	2.0 x 2.0
Unit 8	F	80	2.0 x 2.0
TP01	D	120	1.3 x 0.6
TP02	D	100	1.4 x 0.4
TP03	B	115	1.1 x 0.5
TP05	B	160	1.8 x 0.4
TP07	B	130	1.0 x 0.5
TP08	B	140	2.2 x 0.5
TP14	C	110	1.5 x 0.5

Table 4.1: Depth, area and general location of test pits from 2016 (top) and 2019 (bottom).

4.4.1 Magnetic Susceptibility

Magnetic susceptibility was the first analysis done so that the use of metal equipment for later analyses did not interfere with the magnetic properties of the sediments. Each sample typically weighed between 16 g and 24 g. A Bartington MS2B instrument connected to a laptop was used to record mass specific mass susceptibility and frequency dependence at 0.465 kHz and 4.65 kHz. Measurements were repeated until five reasonably concordant frequency dependence results were obtained. "Reasonably concordant" here means within the same order of magnitude. This was not always satisfactorily possible in the case of very low frequency dependence. However, the mass-specific susceptibility measurements were always reasonably concordant indicating that the differences between measurements at low and high frequency for many samples were too small to be accurately measured by the instrument. It was found that moving the instrument to the centre of the room away from electrical outlets and wiring, and especially ensuring the laptop's wireless network adaptor was disabled, helped tremendously in getting more consistent result. People taking phone calls and moving metal trolleys around in the room always necessitated a new measurement. The purpose of testing magnetic susceptibility and frequency dependence was to determine degree of pedogenesis and possible burning in the sample. Soil formation causes increased magnetic susceptibility as iron-bearing minerals are converted into magnetite. The intense heat from human burning activities increases this to a substantial degree as it allows for the more intense formation of highly magnetic magnetite and maghaemite (Clark 1996, pp. 100–1). Frequency dependence in particular allows for the better identification of human occupied surfaces as those tend to

accumulate very tiny superparamagnetic grains. Such grains display lower susceptibility under a higher frequency magnetic field (Clark 1996, p. 103).

4.4.2 Sieving

Next the sediments were sieved using a series of meshes ranging from 4 mm to 62.5 µm which were stacked on top of each other in order of coarsest at the top and finest at the bottom. The sequence of mesh sizes came in powers of two millimetres so that each fraction's grain size range was half of the previous in accordance with the Wentworth size classification of grain size (Boggs 1995, p. 81). The sediment sample was first lightly broken up using a mortar and pestle (being sure not to crush the sample) then placed into the top sieve. The entire stack was vibrated for five minutes to ensure all of the particles had been thoroughly sorted. Each fraction was weighed along with the total amount both before and after. A brush was used to sweep remaining sediment from the sieve to minimise sediment loss. The percentage loss of sediment was generally under 1%.

4.4.3 X-Ray Fluorescence

X-ray fluorescence was done using a Bruker Tracer 5i pXRF instrument to obtain the elemental composition of each sample. The samples were placed inside plastic bags to avoid contamination of the measurements. A calibration sample (OREAS 45d) was measured five times over the course of the measurements and one of the samples was measured thrice to determine how variable the measurements could be. The acquisition method used was GeoExploration 2020 which is designed for geological materials. The results were output as a spreadsheet containing the amounts (ppm) and errors for a wide range of elements ($Z \geq 12$).

4.4.4 Loss on Ignition

A small amount of each sample (10 – 15 g) was taken from each bag for use in loss on ignition. The sub-samples were placed into crucibles (fig. 4.7). Care was taken not to touch any of the crucibles with bare hands which would leave oily residues and reduce the accuracy of the results. Instead plastic tongs or nitrile gloves were used to handle them. Because the crucibles could not be labelled, it was necessary to organise them into a grid and record the location of each relative to the back of the oven. The loss on ignition procedure was broken up into three stages. The samples are first heated to 105 °C for 12 hours in a forced convection oven, then to 550 °C for four hours, and finally to 1000 °C for two hours in a programmable muffle furnace. These steps were chosen in order to ascertain the dry weight of the sample, the weight of organic carbon material contained and the weight of inorganic carbonates contained respectively. Measurements of the weight of the sample plus crucible were made before and after each step as well as the empty crucible at the beginning. All weights were measured without the crucible lid.

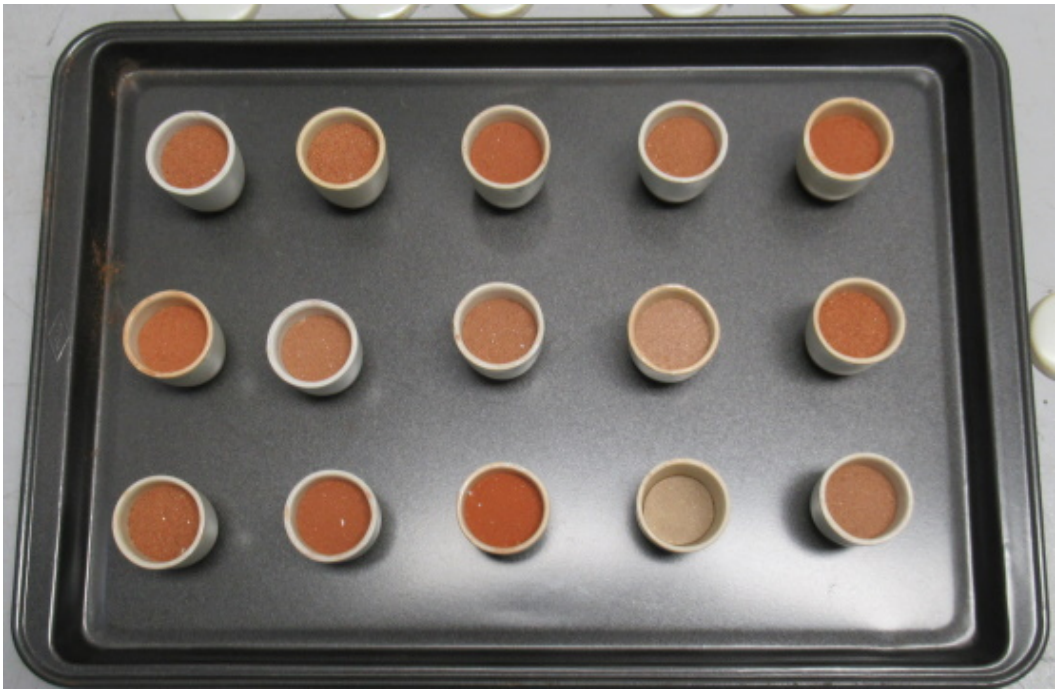

Figure 4.7: Image of sediment samples after LoI treatment.

4.5 Geopositioning

Positioning at Soyo was done using a Leica total station and Emlid RTK. When the total station was used, it was resectioned off the RTK base station locations. The start and end points of every ERT line was decided in advance in order to cover the same area as the GPR survey. These points were found in the field using the RTK. As each ERT survey was being conducted, a position was taken at every electrode for more accurate positions and so that elevation data could be obtained for the inversion process. The magnetometry grids were constructed in an *ad hoc* way using tapes to cover approximately the same area as the ERT and GPR surveys. The co-ordinates of the grid corners were collected as well as the corners of each test pit and other notable features at the site. Co-ordinates from the RTK were output in WGS84 in the UTM 47N projection which was used as the project co-ordinate system throughout the data processing. The geographic datum used in Mongolia is Monref 97 which is based on WGS84 with a UTM projection. However, elevations are still done under the old System 42 Baltic datum (Mugnier 2003). Therefore, we used GNSS elevations which had to be corrected for geoidal separation after the fact. Afterwards, the points were imported into QGIS along with the orthophoto and DEM of the site so that inconsistencies in naming could be fixed and stray or wildly incorrect data points could be removed. Positioning data inherited from the 2016 field season was taken using a CHCX90+ Static GPS for control points and post-processed by AUSPOS (Vella 2018, p. 37).

4.6 Radiocarbon Dating

Carbon dating was used to give chronological control to the stratigraphic layers. Carbon samples ($N = 23$) were retrieved from most test pits in 2019. The vast majority of these were of charcoal or wood. Seven of these – collected from four pits – were selected for AMS carbon dating on the basis of being at or below the most recent palaeosol to minimise the risk of dating modern samples and contamination from modern roots (table 4.2). Furthermore, these samples would have the greatest potential to address problems with previous dating of the site in 2016. Twelve bone samples had been collected from a single excavation unit, of which nine underwent AMS dating, but the results encompassed a bigger age range than expected (Vella 2018, p. 53). The 2019 collection aimed to confirm the previous results and resolve the chronology in more detail. The samples were sent to Australia's Nuclear Science and Technology Organisation (AP12910) where they were cleaned with a scalpel and checked for rootlets. An acid wash of 2 mol L^{-1} HCl at 60 °C was done for over an hour to dissolve carbonates and fulvic acids followed by repeated alkali washes of NaOH until all humic acids had been dissolved. The samples were then put back into 2 mol L^{-1} HCl to remove any CO2 that may have been absorbed during treatment. Finally, the samples were freeze dried and converted to graphite using the H_2/Fe method. This process converts CO_2 to graphite by the following equation (Vogel *et al*. 1984).

$$CO_2 + H_2 \xrightarrow[600°C]{Fe\ catalyst} C + 2H_2O$$

Pit	Unit	Depth (cm)	Weight (g)	Material
TP03		83	0.43	Charcoal
TP08		68-73	4.08	Charcoal
TP08		81-100	0.43	Charcoal
TP08		100-120	0.43	Charcoal
TP14		60	0.97	Charcoal
TP14		75	0.45	Charcoal
TP02		68/89	0.33	Wood

Table 4.2: Carbon samples taken from test pits during the 2019 field season at Soyo.

Once the final results had been reported, they were calibrated using the R package "rcarbon" with the IntCal20 calibration curve.

Chapter 5

Results

5.1 Photogrammetry

The two products obtained from photogrammetry using Agisoft's Metshape were an orthophoto and digital terrain model (DTM) of the part of Soyo that has been surveyed under this project to date. Both were exported as georeferenced TIFF files. On the orthophoto it is possible to see both fine details on a scale of centimetres (each pixel is 1.5 cm across) and thus how the surface features change across the whole site. Two areas of significant sand coverage dominate the western and eastern ends of the site. Both have erosional escarpments that reveal palaeosols. These zones of bare sand are partially ringed with marginal bands of patchy tussock grass in sand which give way to turf. Towards the north and east of the rectangular enclosure that sits in the middle of the site, there extends a field of boulders in varying degrees of submersion below the ground. The site is flanked on the north by the Hog River and on the south by a lateral moraine with exposed boulders and scree.

Looking at the DTM (fig. 5.1), it becomes clear that the axis of the site, in terms of topography, runs from East to West. There is an elevated ridge through the middle which slopes down to the river on its northern side. On its southern side, a slight decrease in elevation (up to a metre) sits between the ridge and the southern lateral moraine. At the western and eastern ends the elevation changes more drastically due to the mobile dunes and erosional escarpments that lie there.

5.2 Surface Geology

The orthophoto was used as the basemap for most of the geographic data interpretation and presentation in QGIS because it makes visible the surface features of Soyo. The surface of the site is divided into a few geological facies which are shown in the surface geology map in figure 5.2.

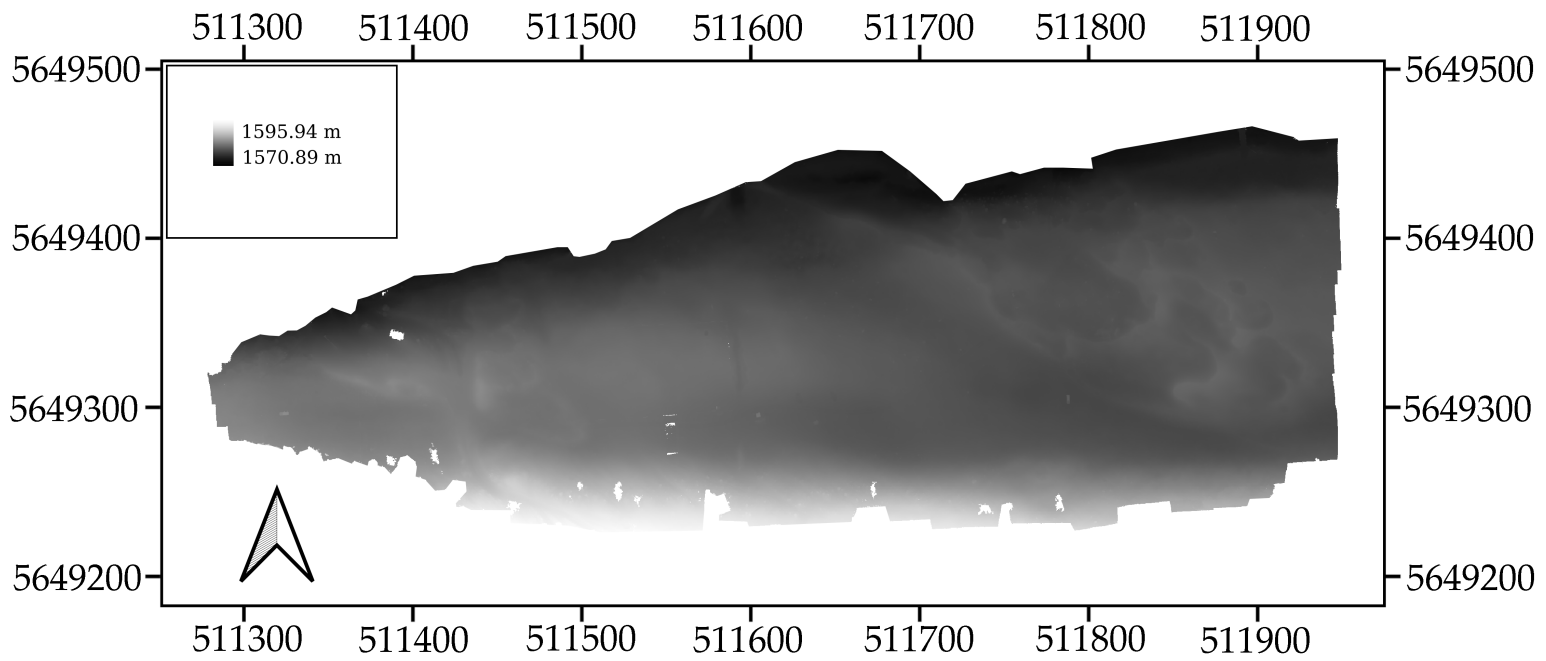

Figure 5.1: Digital terrain model of Soyo.

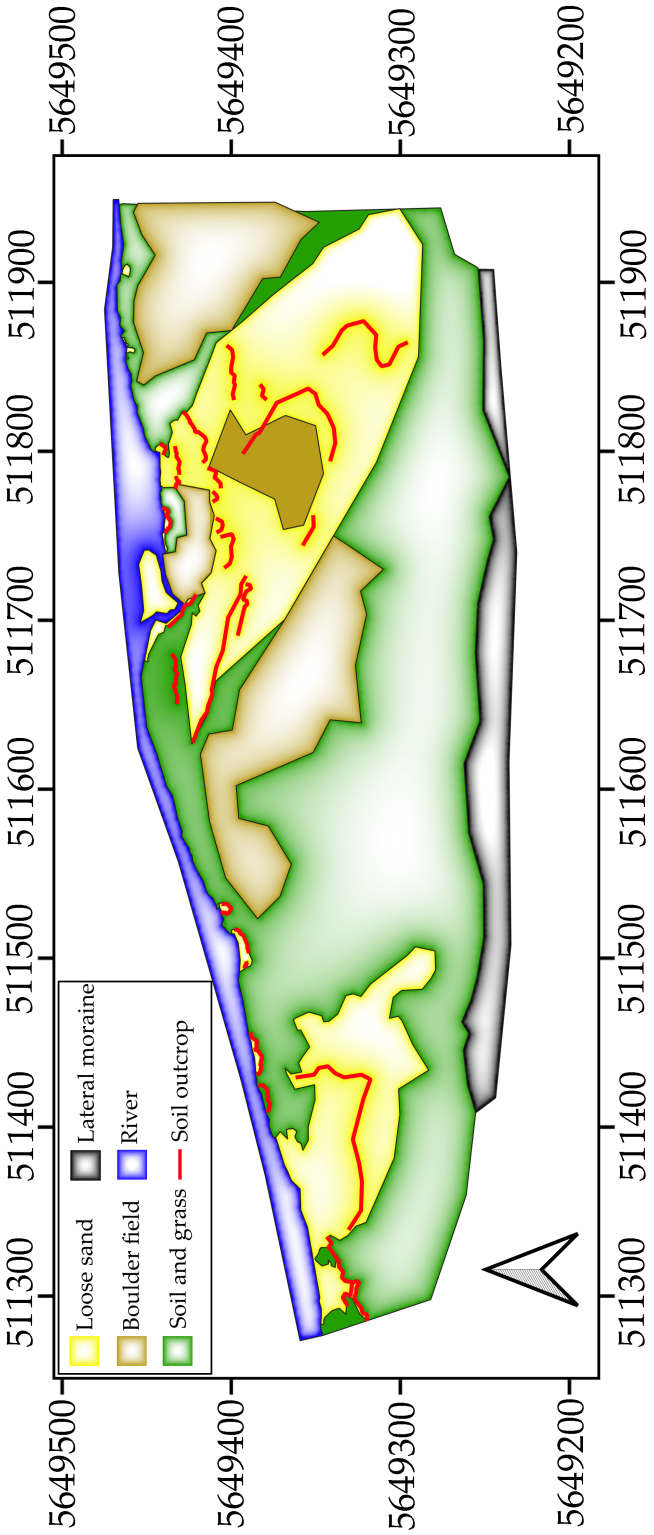

Figure 5.2: Surface map showing the extent of the different geological facies at Soyo.

First, the site is bounded on the southern side by a lateral moraine (over 15 m high as seen from the modern topograpy) and associated scree. The moraine extends from Soyo Hill (just off the map to the southwest) eastward. Much of the moraine is capped by soil and grass but there are many boulders protruding through the ground surface and collected at the bottom of the slope. On the northern side lies the River Hog which exits the Sayan Mountains and winds its way within the glacial moraine valley. The bed of the river is made of pebbles and sand.

There are two large regions of loose sand at Soyo. At the western end, the sand forms a series of dunes. These dunes have patches of tussock grass growing around the margins. To the North of the dunes is loose, eroded sand extending downslope to the river. The eastern zone of loose sand covers the majority of the eastern third of the site and is mainly exposed by blowouts and erosion. Loose surface sand also occurs in several small beach coves along the river bank as well as on islands in the river.

A great number of exposed soil and palaeosol outcrops are associated with the areas of loose sand. The western sands host one line of exposed palaeosol which divides that patch of sand in half. It extends broadly east to west but curves around northwards to the river at its eastern end. At the western extremity of this unit, there appear to be two palaeosols close together. The eastern zone of sand is riddled with multiple palaeosol outcrops and it is not clear how these relate to each other. They may represent either two or three horizons. Along the river there are multiple small erosional exposures which are from the modern surface soil being eroded into the water.

The boulder field is extensive across the eastern half of Soyo. There are four main subfields: one lies within the eastern blowouts, one wedged between the northern blowout margin and the river, and one each to the east and west of the blowouts. The boulder field is situated on the northern margin of the south bank where the terrain slopes down from the elevated part of the site to the river. It also lies to the east of the elevated central portion of the site. Grass grows between the boulders throughout the field.

The remainder of the site is covered by soil in which grass is growing. This is concentrated mainly in the central region of Soyo and along the the moraine and river margins. Where this soil coverage meets the bare sand, there is often a transition zone of patchy tussock grass. At the western end of Soyo and along the river, the grass is a deep green but it takes on a bluish hue in the centre, along the moraine and within the boulder field.

5.3 Geophysics

5.3.1 Electrical Resistivity Tomography

The resistivity survey covers the approximate area of the other geophysical surveys. Each profile was taken with both the Wenner and dipole-dipole arrays and were processed us-

ing the L^1 and L^2 norms using BERT. See Section 4.1.1 for further details. All of the L^2 norm inversions completed within the maximum set iteration limit (almost always after four or five iterations) and so for all of these models the iterative change in the objective function to be minimised has reached a suitable small percentage ($\Delta\Phi < 2\%$). The two exceptions were Wenner lines 15 and 16 which terminated inversion because they reached a χ^2 error value of less than one. Because of this, most of the L^2 inversions have larger χ^2 values than the L^1 inversions. This is usually around one to five but extremely high values do occur such as 130.60 for Wenner line 5. For the L^1 norm inversions, the process in some cases reached the maximum set number of iterations (20) and so some of the results have higher than desired χ^2 errors but much less than for the L^2 inversion. In particular, for the dipole-dipole inversions, line 18 ($\chi^2 = 1.65$), line 19 ($\chi^2 = 1.27$), line 22 ($\chi^2 = 1.07$) and line 23 ($\chi^2 = 1.19$) had values greater than 1.00. For the Wenner inversions, line 2 ($\chi^2 = 1.17$), line 5 ($\chi^2 = 5.60$) and line 18 ($\chi^2 = 1.16$) had large errors. The χ^2 values for every inversion can be seen in table 5.1.

Three main facies of resistivity are made apparent. The underlying basal facies of the site is highly resistive (3000-10,000+ Ωm) with an irregular geometry. That is to say, this facies does not have a flat upper boundary and it does not usually extend across the whole North-South width of Soyo but is instead bounded laterally (see fig. 5.3). In some places it also seems as if there are deep channels (several metres deep) cut into this facies but these do not line up from profile to profile (see fig. 5.4 for example). The upper boundary lies at a depth of at least 2-3 m and often deeper. The lower boundary is not visible and the facies extends at least 10-15 m below the modern surface. A moderately resistive (1000-3000 Ωm) facies sits on top and around the first. In some lines the boundary between the basal high resistivity facies and the moderate resistivity facies is sharp and in other lines the boundary is gradual. There does not seem to be any systematic distribution to this difference. The upper boundary of this facies is much more level that that of the deeper, resistive facies and usually follows the topography at a depth of 2-3 m. The third facies has the lowest resistivity (300-700 Ωm) and blankets the site. It is nearly always distinguished from the other two by a sharp boundary. It was expected and initially thought that the highest resistivity facies would correspond to underlying coarse glacial till deposits and that the low and medium resistivity would represent different sedimentary units on top of that. However, after a comparison of the available data sets, it was judged that the glacial till is actually represented in the medium resistivity facies and that the highest resisitivty probably represents a deeper bedrock. Therefore, almost the entire package of overlying sediments at Soyo is contained within the lowest resistivity facies. This interpretation is further elaborated on in section 6.3.1.

The distribution of resistivity values can be seen in fig. 5.5. The exact values were extracted from the inverted L^2 data. This plot suggests that there is a normally distributed subset of the data (transformed with the natural logarithm) with a mean resistivity of about 6.35 (570 Ωm) and standard deviation of approximately 0.6. The frequency of values in this

Line	L^2 Wenner	L^2 DpDp	L^1 Wenner	L^1 DpDp
0	2.44	0.98	0.88	0.45
1				
2	3.26	4.28	1.17	0.74
3	2.74	3.54	0.70	0.82
4	2.77	20.20	0.98	0.94
5	130.60	2.47	5.60	0.52
6	1.80	2.53	0.96	1.00
7	2.63	5.03	0.83	0.95
8	2.37	4.77	0.89	0.97
9	3.29	10.81	0.95	1.00
10	4.41	15.45	0.97	1.00
11	2.74	6.92	0.94	0.99
12	3.35	13.90	0.88	0.94
13	2.35	16.28	0.98	0.99
14	2.41	6.23	0.87	0.98
15	0.74	1.73	0.63	0.61
16	0.98	26.50	0.48	0.94
17	1.68	4.85	0.97	0.91
18	7.35	19.00	1.16	1.65
19	5.95	11.23	0.99	1.27
20	1.97	5.33	0.99	0.98
21	1.53	4.98	0.52	0.91
22	2.69	7.46	0.96	1.07
23	3.57	8.37	0.98	1.19
24	2.58	5.52	0.96	0.86
25	1.65	4.91	0.80	1.02

Table 5.1: Table of ERT inversion errors.

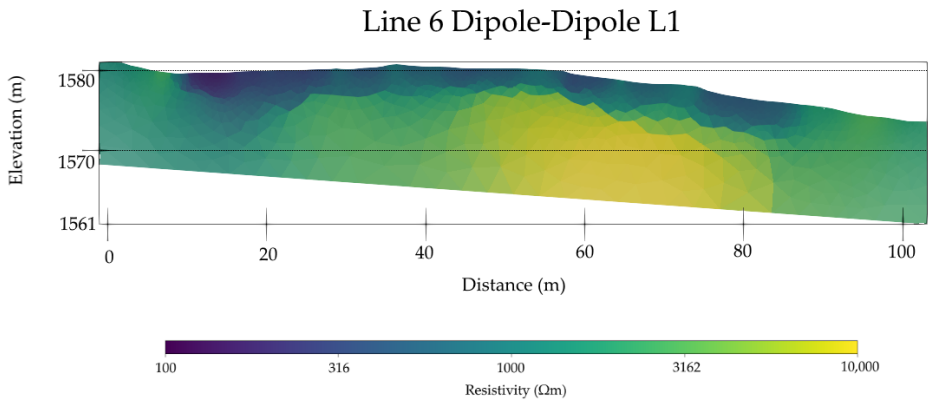

Figure 5.3: ERT line 6 dipole-dipole L^1 inversion.

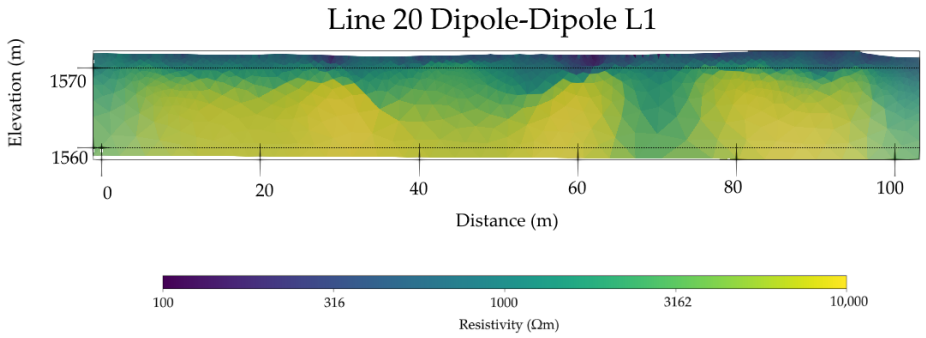

Figure 5.4: ERT line 2 dipole-dipole L^1 inversion showing presence of channel at 70 m.

range is disproportionately high compared to the low area taken up by such low resistivity cells on the inverted profiles because the mesh grows in cell size with depth. Therefore, there are many small cells near the surface with lower resistivity and comparatively few deep cells where the highest resistivity was located. This makes it difficult to discern if there are any further categories distinguishable solely from the distribution of resistivity values. However, the moderate facies was distinguished from the highly resistive one in order to characterise the morphology of the resistivity changes in the ground. The highest resistivity areas appear as ”blocks” within moderate resistivity surrounds in many lines but only under the L2 inversion (see fig. 5.6 for an example).

The differences between the results for the L^1 and L^2 inversions is showcased for line 11 in fig. 5.7. All four show the same approximate situation. There is a basal layer of a few to several thousand ohm-metres resistivity. This layer is at its most resistive in a zone at x = 65 m to x = 85 m. On top of this sits a layer a few metres thick of sub-1000 Ωm. The

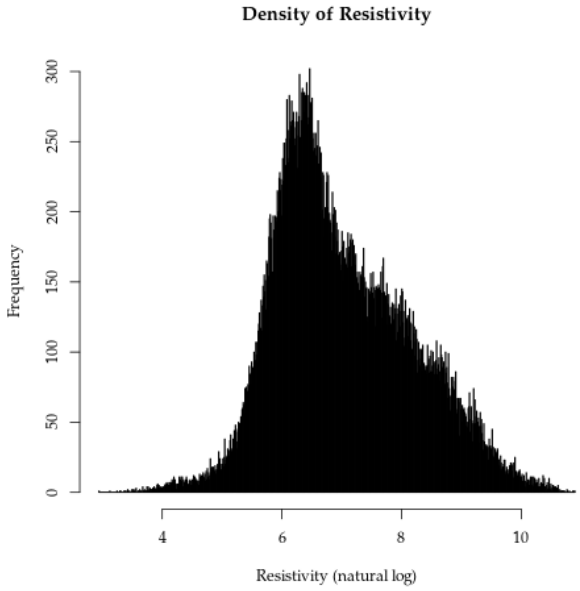

Figure 5.5: Histogram showing the frequency of log resistivity values for ERT at Soyo.

sharpness of the resistivity facies boundaries in the two L^1 inversions is the salient differentiating feature. This is due to the use of the L^1 norm during inversion which allows for steep changes in resistivity between neighbouring cells. This allows for greater confidence in identifying geological boundaries in the ground. However, the L^2 dipole-dipole inversion contains information that the other three do not. Particularly, a series of round features of about 2000 Ωm within the low resistivity facies. This feature is present in many of the other L^2 dipole-dipole inversions but not on the L^1 dipole-dipole inversions. This many be because of the use of the BERT inversion parameter ROBUSTDATA=1 which may reduce resolution in the inverted profile (Günther and Rücker 2019, pp. 10–1). Another feature in the L^2 dipole-dipole inversion is the apparent change in the resistive facies at x = 60 m. This is indistinct in the L^1 inversion and not present in the two Wenner inversions which is unsurprising since the Wenner array is ill-suited for defining vertical features. However, they do display a general zone of moderated resistivity in the middle section of the profile (40-60 m). In general, these differences between the inversions are replicated in other lines. In the end, the dipole-dipole array (and particularly the L^1 inversion of such) was used for the interpretation of the electrical model of the ground at Soyo. This is because of its visibly higher resolution so that smaller features are visible and its lower errors as seen in table 5.1. The L^1 inversion was especially relied on because of the sharper and more distinct boundaries between resistivity facies it allows. It is expected that this will be more useful for the interpretation of stratigraphy at Soyo since the stratigraphic units in a glacial setting will contain varying amounts of gravel and boulder sized clasts that will affect the bulk resistance of the ground. This means it would be expected that resistivity should change dramatically and (relatively) sharply across stratigraphic boundaries rather than over a gradual gradient.

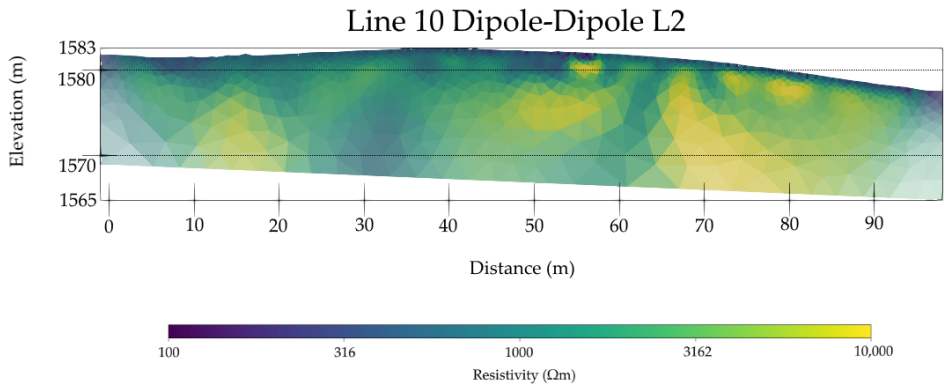

Figure 5.6: ERT line 10 dipole-dipole L^2 inversion.

5.3.2 Ground-Penetrating Radar

The GPR profiles reveal several recurrent features. These are later associated with a Greek letter coded stratigraphic scheme in Chapter 6 with α at the top of the sequence and η at the bottom. A schematic representation of this, along with the sedimentary interpretation of the facies that will be reached, is available in fig. 5.8 to orient the reader for this section. One of the most prominent is a strong, mostly unbroken reflection that is present in grids A and B which are to the west (see fig. 4.5 for locations of GPR grids throughout this section). The feature corresponding to this reflection (labelled gamma) is buried up to a metre underneath the modern surface for much of the length of each GPR profile but emerges at the surface where the palaeosol outcrops on the slope down to the river. This reflection is easy to track between GPR lines and decreases in depth until it disappears into the ground wave towards the eastern extremity of grid B. This reflection is highlighted in purple in figs. 5.9 and 5.10. Further GPR lines are given

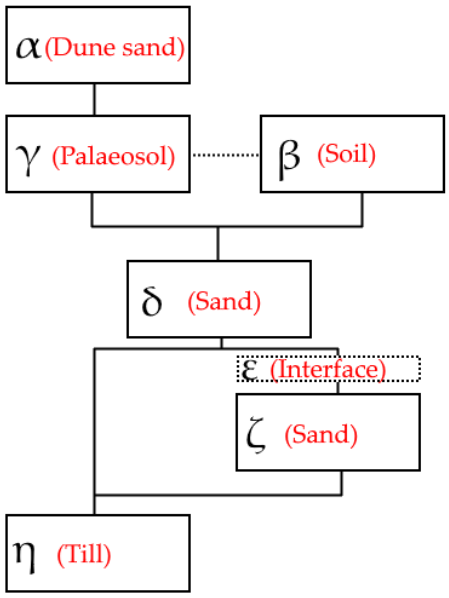

Figure 5.8: Harris matrix of the stratigraphic scheme derived from the GPR and sediment analysis along with the basic interpretation of each unit.

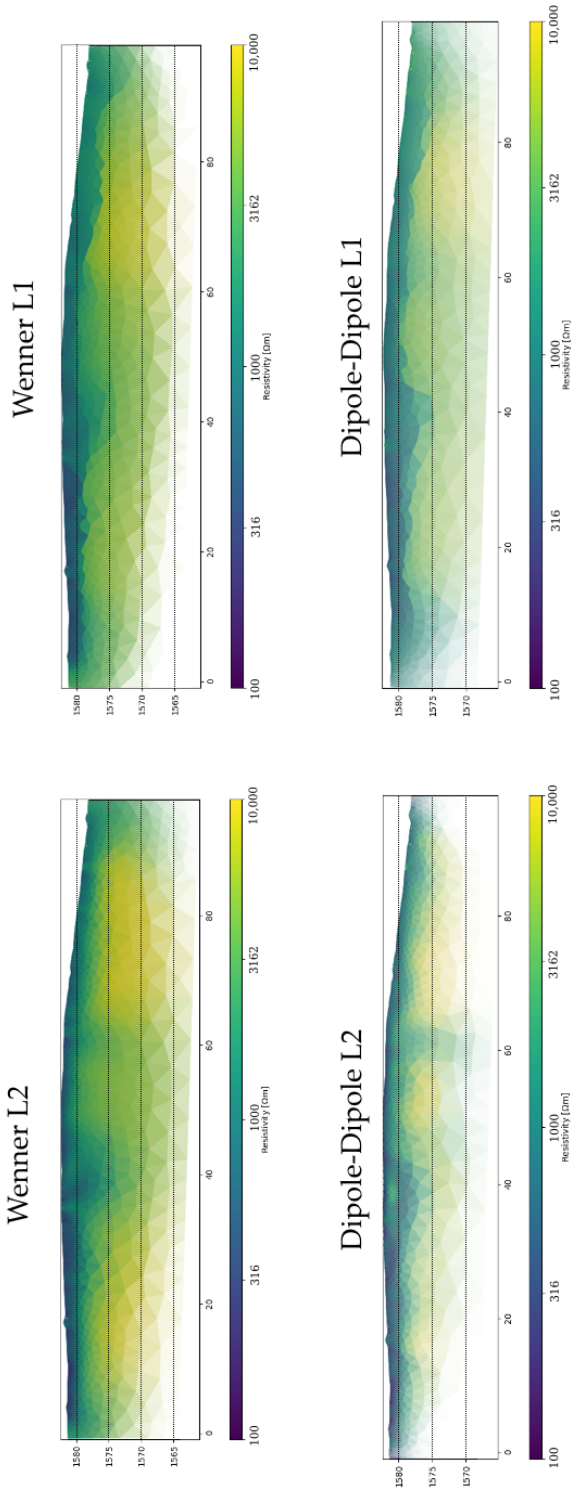

Figure 5.7: Comparison of ERT inversions using line 11.

in appendix B. In the subsequent grids to the east, it was possible to follow a related reflection (fig. 5.11) which is identified as marking the lower boundary of this feature (now the soil on the surface) and the top of the next feature below. This reflection covers most of the central portion of the survey area but becomes less represented in the boulder field and terminates before the eastern blowouts.

The isopach map for the deposit of sand above this feature (called alpha) can be seen in fig. 5.12. Isopach maps show the variation in thickness for a stratigraphic unit. In this thesis, "thickness" means vertical thickness so that the isopach map is the elevation map for the top interface minus the elevation map for the bottom interface of a stratum. The isopach map for unit α shows that the thickest part of the sand overburden corresponds to the dunes which are visible on the surface with a maximum thickness of 1.6 m on the central, round dune (about 17 m by 25 m across) and 1.3 m on the elongated dune (70 m long) to the west. Another area of greater thickness was on the southern margin (74 m long) at the base of Soyo Hill where the thickness increases to at least 1.4 m. The areas of lowest thickness were around the northern edge where the thickness was a few centimetres thick at most. This corresponds to where the palaeosol had been exposed on the surface and was eroding away. Where the lower boundary of the gamma unit was identifiable, the thickness between that and the modern surface was uniformly 30-40 cm (fig. 5.13).

The most prevalent feature across all GPR grids was a mass of broken reflections and hyperbolae (labelled eta). This is marked in blue in figs. 5.9, 5.10 and 5.11. This occurred below almost all other reflections at a depth of around one to two metres in grids A and B. This depth reduces to half a metre or less by grid F. Therefore, the layer of material above this feature becomes less thick heading east. In some places, it protrudes through the overlying layers as seen in fig. 5.10. Another change that occurs is that in grid A and part of grid B, this feature does not underlie the entire length of the GPR line. Instead there is a large gap in the southern half of the line which separates the two sections of this feature. This gap disappears elsewhere in the site.

The entire thickness of all the sediments overlying this reflection eta (fig. 5.14) decreases from west (up to 2.2 m beneath the dunes; typically 0.7-1.5 m elsewhere) to east (typically 10-50 cm). These lowest easterly values correspond to the boulder field regions. There is a substantially thicker strip of sediment between the two main fields covered by the GPR survey (1.0-1.5 m).

The thickness of the sediments between eta and gamma (including the latter) is lowest to the west in the range of 10-50 cm (fig. 5.15). This rises to about 60-120 cm on average further east (a distance of about 150 m). There are multiple dark and light features (a few metres across in size) which correspond to abrupt and limited changes in thickness. This

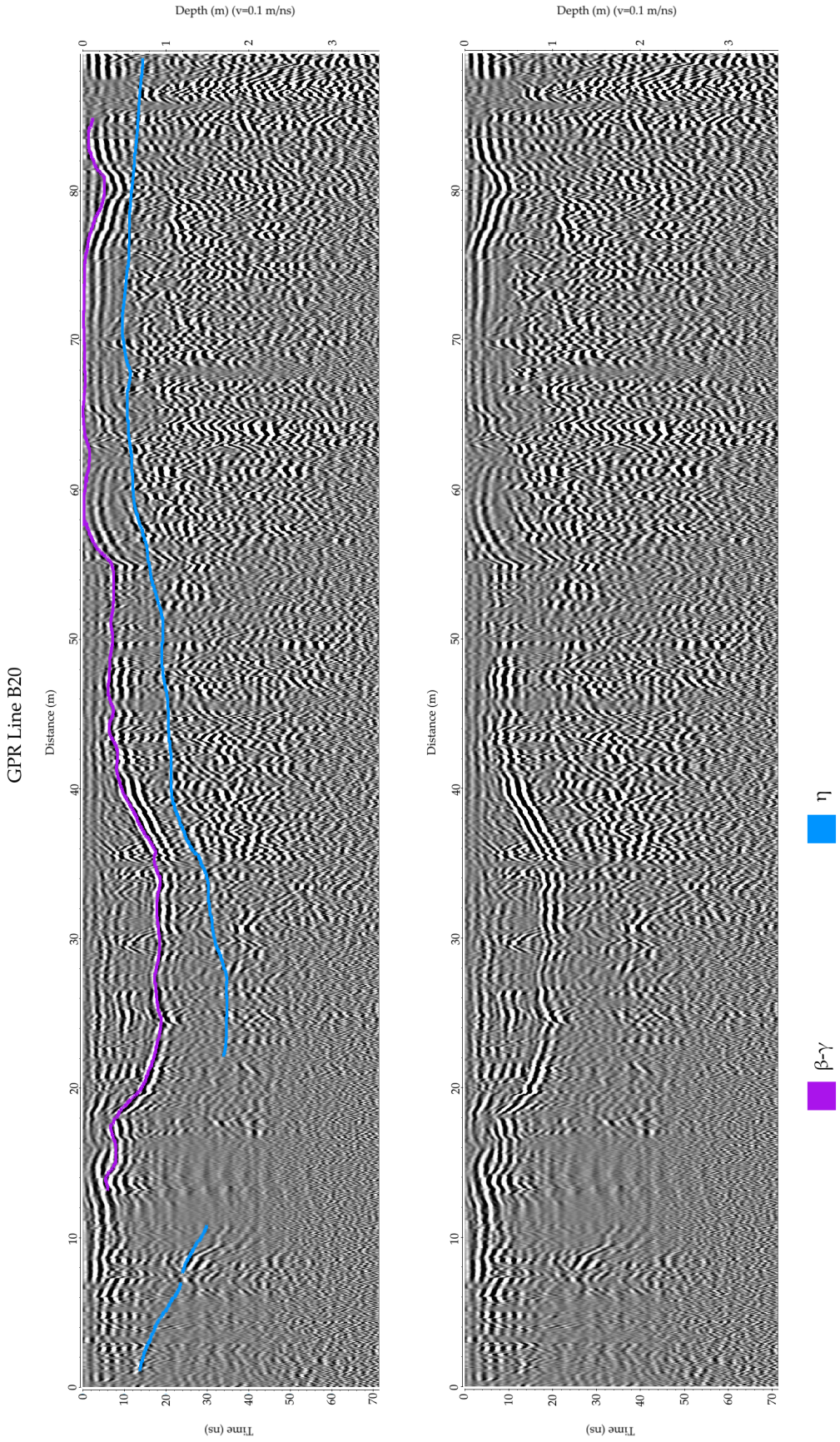

Figure 5.9: GPR grid B profile 20 showing gamma (palaeosol) reflection in purple and eta (till) reflection in blue.

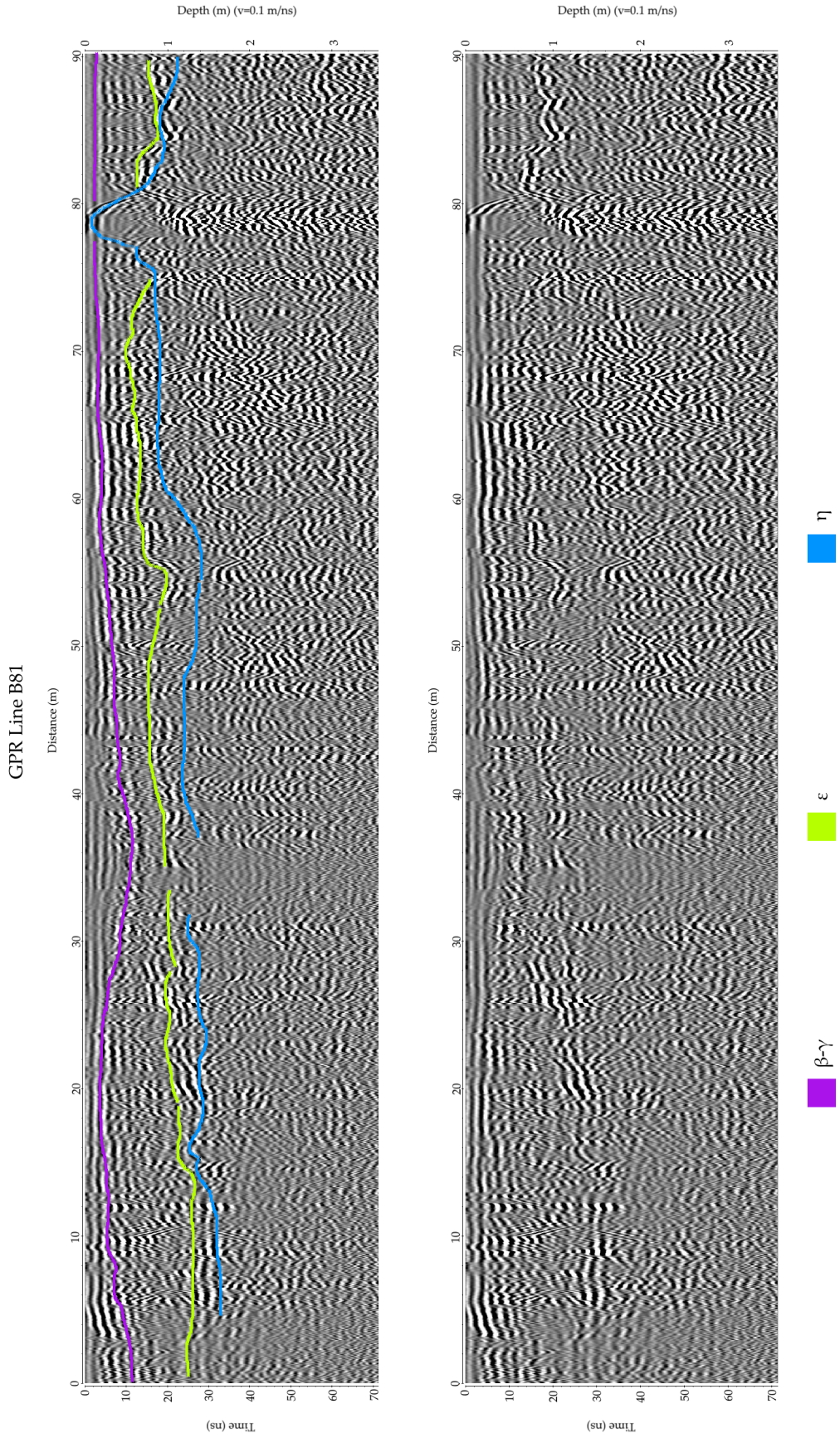

Figure 5.10: GPR grid B profile 81 showing gamma (palaeosol) reflection in purple, eta reflection in green and eta (till) reflection in blue.

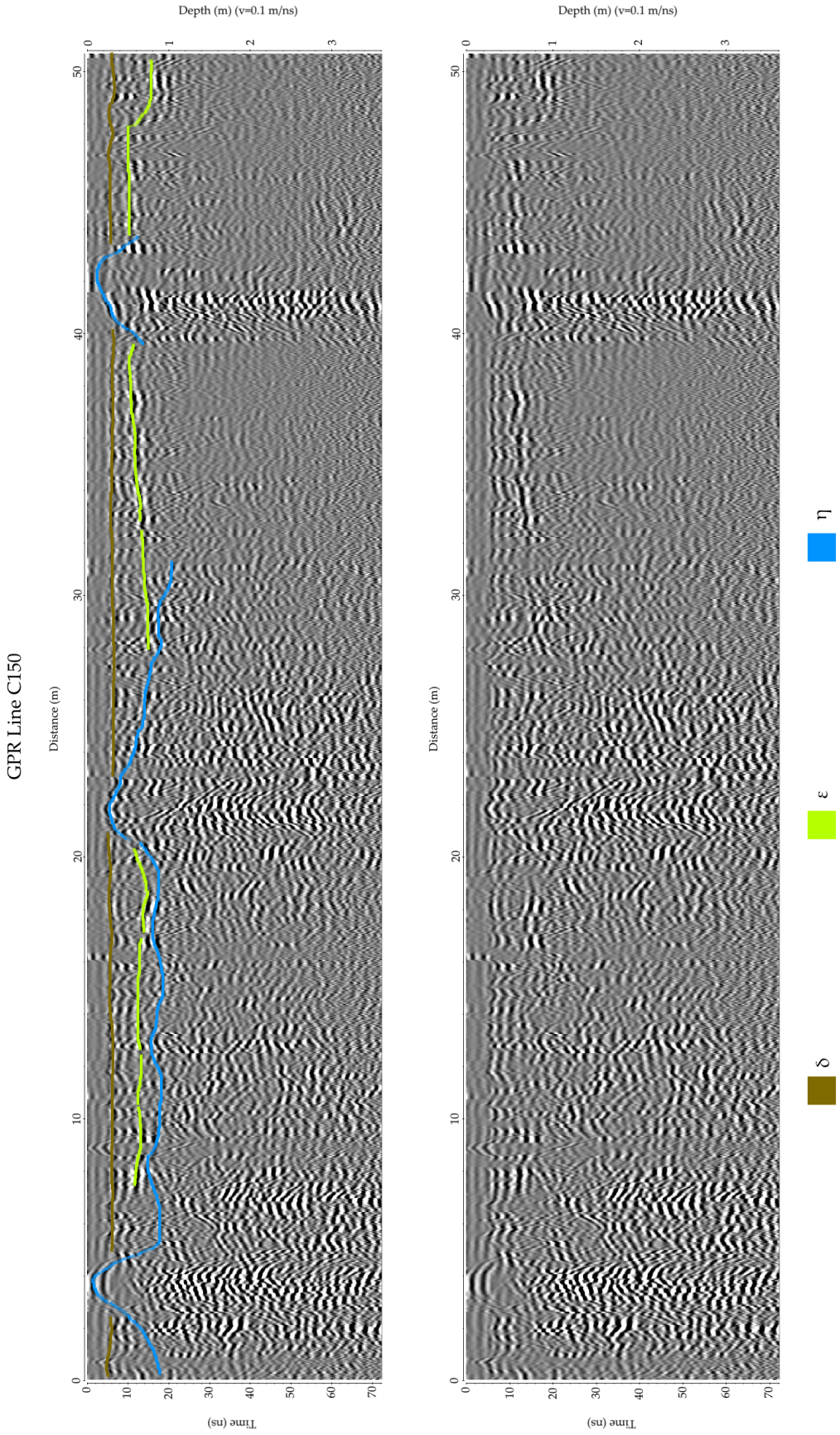

Figure 5.11: GPR grid C profile 150 showing delta reflection in brown, eta reflection in green and eta (till) reflection in blue.

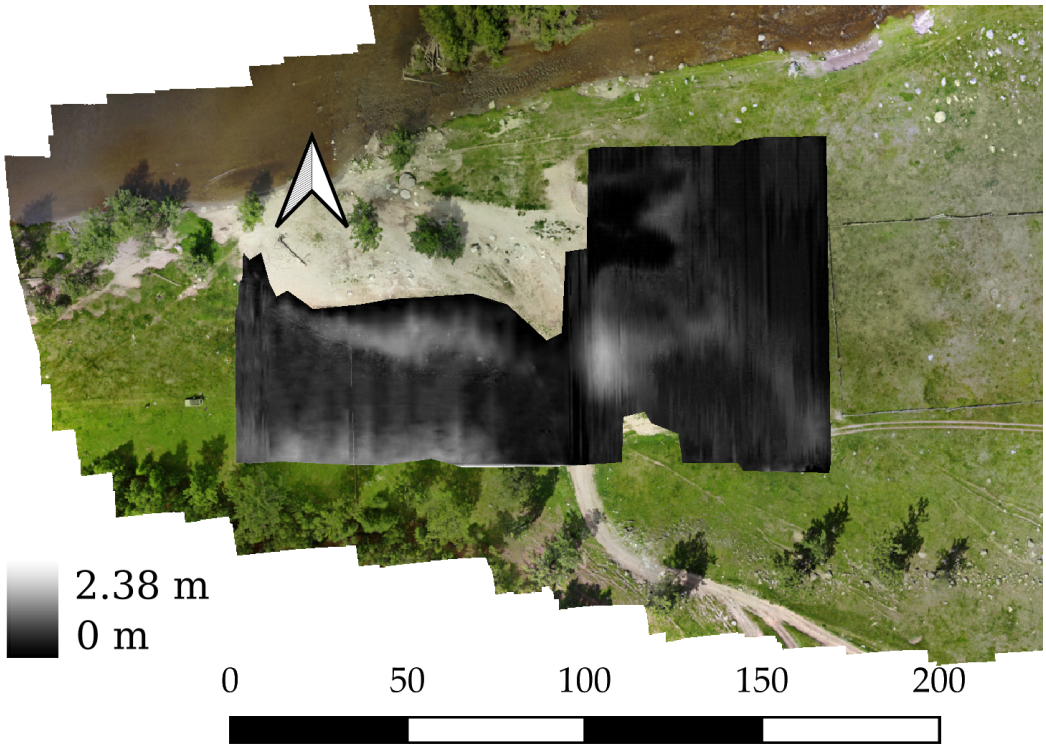

Figure 5.12: Isopach map of alpha facies.

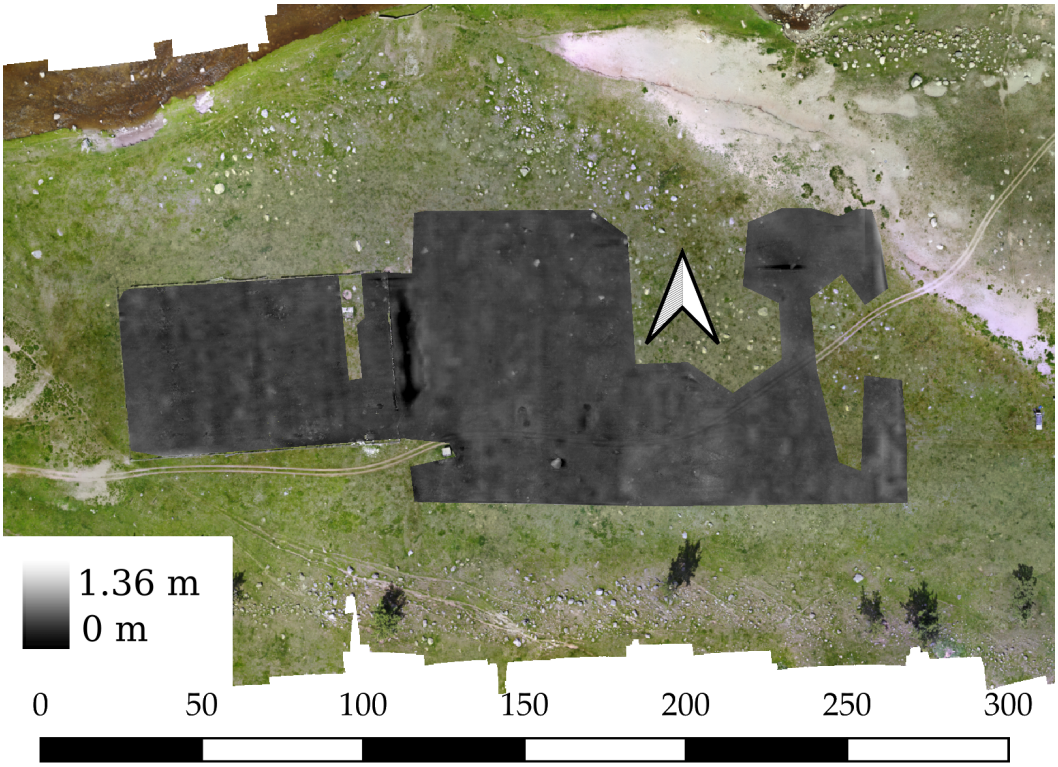

Figure 5.13: Isopach map of surface soil facies.

Figure 5.14: Isopach map of all sediments overlying eta facies.

is due to changes in the topography of the eta unit surface.

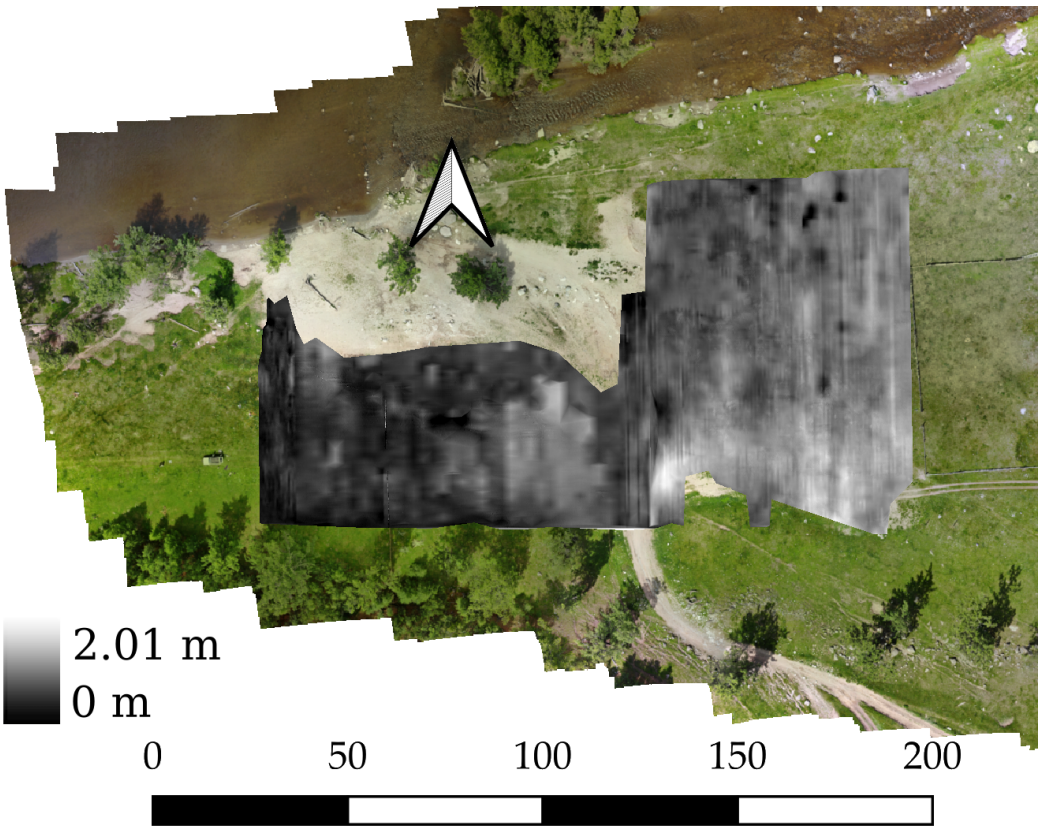

Figure 5.15: Isopach map of Sediments between gamma and eta reflections.

Moving to the east, the thickness of sediments between eta and the bottom of the gamma unit begins at around 60-130 cm in the area immediately adjacent to the thickest part of the previous isopach map. This steadily declines to the east (over a distance of approximately 200 m) until the thickness is reduced to 0-10 cm at which point the unit has tapered out (fig. 5.16).

Another reflection, which is constrained to grids B and C in the middle of the survey area, is labeled as ”epsilon” (see figs. **??** and 5.11). It generally sits between 0 cm and 50 cm above the eta facies and is 140 m long and 95 m at its widest point. This reflection divides the sediments that lie between the gamma and eta facies into two. The upper is called delta while the lower is called zeta.

The thickness of the delta facies is slightly higher to the west at 30-70 cm (increasing to 140 cm at the southern margin of the survey area). At the eastern end of GPR grid C, the thickness decreases to a range between 0 cm and 60 cm (fig. 5.17).

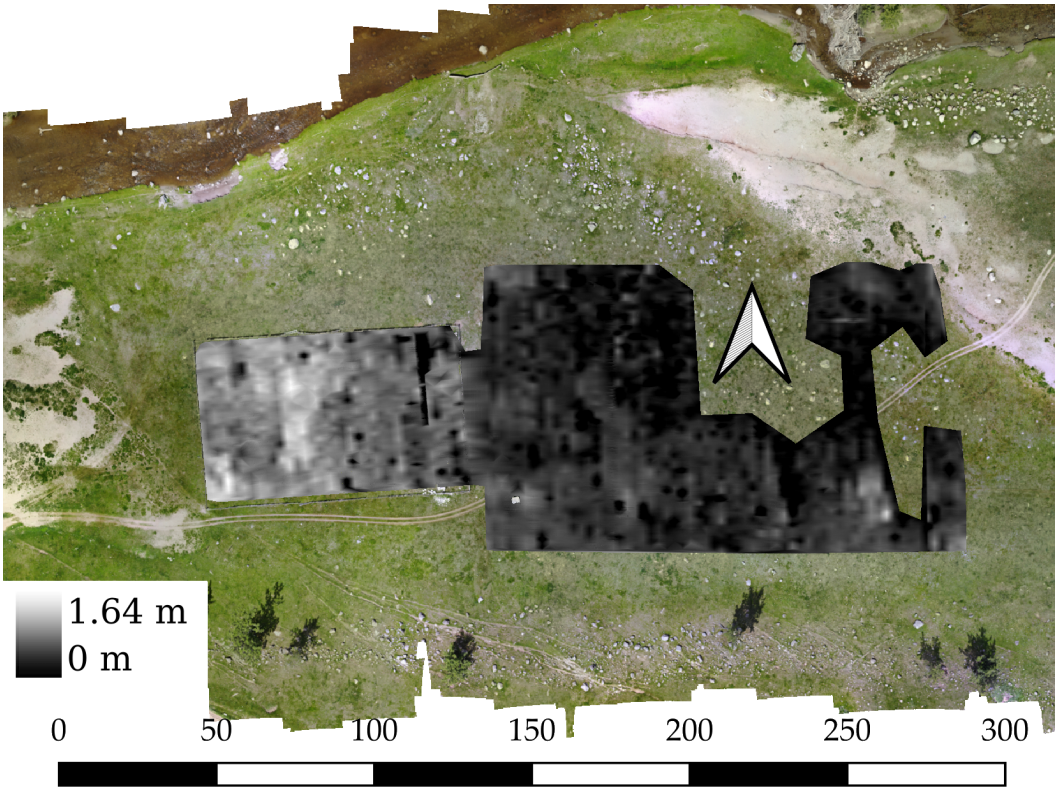

Figure 5.16: Isopach map of sediments between the surface soil and the eta facies.

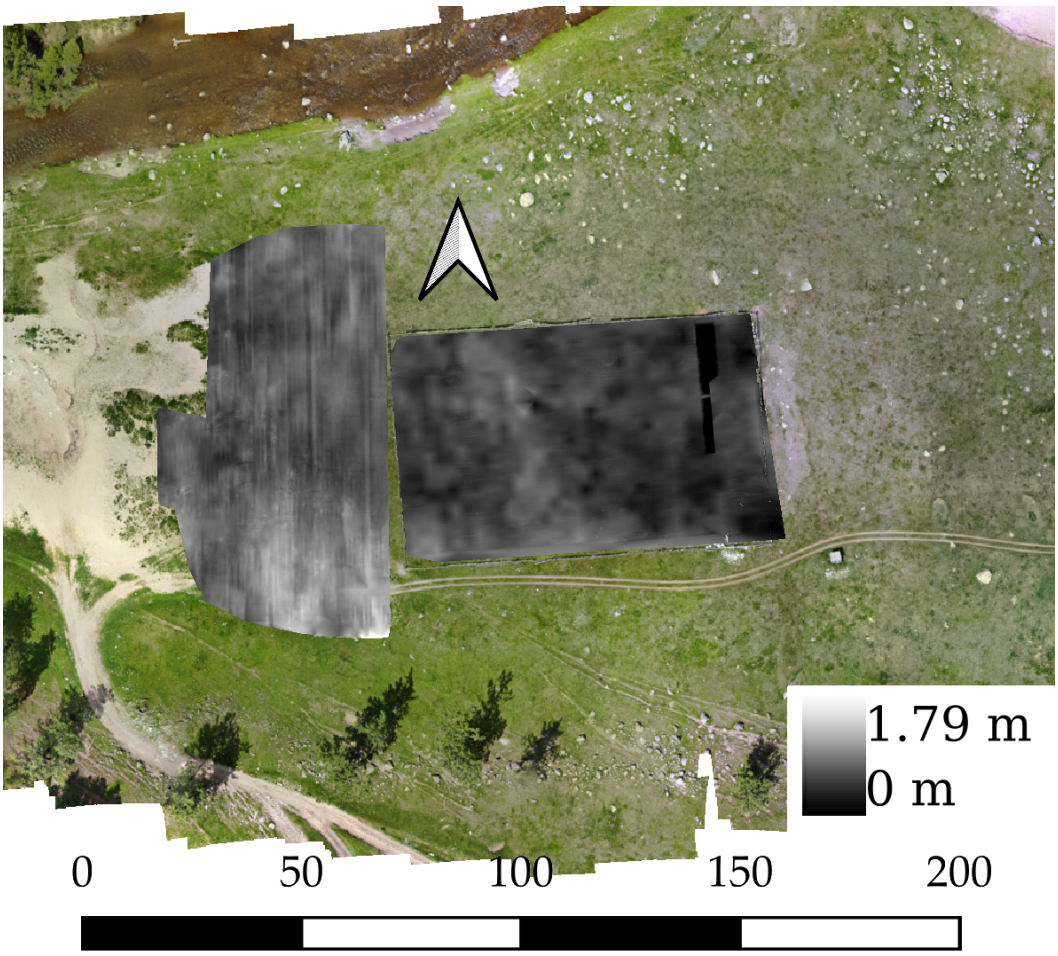

Figure 5.17: Isopach map of delta facies.

The thickness of the zeta facies varies wildly up to 110 cm. On average, it is slightly thicker in the middle of its area (20-110 cm) and thinner around the edges (0-40 cm). Throughout the isopach map (fig. 5.18), but especially at its extremities, there are numerous features (typically 2-8 m across) that represent "thicknesses" of less than 0 cm. These are where the undulations of the eta facies surface break through and interrupt the epsilon reflective feature.

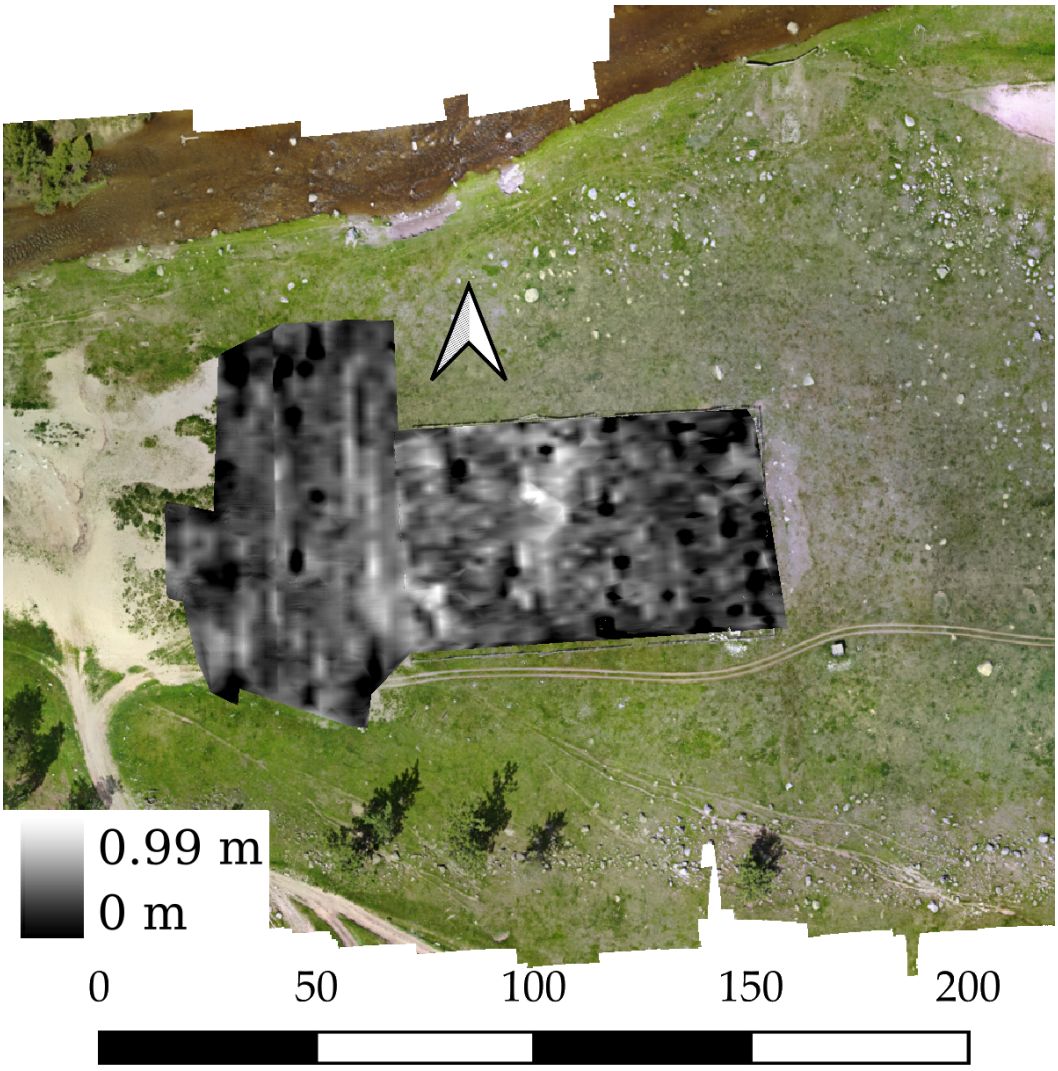

Figure 5.18: Isopach map of zeta facies.

5.3.3 Magnetometry

The magnetometry survey grids were divided into their contiguous blocks and georectified in GIS as seen in fig. 5.19. The data is plotted on a scale between -20 nT (white) and

+20 nT (black). Beginning from the western block of grids, there two features visible on the northern edge which is a total of 60 m from west to east. The second one appears V-shaped with the point of the "V" pointing south and the arms disappearing off the grid. Its dimensions are approximately 23 m by 25 m. These features are overlain with numerous magnetic dipoles and positive magnetic poles with values typically in the range of ±20 nT. In the centre of the survey is a linear feature (width varies between 3-4 m) that runs north-south for about 40 m. The magnetic strength of this feature is mostly between ±30 nT. The northern end overlaps a dense, elongated cluster of strong magnetic poles that is oriented East-West. This field of magnetic readings is 170 m across its longest axis and 50 m across but it is almost certainly longer than that as it likely extends beyond the reach of the survey bounds. The strength of individual magnetic poles varied widely up to ±100 nT but typical common values lay around ±30 nT to ±50 nT. To the east of this is another, smaller cluster of strong poles separated by a relatively quiet (magnetic strength within ±10 nT) strip. This second cluster is smaller at only 80 m by 30 m across but also likely extends outside the survey area. The range is magnetic strength is the same as for the first cluster. There is a sinuous feature (total curve length of 75 m, width between 1-3 m) at the eastern extremity that sits in an otherwise quiet (between ±1 nT) region. This had a low magnetic strength of around ±10 nT. Throughout many of the survey grids, there are numerous, more widely spaced magnetic poles which do not appear to be part of any particular structure but are strongly associated with the modern, topsoil unit, palaeosol outcrops and the boulder field (fig. 5.2). These reach comparatively extreme magnetic strength deviations of over 100 nT which can make the identification of weaker signals difficult.

5.4 Stratigraphic Pits

The locations of the seven pits from 2019 can be seen in the map in fig. 4.1. This shows how the newer pits are spatially related to the previously excavated ones. The stratigraphic logs from each pit have been digitised as figures.

Test pit 01 (fig. 5.20), lying within the area of the boulder field with topsoil cover, is one of the most complicated at the site. It has the most number of separately labelled units (8). The boundaries between the upper strata are fairly flat and there are roots visible in the sediments but the lower strata have no roots and display signs of significant disturbance or discontinuity. This is seen by the undulating, and sometimes unclear boundaries. In one such disturbed area, there is a region of reddish discolouration as unit 01D protrudes into unit 01F. A boulder appears at the bottom of the pit beginning at one metre below the ground surface. The top layer was a soil interspersed with many roots. It was noted that mica grains were found throughout most of the layers except 01F and 01E. Unit 01E had some flecks of a dark mineral.

Test pit 02 (fig. 5.21) was located in the soil-covered area central to the area of investiga-

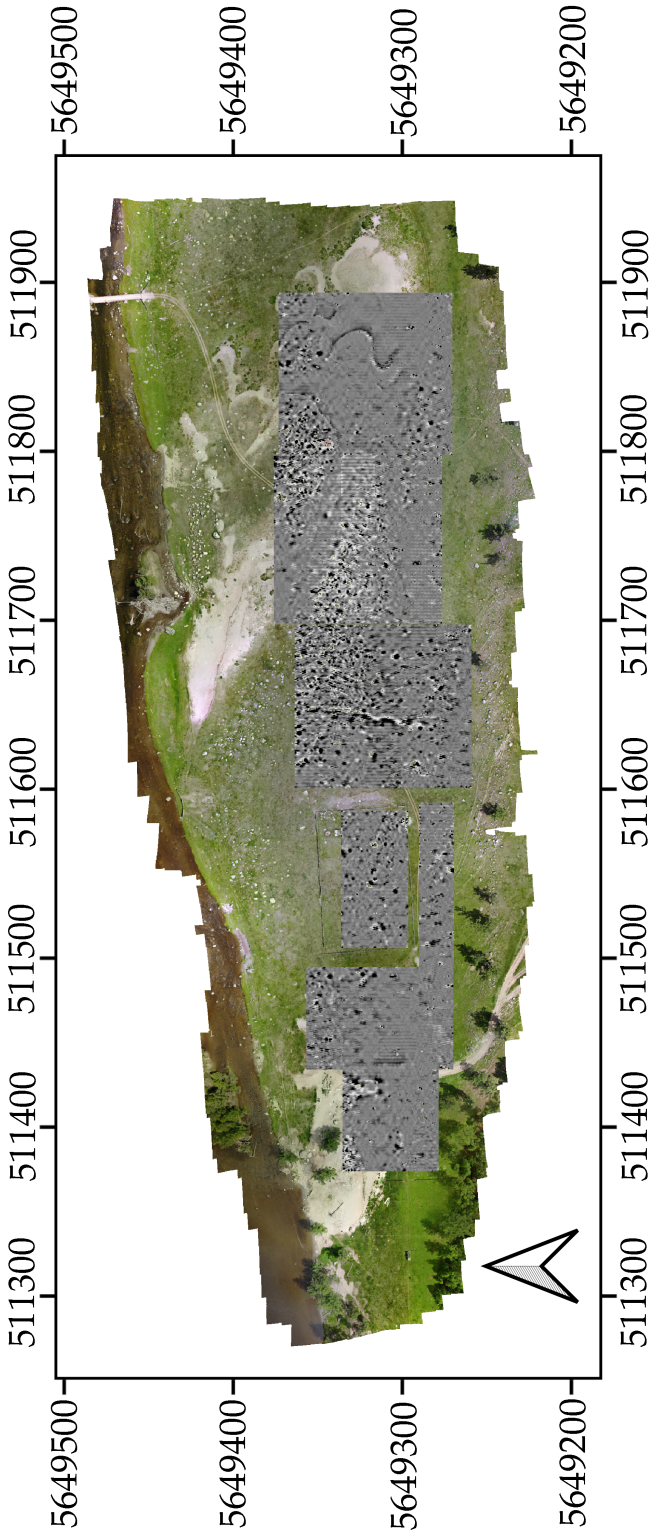

Figure 5.19: Map of magnetometry survey. Scale is ±20 nT.

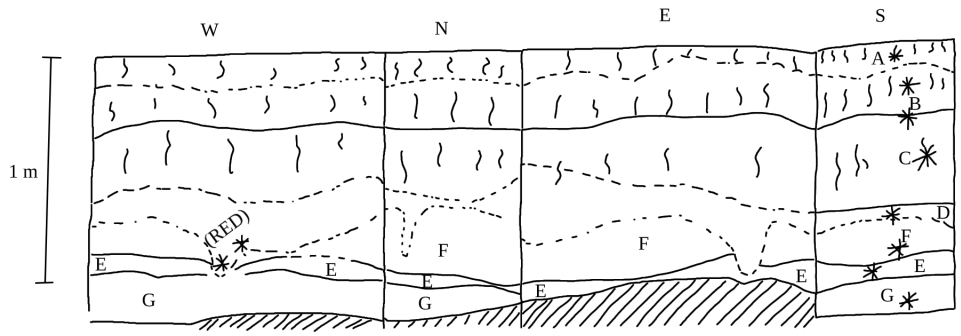

1A: Silt with occasional very fine sand grains. organic rich, heavily rooted. 10YR 2/2 "very dark brown."
1B: Very fine sand with abundant silt (~40%) and common mica grains. Abundant roots. Diffuse boundary with IA. Mottled 2.5Y 4/3 "olive brown."
1C: Fine grained sand with sporadic mica grains, moderately sorted and rounded. Clear border with 1B. Coarsening upwards from very fine - fine grained. 2.5Y 3/4 "light olive brown."
1D: Fine grained sand with mica particles and common organics, weakly developed palaeosol? 2.5Y 4/2 "dark greyish brown."
1E: Very fine grained sand with rare dark minerals. Very well sorted, subrounded and low sphericity. Appears as an obvious light coloured layer. 10YR 6/2 "light brownish grey."
1F: Very fine grained sand and very well sorted, subrounded and high sphericity. Clear border with 1E. 10YR 5/3 "yellowish brown."
1G: Fine grained sand, moderately sorted, rare mica particles, subrounded, low sphericity. 10YR 6/2 "light brownish grey."
1H: Granite boulder, decaying, onion skin weathering.

Figure 5.20: Stratigraphic log for test pit 01. Star indicates location of sediment sample taken. ”S” marks indicate roots present.

tion at Soyo. It was comprised of three identified units although the middle one was only partially laterally traceable. It was a moderately sorted, subrounded fine to very fine sand. The sediment sample for that unit was taken from the most identifiable region of that unit. The top of a boulder appears at 90 - 100 cm but there are no other notable features. The top layer was an organic rich soil containing some mica grains while the lowermost sand was lighter coloured and well sorted very fine sand.

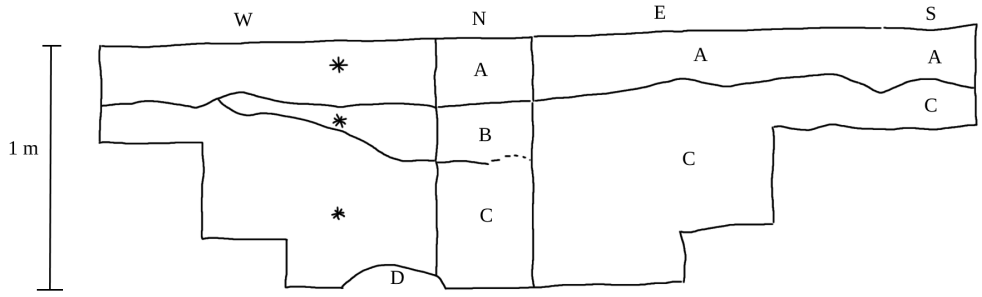

2A: Silt with 10-15% very fine sand. Organic rich, heavily rooted with grass. Well developed soil. 2.5YR 2.5/1 "reddish black."
2B: Fine to very fine sand, moderately sorted, subrounded, subspherical. No trend in grain size within the unit. 2.5Y 5/4 "light olive brown."
2C: Very fine sand, well sorted. 2.5Y 6/4 "light yellowish brown."
2D: Granite boulder.

Figure 5.21: Stratigraphic log for test pit 02. Star indicates location of sediment sample taken.

Test pit 03 (fig. 5.22) was located in a sandy area with tussock grass cover. In this pit was

uncovered a palaeosol which lay around 70 cm beneath the ground and was 10 - 20 cm thick. Above this were two separate layers of fine sand. The upper was well rounded and sorted with some clay while the lower was subrounded and less well sorted with mica grains. Below the palaeosol was another fine sand, well rounded and sorted with mica grains visible. The boundary layers were horizontal and there was no note of any significant disturbance except in that the unit boundaries were diffuse in some places. Both plant roots and mica grains were found throughout the pit. This pit terminated in unconsolidated sand.

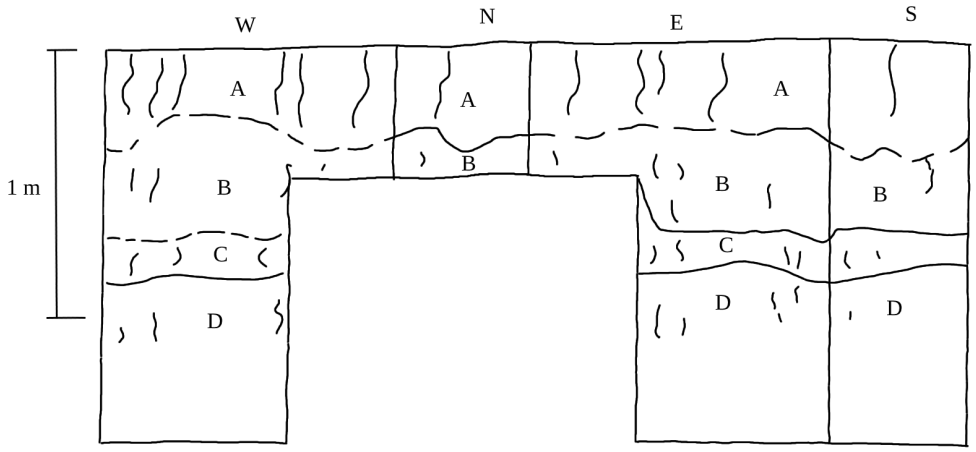

3A: Fine sand, well sorted, well rounded, high sphericity, well rooted, some clay present. 7.5YR 4/4 "normal brown."
3B: Very fin sand with a bundle of mica grains, high sphericity, subrounded, poorly sorted. 2.5Y 5/3 "light olive brown."
3C: Palaeosol. Fine sand, some clay present, high sphericity, well rounded, well sorted. 2.5Y 3/3 "dark olive brown."
3D: Fine sand, roots present, evidence of mica grains, high sphericity, well rounded, well sorted. 5Y 4/3 "olive."

Figure 5.22: Stratigraphic log for test pit 03. ”S” marks indicate roots present.

Test pit 05 (fig. 5.23) was opened on top of a sand dune in the western part of Soyo. The idea was to test the thickness of the dune above the palaeosol so the pit was only taken down so far. Most of the removed sediment was a fine grained sand with rare, if any, mica and some organic material in at least the upper portions. This sand is interposed by a darker layer with undulating boundaries. Roots dominate this layer and the sand above. The sand above and below the interposing layer was thought to be the same unit by the excavators and there is accordingly no sediment sample from the lower unit. Nevertheless, there is obviously at least a difference in plant activity between the two strata. At the base of the pit (120 - 140 cm) there was found a developed palaeosol unit; however, the pit was not continued past this point so its thickness and substrate material is unknown.

Test pit 07 (fig. 5.24) was opened in an area of topsoil cover but close to the sand dunes to the west. It shows some complex stratigraphy. Below the surface soil there was an olive brown layer with decayed roots whose boundary was difficult to trace. The layer pinches out and has wildly varying thickness up to 55 cm indicating that post-depositional processes had disturbed the sediment in this pit. Near the base of the pit, a distinct lens of

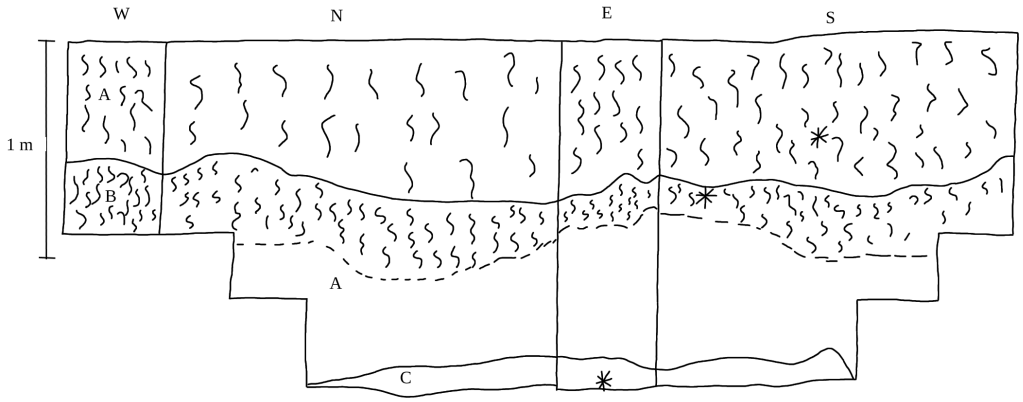

Figure 5.23: Stratigraphic log for test pit 05. Star indicates location of sediment sample taken. ”S” marks indicate roots present.

well sorted, high sphericity, subrounded very fine sand (unit 07D) lay horizontally. This lens displayed climbing ripples (fig. **??**) but it did not appear to compass the entire perimeter of the pit. The surrounding matrix of light-coloured, well sorted fine sand was given the label of unit 07C but a sediment sample was taken from both above and below unit 07D. This light sand contained occasional mica, roots and some white laminations. No palaeosol or boulder was discovered in pit 07.

Test pit 08 (fig. 5.25), located in the middle of the site and west of the fenced enclosure, showed level stratification without significant disturbance although the boundaries were often indistinct. The topsoil layer contained frequent roots but these were not noted throughout the rest of the layers. Like pits 03 and 05, there was a palaeosol: this time at a depth of 30 - 40 cm and 10 - 40 cm thick. The soil rests in fine grained sands which were distinguished based on their colour. As in pit 01 there was a red discolouration in one of the units (unit 08D). Unfortunately, the depth and location at which this sample was taken is unknown. However, the sample bag records it as ”red leeching into E.” Therefore, a depth of 100 cm has been assigned to this sample which is about the depth of the boundary between unit 08D (very fine sand, angular, low sphericity, well sorted) and unit 08E (fine sand, moderate to well sorted, subangular with black flecks throughout). Below 130 cm depth lay a large boulder which prevented further digging.

Test pit 14 (fig. 5.26) was the only pit to lie within the fenced enclosure in the middle of Soyo. The pit is capped by soil which sits on a light coloured sand (unit 14B). This sand was noted to have occasional roots in the upper portion and undergoes a mottled brown colour change which led to multiple sediment samples being taken. Two structures appear towards the bottom of the pit. Unit 14C is a light sand with black flecks that forms a narrow intrusion into unit 14B. Given the shape of it, it is possible that it was an animal burrow. Unit 14D is less clear and may be sedimentary or biogenic. It forms a horizontal

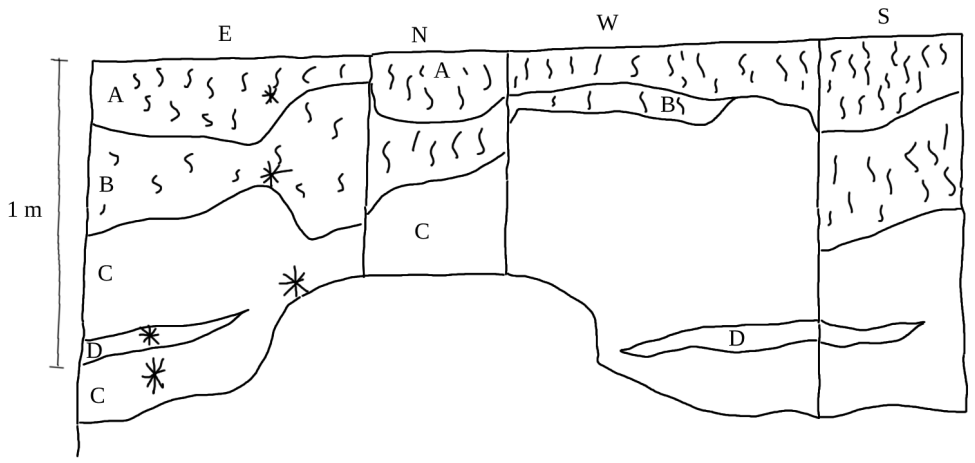

7A: Very fine sand with abundant silt, well sorted, subrounded to rounded, high sphericity grains. Well rooted. 10YR 2/2 "very dark brown."
7B: Very fine grained sand, moderately sorted with occasional mica particles. Subrounded, low sphericity, moderately rooted. Decayed root structures throughout unit. 2.5Y 4/4 "olive brown."
7C: Fine sand and well sorted, subrounded, high sphericity, occasional mica present. Occasional root structures evident in unit, occasional white laminations, occasional bioturbation. 2.5Y 6/3 "light yellowish brown."
7D: Very fine sand, well sorted, high sphericity, subrounded grains. More quartz? Laminations, rippling with various degrees of dipping, distorted bedding. Climbing ripples? 2.5Y 6/2 "light brownish grey."

Figure 5.24: Stratigraphic log for test pit 07. Star indicates location of sediment sample taken. ”S” marks indicate roots present.

lens of light sand. This time no black flecks are noted. A reddish discolouration was again noted in this pit and a sediment sample was collected at a depth of 76 cm (marked on the sample bag). Unfortunately, it was not recorded on the stratigraphic diagram where it was taken but that depth would place it immediately above unit 14D. There was no boulder recorded in this pit. Excavation was ended because of time constraints.

5.5 Sediments

The sediment samples were taken per stratigraphic unit (table 5.2): the assumption being that each was sufficiently representative of the layer. The depth of each sample is represented by a light grey, dotted line on the stratigraphic plots in each of the figures in appendix C. However, there were some peculiarities that need to be noted. First is the case of ”subunits” that had a different appearance but were not judged in the field as being worthy of their own unit label. This occurs in TP01 where unit D has a ”black” sample and a ”red” sample which was noted to cut into the underlying unit F on the form. This also happens in TP08 where there is a similar ”red” part that is wedged between units D and E. As stated earlier, the location of this sample went unrecorded and an estimated depth had to be determined from the description on the sample bag. It also was found in TP14 where there were three different samples taken from unit B. Furthermore in TP14 there were two structures labelled as units C and D from which a sample each was taken. These were taken from almost the same depth but from different sides of the pit. Nevertheless,

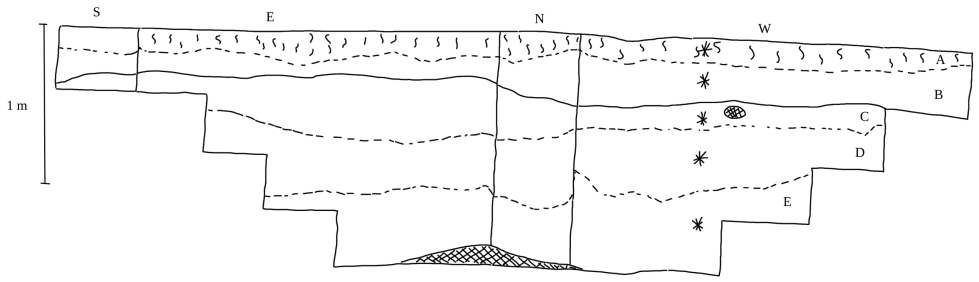

8A: Fine grained, subangular, high sphericity sand. Well sorted with moderate rooting. Dark organic visible, soil formation. 10YR 3/2 "very dark greyish brown."
8B: Fine to very fine grained sand, moderately sorted, medium to high sphericity, subrounded or subangular grains. 2.5Y 4/3 "olive brown."
8C: Very fine grained sand, well sorted, mostly homogeneous, medium sphericity, subangular to subrounded, moderately developed palaeosol. 2.5Y 3/2 "very dark greyish brown."
8D: Very fine grained sand, angular, low sphericity and well sorted (some larger grains visible). 10YR 5/4 "yellowish brown."
8E: Fine grained, moderately to well sorted, subangular grains. Black flecks throughout unit. 2.5Y 5/2 "greyish brown."
8F: Large rock.

Figure 5.25: Stratigraphic log for test pit 08. Star indicates location of sediment sample taken. ″S″ marks indicate roots present.

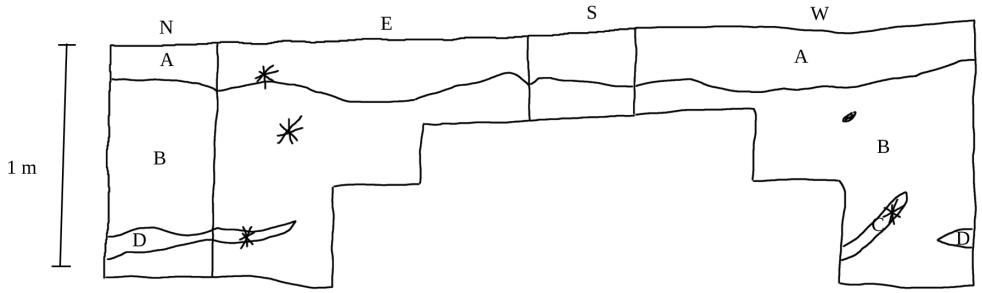

14A: Very fine, well sorted, organic rich sand with roots. High sphericity, subrounded. 10YR 3/2 "very dark greyish brown."
14B Very fine, well sorted, occasional roots in upper portions, high sphericity, subrounded. 2.5Y 6/4 "light yellowish brown."
Undergoes colour change (mottled). Mottling is 7.5 YR 5/4 "brown" and 7.5YR 6/4 "light brown."
14C: Fine sand, well sorted, subangular, medium sphericity, no roots, contains some black flecks/minerals. 2.5Y 6/3 "light yellowish brown."
14D: Very fine, high sphericity, subrounded. 2.5Y 6/3 "light yellowish brown."

Figure 5.26: Stratigraphic log for test pit 14. Star indicates location of sediment sample taken.

it seems likely that unit C represents a burrow rather than primary deposition. Second is the case of one interpreted unit being split into two parts by an intervening unit. This is the case in TP05 where both the top and third-from-top units were interpreted in the field to be the same and a sample was only taken from the top portion. Likewise in TP14 where a sliver of unit B lies at the bottom of the pit but not in TP07 where a sample was taken from both the top and bottom sections of unit C.

5.5.1 Magnetic Susceptibility

The magnetic susceptibility reported here is the low frequency (0.465 kHz) mass susceptibility (χ) in m^3 kg^{-1}. These values had typical ranges of between 5×10^{-7} and 1.5×10^{-6} m^3 kg^{-1}. The frequency dependency was generally quite low (under 2%) but the higher values corresponded to soil formation, either ancient or modern, which was to be expected.

The magnetic susceptibility of TP01 shows two phases. The upper strata hold steady at a high susceptibility (around 1.0×10^{-6} m^3 kg^{-1}) while the lower levels are quite lower (around 6.0×10^{-7} m^3 kg^{-1}) but with a peak in magnetic susceptibility (1.2×10^{-6} m^3 kg^{-1}) at around 95 cm. The frequency dependence is uniformly low (0% to 0.4%) except for near the surface where it jumps to 2.1%. This coincides with the surface soil layer at that location.

In TP02 both the magnetic susceptibility and frequency dependence undergo a uniform decrease. Both are at their highest in the topsoil (8.5×10^{-7} m^3 kg^{-1}, 1.7%) and lowest in the underlying very fine sand (6.3×10^{-7} m^3 kg^{-1}, 0%).

Test pit 03 has a noticeable spike in frequency dependence (1.1% compared to 0.14% - 0.25%) at a depth of 78 cm which is within the palaeosol unit found in that pit. However, the magnetic susceptibility does not see a significant corresponding elevation there but rather at the top of the column instead (1.4×10^{-6} m^3 kg^{-1}).

Test pit 05 likewise has a higher frequency dependence (0.9% compared to 0.0% - 0.1%) for its palaeosol but a significantly reduced magnetic susceptibility (8.6×10^{-7} m^3 kg^{-1} compared to 1.5×10^{-6} m^3 kg^{-1}) for the other two layers.

Test pit 07 has an increase in frequency dependence (1.5% compared to 0.0% - 0.3%) in its soil layer and a gentle decline in magnetic susceptibility down the pit from 1.1×10^{-6} m^3 kg^{-1} to 4.0×10^{-7} m^3 kg^{-1}. There is a spike

Pit	Unit	Depth (cm)
TP01	1A	5
	1B	23
	1C	50
	1Dred	74
	1Dblack	76
	1F	86
	1E	95
	1G	112
TP02	2A	10
	2B	32
	2C	70
TP03	3A	18
	3B	50
	3C	78
	3D	113
TP05	5A	45
	5B	80
	5C	162
TP07	7A	12
	7B	44
	7Ctop	80
	7D	99
	7Cbottom	110
TP08	8A	12
	8B	33
	8C	53
	8D	79
	8Dred	
	8E	112
TP14	14A	13
	14Bupper	33
	14B	40
	14Bred	76
	14C	87
	14D	89

Table 5.2: Table of sediment samples obtained from 2019 test pits.

in magnetic susceptibility (1.4×10^{-6} m^3 kg^{-1}) in unit D towards the bottom of the pit which was the lens in which climbing ripples were identified.

Test pit 08 has two levels of magnetic susceptibility. The upper strata sit at 1.1×10^{-6} m^3 kg^{-1} while the lower sit at around 5×10^{-7} m^3 kg^{-1}. Frequency dependence is highest at 0.8% at a depth of 53 cm. This corresponds to the palaeosol level in this pit. Other samples with moderately elevated frequency dependence include near the surface (0.4%) and in a very fine sand at a depth of 79 cm (0.5%). Otherwise, frequency dependence ranged from 0.1% to 0.2%.

Test pit 14 showed elevated frequency dependence only in its uppermost two layers (1.6% and 0.8%). Otherwise the frequency dependence was below 0.25%. Magnetic susceptibility was higher in the upper three layers (1.1×10^{-6} m^3 kg^{-1}) and lower below that (down to 5.8×10^{-7} m^3 kg^{-1}) except for a sharp increase in the lens of unit D which is at 1.3×10^{-6} m^3 kg^{-1}.

5.5.2 Grain Size

The grain size of sediments at Soyo was categorised into five bins which corresponded to Wentworth size classes from coarse sand to silt and clay (Boggs 1995, tbl. 4.1). The coarsest bin coalesced all of the fraction sizes greater than 0.5 mm which is coarse sand and above. The other fractions were 0.5-0.25 mm (medium sand), 0.25-0.125 mm (fine sand), 0.125-0.0625 mm (very fine sand) and under 0.0625 mm (silt and clay). Each fraction cutoff was half the size of the previous. In general, the sediments at Soyo were very fine grained with substantial fractions in the smaller three sizes and comparatively little above 0.25 mm. The grain size plots seen in the figures in appendix C show the "shape" of the fraction proportions for each sediment sample with coarse sand on the left and silt plus clay on the right. The y-axis of each subplot follows a common scale so that the thickness of each can be fairly compared. The plot forms can be broadly categorised into five shapes as seen in fig. 5.27. The first form's most abundant grain size is very fine sand (0.125-0.0625 mm). It also has abundant silt/clay and fine sand fractions with gentle tapering into the medium and coarse sand range. This indicates poorer sorting No doubt with finer sieving, the shape of the plot would become a lozenge. The second form is like the first except that it has a more extreme concentration in the very fine sand range with a sharp drop off into the coarser ranges indicating that the sediment was well sorted. There is still a strong proportion of silt and clay. The third form, on the other hand, is most dominated by fine sand (0.25-0.125 mm). It has a very sharp drop off in material bigger than 0.25 mm but the amount of finer material tapers off evenly. This indicates biased sorting. The fourth form is also centred around the fine sand fraction but has a gentler taper into the medium and coarse fractions. This is the rarest of the five since there was not a lot of these grain sizes in any of the sediment samples. The final form had equally abundant very fine sand and silt/clay with little and any of the larger fraction sizes. This form was also rare and could be considered a sub-type of the second form.

Test pit 01 began with poorly sorted sediments with a large fine sand fraction (32% - 47%) but predominantly changes to mostly very fine sands (38% - 53%) with varying degrees of sorting. A notable change occurs at the level at a depth of 76 cm. The sediments revert back to being fine sand-dominated (50%). Overall, the sorting in this pit appears to stay moderate.

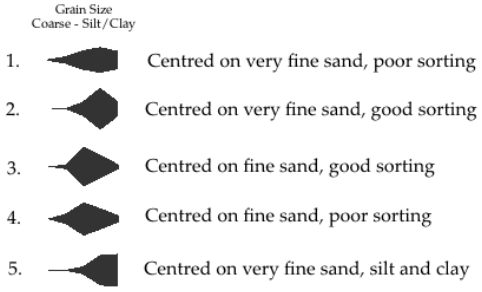

Figure 5.27: The five categories of sediment by grain size.

Test pit 02 showed no change in grain size or sorting with all three samples being of the poorly sorted very fine sands. The percentage of each fraction that was made up by very fine sand ranged from 39% to 48%.

The sands above the palaeosol (depth 78 cm) in TP03 were primarily composed of fine sand (52% - 58%). The plots change to be more dominated by very fine sands (34% - 48%) within the palaeosol and below. The palaeosol sample also shows the least sorting in this pit.

Test pit 05 shows a very similar situation to TP03. The upper sands are dominated by fine sand (55% - 56%) while the palaeosol, at the bottom of the column, is less sorted and has more very fine (38%) than fine sand.

The sediment plots for TP07 show poorly sorted sediments centred around the very fine fraction except for the two samples from unit 7C (depths 80 cm and 110 cm) which are more highly sorted. This indicates a change from poorly sorted but still mostly very fine sand (36% - 40%) to well sorted very fine sand (57% - 59%). An exception occurs in the lens of sediment at 99 cm which is poorly sorted again but most characterised by fine sand (39%).

Test pit 08 is much like TP03 and TP05 in that its upper sands are dominated by well sorted fine sand (48% - 52%) and sit on a sequence of very fine sands (36% - 44%) capped by a palaeosol (depth 53 cm). The sample with the higher-than-normal proportion of silt and clay at a depth of 100 cm was the reddish sediment described above.

The sediments from TP14 are almost completely poorly sorted with the largest fraction being very fine sand. The size of the very fine fraction ranges from 35% to 46%. The two exceptions at the bottom of the pit come from lenses or burrows. The upper (87 cm) is centred around the fine sand fraction (46%) while the lower (89 cm) has a great abundance of both very fine sand (42%) and silt/clay (46%).

5.5.3 X-Ray Fluorescence

The elemental composition obtained from each sample included a large range of elements from magnesium to uranium. Most of the concentrations of these elements were either negligible or had error ranges larger than the actual results. A selection of eight elements (Al, Si, S, K, Ca, Ti, Mn, Fe) to analyse was made on the basis of their being present in appreciable amounts and having low enough error to be usable. This list was further trimmed to just five (Al, Si, K, Ca, Fe) as the most meaningful and important elements for a geological interpretation. These five are the five included in the stratigraphic plots. Of them, aluminium and potassium stand out as being the more minor elements. Aluminium ranged between 3000 ppm and 6000 ppm while potassium was between 6000 ppm and 11,000 ppm. Silicon was expected to be high since it is a principal component of quartz and thus sand. Indeed it was an abundant element at concentrations of 15,000 - 50,000 ppm. Interestingly, its rise and fall through the stratigraphy was the reverse of calcium so that high calcium corresponded to low silicon and *vice versa*. Calcium displayed the most extreme range in concentration with most samples falling in a similar range as silicon but those samples marked as "red" reaching as high as 150,000 ppm. The final element, iron, ranged between 20,000 ppm and 45,000 ppm. One might expect it to be more concentrated in soil layers and to follow the magnetic susceptibility curves but it only does so sometimes. In particular, there are notable samples where the iron is lower than normal but magnetic susceptibility spikes or *vice versa* such as in TP01, TP05 and TP14.

The salient feature of TP01 is the abrupt change in silicon, potassium and calcium at 74 cm. This occurred in a particularly reddish sediment. What is most notable is the extremely high calcium content (128,000 ppm) which is significantly higher than most other samples collected from Soyo. Silicon is reduced to 21,900 ppm from the 40,000-50,000 ppm measured from the rest of the pit. Above and below this point, there are two different elemental profiles. The upper sediments contained more potassium (9800-10,000 ppm versus 7200-9100 ppm), more iron (30,700-35,900 ppm vs 22,400-29,700 ppm), and less calcium (7400-13,400 ppm versus 25,400-41,500 ppm) than the lower sediments. Silicon stays fairly steady with the exception of the drop at 74 cm while aluminium fluctuates within a similar range throughout.

In TP02 there is a decrease in silicon content from 43,800 ppm at 10 cm to 27,300 ppm at 70 cm. There is also a general increase in calcium from 15,500 ppm to 68,100 ppm. Aluminium is highest in the top layer (4700 ppm compared to 4400 ppm) while unit B (32 cm) holds the highest content for potassium (9800 ppm compared to 9300-9400 ppm). Iron is lowest towards the base of the pit at 29,200 ppm as compared to 34,900-36,800 ppm towards the top.

Test pit 03 has relatively low calcium content in the upper two samples (12,900-15,100 ppm) which increases with depth up to 20,900 ppm. The content of the other four elements fluctuate throughout the pit. Unit B (at 50 cm depth) contains the highest proportion of

aluminium (4500 ppm) and silicon (53,400 ppm). The palaeosol (78 cm) contains the most potassium (10,600 ppm) and iron (36,900 ppm) and the least silicon (34,400 ppm).

In TP05 there is an increase in all elements except silicon in the lowermost sample (162 cm) which is a palaeosol. Aluminium (5800 ppm compared to 3200-4300 ppm), potassium (11,300 ppm compared to 7400-9100 ppm), calcium (29,800 ppm compared to 18,500-20,700 ppm), and iron (46,000 ppm compared to 27,400-28,700 ppm) are all higher in the palaeosol than in the overlying sands. The one exception is silicon which was highest at 80 cm (40,200 ppm) compared to the palaeosol (38,500 ppm) and uppermost sand (37,500 ppm).

The unusual sample from TP07 is from unit D (99 cm) which was the lens of sand showing climbing ripples. This sample contained significantly lower aluminium (2900 ppm compared to 3600-4600 ppm), potassium (6900 ppm compared to 9000-9900 ppm), and iron (18,800 ppm compared to 31,700-36,200 ppm). Silicon fluctuates between 35,500 ppm and 42,900 ppm without any strong pattern. Calcium steadily increases from 13,500 ppm to 31,000 ppm going down the stratigraphic column with a slight bump to 35,500 ppm at 99 cm.

Test pit 08 likewise has a sample which strongly differs from the rest which is the reddish pocket of sediment at a depth of 100 cm. This possessed lower silicon (15,700 ppm compared to 34,300-46,800 ppm), potassium (6300 ppm compared to 8800-10,300 ppm), and iron (22,300 ppm compared to 28,500-40,000 ppm). It also had higher aluminium (5600 ppm compared to 4100-5100 ppm) and extremely high calcium (150,000 ppm compared to 12,900-17,500 ppm). The lowermost sand sample (112 cm) also had an elevated calcium content at 43,400 ppm. Units C (53 cm, palaeosol) and D (79 cm, sand) show increased iron (36,600-40,000 ppm) and decreased aluminium (4100-4500 ppm) compared to the overlying sands (Fe: 28,500-30,700 ppm; Al: 4700-5100 ppm).

The sample from a depth of 76 cm in TP14 shows significantly different elemental composition to the three samples high up the pit. This was another reddish-coloured sediment of the same type as found in TP01 and TP08. Compared to the overlying sediments, this unit has significantly decreased silicon (14,200 ppm compared to 38,700-44,700 ppm), potassium (6500 ppm compared to 9200-10,300 ppm), and iron (21,400 ppm compared to 31,700-37,400 ppm) while having increased aluminium (5900 ppm compared to 4600-5100 ppm) and extremely high calcium (148,000 ppm compared to 13,400-14,800 ppm). The two lowermost samples, from lenses or pockets of sediment, at depths 87 cm and 89 cm are similar to the upper sediments in terms of aluminium (4600-5200 ppm) content with slightly increased silicon (47,900-52,200 ppm) and moderately increased calcium (30,000-38,900 ppm). Their iron content (25,100-25,600 ppm) is more in line with the reddish outlier sediment and they are split both ways with potassium (9300 ppm and 7600 ppm).

5.5.4 Loss on Ignition

The values for loss on ignition are given as the percent weight of the carbon and carbonate. For the organic carbon this was calculated as the mass lost between heating the sample to 105 °C and 550 °C times the molar mass of carbon (12 g mol^{-1}) and divided by the molar mass of carbon dioxide (44 g mol^{-1}). For carbonate this was calculated by taking the mass lost between heating the sample to 550 °C and 1000 °C, multiplying it by the molar mass of carbonate ions (60 g mol^{-1}) and dividing by the molar mass of carbon dioxide. Therefore, the results represent the percent weight of the carbon atoms themselves (not the total weight of organic molecules) and the percent weight of just the carbonate ions themselves rather than of calcium carbonate. The assumption made here is that loss of water of hydration from clay particles was negligible. Soyo is a sandy site and there is not a lot of clay but at least a small amount was reported from some of the stratigraphic units. In general the carbonate levels go up and down with the levels of calcium derived from XRF with only a few exceptions which supports this assumption. Typically the values lie in the range of 6% or less with three exceptions clustered around the 15% mark. The values for organic carbon all lay below 2.6% and mostly increase in units that have undergone soil formation. Higher organic content in non-soil units might indicate some incipient soil formation that was not visible to the eye or else it might indicate the localised breakdown of roots.

Test pit 01 had an elevated level of organic carbon (1.8%) in its surface soil layer compared to the baseline of sub-0.4%. Both organic carbon (1.4%) and carbonate (14.5%) content are increased in the reddish sample at 74 cm. The carbonate content is much lower for the rest of the pit but the sediments above this point have lower (0.7% - 0.8%) carbonate than the sediments below (3.8% - 6.0%).

Test pit 02 also displayed elevated organic carbon (2.3%) in its surface soil. However, there is more of it in the underlying layers (1.1% and 0.8%) than in TP01. Carbonate increases with depth from 1.0% to 6.3%.

In TP03 organic carbon is noticeably increased (1.9%) in the palaeosol at 78 cm depth compared to the sub-0.4% in the other three units. Conversely, carbonate drops at this point to 1.0% from its otherwise 1.8% - 2.2%.

The same situation occurs in TP05 where the palaeosol at 162 cm contains more organic carbon (2.6%) and less carbonate (1.5%) than the other two samples which were 0.3% - 0.4% and 2.3% - 2.4% respectively.

In TP07 the organic carbon content is relatively constant (0.1% - 0.5%) except in the soil at the top of the pit where it jumps to 1.6%). Carbonate content generally increases down the pit from 0.8% at the top to 5.5% at the bottom. There is a slight reversal of this trend at 99 cm depth where the carbonate content dips to 3.1%.

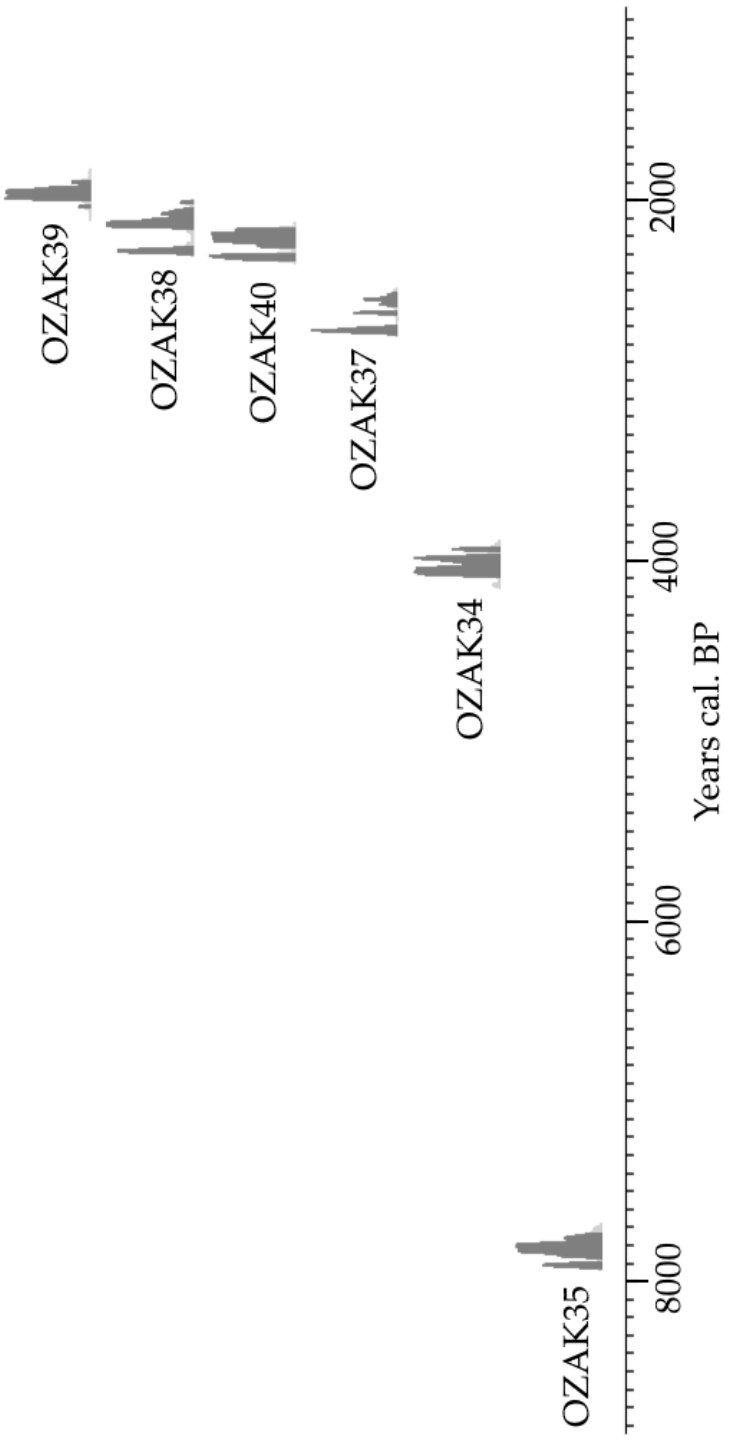

Figure 5.28: Probability distributions of the six non-modern dates from Soyo 2019. The 95% confidence intervals are highlighted in darker grey.

ANSTO Code	Pit	Depth (cm)	Material	Weight (g)	% C	BP	Error (σ1)	cal. BP (σ2)
OZAK34	TP14	60	Charcoal	0.97	60.90	3680	20	4088-3965
								3946-3927
OZAK35	TP14	75	Charcoal	0.45	63.87	6985	25	7927-7896
								7870-7732
OZAK36	TP02	68/89	Wood	0.33	48.72	80	20	Modern
OZAK37	TP08	69-73	Charcoal	4.08	64.96	2545	20	2742-2699
								2634-2616
								2587-2534
								2532-2518
OZAK38	TP08	81-100	Charcoal	0.43	62.03	2150	20	2298-2257
								2155-2048
								2018-2007
OZAK39	TP08	100-120	Charcoal	0.43	67.32	2025	20	2039-2029
								2002-1921
								1908-1891
OZAK40	TP03	83	Charcoal	0.43	58.80	2240	20	2333-2298
								2260-2156

Table 5.3: Table of 2019 carbon dates. Calibrated using IntCal20.

Test pit 08 contains comparatively little carbonate in the upper layers (0.9% - 1.8%) but a large amount (16.2%) in the reddish sample from 100 cm. The unit below this (112 cm) contains a lesser, but still elevated, amount of carbonate (5.9%). The organic content fluctuates in this pit. The highest amount was 1.6% from the palaeosol at 53 cm depth. The reddish sample with high carbonate also had high organic content of 1.3%. Organic carbon throughout the rest of the samples ranged from 0.3% to 0.6%.

The soil layer at the surface in TP14 has notably higher organic carbon (1.8%) than most of the rest of the samples (0.2% - 0.6%). The exception is the reddish sample at a depth of 76 cm which was 1.3%. This reddish sample also contained 14.0% carbonate which was much higher than the rest of the pit. The two sediment samples below (87 cm and 89 cm) had a moderate 3.8% and 4.6% carbonate but the samples in the upper half of the pit had very little carbonate content (0.9% - 1.2%).

5.6 Radiocarbon Dates

The carbon dates obtained from ANSTO are summarised in table 5.3. These dates are well within the range of dates previously established at Soyo. The oldest two at 7927-7732 *cal* BP and 4088-3927 *cal* BP come from TP14 in the middle part of the site. They were taken from within a sand layer beneath the modern topsoil at depths of 75 cm and 60 cm. One sample was taken directly from the palaeosol in TP03 and is dated to 2333-2156 *cal* BP. Three further samples from beneath this same palaeosol but in TP08 to the North date to 2742-2518 *cal* BP, 2298-2007 *cal* BP and 2039-1891 *cal* BP. The final sample was from a different part of the site and was found to be modern. All of the non-modern samples

were charcoal and contained between 58.80% and 67.32% carbon. The weights of each sample ranged from a third to one gram with the exception of one sample which was just over four grams. Figure 5.28 shows the six relevant dates from Soyo plotted as probability distributions with $\sigma 2$ probability in darker shading.

Chapter 6

Discussion

This chapter continues from the previous by integrating the results into a unified model for the stratigraphy and chronology of Soyo. First the stratigraphic layers from each test pit are correlated into a master stratigraphy using the GPR, ERT and sediment analysis results. A comparison with previous interpretations of the stratigraphy at Soyo is made. The full synthesis of all geological and archaeological data obtained as Soyo follows. This dates the stratigraphic layers at Soyo and compares the ages with the regional climate record to help inform depositional environments for each of them. The archaeology found in previous years at Soyo is given stratigraphic and chronological context. Finally, the implications for this kind of geoarchaeological research and for Mongolian archaeology in general are explored and some lines for future research are suggested.

6.1 A Correlation of Data and a Model of Soyo

The stratigraphic pit layer units that have been presented in Latin letters (A, B, etc) are specific to the pit they were found in (see Section 5.4 for these). The first step, therefore, towards an overarching model of Soyo's structure and site history is to draw all of the individual pits into one master stratigraphic scheme. Based on the geophysical results, the sediment analysis and the surface features, it is possible to construct such a scheme.

There are seven master stratigraphic units (marked in Greek letters) that have been identified in this study. They are, starting from the modern surface, α deposits of modern aeolian sands which have collected in dunes across the site; β the modern topsoil which covers much of the central part of the survey area including within the boulder field; γ the main upper palaeosol in the western part of Soyo which appears to have a relationship to unit β; δ the substrate sand unit in which palaeosol γ lies and which topsoil β also overlies; ε which is not a layer as such but appears in the lower part of δ and is comprised of the pockets of unusual reddish calcium carbonate sediments mentioned in chapter five; ζ a lower unit of sand which has many distinctive characteristics that differ from unit δ; η the glacial lodgement till underneath Soyo. These are summarised in table 6.1. This section aims to demonstrate the existence of these seven units and to explain the precise relation-

Stratum	Unit	TP05	TP03	TP08	TP07	TP14	TP02	TP01
Modern dunes	α	A,B	A,B	A,B				
Topsoil	β				A	A, B_{upper}	A,B	A,B
Palaeosol	γ	C	C	C				
Upper sands	δ		D	D	B	B	C	C
	ε			D_{red}		B_{red}		D_{red}
Lower sands	ζ			E	C_{top},D,C_{bottom}			G
Till	η			F			D	H

Table 6.1: Master stratigraphy scheme for Soyo showing correlation of 2019 test pits.

ship between them. The test pits with the clearest correlation are from GPR grid B (fig. 4.5) (TP08, TP07, TP03 and TP05) so it is sensible to begin there and discuss the easterly pits afterwards. Furthermore, the palaeosol identified in this part of the site is the clearest feature imaged in the GPR and the most salient feature there. Correlation of the palaeosol to the correct set of GPR reflections will provide a foundation for the interpretation of the rest of the site.

The first fact known about the palaeosol is that its northern extent is known from its outcropping. The identification of the palaeosol in the GPR should be made on a reflection that is bounded by its erosional limit. The palaeosol was identified in TP08, TP03 and TP05. In TP08 it appears at a depth of 30-40 cm. In the GPR lines that cross the pit, there is a reflection at 30 cm to correspond to this (fig. 6.1). Likewise, the palaeosol in TP03 occurs at 70 cm depth which corresponds to a strong reflection at the same depth in the GPR (fig. 6.2). Importantly, the two reflections identified here correlate horizontally to each other in the GPR data as one γ feature. This γ feature is easy to correlate between lines and to mark where it outcrops at the surface in the GPR data. Regarding TP05, the palaeosol appears at the bottom of the pit at a depth of 150 cm. In the GPR, the γ reflection which extends from the previous interpretation of palaeosol is at a depth of 100 cm (fig. 6.3). This is likely due to a substantial dune of loose aeolian sand which has a different dielectric permittivity to the site average and has caused the depth estimates at this particular point to be incorrect. The grain size plots for this sand (α) indicate that it is generally coarser-grained than most other sediments at Soyo (mode size fine sand) and its position on top of the site (and the fact that the GPR survey was taken in Summer) suggests the possibility that the dune is drier due to evaporation. Therefore, the radar waves would pass through with a higher velocity because the energy is propagated less by the slower alignment and relaxation of water molecules and more by the faster atomic displacement and relaxation in sand. Extrapolating the γ reflection interpreted as palaeosol produces the desired northern boundary (fig. 6.4) so it is doubtlessly the correct interpretation regardless of depth inconsistencies in TP05. This interpretation also matches the previous GPR interpretation made by Vella (2018) which will be discussed in detail later.

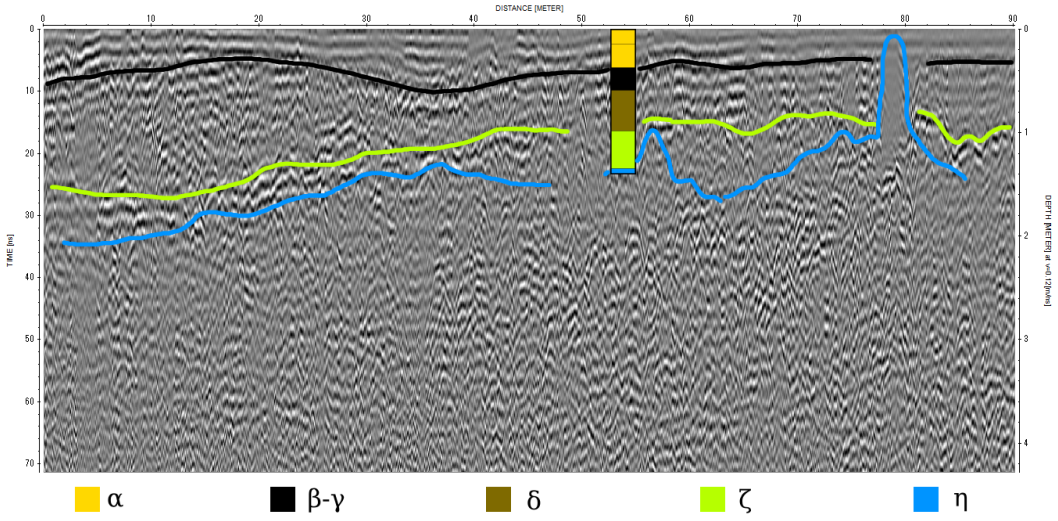

Figure 6.1: GPR profile over TP08 showing the interpretation of stratigraphy.

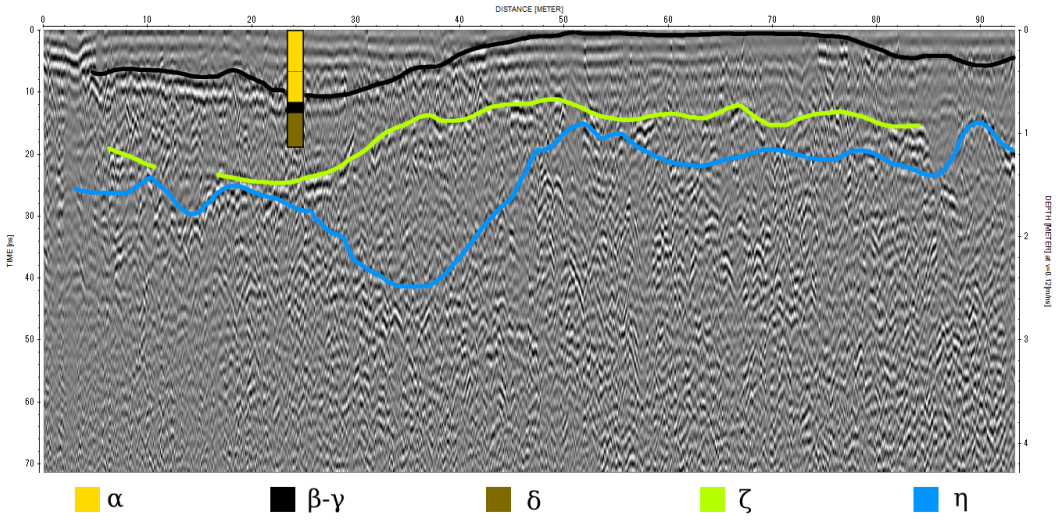

Figure 6.2: GPR profile over TP03 showing the interpretation of stratigraphy.

The other GPR facies that is easy to identify is the mass of hyperbolae and broken reflections labelled η which makes up a large part of the GPR profiles across Soyo. This facies is identified as the glacial lodgement till that forms the base of the site. Three of the pits dug in 2019 were taken down to a boulder (TP01, TP02 and TP08). In TP01 the top of the boulder lies at a depth of 100-120 cm. The η facies at this point in the GPR lies at a depth of 100 cm (fig. 6.5). The very top of the small boulder in TP02 is at 90 cm depth which is

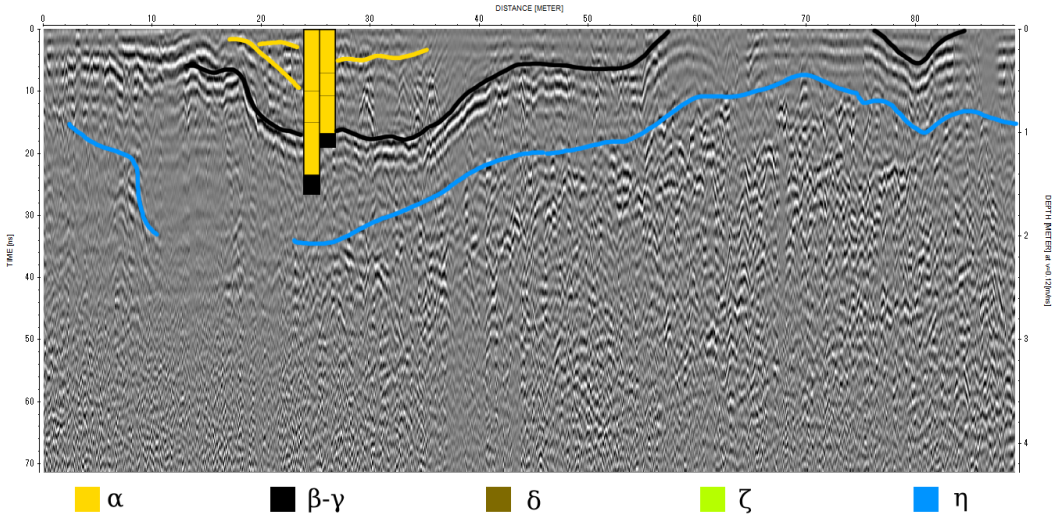

Figure 6.3: GPR profile over TP05 showing the interpretation of stratigraphy. The left half shows the test pit stratigraphy with its true depths while the right half has been compressed so that the palaeosol aligns with the correct GPR reflection.

the same depth as the η facies there as well (fig. 6.6). Test pit 08 was excavated down to a boulder at 130-140 cm which is close to the 150 cm depth of the η facies in that location (fig. 6.1). For the remaining test pits (TP03, TP05, TP07 and TP14), it is easy to verify that the η facies in the GPR is too deep to have been reached. Test pit 03 reached a maximum depth of 115 cm but the GPR shows the η facies as being at a depth of 180 cm (fig. 6.2). The GPR shows a depth of around 210 cm for the η facies underneath TP05 (fig. 6.3) so, even without considering the likely underestimation of depth (see previous paragraph on the palaeosol), that pit was too shallow to reach it. Test pit 07 was 130 cm deep while the GPR shows η facies depth of around 110 cm (fig. 6.7). However, it appears that the pit was dug between two hyperbolae so it is possible that the excavation just missed hitting a boulder. In the location of TP14, the GPR does not show any of facies η underneath (fig. 6.8). There is a large, quiet region in the GPR which may indicate high attenuation in this area or it may indicate a buried topographic shallow with a fairly homogeneous fill.

In between the palaeosol and till levels, there is sand which is divided into two parts (δ and ζ) by one further stratigraphic boundary which can be identified in the GPR. The upper sand (δ) contains pockets of reddish sediment which are denoted by stratigraphic level ε. The ε level appears in pits 01, 08 and 14 as a reddish, calcium carbonate-rich sediment. In TP08 the boundary between δ and ζ lies at a depth of 90-100 cm. In the GPR profiles that cross this pit, there is a clear reflection at 95 cm which corresponds to this. In TP07 the GPR reflection is visible at a depth of 55 cm which is approximately the depth of the

Figure 6.4: Map showing the extent of γ palaeosol from GPR (lines of cyan dots) compared to the palaeosol outcrop (solid red line).

boundary between pit units 07B and 07C although the boundary between those units in the pit undulated quite a lot. In TP14 there is no evidence of the boundary within the pit itself. However, it is visible in the GPR on either side of the pit with an appropriate break in the reflection. The depth this reflection *would* be at for TP14 is about 100 cm which is surprisingly close to the lens of very fine sand to silty clay (14D) between 80 cm and 100 cm depth and a potential burrow (14C) which is found between 70 cm and 100 cm depth (perhaps there was build up of sediment around the mouth of the burrow to explain its shallower depth compared to the lens). This might indicate the existence of a surface at this location although there was no discernible corresponding stratigraphic change. Test pit 01 is difficult to understand in relation to the rest of the site due to having more stratigraphic units than the other pits and being situated on the marginal edge of many of the GPR facies that are more clearly represented in the pits farther to the west. However, it is plausible that the spatially limited, upward-bowing GPR reflection siting just above the till facies (80-90 cm depth at the location of TP01) is this boundary. Unfortunately, the fact that this reflection only horizontally extends for five metres before disappearing into the till reflections means this boundary is very difficult to correlate with any certainty to the other pits. The fact that it becomes difficult to trace in this part of the site is a consequence of the overall thinning to the east of the entire sediment package above the lodgement till as seen in the isopach map fig. 5.14. Whether this level truly ends somewhere between GPR grids C and D (fig. 4.5) or continues on within the till level is a question that is impossible to answer with the data at present. The boundary is not visible at all in TP02 or in the GPR profiles there which further supports the conclusion that it has already begun to disappear from the super-till sediments by GPR grid D. The level is also not visible in TP03 and TP05 because neither of these pits were deep enough. The is no indication of an

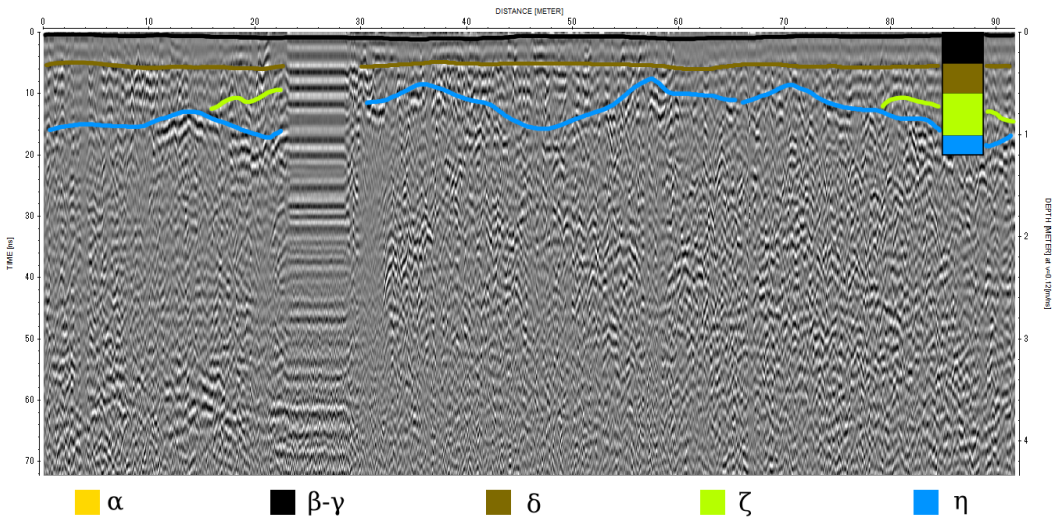

Figure 6.5: GPR profile over TP01 showing the interpretation of stratigraphy.

appropriate GPR reflection between the palaeosol and till facies for TP05 which indicates a western limit as well. In the GPR profiles over TP03, the reflection at a depth of 140 cm corresponds to this. Overall, the data shows that the sand that lies between the lodgement till and the soil levels is divided into two parts with an unclear event between them.

The structural interpretation of the site developed above can be further supported with the sediment analysis data. The data shows clear clustering in all four analyses (magnetic susceptibility, grain size, XRF and loss on ignition) which supports the stratigraphic model of Soyo. Plotting the carbonate content against organic carbon content for each sample results in fig. 6.9. The points naturally split into four categories. A high carbonate cluster which is the three reddish samples from TP01, TP08 and TP14; a high organic carbon cluster which is the soils and palaeosols from each pit; and two further clusters, one with moderately higher carbonate and one with moderately higher organic carbon content. The distinction between these last two clusters is as follows. For the cluster with more organic carbon and less carbonate, the samples come from master stratigraphic units α (modern dunes above the palaeosol) and δ (upper sand unit below palaeosol and top soil). Two further samples (1B and 14Bupper) are included here which are not fully part of either unit but are instead probably transitional units between δ and β (top soil). The cluster with more carbonate and less organic carbon is comprised of the samples belonging to master stratigraphic unit ζ. The two lower stratigraphic units from TP02 (02B and 02C) are rather anomalous by having significantly more organic carbon content than the main clusters.

A plot (fig. 6.10) showing the scatter of frequency dependence and magnetic susceptibility is similarly revealing. First of all, the data is fairly continuous along the magnetic susceptibility axis while there is some more obvious clustering along the frequency dependence axis. The four clustered points at the top of the frequency dependence axis are in fact the

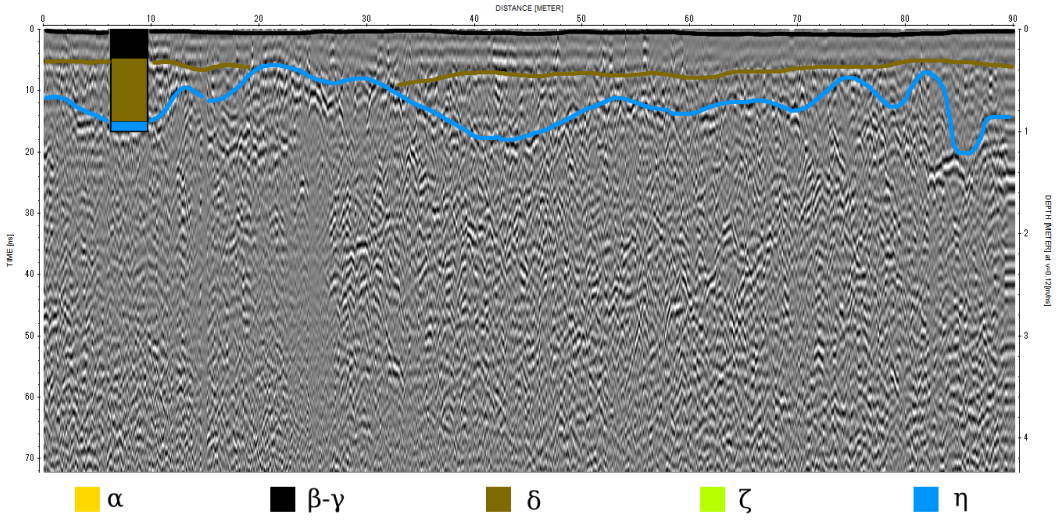

Figure 6.6: GPR profile over TP02 showing the interpretation of stratigraphy.

four modern top soil samples from TP01, TP02, TP07 and TP14. The palaeosol units are found in the two clusters of points with moderate frequency dependence along with two more samples that are probably sub units of the top soil (02B and $14B_{upper}$). The remaining collection of points with low frequency dependence and the full range of magnetic susceptibility can be divided into three parts. The sediments belonging to master unit ζ are almost entirely in the low susceptibility region. The sediments belonging to master unit δ are entirely in the middle range of susceptibilities. The sediments from the upper dune sands α are a mix of medium and high susceptibilities. This once again shows a clear distinction between the master units δ and ζ and less of a distinction between δ and α.

Because the grain size data has five dimensions (one for each of the five size categories), it was necessary to reduce the number of dimensions using principal component analysis. In this analysis, 60% of the variation is explained by PC1 and 30% by PC2. The modern dune sands α form a group of their own in the low PC1 and high PC2 corner of the plot. This group is quite separated from the other points with the exception of two to four outliers which will be discussed later. The samples from master stratigraphic units β, γ, δ and ζ form a sequence from the upper right (high PC1, high PC2) to the centre of the plot. The samples from unit ζare spread over the high PC1 half of this range. The samples from unit δ form a tighter cluster that overlaps with the lower PC1 end of the range encompassed by unit ζ. Most of the palaeosol (γ) and top soil (β) samples also form their own cluster at the opposite end of the continuum to unit ζ with two exceptions. Test pit unit 01A is an outlier point at the extreme low ends of both principal components. Unit 01B from the same pit is within the cluster of unit α points previously mentioned. Other outlier points include $01D_{black}$ which is also close to the unit α points; unit 14C which is likely to be infill from a burrow, 14D which has very different grain size characteristics to 14C despite the potential for them to have been the same structure; and 7D which displays unique climb-

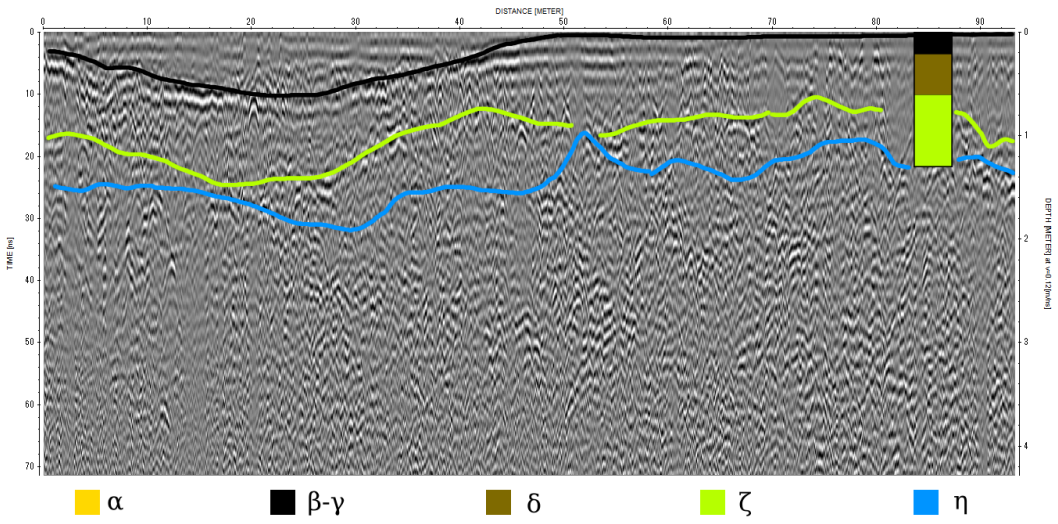

Figure 6.7: GPR profile over TP07 showing the interpretation of stratigraphy.

ing ripples at the site and so it's outlier grain size composition may reflect the process that caused those ripples to be formed. It was expected that the three reddish sediments should form a tight cluster due to their unusual chemistry and other properties but this did not turn out to be the case. None of the three points are close to each other (as compared to the closeness of points for the other master stratigraphic units) although two of them are within the range of the β-γ-δ-ζ sequence.

The master stratigraphic units were the least clearly distinguished in the principle component analysis for the XRF data (fig. 6.12) of all the sediment analyses. It is possible this is because the variation in the data is not well explained with only two dimensions. Forty-three percent of the variation could be explained by PC1 and 30% by PC2. Principle component three was responsible for a further 21% of the variation. Therefore, there is a substantial amount of differentiation between different samples that cannot be captured in a two-dimensional chart. First it should be noted that the three reddish sediments are not included in the chart. This is because their extremely high calcium content dominates the variance and makes it difficult to differentiate between the other samples. The three reddish sediment samples, when they are included, form a distinct cluster far from the rest of the samples. There is a large overlap between the samples from units β, γ and δ which are on the low end of PC1. This is fitting with the interpretation that the soil levels β and γ are formed within the δ substrate. Units α and ζ have a wider spread in the middle and upper ranges of PC1. They also overlap. No master stratigraphic unit seemed to show any patterning along the PC2 axis.

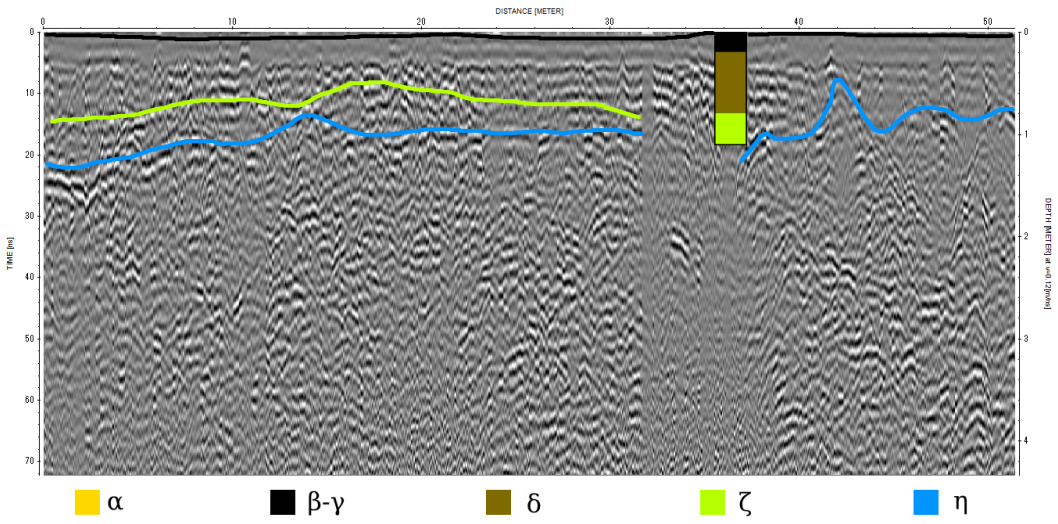

Figure 6.8: GPR profile over TP14 showing the interpretation of stratigraphy.

6.2 Comparison and Integration with Previous Geophysical Interpretations at Soyo

The previous study of the stratigraphy at Soyo (Vella 2018) identified many units of sediment in stratigraphic pits. Of these, two palaeosols and the lodgement till (labelled moraine) were interpreted into the GPR profiles. The upper palaeosol in Vella (2018) is the same as the palaeosol identified in this study (γ). The strong reflection in the GPR profiles clearly link this upper palaeosol (unit C in the 2016 excavation unit 6) to the ones found in the 2019 test pits. The lower palaeosol found in the 2016 test pits was not found in 2019. This suggests that it is spatially limited to the western part of Soyo. The GPR reflections identified as the lower palaeosol have a limited presence within each profile of GPR grid A (fig. 4.5) although they are reported as being present in the majority of those profiles. It is suggested here that these reflections may actually be due to the lodgement till or else the Soyo Hill limestone. Apart from this, the identification of lodgement till in the GPR is the same between both studies.

One major difficulty in joining the two studies together is the much greater complexity of stratigraphy in the 2015-2016 pits as opposed to the 2019 pits. While the boundaries between the latter strata were by no means perfectly horizontal, they were approximately so most of the time and deviated within only about ten to twenty centimetres. The former pits displayed stratigraphy that was not only non-horizontal, with units cross-cutting into one another in many cases, but that also differed remarkably between the four walls of the pit. This makes it effectively impossible to produce a simple schema of one sedimentary unit stacked on the next with boundaries between units given an approximate or average depth. Therefore, it becomes difficult to match them with GPR reflections. This issue is compounded by confusions and inconsistencies in the reports and primary data available.

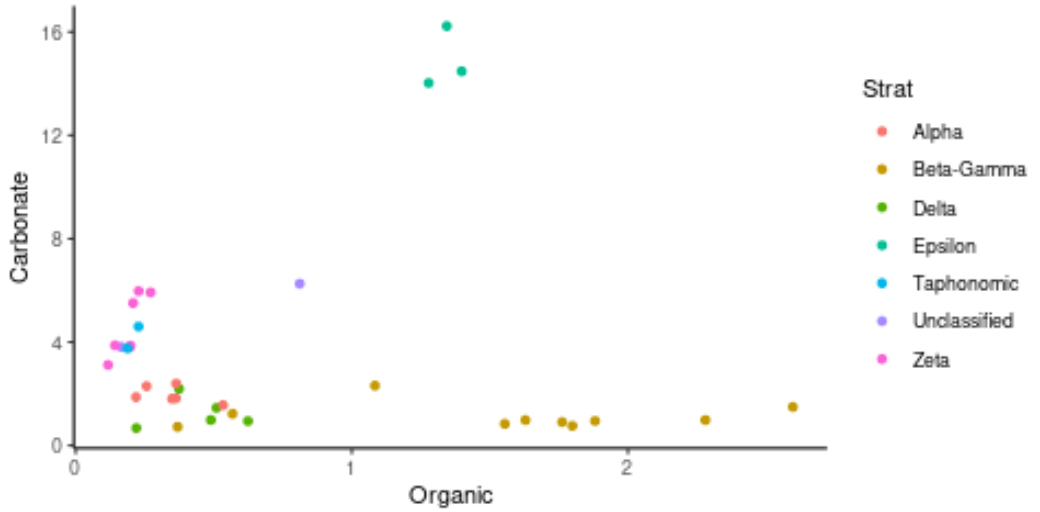

Figure 6.9: Plot showing the relationship between organic carbon and carbonate percent by weight for each sediment sample. Data points are coloured according to their master stratigraphic interpretation.

Many of the digitised stratigraphic drawings provided by Vella (2018, app. B) are not labelled consistently with the original drawings which raises some questions over which drawings belong to which pit. It is assumed here that the original drawings provide correct information where this differs from the published drawings. Lastly, the categorisation of sediments provided in Vella (2018, sec. 5.4) is inconsistent with itself both in terms of the total number of sediment categories present and in their names. Because of this and the generally mixed stratigraphy in much of the pits, the collation of adjacent and similar sands is unavoidable. Unfortunately, this means that the complexity of stratigraphy at the scale of one pit makes it impossible to see any broad-scale subtle changes. In particular, it may not be possible to find any evidence of a boundary between two sand layers corresponding to units δ and ζ as it was in the 2019 pits. This extra sedimentary complexity in the west of Soyo may be why the δ-ζ boundary disappeared from the GPR towards the western end of GPR grid B (fig. 4.5). One possible explanation for this added complexity is that this part of the site lies adjacent to the northern side of the Soyo Hill meaning it may lie in shadow for much of the day during parts of the year. Permafrost and frost wedging was discovered in the 2016 field season in some of the pits but this was not found in any of the pits dug in 2019 farther east. Therefore, it is proposed that the difference in complexity in the stratigraphy between field seasons is related to a difference in taphonomic ice action.

The stratigraphic model produced by this thesis compares favourably with the preliminary interpretation offered by Putnam (2016). His stratum I (limestone bedrock) was only visible in the ERT data and does not appear in the model here which starts with the glacial till (η). This corresponds to Putnam's stratum II. Stratum III is reported as a glaciofluvial gravel and possibly glaciolacustrine sand that was deposited within the interstices of the till. No gravel sized clasts were found in the pits in 2019 but this stratum is very likely

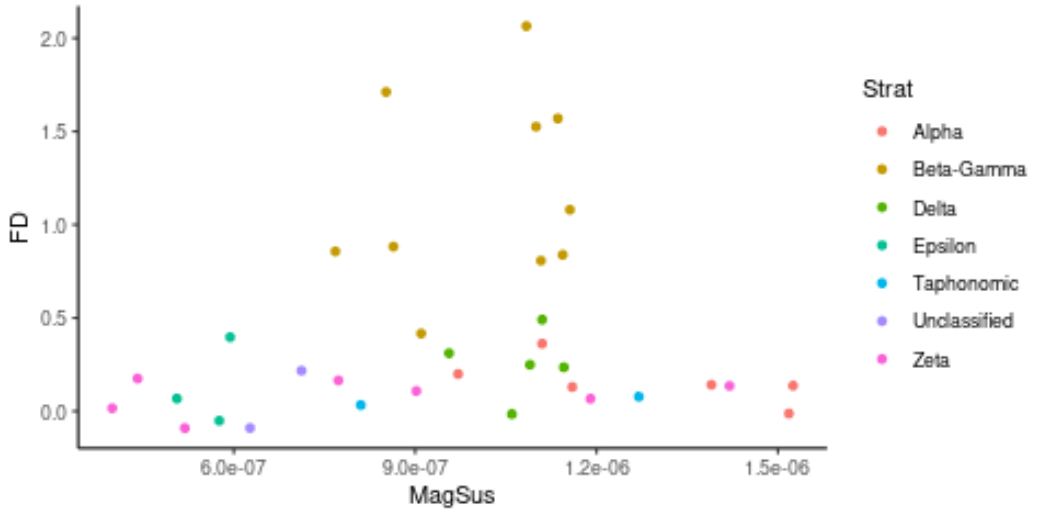

Figure 6.10: Plot showing the relationship between magnetic susceptibility and frequency dependence for each sediment sample. Data points are coloured according to their master stratigraphic interpretation.

to be the lower, fluvially reworked sand ζ. The gravel reported by Putnam is likely to be specific to the western end of the site where it was found. Stratum IV (angular limestone colluvium) was not represented at all in the 2019 pits or in the stratigraphic model presented here. This is probably another feature that is specific to the part of the site that is close to the Soyo hill. Stratum V was a lower palaeosol which was also not found in 2019. As argued in this thesis, it is probably spatially limited to the western end of Soyo. Stratum VI is reported as an aeolian sand with incipient palaeosol formation. It was also suggested that this sand corresponds to the earliest archaeological finds at Soyo. This layer corresponds to unit δ in the model here. This interpretation is supported by the results of this thesis which has produced two firm dates for this unit of 7732-7927 cal. BP and 3927-4088 cal. BP (see Section 6.3.2 for the dating of layers). This encompasses the date of 5938-6546 cal. BP reported for the Mesolithic-Neolithic hearth found at Soyo (Bayarsaikhan *et al.* 2005, Fitzhugh 2005). Stratum VII was the upper palaeosol which corresponds to master stratigraphic unit γ in this thesis. Putnam noted that this unit is continuous with the modern surface soil (corresponding to β here) which is again supported by the results of this thesis. The final layer (stratum VIII) is the dune sands present on the surface of Soyo. This corresponds to unit α here. It was noted that the sand for this unit likely comes from the channel bars of the Hogiin Gol. This interpretation is in agreement with this research (see Section 6.3.2).

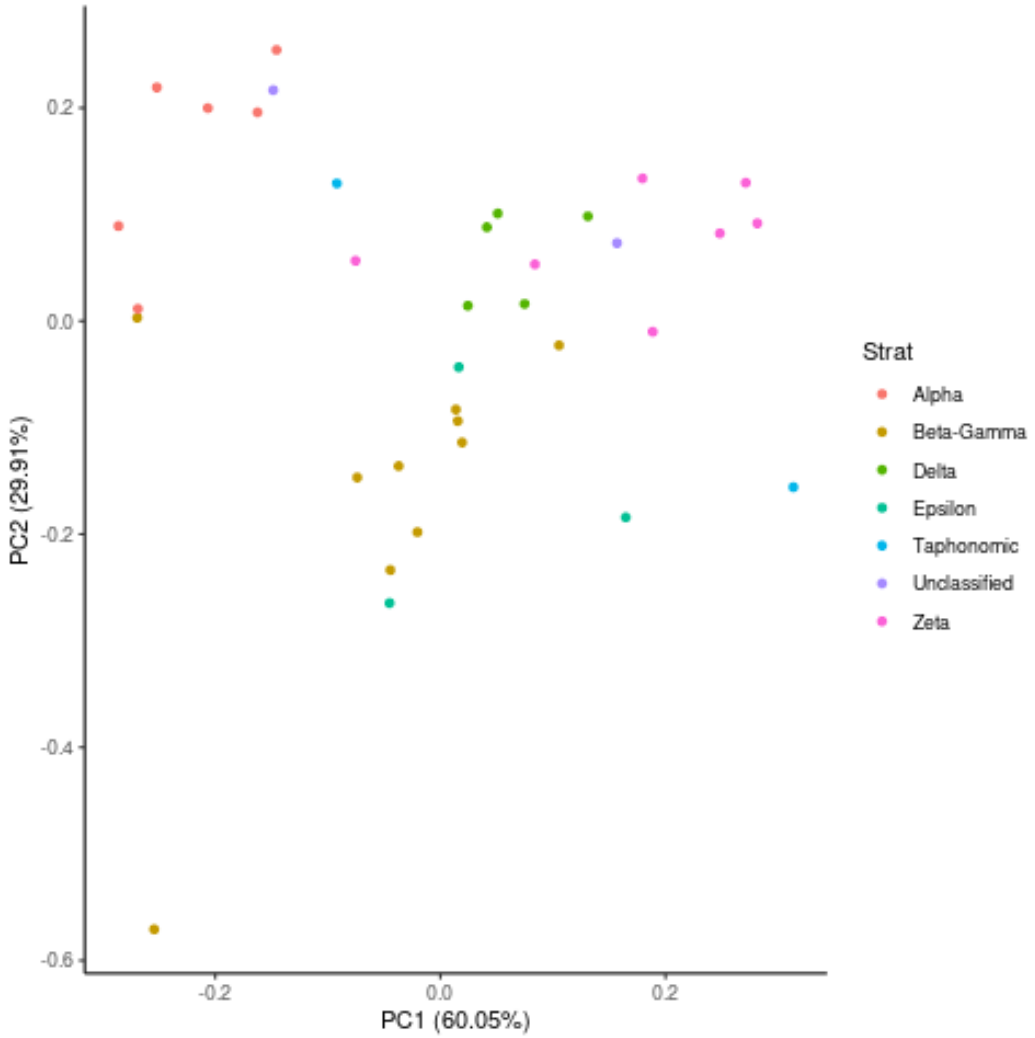

Figure 6.11: PCA chart of the range of grain sizes across all samples. Data points are coloured according to their master stratigraphic interpretation.

6.3 Full Synthesis of all Information Related to Soyo

6.3.1 Comparison between GPR and ERT

The resistivity profiles have less resolution than the GPR profiles (1.0 m horizontal, 0.2 m vertical for dipole-dipole ERT; 1.0 m horizontal, 0.5 m vertical for Wenner ERT; 1.9 cm horizontal, 15 cm vertical for GPR) but much greater depth. In order to see how these two data sets compare, each ERT profile was lain over its corresponding GPR profile. Effectively, the GPR profile is coloured according to resistivity. What is revealed is that the palaeosol (unit γ) and the underlying sand units (δ and ζ) on the GPR occupy the facies with lowest resistivity (under 1000 Ωm) on the ERT. This is likely because of moisture held in these sands and the lack of massive resistive objects like rocks to obstruct the flow of current. These sands, comprising the bulk of the material studied at Soyo, provide the best

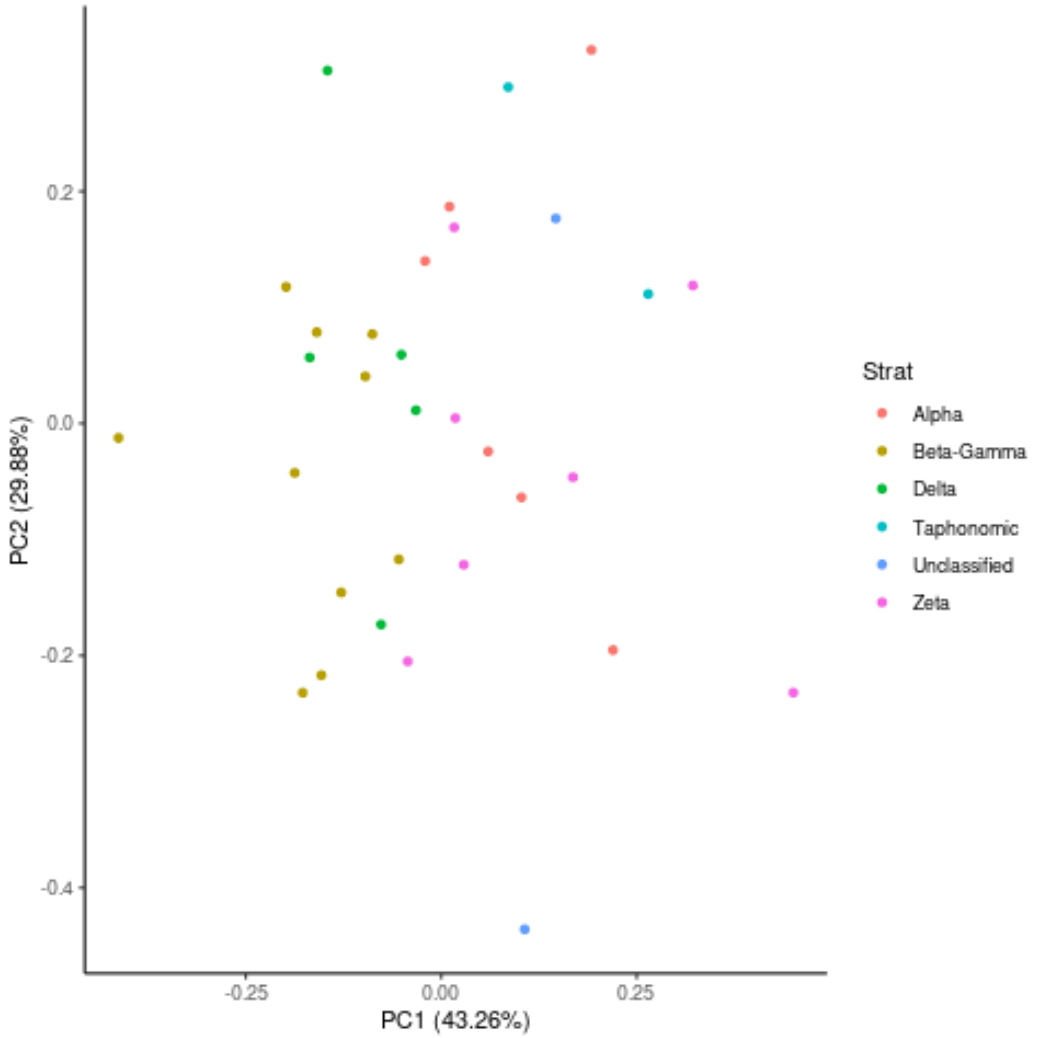

Figure 6.12: PCA chart of the elemental composition across all samples. Data points are coloured according to their master stratigraphic interpretation. The three reddish ε sediments are not included because their extreme calcium content dominates the results.

conditions for electric conduction at the site.

The modern sand dunes (α) perched on top of the palaeosol are clearly of a higher resistivity (approximately 600-1500 Ωm) than the palaeosol and underlying sands although this is only visible in ERT line 5 (fig. 6.13. Note the layer of medium resistivity above the palaeosol (γ) pick in that line. This is probably because this unit has a coarser grain size (mode size fine as opposed to very fine sand) and so the moisture within either drains to lower strata or evaporates more readily due to the increased pore space in the sediment. This would give stratigraphic unit α a lower water saturation than the other sediments. An alternative explanation could be that the highly conductive sands (δ and ζ) have higher clay content which would greatly improve the conductivity of the soil through their own conductivity and electrostatic attraction of water. While these sands do contain a lot more

clay and silt-sized clasts than the coarser, resistive sand (α), they did not display any particularly noticeable plasticity in the field characteristic of clay sediments. Neither does the GPR support such an explanation. If there were significant amounts of conductive clays present, it would be expected that the radar signal would have attenuated. However, reflections are clearly visible from the underlying lodgement till so it is likely the the difference in resistivity is primarily a difference in moisture content. The reason this sand only clearly shows up in ERT line 5 is probably because that is the location where the modern dunes are the thickest (over a metre). The α stratum is probably not thick enough elsewhere to be visible. Notably, this medium resistivity sand overlying the palaeosol in the west of Soyo does not appear to overlie the potentially unrelated palaeosols in the eastern blowouts area. There, the palaeosol is overlain by more low resistivity sands as seen in fig. 6.16 and more in appendix of picked ERT lines.

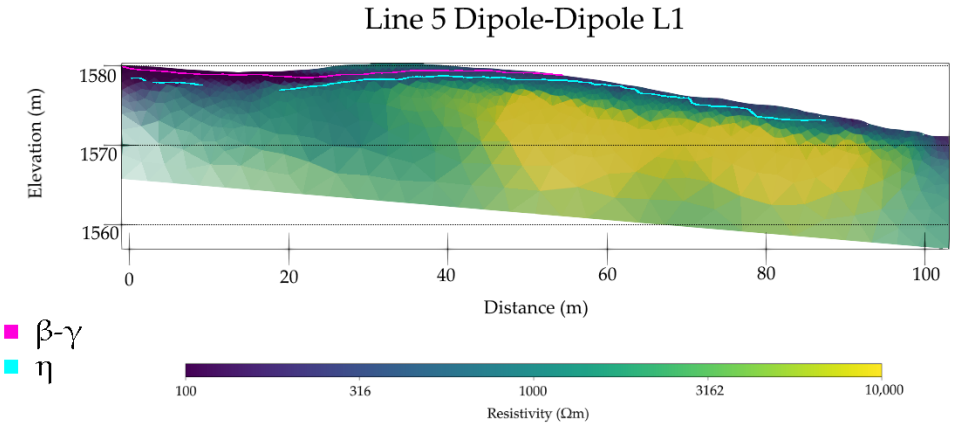

Figure 6.13: Overlay of GPR picks onto ERT line 5.

The glacial lodgement till as seen in the GPR did not correspond to the highest resistivity facies as was expected but rather to the medium resistivity facies (1000-3000 Ωm). This suggests two alternate hypotheses: that the lodgement till unit η is not a densely packed mass of rock but contains quite a bit of sediment between boulders and rock fragments; and that the ERT has detected a much higher resistivity feature underneath the lodgement till which may be bedrock or permafrost. Given the undulating top interface of this facies (elevation varies by at least several metres), the bedrock hypothesis is more believable. Bedrock to glacier interfaces can exhibit complex scouring patterns from glacial erosion even over short scales of tens of metres (Nishiyama *et al*. 2019). It is feasible that the complex, undulating interface between high and moderate resistivity facies at Soyo is a result of glacial action. If this were a permafrost surface, it would be expected that its topography would more closely match the modern surface.

The profile that best illustrates the overlap of these features is ERT line 5 in figure 6.13. There the modern dune above the palaeosol is shown to reach up to 1500 Ωm while the

palaeosol itself and the sand units it overlies range from as low as 40 Ωm to 500 Ωm in this particular part of the site. The very low resistivity found there on the southern end of the profile is likely due to water collection in the local topographic low. The same pattern is found on other ERT lines and the GPR profiles show strong reflections there even in the unprocessed data. This is the area just north of the southern moraine and lies in a shallow dip as seen on the topography. Throughout the field season, it rained on several days and it appears as though this dip collects water without draining as readily as other areas at Soyo. The till facies as seen in the GPR profile corresponds not to the highest resistivity values but primarily to values in the 1000 Ωm to 3000 Ωm range. This is seen in the following figures 6.14, 6.15 and 6.16 where the top of the till facies η in the GPR broadly corresponds to the boundary between the medium resistivity facies and the overlying low resistivity facies. At the deepest level reached by the GPR and below, the resistivity increases beyond that to as high as 20,000 Ωm.

6.3.2 The Stratigraphic Structure of Soyo and its Depositional Environment

The proposed overall structural model of Soyo can be seen in the cross-section in fig. 6.17. This shows how the major stratigraphic units sit in relation to each other on an East-West axis. The location of the line was chosen to be central along the axis of the site and to cover as many features as possible. The bedrock surface was derived from the L^1 norm dipole-dipole resistivity profiles because they showed the clearest, sharpest boundaries between the bedrock and the overlying units. The apparent jagged nature of the contact is a result of the coarse 20 m line spacing between ERT surveys.

From this diagram, it becomes apparent that there is a general downward slope of strata to the East. The bedrock surface has peaks and troughs with a range in elevation of over ten metres. This is something that is seen in individual (North-South) ERT lines so there is a complex pattern of glacial scouring. That is, it is not a matter of simple, straight channels. There are three major troughs along the profile line shown. These are at 210 m, 300 m and 430 m. These are filled with moderate resistivity material which is likely to be the glacial till since it is indistinguishable in the ERT profiles from that (6.18). It is possible that the overall decrease in elevation represents the buried slope of Soyo Hill or it may simply represent the grade of the glacier. The till facies sits upon the bedrock and follows a slightly different topography. Its western end is highest as with the bedrock but it forms a shelf from about 230 m to 300 m. This causes the till to increase in thickness over the central portion of the profile. It is not clear what caused this.

This facies has been hitherto interpreted as glacial lodgement till that was laid down un-

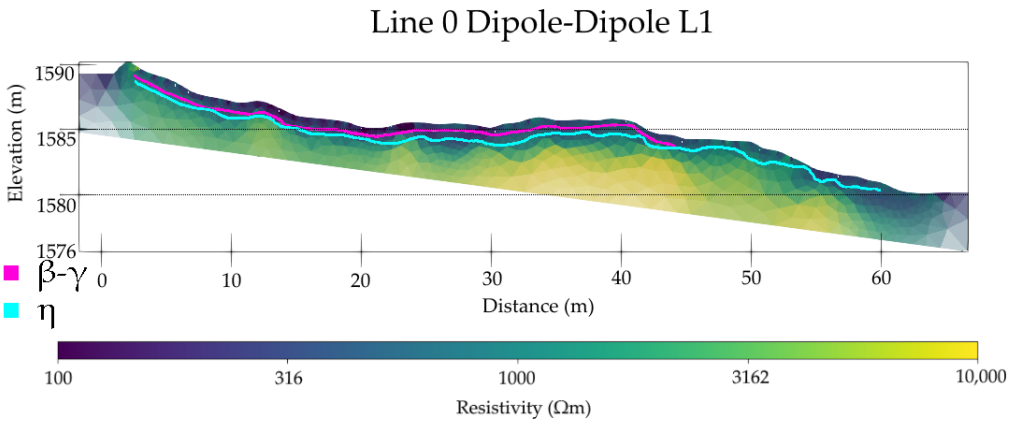

Figure 6.14: Overlay of GPR picks onto ERT line 0.

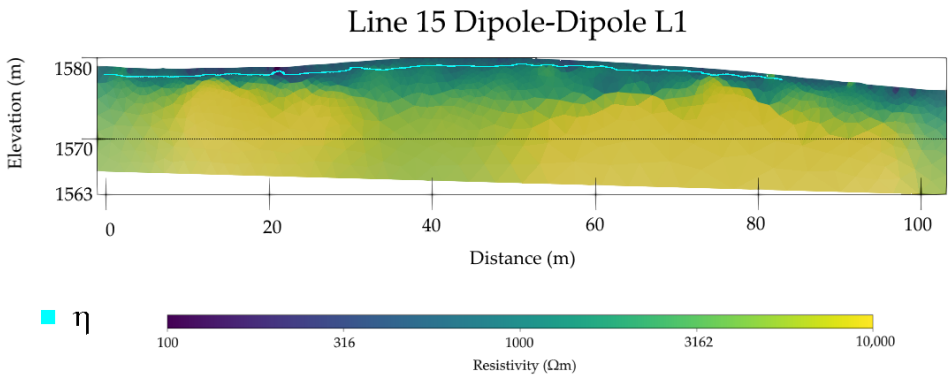

Figure 6.15: Overlay of GPR picks onto ERT line 15.

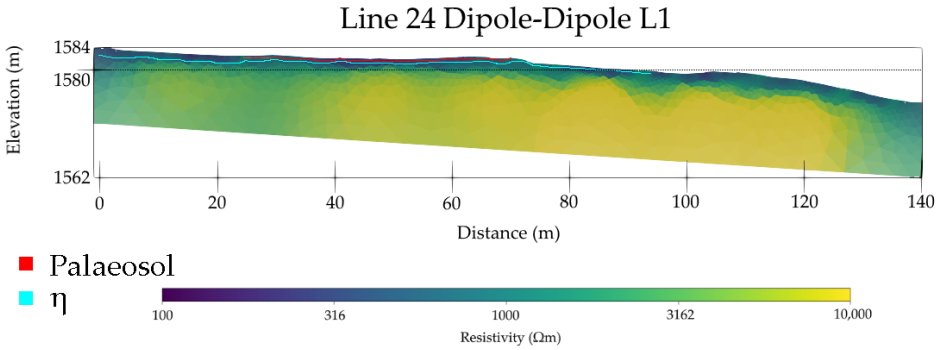

Figure 6.16: Overlay of GPR picks onto ERT line 24.

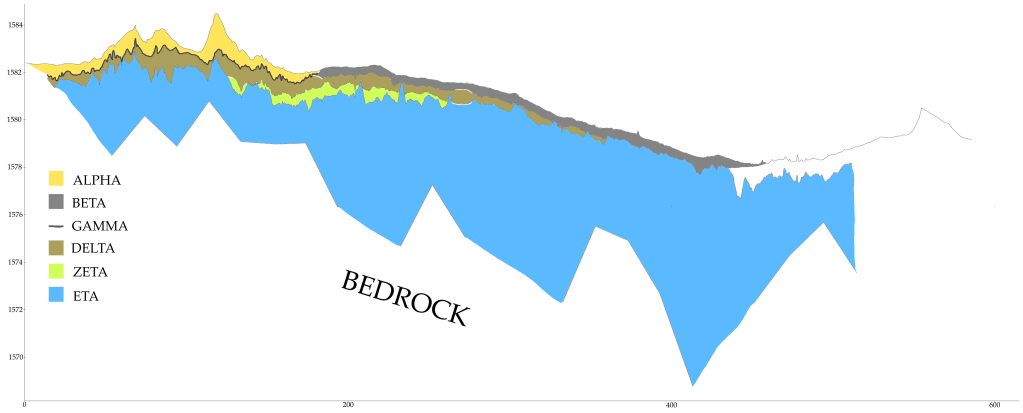

Figure 6.17: Cross section of Soyo stratigraphy from West to East. Stratigraphic units are colour coded according to the legend.

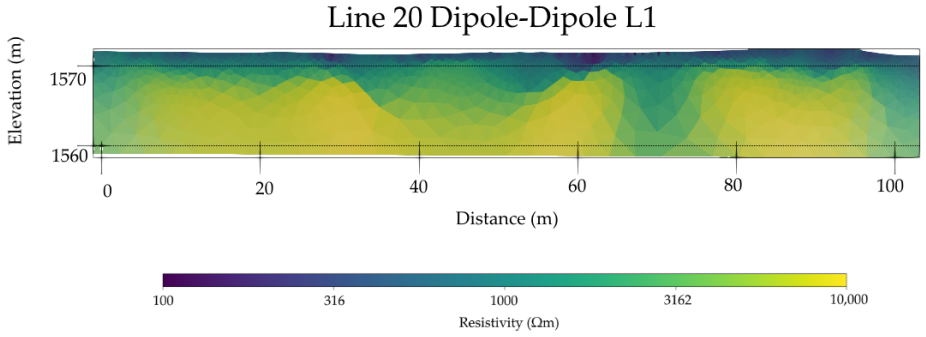

Figure 6.18: The L^1 dipole-dipole inversion of ERT line 20 showing troughs in the bedrock that are filled with the medium resistivity facies which is interpreted as lodgement till fill.

derneath the glacier as it retreated. However, there is another possible explanation. It may be that the majority of the surveyed area of Soyo does in fact rest on a recessional moraine. The main reason for suspecting this comes from the morphology of the glacial deposit. Not far west of the site under investigation here, the modern topography abruptly drops several metres to the level of the river. This suggests a broadly wedge-shaped glacial deposit that may be either a recessional moraine or a later terminal moraine. There are potential problems with this interpretation such as the subroundedness of the boulders (fig. 6.19) which is something that is typical of active transport such as basal transport (Benn and Evans 2010, p. 360) although non-basal transport within glaciers can also be active transport (Benn and Evans 2010, p. 356). The example shown does not bear parallel striations which would be indicative of basal lodgement but striations do not always clearly appear on rocks with different resistances to erosion (Benn and Evans 2010, p. 361) as is evident from the relief on the surface. The parallel linear features seen in the figure are in relief not

Figure 6.19: Example of a schist boulder from the boulder field at Soyo.

abraded and are likely to be intrusions from processes prior and unrelated to glacial transport. The bimodal distribution of grain size (boulders and sand-silt-clay with no gravel or cobbles in between) is also unusual whether it is interpreted as lodgement till or moraine. Glacially deposited materials tends to contain a full range of sizes but there was very little gravel-sized material found at Soyo. Finally, the steep drop which would be the ice-contact side of the hypothetical recessional moraine is situated between Soyo Hill (limestone) and a limestone outcrop (a few metres across and several metres high) (fig. 6.20). On the other side of the outcrop is the river. The presence of the outcrop here presents a problem. It is undoubtedly in the path of a former glacier since there are multiple lateral moraines downriver. Therefore, the glacier must have either gone entirely around it or split into two with the outcrop as a midglacial ridge. The question is whether the full difference in elevation from the river to the top of the steep slope is due to entirely to glacial and post-glacial deposition or whether the Soyo Hill limestone bedrock contributes significantly. It is to be expected that the River Hog has carved into the underlying glacial deposits and possible bedrock on the northern side of the valley where it currently is. Therefore, it would not be too surprising if the bedrock was elevated on the southern side of the valley as opposed to the northern side. If there is a difference in bedrock elevation, it might indicate that there was no recessional moraine and that the landform was caused by fluvial erosion. If there was no difference, it would indicate a recessional or terminal moraine. In order to test this idea, it would be necessary to do further survey work at this part of the site.

Figure 6.20: The limestone precipice marking the western end of Soyo. Soyo Hill is to the right out of frame. The photo looks downriver in the direction of the site which is hidden from view.

Unfortunately, the cosmogenic dating planned to be done on 21 boulders from the site was unable to be undertaken so there is still no firm idea of the timing of glaciation at the site of Soyo itself except that it probably postdates the large terminal moraine south and southwest of Soyo from which three dates have been obtained (38.6 *kya*, 24.9 *kya* and 14.2 *kya*). Although these dates have a large range, it is thought that the moraine dates to MIS2 with the older dated boulder having inherited beryllium (Gillespie *et al*. 2008, p. 178). Cosmogenic dates are exposure dates so the younger date could easily be due to that boulder being buried within the moraine for significant periods of time and exposed by erosion later. This would give time for the smaller glacial valley, in which Soyo sits, to be cut through the large terminal moraine with potentially multiple advances and retreats.

The ζ sand unit is nestled on a shelf in the till surface from 125 m to 265 m in fig. 6.17. It is bounded on the western side by a rise in the till's elevation. On the eastern side, it is lost in the transition between GPR grids C and D (fig. 4.5). Boulders sit above or protrude above this sand unit in multiple places. It is probably more accurate to say that unit ζ is a deposit which largely lies in the spaces between glacial boulders. It would be impossible to determine from the GPR data whether or not it extends farther west as the reflection would be completely obscured by boulder reflections. The only test pits in the relevant

area to test this were made during the 2016 field season. It is entirely plausible that some of the deep sands uncovered between the boulders there also belong to unit ζ. Unfortunately, it is not possible to satisfactorily answer this question with the data available at the present time. The interpretation of this facies is glacial deposits reworked by either a braided stream or alluvial fan. The braided stream interpretation is slightly favoured due to the presence of climbing ripples in one of the test pits. One further reason for believing that unit ζ is water-deposited rather than wind-deposited is its higher content of calcium carbonate *in comparison to the other sand units at Soyo*. Since limestone bedrock is present in the region (and importantly upstream from Soyo), it is easy to suggest it as the source for calcium carbonate within the sediments at Soyo and for the River Hog to be its mode of transport. The calcium carbonate was probably precipitated from solution as there is no evidence of larger clasts. However, it is unknown where it fits into the range of grain sizes within the total sediment. The possibility of aeolian transport for this sediment cannot be ruled out entirely since it is possible that it was drawn from an already calcareous source or that the calcium carbonate was precipitated out into an aeolian sand.

There was only one carbon date retrieved from unit ζ and it is unfortunately younger than dates from overlying units even within the same pit. The sample in question dated to 1891-2039 cal. BP while two more samples from superior positions in the same pit dated to 2007-2298 cal. BP and 2518-2742 cal. BP. This inversion of dates could be explained by mixing of sediments which leaves the time period of ζ sediments in question. This sample was likely to have intruded into the ζ unit from above. Given the large depth range given for the sample in question (100-120 cm), it is also not especially clear whether it was found on the boundary between strata or deep within unit ζ. It is not possible to definitively correlate this unit to the western stratigraphic pits excavated in 2016 but, if it does extend that far, it is likely found in the disturbed pockets of sediment found between boulders there which might be indicative also of a braided stream environment. The dates from those sediments cover a huge span of time from 1060-1242 cal. BP to 12,747-12,892 cal. BP. It is very likely that the pockets and lenses of sediment (units E to Q) in excavation unit 6 below the palaeosol and associated sand represent intense post-depositional disturbance. Likely this was cryogenic given the presence of permafrost in one corner of that pit.

The δ sand unit blankets much of this part of Soyo (0 - 360 m on the diagram). West of around 125 m it appears to partially lie within the glacial till (η) and likewise east after 270 m (fig. 6.17). Beyond 360 m, it appears to wholly submerge into the till facies. It is difficult to understand what the mode of deposition could be. One of the chief problems with the interpretation (of all the sand units: not just this one) is that it is a massive sand deposit without any visible internal structure. It is possible that this is due to biological and ice activity mixing the material. If that is the case the the mixing must be substantially limited to within each unit identified. Further evidence for at least some disturbance comes from a possible burrow identified in TP14 although this was burrowed into the sediments of ζ. As well as that, the inversion of carbon dates discussed below might suggest that the sediments of unit δ have been disturbed after deposition. It may also be that the

sand deposit was originally deposited as a massive bed and there never was any visible stratification. Taphonomic processes may have still played a role in the inversion of dates but, additionally, it may be the case that the charcoal collected came from in situ roots that had been burned. The dates would then have represented the age of the surface for that plant (wherever that may be) rather than the age of deposition at the location of the sample. Unlike in unit ζ, there were found no surviving sedimentary structures in unit δ that might give a clue as to its depositional environment. However, it has been interpreted as aeolian sands for these reasons. First, the chemistry and physical properties of sands δ and ζ are different and particularly in regards to carbonate content. This mildly suggests a different source for the material but it's not conclusive. Second, the likely presence of a burrow within the unit in TP14 indicates that it was not submerged under water since the mouth of the burrow was well within stratigraphic unit δ. Third, the increased amount of organic carbon in unit δ possibly indicates periods of long term stability and incipient (but invisible or disturbed) palaeosol formation which would be conducive to an interpretation of a dune system that has periods of growth and stabilisation culminating in one major period of stabilisation in which the palaeosol γ formed. Fourth, the present day deposition is primarily wind-dominated and it is easy to imagine that this situation extended back into the past especially considering the more arid conditions present during much of the age range (see Section 2.5).

Four (possibly five) dates were obtained from unit δ which indicate a lengthy period of deposition. Two dates from TP08 were 2518-2742 cal. BP and 2007-2298 cal. BP. If the sample from unit ζ discussed previously was intrusive, it would also belong here. Two further samples came from TP14 and were dated to 7732-7927 cal. BP and 3927-4088 cal. BP. This represents a total age range of some six thousand years. However, there are some problems with the results from TP08. There is an inversion in the three dates with the oldest at the top and the youngest at the bottom. As suggested earlier, this might be explained by post-depositional disturbance. However, it might also be explained as *in situ* root charcoal. This would suggest, rather, an older and narrower age range for the δ sediments as the younger, first millennium BC dates would correspond to a vegetated surface (probably the palaeosol; see below). Not only would this explanation be parsimonious with the date of the palaeosol obtained, it would explain how an inversion could occur across a stratigraphic boundary while keeping that boundary largely intact (although it is true that the ζ-δ boundary is the most poorly understood of the stratigraphic boundaries at Soyo).

Within the δ sand were found pockets of reddish sediment in three pits (TP01, TP08 and TP14) (figs. 6.21, 6.22, 6.23). These pockets of sediment were highly rich in calcium carbonate and relatively low in quartz as indicated by the XRF and loss on ignition results. The explanation for these pockets is obscure. One possibility is that calcium carbonate was precipitated out from ground water or river water. One then has to ask the question why it was precipitated in such a local fashion and not as sheet-like calcrete structures as would be expected in that case. Furthermore, the sediments are loose rather than accreted into a calcrete structure. Another possibility is that limestone rocks (which had

Figure 6.21: The reddish sediment from TP01 on the left. The contrast and brightness of the photograph have been altered to improve its visibility.

Figure 6.22: The reddish sediment from TP08 in the centre left. The contrast and brightness of the photograph have been altered to improve its visibility.

Figure 6.23: The reddish sediment from TP14 in the top right. The contrast and brightness of the photograph have been altered to improve its visibility.

been deposited by water or gravity) disintegrated due to weathering and left behind the sediments in question. To this it must be asked how the limestone could break down so perfectly into very fine sand to silt that not even small fragments remained. It might also be expected that, if this were the result of limestone weathering, the calcium carbonate would be dissolved away rather than remaining in concentration. Furthermore, limestone was not generally found in the pits except in two that were dug during 2016 which were closer to Soyo Hill. Neither of these solutions are particularly satisfying. One other, and perhaps very surprising, consideration is that these pockets of sediments are the remains of ancient fires. It has been shown that the major component of wood ash is calcium carbonate (especially in pine which is common in Mongolia) and related minerals such as potassium-calcium carbonates (Karkanas 2021). To further bolster this idea, each of the three sediment samples also contained elevated quantities of organic carbon matter. There are some difficulties with this interpretation. First, the nature of the fire. The pockets of sediment are not very large (several centimetres across). Furthermore, the vertical dimension of the sediments is significant and their boundaries can be quite irregular. Therefore, an interpretation of anthropogenic fire is not supported by their geometry. To counter this, we may suggest that in all three cases only a corner of a hypothetical larger unit was seen in the test pits. It is also noted in the previously cited paper that, while many fires would be necessary to produce the thickness of these deposits, the overall area of the ash deposits does not change according to the number of fire events (Karkanas 2021, p. 34). If these were the remains of campfire, that would, therefore, indicate long lived use of the same spot (perhaps weeks or months at a time). Given that three out of seven test pits opened in 2019 contained these deposits, we should expect them to be reasonably common across Soyo as well. This would make Soyo quite an active site in terms of human occupation. This was not borne out in the finding of any associated artefacts or other archaeological remains in the relevant test pits. It is also possible that the calcium carbonate remains of the fire have leeched into the surrounding sands creating a deeper affected zone and leading to an overestimation of the length of occupation. An interpretation of natural fire is much more attractive as two of the three sediments were found in proximity to large root structures. It is more likely the case that these sediments are the result of these particularly deeper roots burning (which would shield them from being eroded by wind) followed by the calcium carbonate leeching out into the surrounding sediments. The second major problem with the fire hypothesis is the fact that the magnetic susceptibility of all three samples was low. Had there been significant heating of these sediments, one would expect the formation of more magnetic iron minerals. To this it can be said that, while the magnetic susceptibility is low, so too is the concentration of iron. The former may simply be due to the latter. The interpretation of root burning from natural fire is the probable explanation. One final note is the markedly lower potassium in all three samples. This may be illuminating in regards to the species and firing temperature experienced as discussed in Karkanas (2021).

Appearing at the top of unit δ from 0 - 180 m on the diagram is the main palaeosol at Soyo which is denoted by the Greek letter γ. This is a layer of soil formation that lies

within the underlying sand and represents a stable, long-lived period for the dune system in that area. There was only one sample retrieved in 2019 for dating from within the palaeosol which came from TP03 and has been dated to 2156-2333 cal. BP. This is interesting because it fits in the range of the three out-of-sequence dates from TP08 discussed previously (2518-2742 cal. BP; 2007-2298 cal. BP; and 1891-2039 cal. BP). If we accept the possibility of these being *in situ* root charcoal, a broad period of at least 800 years (c. 1.9 kya to c. 2.6 kya) appears as part of the age range for soil formation at this part of Soyo. The lifespan of the palaeosol may, of course, extend earlier or later than that range. The 2016 carbon dates indicate that it extended at least in the younger direction. Two samples came from within the palaeosol and one below it. The two within were dated to 32-256 cal. BP and 156-424 cal. BP. The date from the stratum below the palaeosol was 734-907 cal. BP. This shows it was present at a substantially more modern time as well. The early date is assumed to be associated with the period of soil formation and was disturbed from its original position. Since it was a bone sample, it cannot have been derived from burned roots. It is most likely that the period of dune stability and soil formation lasted a long period of time from the early to mid-first millennium BC to relatively recent. At the eastern limit of the palaeosol, it emerges at the surface and becomes the modern topsoil (denoted by β). This is also a layer of soil formation within the sand unit δ and it is taken as all but certain that the two soil layers are, in fact, one. This means that the soil β probably had an even longer lifespan than γ since they must have begun formation at approximately the same time. No dates were taken from unit β anywhere on the site since it was assumed any samples would be modern. Given that unit β is definitely on the surface today and it is taken to be continuous with the palaeosol γ, that provides further support for a hypothesis of very long term stabilisation and soil formation into present times.

The magnetometry data (fig. 5.19) reveals an interesting connection between the numerous magnetic poles visible and this β-γ combined soil complex since most of them are located in areas of modern topsoil, areas where palaeosols are outcropping on the surface, but also especially within the boulder field. The one major exception to this is that there are no such poles visible in association with the S-shaped palaeosol at the far eastern end of the survey. The magnetic features within the boulder field can be assumed to result from the increased magnetism of igneous rocks since many of the boulders are granitic. The dipoles and positive poles that appear in association with the palaeosol outcrop at the western end of the survey may represent anthropogenic burning in hearths. Hearths have been found in this part of the site previously (Bayarsaikhan *et al*. 2005, Fitzhugh 2005). Other such magnetic features scattered around areas located far from the boulder field (especially in GPR grids A, B and C) may also represent either anthropogenic or natural burning. A despike filter was applied to the data to remove features caused by iron objects; however, it is still difficult to definitively determine if the remaining features represent burning or not. In and near the area of the boulder field, it is impossible to tell if there are any potential areas of burning since the magnetism of boulders on and just under the surface is a reasonable explanation for any magnetic feature found there.

Stratigraphic Unit	Dates cal. BP
α	24-263; modern; modern
β-γ	2518-2742(r); 2156-2333; 2007-2298(r); 1891-2039(r); 734-907; 156-424; 32-256
δ	7732-7927; 3927-4088
ζ	12,747-12,892

Table 6.2: Table of stratigraphic units and dates associated with them. (r) indicates samples found in a lower stratum but believed to be derived from roots.

On top of the elevated, western end of the diagram lies the modern sand unit α which has coalesced into a few dunes on the surface. This unit pinches out at around 180 m but it extends farther westward beyond the surveyed area. In fact it appears to grow in thickness towards the westernmost extremity compared to the δ sand unit it overlies. This unit has been interpreted as an aeolian sand as well. However, while δ was formed by windblown grains, the source of the sand in α is proposed to be deposited fluvial sand from the nearby River Hog. This sand would have been transported via saltation or traction to its present location. This would explain the larger grain size for unit α as compared to other aeolian sands at the site (since it was originally fluvial rather than aeolian). It is not known what the original source of the δ sediments was. It may have been from ten metres away or from a hundred kilometres away. However, the small separation between α and δ samples on the elemental PCA chart on the axis of PC1 (fig. 6.12) suggests a different source. No dates were taken from this unit in 2019 but there were three from 2016. Two of them were dated as modern with the third falling in the range of 24-263 cal. BP. These dates combine with the *terminus post quem* dates from the underlying palaeosol indicate a very young age for the α dune sands. The ages for all of the sediment layers is summarised in table 6.2.

6.3.3 Climate

From the LGM through MIS2, the Darkhad Basin was submerged under a large palaeolake which reached a maximum elevation of either 1711 m a.s.l. or 1670-1679 m a.s.l. (Gillespie *et al*. 2008). The level of the lake was 1670 m a.s.l. by 14 kya after which it declined precipitously (Batbaatar and Gillespie 2016, p. 1771). Such high lake levels would have meant Soyo was under water until after this point. Unfortunately, the state of the lake during the subsequent period until 9.5 *kya* is contested. The two competing views are that there was a low lake level of around 1560 m a.s.l. for most of that time followed by a medium lake level at 1602 m a.s.l. between 11-10 *kya* (Gillespie *et al*. 2008); and that there was no lake during that period (Krivonogov *et al*. 2012, Narantsetseg *et al*. 2013). In either case, the lake level is not expected to have reached Soyo during this time. Although this is much higher than the elevations at Soyo reported here, the elevations reported in the literature are 40 m higher than the elevations from the Soyo project. This is almost certainly due to a mistake in this thesis taking the height above ellipsoid instead of the height above geoid which is a 40 m difference according to the GPS processing report files.

The fact that there is bone dated to 12,747-12,892 cal. BP from the lowest reachable levels at Soyo (sands within the boulder till η) demonstrates that the site had emerged as dry land. Unfortunately, the identification of the animal is unknown. The climate for this period of time after 14 *kya* according to the records within the Darkhad basin was cold and dry. Since the valley in which Soyo sits develops out of the breach in the large terminal moraine (MIS2) west of Soyo and given its much smaller width, it is likely that the "Soyo glacier" postdated it. Furthermore, no terminal moraine has ever been discovered for this glacier but only lateral moraines which end a few kilometres downstream. Critically, the lateral moraines end at close to the same elevation (1580 m a.s.l.) as a hypothesised elevated lake level which reached a new local maximum during 11-10 *kya* and which was dammed by the Tengis Gol outwash fan (Gillespie *et al*. 2008, p. 180). It is also close to the same elevation as beach deposits at the Jarai Gol exit into the Darkhad Basin (Gillespie *et al*. 2008, p. 173). Therefore, it is suggested that the "Soyo glacier" calved directly into the palaeolake as it was rising to its maximum level and was active during the period following lake level fall at 14 *kya* (since lateral moraines are not expected to have formed under water) and before about 12.8 *kya* due to the presence of carbon dated material. There was a cosmogenic date from the terminal moraine upstream from Soyo from 14 *kya* which demonstrates that glaciation may have been active at this time. However, if the 1602 m a.s.l. lake was glacially dammed, it seems unlikely that its bursting could be associated with glacial advance. This is also earlier than the reported time for renewed lake level rise. Multiple clam and snail shells supposedly associated with this lake level were dated to 14-13 *kya* by Gillespie *et al*. (2008) including specimens from about 10 km SSE of Soyo but a later date was chosen on the basis of larch charcoal due to the likelihood of a hard water effect for the mollusc remains (Gillespie *et al*. 2008, p. 180). This puts the proposed timeframe for the lake later that the animal bone date from Soyo. Therefore, the Soyo glacier cannot have been at the same time of maximal lake extent. It may still be possible that the 1602 m a.s.l. lake existed earlier than the stated range of 11-10 *kya* at a lower level before reaching its maximum. However, given all the evidence available, it is difficult to be confident of a 14-13 *kya* extensive glaciation building the lateral moraines at Soyo.

Perhaps the more likely possibility is that the Soyo glacier is much older and dates to the 19-17 *kya* glaciation. Under this hypothesis, the Hogiin Gol glacier would have reached the large terminal moraine at which point a finger of ice protruded from an existing breach where the river flows through today. Glaciers are able to be hemmed in by their own moraines given sufficient sediment deposition and may be constrained to exiting through a breach left by a previous proglacial lake outburst (Benn and Evans 2010, p. 489). This glacial finger advanced to meet the rising palaeolake where it terminated without an end moraine. While perhaps this explanation is easier to fit into the proposed timeline of palaeolakes and glaciation in the Darkhad, it does run into one problem. The glacial valley cuts through the lake deposits on the plains surrounding Soyo. Furthermore, no evidence for lake deposits has been found within the site. Therefore, it is more parsimonious on this basis to assume that the Soyo glacier postdates the Darkhad palaeolakes that reached to

that elevation and that the glacier simply ploughed through the lake sediments removing them entirely.

During the period following lake drainage at 14 *kya*, whether there was a glacier at Soyo or not, it is to be expected that the climate there was harsh and cold. The climate in the Darkhad has been projected to be cold and dry during the Late Pleistocene and Early Holocene with precipitation only increasing around 9.5 *kya* (Narantsetseg *et al*. 2013). This stands in contrast to neighbouring Lakes Hovsgol and Baikal where climate amelioration began two millennia earlier. Although the dating of layer ζ is uncertain, it can be said that it probably formed under cold but wettening conditions in the Darkhad prior to 8 *kya*. At the time of the 1602 m a.s.l. lake, Soyo lay four to six kilometres from the nearest shorelines (fig. 2.22). The surrounding dry but low lying land beyond the terminal moraine (area about 40 km^2) was connected to other such areas in the southern part of the basin by a thin strip of land between the lake and mountain (325 m between 1600 m a.s.l. and 1700 m a.s.l. contours). The site itself doubtlessly hosted a braided stream of glacial meltwater. It is entirely possible that humans or animals occupied the area at this time.

The deposition of unit δ took place during the warm Holocene optimum and the subsequent mid-Holocene arid phase of northern Mongolia. At the time, the lake level was supposed to be lower again (under 1570 m a.s.l.) which puts Soyo at least 10 km from the palaeolake shoreline at this time (fig. 2.23). The site and its surrounding landscape would have been far more easily accessible to humans and wildlife due to the lowered lake level.

The timing of the local Holocene optimum in the Darkhad is suggestive as it begins around the same time as the earliest date for layer δ (7732-7927 cal. BP) which is proposed to represent a change in depositional mode from fluvial to aeolian. This aeolian regime apparently predominated at Soyo from prior to 7.8 *kya* to 2.6 *kya* which spans a range of climatic conditions proposed in the literature. Aeolian-palaeosol sequences in Mongolia have been previously interpreted in terms of climatic history over very large time scales. Palaeosol formation is supposed to have occurred under warm, wet conditions and aeolian deposition under colder, dryer conditions (Feng *et al*. 2007, p. 515). At Soyo the aeolian sequence begins with, or at least covers, the warm, dry Holocene optimum in northern Mongolia and continues through the subsequent arid period in the mid-Holocene. Why aeolian accumulation occurred during a time when soil formation might be expected and why the deposition did not appear to change moving into a more arid climate is a challenging question. The answer probably lies in the local conditions at Soyo. One can never quite forget the possibility of erosion hiding large portions of the past. With aeolian dunes, it is quite reasonable to suppose there may have been both deposition and erosion even at the same time as dunes shift across the site. This is true of Soyo today. There are recent accumulations of sand into dunes in some parts of the site and erosion happening in others. Therefore, it may be that the apparent homogeneity in environment is false and that the true depositional history is more complex. Multiple weaker and localised palaeosols were found elsewhere at Soyo so perhaps there was additional subdivision of unit δ that

has become lost over most of the site. Another local reason for the change in deposition may be a change in the river system such that it no longer was able to deposit material on top of the site in the normal course of events (outside of flash flooding). The upstream end of the site is marked by an abrupt drop in elevation to the river with large limestone outcropping. Therefore, it may be the case that the Soyo site has been shielded from fluvial action. Finally, the change in deposition may be due to a greater availability of airborne dust in the region. This may be due to a decrease in vegetation. However, pollen records in northern Mongolia (Ma *et al*. 2013, Fukumoto *et al*. 2014), Lake Baikal (Tarasov *et al*. 2007), and the Altai (Blyakharchuk *et al*. 2004) all show that tree cover (mainly pine) was high during much or all of the relevant period from 8 *kya* to 3 *kya* (indicating a trend away from desertification). There is significant local variation between these records so it remains possible that plant cover had diminished within the Darkhad basin.

The later Holocene is represented in Dood Nuur sedimentary cores by a clay which is described to have formed under wetter conditions after 5.8 *kya* but during a time of lake level decline supposedly due to drying conditions (Narantsetseg *et al*. 2013, p. 20). In a study on Lake Hovsgol (Prokopenko *et al*. 2007), it was found that the ratio of precipitation to evaporation increased after 3 *kya*. A similar result was obtained from pollen records in northern Mongolia (Ma *et al*. 2013). At Soyo, the main palaeosol (γ) is dated to the millennium following this event. This might indicate that the climate had shifted to favour pedogenesis or simply that the local dune system at Soyo had stabilised at this time as has been explored above. The aeolian deposits at the confluence of the Orkhon and Selenge Rivers show that the late Holocene was marked by intermittent palaeosol formation in that area including one projected (but not dated) to around 3 *kya* (Feng *et al*. 2007, Ma *et al*. 2013). Critically, a palaeosol from the northern Darkhad basin yielded two carbon dates of 3410-3620 cal. BP and 3360-3560 cal. BP which was attributed to an end in post-glacial loess deposition (Gillespie *et al*. 2008, p. 180). This, combined with the results from Soyo, suggest the possibility of basin-wide palaeosol development at this time. In any case, it appears that the period of palaeosol formation and subsequent dune sands (α) was a period where the climate was approaching the modern one.

6.3.4 The Archaeology of Soyo

The most common artefacts found at Soyo are lithic tools, flakes and fragments. Other archaeological materials include pottery and evidence of fire and there was also animal bone found at the site. Several monumental structures (deer stones and khirigsuurs) and other stone structures are present in the surrounding area. The total surveyed area surrounding Soyo as of 2017 is about 13.5 km^2 (Clark and Bayarsaikhan 2017, pp. 31–2). Over 100 "sites" as defined and mapped in Section 2.3.2 *Regional Survey Surround Soyo* have been identified in the area. Over the course of 2015 to 2016, thousands of artefacts from from at and around Soyo were collected and recorded during excavation and pedestrian survey. This included a total of 1667 lithics, 590 ceramic fragments and 1299 bone fragments (Clark 2015, Clark and Bayarsaikhan 2016). Detailed study on most of these has not been

done; however, there has been one study on a select sample of stone artefacts from the excavation units which will be discussed below.

There were 189 ceramic fragments recovered from the excavation units of 2015 and 2016. Most of these (127) were found together in excavation unit 1 at a depth of 45-50 cm. A further 39 were found in the subsequent 5 cm spit below. All of the ceramic fragments in excavation unit 1 were located within the group of palaeosol horizons as identified by the excavators. Despite the numerous hearth features in excavation unit 4, only 12 ceramic fragments were found. All of them were located at a depth of 55-60 cm. It is not clear whether these fragments were found within a hearth feature or not but it is interesting that 634 bone fragments were recovered from the same spit. This (along with the stone artefacts) suggests intensive use of this area and the multiple hearths at different levels indicates this use went on for a long period of time. In excavation unit 6, only six ceramic fragments were found which were at a depth of 70-85 cm. This puts them below the well defined stratigraphic layers (A-D in the local pit nomenclature) and in the highly turbated sediments below. Therefore, it unlikely these were *in situ*. None of the other excavation units contained any ceramics (with the exception of excavation unit 8 which contained a single specimen) nor did any of the stratigraphic test pits dug in 2016. Ceramics were less represented among the pits than stone artefacts but, where they were present, were present at the same depths reached by the lithic artefacts. That is to say, there was no obvious pre-ceramic cultural level at Soyo. The one exception is in excavation unit 6 where there were lithic artefacts found up to 45 cm below the lowermost ceramics. Due to the turbation in this pit, a sorting effect on the artefacts can't be ruled out. The ceramics may have had more of a tendency to move upwards as compared to the stone artefacts. Since pottery is the defining feature of the Mesolithic-Neolithic in this part of the world, that means there was likely not a Palaeolithic occupation of the site after the last glacial retreat. That is likely to be the case in at least the studied area of Soyo but it does not preclude earlier Palaeolithic activity prior to the last glaciation that may have been stripped away. Excavation unit 6 contained the oldest date at Soyo (12.8 *kya*) so, if there is any place within Soyo that might contain such material, it may be there. The type of ceramic was not recorded by depth in any of the excavation units so it is unknown how the ceramic technology changed over time. However, the coarse, sandy greyware and redware are thought to be from the Mesolithic-Neolithic and Bronze Age respectively which is reminiscent of the Gobi ceramic scheme put forth by Janz *et al*. (2012, 2017, 2021). A lot more study needs to be done before any definite link can be made (Julia Clark pers. comm. 2023).

The general landscape beyond Soyo itself is full of archaeological features and sites (fig. 2.17). The pedestrian survey done both upriver and downriver of Soyo has revealed extensive activity in the area. The most common type of feature found were unspecified stone features (such as rings and mounds) and lithic scatters. These were found in two distinct clusters along the Hogiin Gol: one directly surrounding Soyo and extending upriver and one further downstream at a bend in the river. Given the distinct clustering, this may represent a temporal shift in land occupation or a contemporaneous territorial

distinction. Further work would need to be done to explore these possibilities. Khirigsuurs were clustered within a 0.5 km^2 area about 6 km ENE of Soyo in this second cluster of stone features. There was also a deer stone 2 km SE from this and 7 km from Soyo. Given these kinds of LBA monuments may have served (among other functions) to mark territory (Wright 2006), this cluster of monuments suggests that the area might have been important to people of that time. Furthermore, the stone features in the Soyo cluster of sites appear along the pass into the larger glacial valley upriver, on the southern side of Soyo Tolgoi and eastward along the river. This would put them in the path of any visitor to Soyo. Although these stone features are not khirigsuurs and they remain undated, this pattern might strengthen arguments connecting monuments and territoriality.

At least four other non-monumental sites along the river aside from Soyo have been investigated. Bayanii Am 1, on the northern side of the river across from the Soyo hill, produced 1096 stone artefacts (mostly bladelet and microbladelet fragments) and 424 faunal remains (Clark and Bayarsaikhan 2017). This shows that the archaeological landscape around Soyo does locally extend beyond the confines of the area studied in this work. Bayanii Am 3, located about 2 km upriver, was mentioned as a possible pre-LGM site that had survived the glaciation on a terrace in the mountain valley. Four quartz artefacts were found (two unipolar flake cores, a core-edge removal piece, and a scraper) (Clark and Bayarsaikhan 2017). If this is true, it provides direct evidence that the area around Soyo was indeed utilised by pre-LGM populations. Any trace of their activity near Soyo will have been obliterated by glaciation, outburst floods and the formation of the Soyo glacial valley but further remains may be found on similar terraces. This might be a promising future line of inquiry. The most important site (archaeologically speaking) near to Soyo is Bagsagiin Bulan. This site (4 km ENE of Soyo in the direction of the khirigsuur cluster) was identified as a LBA habitation site on the basis of the ceramics and the presence of a (structural) post hole (Clark and Bayarsaikhan 2017, 2018). This demonstrates that people were camping along the Hogiin Gol during at least the LBA. Numerous smaller scatters of lithics and ceramics along the river attest to more occupation in the area than just what is seen at the named sites. The spatial distribution of these correspond well with that of the monuments meaning they also form two clusters in the same locations. This suggests that the choice of occupation sites and monument sites are related. This stands in contrast with the findings of Clark (2014). However, it is possible that this clustering is spurious and derives from the small sample size (the "small sample size" in this case meaning the smallness of the survey area compared to the size of the clusters). The clustering may disappear once the survey area is extended significantly as new sites are discovered in the landscape.

It is tempting to consider interpreting the occupation at Soyo in light of other habitation studies elsewhere in Mongolia. For example, Houle (2010) identified a system of short range LBA migrations between Summer camps by the Khanuy River and Winter camps in the nearby sheltered valleys. Summer camps were noted by Houle to yield far lower quantities of archaeological material than Winter camps (Houle 2010, p. 52) which may indicate that Soyo was primarily occupied in Winter after the rise of nomadic pastoral-

ism as archaeological material is highly concentrated there compared to elsewhere in the area (Julia Clark pers. comm. 2023). Soyo lies between the areas for modern Summer, Winter/Spring and Autumn campsites (but on the margins of the Winter distribution) according to a local map drawn in 2016 (Clark 2017). Using modern campsite distribution to talk about past practices is, of course, questionable at best. The boundaries between camping areas probably shifted quite a lot over time but it does show that it is reasonable for Soyo to be a Winter camp depending on the climate and environment at the time. A trail of artefact scatters upriver from Soyo is suggestive of a possible movement route further into the valleys although it is impossible to say whether these are of the same time period as the occupation at Soyo. Unfortunately, since the bounds of the pedestrian survey are still largely limited to a small stretch of the river, it is impossible to do much more than speculate and await further data. Nevertheless, the monumental landscape and occupation pattern around Soyo indicate a long period of use and that Soyo is just one of many important locations in that part of the Darkhad.

The most extensive study on the stone artefacts of Soyo was undertaken by Gribble (2021). Multiple macroscopic metrics plus XRF were used to detect changes in the record over time. It was argued that there was a change towards longer-duration habitation episodes combine with more developed trade networks. This was tentatively interpreted as representing the Mesolithic-Neolithic to Bronze Age transition (Gribble 2021, p. 124). The new understanding of site stratigraphy developed in this thesis will be of some help towards the dating of the archaeological record.

The sample used by Gribble (2021) consisted of 92 lithics which were discovered in six different excavation units (1, 2, 4, 5, 6, 7) across 2015-2016 (fig. 4.1) and four lithics found on the surface for 96 total. Of these, two (units 2 and 7) are located outside the bounds of the geophysical survey so it is presently impossible to correlate the strata for these pits on the basis of the geophysical data. This represents 30% of the total sample. Unfortunately, the most productive excavation (containing 40% of the lithics in the sample) was located in the eastern part of Soyo which has not been confidently correlated to the rest of the site. This is due to the shallower stratigraphy compressing detail in the GPR profiles and the fact the the geophysical survey area did not cover all of the exposed palaeosols in the dune blowout area. Nevertheless, it is possible to give some likely time frames here. The remaining three excavation units (4, 5 and 6) contained the last 30% of the material (N=18, N=7, N=1 respectively). Most of the following accounts of the excavated finds are derived from Gribble (2021).

In excavation unit 1, the largest share of the lithic material was buried at 50 cm below the datum used (cmbd) which is within the "B soil horizon" (as described on the field diagrams using soil horizon notation (Retallack 1990, pp. 30–4)) of the middle palaeosol of the eastern blowouts. This was at the bottom of the excavation pit although an augur was used to continue for another metre below that. This B soil horizon contained the most lithic artefacts and the largest variety of lithic materials. It is also the level where a large

number of ceramic fragments were found (see above). Although excavation unit 2 is outside the bounds of the geophysical survey, it is very close (33 m north) to excavation unit 1 and has similar stratigraphy. Excavation unit 2 had fewer artefacts overall but the bulk of them were found at 40 cmbd which corresponds to the same B soil horizon as 50 cmbd in unit 1. This supports the finding of a concentration of lithics in that horizon. Unfortunately, the relation between the palaeosols in the blowouts area and the main stratigraphic model for Soyo is unclear. This means the age of that palaeosol (and associated artefacts is unknown) although it is probable that it formed during the proposed main period of soil formation at Soyo (2.6 *kya* onward).

In excavation unit 4, the majority of artefacts, along with the only non-chert examples, were found at 20-30 cmbd. This places them above the youngest palaeosols. No direct date has been obtained from unit 4 but the sequence of palaeosols here are collectively part of stratigraphic unit γ. Excavation unit 4 is horizontally close to unit 6 so, if we accept this means the palaeosols are close in age, this means that these artefacts are very young (within the last 350 years but probably even younger than that). Another sharp increase in lithic artefacts was found at 60 cmbd in excavation unit 4 possibly in relation to a hearth, charcoal, bone and other artefacts found there below the lowest palaeosol. Multiple examples of these hearth features were found at different levels in excavation unit 4. The early Deer Stone Project reports found similar features. Although it is unclear where that team excavated and collected material for dating, it was in the vicinity of excavation unit 4 based on the descriptions and photographs available. Two palaeosol units were discovered 10 cm apart which accords reasonably well with what was observed in excavation unit 4. One of the lower hearth features excavated in 2003-2004 was identified as Neolithic and dated to 6510-5940 cal. BP (Bayarsaikhan *et al*. 2005, p. 228, Fitzhugh 2005, p. 18). It is not explicitly explained how it related to the palaeosols there but the implication was that it was associated with the lower one. This may not actually be the case considering the existence of at least one hearth in excavation unit 4 below the lowest palaeosol. Putting all this together, the lithic record in unit 4 likely spans a period of time from the mid-Holocene to recent with the bulk of the material being from those two end points. This makes it impossible to reasonably talk about when a change in the lithic technology may have occurred based on the sample presented in this unit.

There were comparatively few lithics found in excavation unit 5. All were located in the first few centimetres of soil (β) that cover the surface in this area (20 cmbd) which, as has been demonstrated in this work, is related to the main palaeosol (γ) found farther west at Soyo. This sub-assemblage contained the variety of artefacts (in this case bifaces, non-chert specimens and chert with alternate chemistry) that was characteristic of upper level artefacts in other pits and was suggested by Gribble (2021) as representing the transition to EBA (defined as being characterised by the advent of pastoralism).

Only a single lithic from excavation unit 6 was included in the sample. This was a black chert flake tool from 125 cmbd which puts it in the same stratigraphic unit (G or adjacent

K) that was dated variously to 12.8 and 1.1 *kya* according to Vella (2018). Unfortunately, very few artefacts total - five according to the full finds catalogue (Julia Clark pers. comm. 2022) - were found in excavation unit 6 despite the promising stratigraphy there.

Most of the lithic sample presented in Gribble (2021) were associated with the complex of soils denoted here by β and γ which has been argued here to have begun forming by 2.6 *kya*. In light of the new model for site stratigraphy proposed here, it is very difficult to maintain the conclusion proffered by Gribble (2021) that the change towards increased artefact variety and material provenance represents the transition from Mesolithic-Neolithic to Bronze Age. Pastoralism in Mongolia is thought to begin in the EBA (*i.e.* prior to the LBA when pastoralism was well established but after the Mesolithic-Neolithic when hunter-gatherers were prevalent) (Clark 2014, p. 52). The Afanasievo culture thought responsible for the introduction of pastoralism into Mongolia has been shown through the dating of monuments to appear from 3000 BC (Taylor *et al*. 2019) making this the likely beginning of the EBA in Mongolia. This is borne out in the changing material culture and subsistence patterns in the Gobi oasis economies (Janz *et al*. 2021, p. 2). In contrast, the LBA is attested from the later second millennium BC through the new deer stone and khirigsuur monumental forms and the domestication of the horse (Clark 2014, pp. 45–6, Taylor *et al*. 2019, Wright 2021, p. 440). The period of soil formation (containing the transition identified by Gribble (2021)) begins well after the start of the LBA and, in fact, after the start of the Iron Age at 800 BC (Wright 2021, p. 451). The full period of palaeosol formation may extend a little further back into the LBA but it is unlikely that the artefacts found within units β and γ are related to the Mesolithic-Neolithic or EBA and the transition identified by Gribble (2021) is likely to be an Iron Age one.

This conclusion presents a conundrum because of the presence of material that has been identified as ”Neolithic” at Soyo. The original identification of Soyo as a ”Neolithic” site on the basis of the small finds combined with the mediaeval dates (Fitzhugh 2005) has caused a difficulty in the understanding of chronology at Soyo that has been a major problem in research at the site to the present. Subsequent radiocarbon dates (Bayarsaikhan *et al*. 2005, Vella 2018) have extended the range of the time period attested without satisfactorily explaining the chronology of archaeological remains. A major part of the problem is that spatially close or related samples have been dated as thousands of years apart. The main examples of this are the ”Iron Age” and ”Neolithic” palaeosols 10 cm apart from the Deer Stone Project and the more than ten thousand year gap between dated bone samples within a single stratigraphic feature in excavation unit 6. It is clear that there is culturally Mesolithic-Neolithic material at Soyo but a definite palaeosurface or definable stratigraphic unit exclusively from that time period has not been found. The practical implication of this is that there is not a convenient way to stratigraphically link this older material culture together across Soyo. It might be necessary to date every Mesolithic-Neolithic feature of interest if temporal correlation between separate features is desired.

As for the explanation of why no widespread Mesolithic-Neolithic palaeosurface or defin-

able stratigraphic unit has been found throughout the rest of Soyo, the culprit is probably erosion. There may have been such a surface (pedogenesis optional) or defined stratigraphic unit but much of the sediment was eroded down before either fresh sediments were deposited on top creating a paraconformity or the land surface stabilised and pedogenesis began. The paraconformity was not evident in the field but it is the best explanation of the facts. It would exist within stratigraphic unit δ. The Mesolithic-Neolithic hearth discovered and dated by the Deer Stone Project was certainly taken from the western end of Soyo where there is an erosional escarpment in GPR grid A (fig. 4.5). Excavation unit 4 (dug 2015) revealed a number of stacked hearths and palaeosols together in the same part of the site. The stratigraphic diagram (fig. 6.24) shows that the lowermost hearth is 10 cm below the lowermost palaeosol indicating that this is not the surface associated with that hearth. It is not clear the precise relation between the hearth and lower palaeosol identified by the Deer Stone Project but it may be a similar situation. There may have been a large erosional time break between two generations of hearths (the ones below the palaeosol and the ones associated). This would mean the palaeosol surface may be younger than the Mesolithic-Neolithic hearths at Soyo. The disparate dates within the same strata in unit 6 was likely caused by severe cryoturbation (and possibly bioturbation) of the sediments as seen in the lower sediments there but a paraconformity may have also played a role in bringing bones fragments with such widely differing ages closer together in the strata. This process would mean that Mesolithic-Neolithic artefacts would be accumulated onto the paraconformity as the sedimentary matrix is eroded and the land surface steadily lowers. It has not been noted in the catalogues if artefacts are found within or without any features (only their depth is recorded) so it cannot be determined if the large clusters of stones tools and bone found at certain depths in excavation unit 4 are a result of this surface lowering or were associated with a hearth. If they were associated with hearths, that would not be surprising as it can be assumed that a lot of material would have been deposited there. If not, that would lend support to the presence of a paraconformity.

Given this explanation, it would seem that whatever erosional process was responsible for eliminating the hypothetical Mesolithic-Neolithic strata was very thorough. No palaeosol at Soyo has been dated to that period assuming the hearth discussed above was unrelated to the palaeosol. Furthermore, no unexplained, site-wide candidate reflections were identified in the GPR data. It would seem, then, that it likely did not survive anywhere within the area of the site that has been studied so far. This does not preclude its survival in the unstudied parts of Soyo (which are extensive) but it does call into doubt the prudence of hunting for it.

A secondary explanation might be that the same or similar lithic and other small finds material culture was used in the Darkhad well into the Bronze and Iron Ages by at least some groups. Given the remoteness of the region and the natural barriers that separate it from the rest of Mongolia, it is not impossible that local traditions may have persisted for longer.

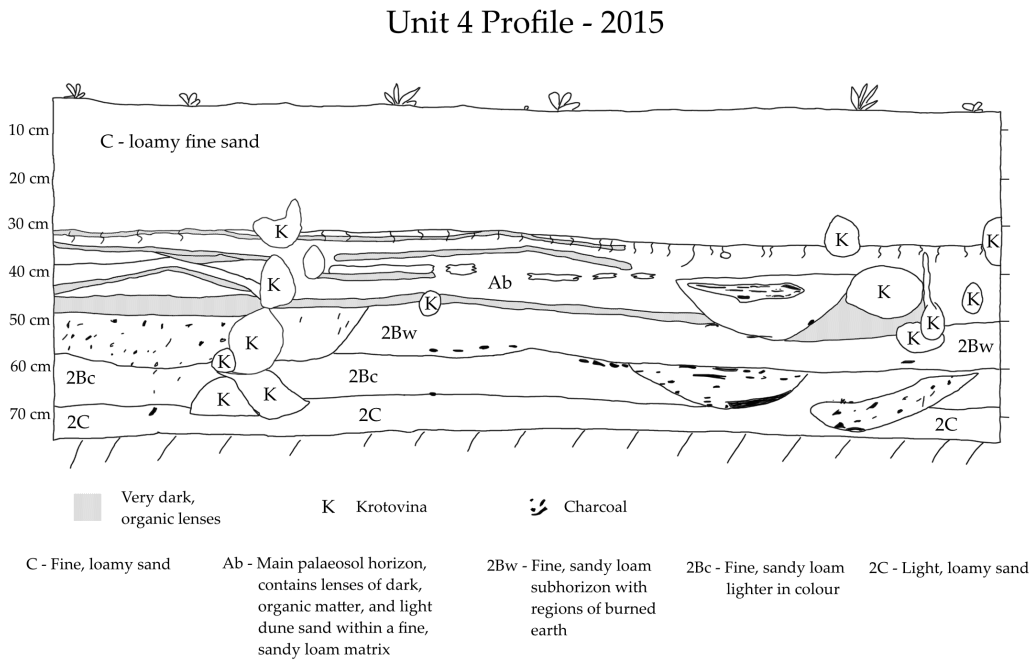

Figure 6.24: Stratigraphic Diagram of the south wall of excavation unit 4 dug 2015.

6.4 Implications for Mongolian Archaeology

There are few well stratified sites that have been discovered in Mongolia and fewer still from the Mesolithic-Neolithic period. It has been a commonly expressed sentiment that Mongolian habitation sites are low visibility and ephemeral with poor potential for detailed study of chronology and domestic practices (Honeychurch *et al*. 2007, p. 373, Houle 2010, p. 49, Clark 2014, p. 175, Honeychurch 2015, p. 132, Wright 2021, p. 450). The reason for this dearth of stratified sites is probably partly because of the fact that Mongolia's landscape is generally non-aggradational meaning sediment is not net accumulated in great quantities to form stratigraphy (Houle 2010, p. 82). Furthermore, the nomadic practices of the ancient inhabitants of Mongolia meant they did not leave as many material remains at each site. Therefore, most sites in Mongolia are shallow palimpsests of material from a wide range of time periods. It is very difficult to then disentangle material culture by time period since excavatable contexts are poorly preserved or absent. The zone of artefacts at habitation sites rarely goes deeper than half a metre (Houle 2010, p. 82, Clark 2014, p. 96). The typically sparse remains per site only compound this problem. It has been hoped that Soyo would be able to shed some light on the chronological changes that took place during this time and into the EBA because Soyo is an aggradational site. In particular, it is not so much the depth of stratigraphy that was promising (although it is deeper than the typical Mongolian site) but that the net aggradation of sediments allowed multiple

palaeosols to be formed. This means that there should be multiple definable, and most importantly dateable, palaeosurfaces that would have been occupied. This is not typically true for other Mongolian sites. However, hoping for stratified sites to solve the problems in Mongolian chronology may be asking too much. Although Soyo promised much, the complex and disturbed stratigraphy, the fact that only one palaeosol appears to be present across most of the site, and the fact that archaeological materials are sparse all mean that the site did not enable a comprehensive and definitive chronology of occupation. The absence of the deeper palaeosols across most of Soyo has huge implications for the location of archaeological material. As mentioned, artefacts at most archaeological sites in Mongolia are shallowly buried and the same is true for Soyo. Taking into account the depth from the nearest palaeosol above (not just the depth from the modern surface), the majority of artefacts at Soyo were buried within a depth of 35 cm. This apparent shallow burial is argued to be the result of the period of erosion or non-deposition of sediment prior to palaeosol formation. The other point about the scarcity of archaeological material is also an important one. Even had the stratigraphy at Soyo been well preserved and easy to understand, the low density of archaeological materials of a campsite may still have hampered the development of a Darkhad archaeological chronology. Barring the discovery of an exceptionally well preserved and extensively occupied site, most sites in Mongolia are likely to be as complex and difficult to understand as Soyo. The reason Soyo is stratified at all has nothing to do with occupation levels being stacked on top of each other (as it is in sedentary settlements with intensive occupation such as Near Eastern tells) but because it sits within a glaciofluvial system where sediment is naturally accumulated. There are probably many similar sites in northern Mongolia but research on early occupation sites in the area is extremely limited. This distinction between modes of stratification is important to note because it means that the sediments themselves are not culturally deposited but rather the cultural deposits lie within naturally deposited sediments. Therefore, the relationship between the archaeological material and the dated stratigraphic layers is less direct. An illustration of this problem arose during this research when there was ambiguity in excavation unit four over whether the Mesolithic-Neolithic hearth feature was connected to any of the palaeosols there. This highlights the importance of still collecting samples for carbon dating from any important features or artefact clusters rather than relying on tenuous and difficult-to-interpret stratigraphic connections to indirectly date features of interest. In fact, dating of individual features in the landscape has already been used with apparent success to build a chronology of burial types (Taylor *et al*. 2019). An acceptance of the limitations of the Mongolian archaeological record may be necessary.

The present work has produced some more dates towards a chronology of Darkhad archaeology. It has been shown that much of the lithic material shedding from the eroding palaeosol at Soyo is probably LBA or later in age. Nevertheless, there is some Mesolithic-Neolithic component at the site as shown by the characteristic artefacts and a securely dated hearth (Fitzhugh 2005). There is a stratigraphic unit (δ) belonging to this approximate age which has probably been an unstable surface with discontinuous periods of deposition, non-deposition and erosion. This study has succeeded in its goal of filling the

large chronological gap in stratigraphy identified by Vella (2018). These new dates have covered a period from 7.9-1.9 *kya* although there is still a substantial five thousand year gap between this and the oldest of dates at Soyo (c. 12.8 *kya*). An investigation of this older gap (if desired) must look to even deeper strata that could not be identified using the methods herein and which were deposited between glacial till boulders. These sediments were probably a mixture of eroded and new sediment as the pro-glacial stream reworked the fine till sediments. The most likely location at Soyo for success in this endeavour would be west of the current survey area and north of the Soyo Hill (west of GPR grid A). Extending the geophysical survey into that area may reveal deeper stratigraphy. However, it is likely that cryoturbation in that area will have made untangling the earliest postglacial period of Soyo's site formation history very difficult indeed. The deepest, most extensive stratigraphy was visible in GPR grid B but no archaeological remains were uncovered in any of the test pits in that area so it is unlikely that future excavations there will find success. The dates presented here complement previous dating programs at Soyo by not only filling much of the chronological gap in stratigraphy at the site but also approximating the general range of previous dates (subtracting the 12.8 *kya* date) beginning with a c. 7 *kya* natural timber horizon and c. 6.5-6.0 *kya* Neolithic hearth (Fitzhugh 2005) and ending with Iron Age to modern deposits.

The interpretation presented here that the stable palaeosol land surface began to form after 2.6 *kya* is significant in the context of other dates taken from the Darkhad basin. Most of the archaeological dating work done there has been on monuments such as deer stones and burials and most of these lie in the range of 4.2-3.6 and 3.2-2.8 *kya*. Therefore, there was an extensive human occupation of the Darkhad prior to the concentration of archaeological material in the Soyo palaeosol complex. The Neolithic hearth at Soyo remains the oldest dated archaeological material in the Darkhad but it must be remembered that most of the dated material there came from the conspicuous Bronze Age monuments (many taken by a research project entitled "The Deer Stone Project") so it is only natural that the acquired dates would be predominantly from that time period and later. Whether Soyo was occupied from a particularly early period compared to the surrounding region is a question that can only be answered with a lot of further research on the pre-Bronze habitation of the Darkhad. It would appear likely *prima facie* that the earliest sites should be found towards the southern (or perhaps northern) margin of the basin as well as near Soyo both because one would expect them to be proximal to the mountain passes and because the southern end of the basin was the most unaffected by the Holocene palaeolake flooding. There are numerous rivers along the southern and eastern sides of the basin which exit the mountains onto tongues of land above 1600 m a.s.l. and could have provided depositional regimes that formed stratified sites even during the 1600 m a.s.l. lake (11-10 *kya*). A search for the earliest human occupation in the Darkhad after 14 *kya* (the end date for the 1670 m a.s.l. palaeolake) should begin along these rivers (fig. 6.25). Whether the areas on the eastern side were above 1600 m a.s.l. at the time (and hadn't emerged above that level due to more recent deposition) is unknown. The range for potentially stratified sites in the Darkhad only increases during the Holocene as the palaeolake from 9.5 *kya* was sig-

nificantly lower and gradually diminished until 3.9 *kya*. Since the main period of general land surface stability at Soyo is now shown to have started in the LBA, it can be said that the artefact assemblage associated with the main palaeosol complex is probably related to this period of monument construction. Particularly, the three unspecified "mounds" at Soyo dating to the range of 3172-2489 cal. BP (Fitzhugh and Leader 2006, p. 78) show that monument construction was already underway by this time. This is not to say that the Soyo camp site was directly related to the construction activity itself but merely that the same groups of people who built the nearby monuments at this time probably sometimes occupied the site itself (and other undiscovered sites as well).

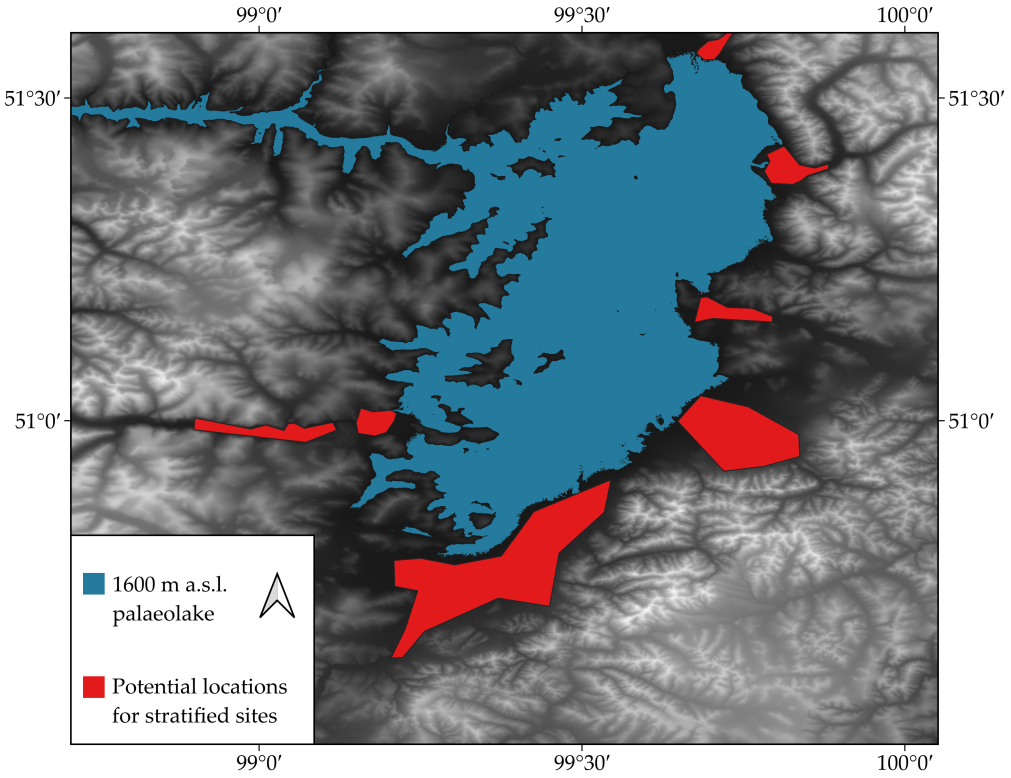

Figure 6.25: Map of the Darkhad showing a 1600 m a.s.l. palaeolake in blue. Areas in red are those where other old and stratified sites similar to Soyo may potentially be found. DEM is JAXA ALOS 3D 30 metre DEM v3.2 (2021).

The overarching question in Mongolian archaeology of the nature and timing of the transition to nomadic pastoralism that is thought to have occurred during the EBA has been the driving question behind the Nomad Science project at Soyo. However, this research suggests that Soyo might not actually be the right site to answer this question. The reason is that, while chronological gaps in the sedimentary record of the site have been partially filled, the key temporal gap between the Mesolithic-Neolithic period and the LBA has been shown to be poorly or not represented at all. Very likely, the desired sediments have been largely eroded away or perhaps this was a period of non-deposition at Soyo. The sole

relevant date thus far obtained from Soyo (4088-3927 cal. BP) comes from an area with little archaeological material and was not itself associated with any archaeological feature or artefacts. It remains possible that unsurveyed areas of Soyo, or perhaps the as of yet poorly understood blowouts, may prove fruitful in this regard. However, there is no indication from the results of the present research that Soyo will be able to provide the archaeological sequence necessary to definitively resolve the timing of transition to nomadic pastoralism.

How pottery spread after its initial invention in East Asia is another ongoing debate with some (Hartz *et al*. 2012, Gibbs and Jordan 2013) advocating for a diffusion of the technology westward while others (Kuzmin 2013a, 2013b) arguing for local invention in Eurasia. The earliest date for pottery at Soyo comes from the hearth feature at 6.5-5.9 *kya*. By comparison, pottery emerged in the Gobi at 9.6 *kya* (Janz *et al*. 2021, tbl. 1), in the Cisbaikal region around 7.8 *kya* (Weber 1995, p. 156) and in the Transbaikal region around 14 *kya* (Tsydenova *et al*. 2017). While the Mesolithic-Neolithic date for the early pottery at Soyo is by no means necessarily representative of the earliest pottery in the Darkhad, it is younger than all three other regions. Possibly this is due to the remoteness of the basin. It is far to early to draw any firm conclusions about how pottery arrived in the Darkhad but, given the younger date here, it is possible that the idea of pottery was able to arrive from either Cisbaikal (there is a pass from there into the Darkhad) or possibly from the Gobi through central Mongolia. A lot of further work needs to be done on the chronology of pottery in the Darkhad and their possible technological or stylistic relation to other pottery traditions before either of these routes can be tested.

6.5 Implications for Geophysics and Landscape Reconstruction Archaeology

One of the chief problems in this research has been the complexity in stratigraphy at Soyo. Cryoturbation and bioturbation appear to have been significant processes which made dating the stratigraphy difficult. That the site was underlain by glacial till deposits proved especially difficult since post-glacial deposition was able to nestle between what would have been a surface boulder field at the time. This made tracing these earlier features with the GPR impossible since their reflections were completely dominated by the reflections from the till boulders. This presents a real difficulty in any geophysical investigations of archaeological sites in former glacial valleys. Original sand, silt and clay clasts deposited by glacial action can be expected to have been reworked and partially eroded by pro-glacial streams with newer, younger deposits replacing them. Therefore, it can be expected that a significant portion of the earliest history of a site like Soyo would be invisible to GPR and probably other geophysical methods as well. Archaeologists who work in rock shelters face a similar problem with roof fall hiding deeper and older stratigraphy. They often use geophysics to try to identify if rock reached in excavation is the true bedrock or merely roof fall. The difference between the two scenarios (glacial sites versus rock shelter sites) is that the latter involves a fairly homogeneous layer of rock fall and the geophysics is used to test

for further sediments beneath it. The former, involves a mixed stratum of boulders and sediment and the archaeologist is interested in material within that stratum. The success of geophysics in solving this problem in rock shelters does not translate to equal success in a glacial environment.

On the other hand, without the GPR data, any correlation of strata across this site would have also been impossible. The massive sands and unhelpful carbon dates made correlation via sedimentological characteristics, as in Vella (2018), very difficult over longer distances. Without GPR, any correlations made on the basis of the sediment analysis would have been tenuous at best. Although the GPR faced some severe limitations at Soyo, it was nevertheless instrumental in piecing together its stratigraphy. One of the main successes of the GPR at Soyo was proving that the palaeosol found in 2019 was the same one as the upper palaeosol found in 2015 and 2016. Based on the reported dates, that would seem unlikely in the extreme. The GPR data was able to prove they are related and form the cornerstone of the stratigraphic reconstruction.

While GPR was able to pick out some more subtle stratigraphic boundaries, the ERT data (both Wenner and dipole-dipole arrays) proved less helpful for this purpose. Most of the sediments lying above the glacial till (with the exception of the modern, loose sand dunes) fell within the same resistivity facies and no distinction could be made within them. The exception was the modern dune system (α) which did show up as a moderately resistive facies (fig. 6.13). In particular, the palaeosol was indistinguishable from the underlying sediments in every relevant ERT profile. The problem was almost certainly a lack of resolution. One metre spacings between electrodes were chosen because of the need to cover a large area but it came at the cost of having a chance to resolve fine detail. The resistivity survey was, however, very useful for understanding the bigger geological picture. It was able to find the bedrock beneath the lodgement till and situate the archaeologically interesting sediment package in its overarching geological context. If ERT is to be used to detect thin layers in the subsurface, a very small spacing (perhaps no more than 25 cm) between electrodes should be used. Unfortunately, this is at odds with the scale of interest for landscape reconstruction. Doing this also sacrifices depth of investigation so it is a difficult balancing act for the geoarchaeologist. Ideally, the choice of parameters should be guided by the research question and previous knowledge of the site.

The differing problems faced by GPR and ERT suggest that using them together is a good idea. Indeed, it was a good idea at Soyo since the alignment between ERT and GPR profiles showed that the glacial till layer, as seen in the GPR, corresponded to the moderate resistivity facies in the ERT. This helped increase understanding of the site by reinforcing the interpretation of till in the GPR and by suggesting that the highly resistive layer beneath this should be bedrock. Having both sets of data increased confidence in the interpretation and sidestepped limitations in both techniques. It should be recommended to use multiple complimentary techniques in any geophysical survey of an archaeological site. It has been found at other sites that the integrated use of ERT and GPR can overcome the weaknesses

of either method (Imai *et al*. 1987, Howard *et al*. 2008, Gaber *et al*. 2021) and particularly that the use of one to constrain the other can help resolve subsurface complexity (Negri *et al*. 2008) and improve depth estimates (Orlando 2013).

6.6 Future Research

The easiest and most immediate continuation of the research project at Soyo should be to date the moraine samples collected from the field in 2019. Cosmogenic dates were originally intended to supplement this research and would have answered currently unresolved questions about the beginning of the stratigraphic sequence at Soyo and, therefore, its potential chronological range in archaeology. In particular, knowing the timing of the multiple generations of lateral moraines north of the site as well as the timing of the final glaciation which carved the valley in which Soyo sits would be greatly beneficial to understanding the geological context that existed prior to human occupation of the site. It may also then help understand the environmental context of human migration into the area. An examination of the stratigraphy of the inter-moraine shelf north of the River Hog may also help towards this end.

A more focused approach to dating the archaeology at Soyo is recommended. The palaeosol complex in the blowouts area of Soyo particularly demands attention and it would be beneficial to have dates from each of the levels. Much of the lithic material examined by Gribble (2021) falls within this part of the site which has no direct dates and whose relation to the main stratigraphic scheme is unknown. Whether or not the palaeosols there can be conclusively demonstrated to be of the same age as the rest of the site would be of great help to clarifying their relation to the rest of the site and assessing Soyo's suitability for direct diachronic research. Targeting specific areas of the site that have sequences of palaeosols would also be useful for disentangling the occupational palimpsests.

Since the site is mostly sand, luminescence dating could be a potentially useful technique. There were about two dozen carbon samples retrieved from Soyo that were not submitted for dating so there is no shortage of suitable material for radiocarbon dating. However, a targeted study involving luminescence dates would be useful if directed at trying to discern exactly where the paraconformity between Mesolithic-Neolithic and LBA dates lies as well as to estimate how much of that time, represented by deposited sediments, is missing. In the case of this specific question, luminescence dating would be the superior dating technique as it can date the last burial of the sediments directly instead of hoping for suitable organic samples to be present in sufficient density.

Clay and pollen analysis would provide a more direct way of investigating the environmental changes over Soyo's formation history. Using X-ray diffraction to investigate the clay types present in sediments is an established tool in the attempt to reconstruct palaeoclimates. In particular, the differences in hydrolisation regimes between warmer and wet-

ter climates and cooler and drier climates has an impact on the clays that are available for deposition (Chamley 1989, chap. 17). Clay analysis has been used at Lake Baikal to make these kinds of inferences about palaeoclimate but also to infer the source of clay sediments and therefore the degree of fluvial transport (Horiuchi *et al*. 2000). Pollen is widely used to reconstruct vegetation cover in the area. In Mongolia this has been used to calculate the presence of steppe versus forest species as well as temperature and moisture indices over time (Feng *et al*. 2007, Tarasov *et al*. 2007, Ma *et al*. 2013). Clay analysis was planned for this research but was cut so indirect comparison by chronology to existing palaeoclimate models had to be made. Furthermore, there is a dearth of climatic data from the Darkhad basin and so studies from the neighbouring Lakes Hovsgol and Baikal as well as from around Mongolia were consulted. This presents a problem as it is not guaranteed that the climatic changes were the same in timing and severity between regions. The existing information available in the literature suggests that indeed they were not. Having this data from Soyo would be invaluable for the study of the relationship between ameliorating climate and migration into the region.

The biggest improvement to the methods used here would be to use a high density sampling strategy in the stratigraphic pits. While this would have undoubtedly greatly increased the time required to analyse the sedimentology, taking only one sample per field-identified stratigraphic unit meant that only broad stratigraphic units that could be identified by eye were analysed and there could be no understanding of internal structure such as, to take one possible example, fining upward sequences which would have been indispensable for a truly robust model of deposition regimes at Soyo. It was always planned to go back to the site in years subsequent to 2019 to take more and better data as need would be indicated from the results of that year. This would have included better stratigraphic control and likely the extra techniques mentioned above. Unfortunately, this became impossible. Taking samples at regular intervals (say every 2 cm) would have resulted in much more detailed information about the stratigraphic sequence and greatly aided the correlation between pits. It would also have been good to use a down-hole sensor for magnetic susceptibility which would have provided more detailed changes of magnetic susceptibility through the stratigraphic sequence without needing to open an excavation to take sediment samples. However, it may be difficult to keep a hole open at Soyo due to the sandy soil (Dalan 2008, p. 5). This would have provided extra (but limited to changes in magnetic susceptibility) stratigraphic control over a wider area.

One final, intriguing possibility for future study would be to map the spatial distribution of sites in the Darkhad basin according to various archaeological categories (presence of pottery, presence of domesticated faunal remains, deer stones, *etc*.) in comparison to the extent of the lower palaeolakes. This should, assuming no preferential use of higher or lower ground, reveal a rough chronology of changes in the material culture. To accomplish this, it would be necessary to conduct large scale survey looking for sites of all, but especially earlier, time periods. This task would be slightly complicated by the fact that sites on dry land during a high lake stand would be available for occupation under a low stand as

well. Therefore, it should contain both early and late material while low lying sites should bear only later material. A further difficulty in this idea is that the chronology for Darkhad palaeolakes is not yet at the fine detail that would be desired by archaeologists. There is also some active disagreement over the level of some of the lakes. In particular, the 1602 m a.s.l. lake supposedly present from 11 *kya* to 10 *kya* according to Gillespie *et al*. (2008) but not according to Krivonogov *et al*. (2012) and Narantsetseg *et al*. (2013). An interdisciplinary project around improving the palaeolake chronology would be rewarding for the archaeologist and geologist alike.

Chapter 7

Conclusion

Existing research on the Mesolithic-Neolithic and EBA periods of Mongolia is limited. These periods are poorly understood and there is an even greater lack of information for them from the Darkhad basin. This is despite the assumption that critical behavioural transitions such as the move towards pastoralism happened during this time (Clark 2014, p. 52). The site of Soyo in northern Mongolia has been intensively studied using a variety of methods. The geophysical surveys, stratigraphic test pits, aerial photography, sediment analysis and radiocarbon dating have been combined to create a stratigraphic model and a history of site formation. This enabled conclusions to be made about the timing of human occupation and the environmental context of that occupation. It was found that, while the site has strata dating back to at least 7900 years ago, the complex system of palaeosol occupation layers found in previous years are spatially limited. General soil formation across Soyo appears to have taken place largely during and after the Iron Age.

7.1 Research Questions

The three research aims presented in Chapter 1 have been achieved. A stratigraphic model for Soyo was able to be built using geophysical survey data in conjunction with direct stratigraphic information from excavations and test pits. All of the major stratigraphic units thus identified were either dated directly with radiocarbon dating or given reasonable interpretations of their likely ages through age constraints. The resulting chronology was able to be compared with palaeoclimate record to infer past environmental conditions at Soyo. This stratigraphic and chronological foundation leads to answering the higher research questions that lie behind this thesis.

How do the dates acquired by Vella (2018) relate to the rest of Soyo and are there surviving, datable strata between 12,900 and 1250 years BP?
The answer to this question is that there was probably significant enough turbation in this part of the site to bring widely disparate dates (10,900 BP to 1200 BP) together into one stratigraphic unit. It is therefore unclear how the oldest date relates to the site stratigraphy since it can be assumed to not be *in situ*. However, it is proposed that this date represents

the earliest period of post-glacial deposition that survives at Soyo. The other recent (under 1000 years old) and modern dates are related to the main palaeosol-soil complex (master stratigraphic units γ and β) which, combined with the dates presented in this thesis, show that the period of general soil formation lasted for at least two and a half millennia. Not all areas of Soyo were stable enough at any given time for soil formation to occur. However, this period marks a phase when at least some parts of the site had sufficient stability for this process. The dates presented by Vella (2018) are in fact unusually young with the exception of the extraordinarily old example. The dates presented here all fall within this large gap (ranging from about 7.9-1.9 *kya*) and help fill in much of that missing period in the stratigraphy. This solves one of the major problems with Soyo's stratigraphy which was a lack of dated strata between 12.8 *kya* and 1.2 *kya*. There is still a substantial gap in dates between the oldest date reported here (7.9 *kya*) and that by Vella (12.8 *kya*). However, it is argued that a well defined stratum dating to this period is unlikely to be found because the deposits would lie within the till as a fluvially reworked sediment. Cryoturbation may also increase in significance at these depths. This is demonstrated in excavation unit 6 where Vella's oldest date was found and such an old date may not represent archaeologically interesting sediment deposits.

What is the date of the material culture at Soyo and particularly the date of the transition in stone tool artefacts identified by Gribble (2021)?
This thesis has shown that much of the site of Soyo only bears one palaeosol or top soil stratigraphic unit and that the multiple palaeosols found in western Soyo in previous field seasons are likely all horizontally related to this unit. To put it another way, the multiple palaeosols (in western Soyo) are part of a combined loess-palaeosol sequence that formed as the palaeolandsurface experienced temporary periods of stability and instability. In the central part of Soyo, the surface appears to have been stable the entire time or, at least, there is no evidence of a cycle of stability and instability. The multiple palaeosols to the eastern end of the currently surveyed area are a possibly separate system of sand and soil but further survey work would need to be done to confirm this. At present, they do not appear to be easily relatable to the current stratigraphic model of Soyo. The main palaeosol-soil complex has been dated from the Iron Age to the present. Therefore, the likely time of the transition in stone technology identified by Gribble (which centred around that complex) is the Iron Age. This is substantially different from the EBA transitional period that was assumed.

Is Soyo a good choice in site for research into the advent of pastoralism in Mongolia which is thought to have taken place in the Early Bronze Age?
It is difficult to make firm statements in the negative but it can be said that the area in western Soyo that has been extensively studied is a poor place to understand transitions taking place in the EBA. This is not only because of the apparently compressed stratigraphy there but also because, as it is argued here, significant sections of the relevant stratigraphy have been eroded away leaving a paraconformity. This means the archaeological record of that time period will be incomplete or not *in situ*. For much of the rest of the area surveyed so

far, there is only one identifiable soil unit. It is possible for archaeological remains to be left on sandy, unstable surfaces as well, of course, but the quantity of them was, in reality, far lower than in the western area with multiple palaeosols and the eastern area with the blowout dunes and multiple palaeosols. It remains possible that suitable areas for investigating the advent of pastoralism exist elsewhere at Soyo. The palaeosol complex in the eastern blowouts is as of yet undated and it may prove to hold distinguishable strata of the right age. Otherwise, there are still large areas at Soyo on both sides of the river that remain largely unexplored. Further geophysical surveys may be able to identify well preserved stratigraphy and potential candidates for future work.

7.2 Problems and Recommendations

The biggest problem faced during this research was undoubtedly the sampling strategy used to take sediment samples from the test pits. Taking one to two bulk samples per discernible stratigraphic unit made it difficult to use them to aid the GPR in correlating between pits. Furthermore, changes within major strata have been averaged into one sample meaning that potential valuable substratigraphic information has been lost. This information may have been valuable for finer reconstruction of depositional environments, palaeoenvironmental reconstruction and stratigraphic correlation.

The complex stratigraphy present at Soyo and particularly the complexity of the GPR profiles made them difficult to interpret. While the palaeosol was easy to identify by GPR, other stratigraphic boundaries were not so easy as they often disappeared and reappeared from line to line. The massed reflections representing the glacial till are presumed to hide potentially significant stratigraphy that is inaccessible to GPR and also to a practical excavation program. This made reconstructing the older history of the site tricky. The ERT survey proved of limited use in this regard since it was unable to distinguish between sediment layers but it was useful for identifying the till bedrock units.

Another big limitation is the area covered by the different methods. It is true that the geophysical surveys only cover approximately a third to half of the area on the south side of the river but, even more importantly, the stratigraphic test pits dug do not extend east beyond the midpoint of the GPR survey area (fig. 4.1). This means the GPR grids E and F (fig. 4.5) are almost entirely without any kind of stratigraphic verification beyond what can be inferred from surface morphology. The one exception is excavation unit 1 (dug 2015) which lies at the eastern extremity of GPR grid F. This means that the stratigraphy in that part of the site is less certain and this is one of the primary reasons why the blowout dunes were not able to be incorporated into the stratigraphic model. The other major reason is that the GPR survey does not cover the entire area but only one of the three palaeosols visible there.

For future work at Soyo, it is recommended that the blowout dune area be fully surveyed

with GPR. ERT is unlikely to be necessary as the partial coverage by existing profiles from this research project will probably be sufficient for the purpose of determining the depth of bedrock. The GPR survey should be augmented with a few more test pits in appropriate locations (particularly over the southern "S-shaped" palaeosol). Exploratory surveys in unexplored parts of Soyo would also be a good idea.

The cosmogenic dating of the moraines and boulder field that was intended to be done for this project should also be a high priority. This would solve certain problems in the timing of glaciation at Soyo and the formation of the glacial valley through the lake sediment plain.

The efforts to understand the chronology of Mongolia's Mesolithic-Neolithic and EBA periods and its pastoral transition would be better redirected to other parts of the site or to other sites. The blowout dunes are a possibility but by no means a certainty.

Nevertheless, Soyo is still an important site for the archaeology of the Darkhad and for Mongolia. The Mesolithic-Neolithic remains that have been found there are still important clues for uncovering past behaviours even if the site does not have well preserved stratigraphy from those periods that can be used to draw conclusions about changes in the material culture across that critical transition. This research project has gone a long way towards understanding the site's formation and putting the archaeological finds in their proper chronological context. This should provide a framework for future research at Soyo moving forward.

Bibliography

Agisoft 2021 Agisoft Metashape User Manual: Professional Ediion, Version 1.7.

Al-Khersan, E.H., J.M.T. Al-Ani, and S.N. Abrahem 2016 Integrated GPR and ERT as Enhanced Detection for Subsurface Historical Structures Inside Babylonian Houses Site, Uruk City, Southern Iraq. *Pure and Applied Geophysics* 173(3):963–982.

Allard, F. and D. Erdenebaatar 2005 Khirigsuurs, ritual and mobility in the Bronze Age of Mongolia. *Antiquity* 79:547–563.

Al-Saadi, O.S., V. Schmidt, M. Becken, and T. Fritsch 2018 Very-high-resolution electrical resistivity imaging of buried foundations of a Roman villa near Nonnweiler, Germany. *Archaeological Prospection* 25(3):209–218.

An, C.-B., F.-H. Chen, and L. Barton 2008 Holocene environmental changes in Mongolia: A review. *Global and Planetary Change* 63(4):283–289.

Annan, A.P. 2005 Ground-Penetrating Radar. In D.K. Butler (ed.), pp.357–438. *Near-surface geophysics*. Tulsa, Okla, Society of Exploration Geophysicists.

Armstrong, B.J., S. Edwards-Baker, P. Penzo-Kajewski, and A.I.R. Herries 2021 Ground-penetrating radar analysis of the Drimolen early Pleistocene fossil-bearing palaeocave, South Africa. *Archaeological Prospection* 28(4):419–433.

Arzhannikov, S., A. Arzhannikova, R. Braucher, and G. Komatsu 2023 Darhad megaflood (southern Siberia): Cause, age and consequence. *Quaternary International* 643:1–21.

Arzhannikov, S.G., R. Braucher, M. Jolivet, A.V. Arzhannikova, R. Vassallo, A. Chauvet, D. Bourlès, and F. Chauvet 2012 History of late Pleistocene glaciations in the central Sayan-Tuva Upland (southern Siberia). *Quaternary Science Reviews* 49:16–32.

Arzhannikova, A.V., S.G. Arzhannikov, V.V. Akulova, Y.V. Danilova, and B.S. Danilov 2014 The origin of sand deposits in the South Minusa basin. *Russian Geology and Geophysics* 1183–1194.

Aspinall, A., C. Gaffney, and A. Schmidt 2008 *Magnetometry for Archaeologists*. Lanham, AltaMira Press.

Ates, A. 2002a Archaeogeophysical investigations around the Bilge Qagan monument in Khosho Tsaidam, Mongolia. *Archaeological Prospection* 9(1):23–33.

Ates, A. 2002b Archaeomagnetic surveys of the anonymous graves in Khosho Tsaidam, Mongolia. *Archaeological Prospection* 9(4):197–205.

Atkinson, R.J.C. 1952 Méthodes Électriques de Prospection en Archéologie. In A. Laming (ed.), pp.59–70. *La Découverte du Passé: Progrès Récents et Techniques Nouvelles en Préhistoire et en Archéologie*. Paris, Éditions A. et J. Picard.

Batbaatar, J. and A.R. Gillespie 2016a Outburst floods of the Maly Yenisei. Part I. *International Geology Review* 58(14):1723–1752.

Batbaatar, J. and A.R. Gillespie 2016b Outburst floods of the Maly Yenisei. Part II – new age constraints from Darhad basin. *International Geology Review* 58(14):1753–1779.

Batmunkh, D., S. Tosun, B. Gündoğdu, M.E. Candansayar, and E.U. Ulugergerli 2004 HLEM and magnetic surveys: examples from the Orkhun Valley, Mongolia. *Archaeological Prospection* 11(3):133–144.

Bayarsaikhan, J. 2005 Shamanistic Elements in Mongolian Deer Stone Art. In W.W. Fitzhugh, Z. Baı͡arsaĭkhan, and P.K. Marsh (eds), pp.41–45. *The Deer Stone Project: anthropological studies in Mongolia, 2002-2004*. Washington, D.C.: Ulaanbaatar, Mongolia, Arctic Studies Center, National Museum of Natural History, Smithsonian Institution; National Museum of Mongolian History.

Bayarsaikhan, J., Ts. Odbaatar, and W. Fitzhugh 2005 Archaeological Reports from the 2004 Deer Stone Project. In W.W. Fitzhugh, Z. Baı͡arsaĭkhan, and P.K. Marsh (eds), pp.225–54. *The Deer Stone Project: anthropological studies in Mongolia, 2002-2004*. Washington, D.C.: Ulaanbaatar, Mongolia, Arctic Studies Center, National Museum of Natural History, Smithsonian Institution; National Museum of Mongolian History.

Becker, H. and J.W.E. Fassbinder 1999 Magnetometry of a Scythian Settlement in Siberia near Cicah in the Baraba Steppe 1999. In J.W.E. Fassbinder and W.E. Irlinger (eds), pp.168–172. *Third International Conference on Archaeological Prospection*. München, Bayerisches Landesamt für Denkmalpflege.

Belfer-Cohen, A. 1991 The Natufian in the Levant. *Annual Review of Anthropology* 20:167–186.

Bellmunt, F., A. Gabàs, A. Macau, B. Benjumea, M. Vilà, and S. Figueras 2022 Sediment characterization in deltas using electrical resistivity

tomography: The Ebro delta case. *Journal of Applied Geophysics* 196:104520.

Bemmann, J., B. Ahrens, C. Grützner, R. Klinger, N. Klitzsch, F. Lehmann, S. Linzen, L. Munkhbayar, G. Nomguunsuren, M. Oczipka, H. Piezonka, B. Schütt, and S. Saran 2011 Geoarchaeology in the Steppe: First results of the multidisciplinary Mongolian-German survey project in the Orkhon Valley, Central Mongolia. *Studia Archaeologica* 30(5):69–97.

Bemmann, J., S. Linzen, S. Reichert, and Lkh. Munkhbayar 2022 Mapping Karakorum, the capital of the Mongol Empire. *Antiquity* 96(385):159–178.

Bendrey, R. 2011 Some like it hot: environmental determinism and the pastoral economies of the later prehistoric Eurasian steppe. *Pastoralism: Research, Policy and Practice* 1(1):8.

Benn, D.I. and D.J.A. Evans 2010 *Glaciers & glaciation*. 2nd ed. London, Hodder education.

Berezowski, V., X. Mallett, J. Ellis, and I. Moffat 2021 Using Ground Penetrating Radar and Resistivity Methods to Locate Unmarked Graves: A Review. *Remote Sensing* 13(15):2880.

Berge, M.A. and M.G. Drahor 2011 Electrical Resistivity Tomography Investigations of Multilayered Archaeological Settlements: Part II - A Case from Old Smyrna Höyük, Turkey: ERT Investigations of Multilayered Settlements at Old Smyrna. *Archaeological Prospection* 18(4):291–302.

Bergman, L.D., B.E. Rogowitz, and L.A. Treinish 1995 A Rule-Based Tool for Assisting Colormap Selection. pp.118-125,. *Proceedings of the 6th*

IEEE Visualization Conference. Atlanta, GA, USA, IEEE Comput. Soc. Press.

Bermejo, L., A.I. Ortega, R. Guérin, A. Benito-Calvo, A. Pérez-González, J.M. Parés, E. Aracil, J.M. Bermúdez De Castro, and E. Carbonell 2017 2D and 3D ERT imaging for identifying karst morphologies in the archaeological sites of Gran Dolina and Galería Complex (Sierra de Atapuerca, Burgos, Spain). *Quaternary International* 433:393–401.

Bevan, B.W. 1991 The search for graves. *Geophysics* 56(9):1310–1319.

Bevan, B.W. 2000 An early geophysical survey at Williamsburg, USA. *Archaeological Prospection* 7:51–58.

Blyakharchuk, T.A., H.E. Wright, P.S. Borodavko, W.O. van der Knaap, and B. Ammann 2004 Late Glacial and Holocene vegetational changes on the Ulagan high-mountain plateau, Altai Mountains, southern Siberia. *Palaeogeography, Palaeoclimatology, Palaeoecology* 209(1–4):259–279.

Boggs, S.Jr. 1995 *Principles of Sedimentology and Stratigraphy*. Second Edition. Upper Saddle River, Prentice Hall.

Boyd, B. 2018 Settled? Recent debates in the archaeology of the Epipalaeolithic and Pre-Pottery Neolithic of Southwest Asia. *Asian Archaeology* 1(1–2):63–73.

Breien, H., F.V. De Blasio, A. Elverhøi, and K. Høeg 2008 Erosion and morphology of a debris flow caused by a glacial lake outburst flood, Western Norway. *Landslides* 5(3):271–280.

Bristow, C.S. and H.M. Jol, editors 2003 *Ground Penetrating Radar in Sediments*. London, Geological Society.

Cai, D., N. Zhang, S. Zhu, Q. Chen, L. Wang, X. Zhao, X. Ma, T.C.A. Royle, H. Zhou, and D.Y. Yang 2018 Ancient DNA reveals evidence of abundant aurochs (Bos primigenius) in Neolithic Northeast China. *Journal of Archaeological Science* 98:72–80.

Campana, S. and S. Piro, editors 2009 *Seeing the unseen: geophysics and landscape archaeology ; [collection of papers presented at the advanced XV International Summer School in Archaeology 'Geophysics for Landscape Archaeology' (Grosseto, Italy, 10 - 18 July 2006)]*. Boca Raton, CRC Press.

Carey, C., A.J. Howard, J. Corcoran, D. Knight, and J. Heathcote 2018 Deposit modeling for archaeological projects: Methods, practice, and future developments. *Geoarchaeology* 34(4):495–505.

Carey, C., A.J. Howard, R. Jackson, and A. Brown 2017 Using geoarchaeological deposit modelling as a framework for archaeological evaluation and mitigation in alluvial environments. *Journal of Archaeological Science: Reports* 11:658–673.

Carey, C.J., T.G. Brown, K.C. Challis, A.J. Howard, and L. Cooper 2006 Predictive modelling of multiperiod geoarchaeological resources at a river confluence: a case study from the Trent–Soar, UK. *Archaeological Prospection* 13(4):241–250.

Cassidy, N. 2009a Electrical and Magnetic Properties of Rocks, Soils and Fluids. In H.M. Jol (ed.), pp.41–72. *Ground Penetrating Radar: Theory and Applications*. 1. ed. Amsterdam, Elsevier Science.

Cassidy, N. 2009b Ground Penetrating Radar Data Processing, Modelling and Analysis. In H.M. Jol (ed.), pp.141–176. *Ground Penetrating Radar: Theory and Applications*. 1. ed. Amsterdam, Elsevier Science.

Challis, K. and A.J. Howard 2006 A review of trends within archaeological remote sensing in alluvial environments. *Archaeological Prospection* 13(4):231–240.

Chamley, H. 1989 *Clay Sedimentology*. Berlin, Heidelberg, Springer Berlin Heidelberg.

Chapman, H., J. Adcock, and J. Gater 2009 An approach to mapping buried prehistoric palaeosols of the Atlantic seaboard in Northwest Europe using GPR, geoarchaeology and GIS and the implications for heritage management. *Journal of Archaeological Science* 36(10):2308–2313.

Chard, C.S. 1958 Mesolithic Sites in Siberia. *Asian Perspectives* 2:118–127.

Cheetham, P., N. 2008 Noninvasive Subsurface Mapping Techniques, Satellite and Aerial Imagery in Landscape Archaeology. In B. David and J. Thomas (eds), pp.562–582. *Handbook of Landscape Archaeology*. Walnut Creek, California, Left Coast Press.

Chikazumi, S. 1964 *Physics of Magnetism*. (S. Charap, tran.). New York, John Wiley & Sons.

Childe, V.G. 1929 *The Most Ancient East: The Oriental Prelude to European Prehistory*. New York, Alfred A. Knopf.

Choi, Y., K.J. Kim, D. Cheong, and Y.H. Kim 2014 Paleoclimate Signals of Lake Hovsgol, Mongolia, Over the Last 19,000 Years Using Authigenic Beryllium Isotopes. *Radiocarbon* 56(3):1139–1150.

Clark, A. 1975 Archaeological prospecting: A progress report. *Journal of Archaeological Science* 2(4):297–314.

Clark, A. 1996 *Seeing Beneath the Soil: Prospecting Methods in Archaeology*. Second edition. London, B. T. Batsford.

Clark, A.J. 1986 Archaeological geophysics in Britain. *Geophysics* 51(7):1404–1413.

Clark, G. 1980 *Mesolithic Prelude: The Palaeolithic-Neolithic Transition in Old World Prehistory*. Edinburgh, Edinburgh University Press.

Clark, J. 2015 Northern Mongolia Archaeology Project Summer 2015: Soyo, Darkhad Depression, Hovsgol Aimag, Northern Mongolia. p.7. Unpublished field report, Northern Mongolia Archaeology Project.

Clark, J. 2017 Shifting Mobility Strategies in Neolithic and Bronze Age Mongolia. Vancouver.

Clark, J. and J. Bayarsaikhan 2016 Монгол-Америкийн Хамтарсан "Умард Монгол" Төслийн 2016 Оны Хээрийн Судалгааны Тайлан. p.24. Unpublished field report.

Clark, J. and J. Bayarsaikhan 2017 End of Fieldwork Report 2017: Soyo Site, Soyo Bag, Ulaan Uul Soum, Huvsgul, Mongolia. p.57. Unpublished field report, Northern Mongolia Archaeology Project.

Clark, J. and J. Bayarsaikhan 2018 Mongolian-American Northern Mongolia Archaeology Project 2018 Research Project. p.11. Unpublished field report, Mongolian-American Northern Mongolia Archaeology Project.

Clark, J.K. 2014 Modeling Late Prehistoric and Early Historic Pastoral Adaptations in Northern Mongolia's Darkhad Depression. Pittsburgh, University of Pittsburgh.

Constable, S.C., R.L. Parker, and C.G. Constable 1987 Occam's inversion: A practical algorithm for generating smooth models from electromagnetic sounding data. *Geophysics* 52(3):289–300.

Conyers, L.B. 2013 *Ground-penetrating radar for archaeology*. Third edition. Lanham, AltaMira Press, a division of Rowman & Littlefield Publishers, Inc.

Conyers, L.B. 2018 *Ground-penetrating Radar and Magnetometry for Buried Landscape Analysis*. Cham, Springer International Publishing.

Conyers, L.B., J.M. Daniels, J.A. Haws, and M.M. Benedetti 2013 An Upper Palaeolithic Landscape Analysis of Coastal Portugal Using Ground-penetrating Radar: Landscape Analysis of Coastal Portugal Using Ground-penetrating Radar. *Archaeological Prospection* 20(1):45–51.

Corradini, E., D. Wilken, M. Zanon, D. Groß, H. Lübke, D. Panning, W. Dörfler, K. Rusch, R. Mecking, E. Erkul, N. Pickartz, I. Feeser, and W. Rabbel 2020 Reconstructing the palaeoenvironment at the early Mesolithic site of Lake Duvensee: Ground-penetrating radar and geoarchaeology for 3D facies mapping. *The Holocene* 1–14.

Correia, A. 2019 Archaeological Geophysics in Portugal: Some Survey Examples. In G. El-Qady and Metwaly, Mohamed (eds), pp.101–124. *Archaeogeophysics: state of the art and case studies*. 1st edition. New York, NY, Springer Berlin Heidelberg.

Cribb, R. 1991 *Nomads in Archaeology*. Cambridge, Cambridge University Press.

Crook, N., A. Binley, R. Knight, D.A. Robinson, J. Zarnetske, and R. Haggerty 2008 Electrical resistivity imaging of the architecture of substream sediments. *Water Resources Research* 44(4):W00D13.

Dalan, R.A. 2008 A review of the role of magnetic susceptibility in archaeogeophysical studies in the USA: recent developments and prospects. *Archaeological Prospection* 15(1):1–31.

Darvill, C.M. 2013 Cosmogenic nuclide analysis. p.25. *Geomorphological Techniques*. British Society for Geomorphology.

David, B. and J. Thomas 2008 Landscape Archaeology: Introduction. In B. David and J. Thomas (eds), pp.27–43. *Handbook of Landscape Archaeology*. Walnut Creek, California, Left Coast Press.

Davis, J.L. and A.P. Annan 1989 Ground-Penetrating Radar for High-Resolution Mapping of Soil and Rock Stratigraphy. *Geophysical Prospecting* 37(5):531–551.

De Giorgi, L. and G. Leucci 2018 The archaeological site of Sagalassos (Turkey): exploring the mysteries of the invisible layers using geophysical methods. *Exploration Geophysics* 49(5):751–761.

Dean, W.E. 1974 Determination of Carbonate and Organic Matter in Calcareous Sediments and Sedimentary Rocks by Loss on Ignition: Comparison With Other Methods. *Journal of Sedimentary Petrology* Vol. 44:242–248.

Dearing, J.A., K.L. Hay, S.M.J. Baban, A.S. Huddleston, E.M.H. Wellington, and P.J. Loveland 1996 Magnetic susceptibility of soil: an evaluation of conflicting theories using a national data set. *Geophysical Journal International* 127(3):728–734.

Derevianko, A.P. and D. Dorj 1992 Neolithic Tribes in Northern Parts of Central Asia. In A.H. Dani and V.M. Masson (eds), pp.169–189. *The dawn of civilization: earliest times to 700 b. c*. Paris, UNESCO Publishing.

Derevianko, A.P., S.A. Gladyshev, T.I. Nohrina, and J.W. Olsen 2003 The Mongolian Early Holocene: Excavations at Chikhen Agui Rockshelter in the Gobi Altai. *The Review of Archaeology* 24(2):50–56.

Derevianko, A.P., S.A. Gladyshev, J.W. Olsen, V.T. Petrin, and Y. Tserendagva 2001 Characteristic Features of the Chikhen Agui Lithic Assemblage (Gobi Altai). *Archaeology, Ethnology and Anthropology of Eurasia* 1(5):25–39.

Derevianko, A.P., J.W. Olsen, D. Tseveendorj, S.A. Gladyshev, T.I. Nokhrina, and A.V. Tabarev 2008 New Insights into the Archaeological Record at Chikhen Agui Rockshelter (Mongolia). *Archaeology, Ethnology and Anthropology of Eurasia* 34(2):2–12.

Donais, M.K. and D.B. George 2018 *X-Ray Fluorescence Spectrometry and Its Applications to Archaeology : An Illustrated Guide*. New York, Momentum Press.

Dorj, D. 1971 *Neolit vostocnoj Mongolii*. Ulaan Baatar.

Easterbrook, D.J. 1969 *Principles of Geomorphology*. New York, McGraw-Hill Book Company.

Edwards, L.S. 1977 A Modified Pseudosection for Resistivity and IP. *Geophysics* 42(5):1020–1036.

El-Qady, G. and Metwaly, M., editors 2019 *Archaeogeophysics: state of the art and case studies*. 1st edition. New York, NY, Springer Berlin Heidelberg.

Ėnkhtör, A., J. Bemmann, and U. Brosseder 2018 The first excavations of bronze and iron age monuments in the middle Orkhon Valley, Central Mongolia: results from rescue investigations in 2006 and 2007. *Asian Archaeology* 1(1–2):3–44.

Evans, J.G. 1978 *An Introduction to Environmental Archaeology*. London, Elek Books.

Evans, M. and F. Heller 2003 *Environmental Magnetism: Principles and Applications of Enviromagnetics*. Academic Press.

Everett, M.E. 2013 *Near-Surface Applied Geophysics*. Cambridge, Cambridge University Press.

Fassbinder, J.W.E. 2015 Seeing beneath the farmland, steppe and desert soil: magnetic prospecting and soil magnetism. *Journal of Archaeological Science* 56:85–95.

Fassbinder, J.W.E. and H. Becker 1999 Magnetic Prospection of a Megalithic Necropolis at Ibbankatuwa (Sri Lanka). In J.W.E. Fassbinder and W.E. Irlinger (eds), pp.106–109. *Third International Conference on Archaeological Prospection*. München, Bayerisches Landesamt für Denkmalpflege.

Fassbinder, J.W.E., H. Stanjekt, and H. Vali 1990 Occurrence of magnetic bacteria in soil. *Nature* 343(6254):161–163.

Fedotov, A.P., E.P. Chebykin, S.M. Yu, S.S. Vorobyova, O.E. Yu, L.P. Golobokova, T.V. Pogodaeva, T.O. Zheleznyakova, M.A. Grachev, D. Tomurhuu, T. Oyunchimeg, T. Narantsetseg, O. Tomurtogoo, P.T. Dolgikh, M.I. Arsenyuk, and M. De Batist 2004 Changes in the volume and salinity of Lake Khubsugul (Mongolia) in response to global climate changes in the upper Pleistocene and the Holocene. *Palaeogeography, Palaeoclimatology, Palaeoecology* 209(1–4):245–257.

Feng, Z.-D., X.W. Zhai, Y.Z. Ma, C.Q. Huang, W.G. Wang, H.C. Zhang, P. Khosbayar, T. Narantsetseg, K.-B. Liu, and N.W. Rutter 2007 Eolian environmental changes in the Northern Mongolian Plateau during the past ~35,000 yr. *Palaeogeography, Palaeoclimatology, Palaeoecology* 245(3–4):505–517.

Fitzhugh, W. 2003 *Mongolia's Arctic Connections: The Hovsgol Deer Stone Project, 2001-2002 Field Report*. Washington, D.C., Arctic Studies Center, National Museum of Natural History, Smithsonian Institution.

Fitzhugh, W. 2005 The Deer Stone Project: Exploring Northern Mongolia and its Arctic Connections. In W.W. Fitzhugh, Z. Baiarsaĭkhan, and P.K. Marsh (eds), pp.3–34. *The Deer Stone Project: anthropological studies in Mongolia, 2002-2004*. Washington, D.C.: Ulaanbaatar, Mongolia, Arctic Studies Center, National Museum of Natural History, Smithsonian Institution; National Museum of Mongolian History.

Fitzhugh, W., J. Bayarsaikhan, and B. Betz, editors 2010 *American-Mongolian Deer Stone Project: Field Report 2009*. Washington, D.C.: Ulaanbaatar, Mongolia, Arctic Studies Center, National Museum of Natural History, Smithsonian Institution; National Museum of Mongolian History.

Fitzhugh, W. and C. Leece, editors 2007 *American-Mongolian Deer Stone Project: Field Report 2006*. Washington, D.C.: Ulaanbaatar, Mongolia, Arctic Studies Center, National Museum of Natural History, Smithsonian Institution; National Museum of Mongolian History.

Fitzhugh, W.W., J. Bayarsaikhan, L. Wynalda, and T. Bertsch, editors 2008 *American-Mongolian Deer Stone Project: Field Report 2007*. Washington, D.C.: Ulaanbaatar, Mongolia, Arctic Studies Center, National Museum of Natural History, Smithsonian Institution; National Museum of Mongolian History.

Fitzhugh, W.W. and G.M. Leader 2006 *Mongolia Deer Stone Project: Field Report 2005*. Washington, D.C.: Ulaanbaatar, Mongolia, Arctic Studies Center, National Museum of Natural History, Smithsonian Institution; National Museum of Mongolian History.

Frachetti, M.D. 2012 Multiregional Emergence of Mobile Pastoralism and Nonuniform Institutional Complexity across Eurasia. *Current Anthropology* 53(1):2–38.

Frederick, C.D. and J.T. Abbott 1992 Magnetic Prospection of Prehistoric Sites in an Alluvial Environment: Examples from NW and West-Central Texas. *Journal of Field Archaeology* 19(2):139–153.

Frohlich, B., T. Amgalantugs, J. Littleton, G. Ganbat, D. Hunt, E. Nittler, S. Karstens, T. Frohlich, and E. Batchatar 2010 Theories and Hypotheses Pertaining to Mongolian Bronze Age Khirigsuurs in Hovsgol Aimag, Mongolia. In W. Fitzhugh, J. Bayarsaikhan, and B. Betz (eds), pp.195–208. *American-Mongolian Deer Stone Project: Field Report 2009*. Washington, D.C.: Ulaanbaatar, Mongolia, Arctic Studies Center, National Museum of Natural History, Smithsonian Institution; National Museum of Mongolian History.

Frohlich, B., N. Bazarsad, and Baatartsogt 2005 Burial Mounds in Hovsgol Aimag, Northern Mongolia: Preliminary Results from 2003 and 2004. In W.W. Fitzhugh, Z. Baĭarsaĭkhan, and P.K. Marsh (eds), pp.57–88. *The Deer Stone Project: anthropological studies in Mongolia, 2002-2004*. Washington, D.C.: Ulaanbaatar, Mongolia, Arctic Studies Center, National Museum of Natural History, Smithsonian Institution; National Museum of Mongolian History.

Fukumoto, Y., K. Kashima, and U. Ganzorig 2014 The Holocene environmental changes in boreal fen peatland of northern Mongolia reconstructed from diatom assemblages. *Quaternary International* 348:66–81.

Gaber, A., K.S. Gemail, A. Kamel, H.M. Atia, and A. Ibrahim 2021 Integration of 2D/3D ground penetrating radar and electrical resistivity tomography surveys as enhanced imaging of archaeological ruins: A case study in San El-Hager (Tanis) site, northeastern Nile Delta, Egypt. *Archaeological Prospection* 28(2):251–267.

Gaffney, C. 2008 Detecting Trends in the Prediction of the Buried Past: A Review of Geophysical Techniques in Archaeology. *Archaeometry* 50(2):313–336.

Gaffney, C. and J. Gater 2003 *Revealing the Buried Past: Geophysics for Archaeologists*. Stroud, Tempus Publishing.

Geotomo Software 2019 Res2dinvx64 ver. 4.09 with Multi-Core and 64-bit Support. User manual, Geotomo Software.

Gibbs, K. and P. Jordan 2013 Bridging the Boreal Forest: Siberian Archaeology and the Emergence of Pottery among Prehistoric Hunter-Gatherers of Northern Eurasia. *Sibirica* 12(1):1–38.

Gilbert, A.S. 1983 On the origins of specialized nomadic pastoralism in western Iran. *World Archaeology* 15(1):105–119.

Gillespie, A.R., R.M. Burke, G. Komatsu, and A. Bayasgalan 2008 Late Pleistocene glaciers in Darhad Basin, northern Mongolia. *Quaternary Research* 69(2):169–187.

Gillespie, R. 1986 *Radiocarbon User's Handbook*. Second edition. Oxford, Oxford University Committee for Archaeology.

Gladyshev, S.A., J.W. Olsen, A.V. Tabarev, and Y.V. Kuzmin 2010 Chronology and Periodization of Upper Palaeolithic Sites in Mongolia. *Archaeology, Ethnology and Anthropology of Eurasia* 38(3):33–40.

Goodman, D. and S. Piro 2013 *GPR Remote Sensing in Archaeology*. New York, Springer-Verlag Berlin Heidelberg.

Gosse, J.C. and F.M. Phillips 2001 Terrestrial in situ cosmogenic nuclides: theory and application. *Quaternary Science Reviews* 20(14):1475–1560.

Goulden, C.E., B. Nandintsetseg, and L. Ariuntsetseg 2011 5. The Geology, Climate, and Ecology of Mongolia. In P.L.W. Sabloff (ed.). *Mapping Mongolia*. Philadelphia, University of Pennsylvania Press.

Gowlett, J. 1987 The Archaeology of Radiocarbon Accelerator Dating. *Journal of World Prehistory* 1(2):127–170.

Grant, F.S. and G.F. West 1965 *Interpretation Theory in Applied Geophysics*. New York, McGraw-Hill Book Company.

Grau-Crespo, R., A.Y. Al-Baitai, I. Saadoune, and N.H. De Leeuw 2010 Vacancy ordering and electronic structure of γ - Fe_2O_3 (maghemite): a theoretical investigation. *Journal of Physics: Condensed Matter* 22(25):255401.

Gribble, L. 2021 An investigation into the Neolithic of Soyo (northern Mongolia) through analysis of lithics. Masters, Adelaide, Flinders University.

Grützner, C., J. Bemmann, J. Berking, M. Frechen, R. Klinger, N. Klitzsch, S. Linzen, S. Mackens, M. Oczipka, H. Piezonka, S. Reichert, M.

Schneider, and B. Schütt 2012 Improving archaeological site analysis: a rampart in the middle Orkhon Valley investigated with combined geoscience techniques. *Journal of Geophysics and Engineering* 9(4):S70–S80.

Günther, T. 2004 Inversion Methods and Resolution Analysis for the 2D/3D Reconstruction of Resistivity Structures from DC Measurements. Freiberg, Technical University of Bergakademie Freiberg.

Günther, T. and C. Rücker 2019 Boundless Electrical Resistivity Tomography BERT 2 – the user tutorial.

Günther, T., C. Rücker, and K. Spitzer 2006 Three-dimensional modelling and inversion of dc resistivity data incorporating topography - II. Inversion. *Geophysical Journal International* 166(2):506–517.

Hallof, P.G. 1957 On the Interpretation of Resistivity and Induced Polarization Field Measurements. Cambridge, Massachusetts, Massachusetts Institute of Technology.

Hanson, R.O., L. Racic, and V.J.S. Grauch 2005 Magnetic Methods in Near-Surface Geophysics. In D.K. Butler (ed.), pp.151–175. *Near-surface geophysics*. Tulsa, Okla, Society of Exploration Geophysicists.

Hartz, S., E. Kostyleva, H. Piezonka, T. Terberger, N. Tsydenova, and M.G. Zhilin 2012 Hunter-Gatherer Pottery and Charred Residue Dating: New Results on Early Ceramics in the North Eurasian Forest Zone. *Radiocarbon* 54(3–4):1033–1048.

Heiri, O., A.F. Lotter, and G. Lemcke 2001 Loss on ignition as a method for estimating organic and carbonate content in sediments:

reproducibility and comparability of results. *Journal of Paleolimnology* 25:101–110.

Heller, F. and L. Tungsheng 1984 Magnetism of Chinese loess deposits. *Geophysical Journal International* 77(1):125–141.

Honeychurch, W. 2015 *Inner Asia and the Spatial Politics of Empire: Archaeology, Mobility, and Culture Contact*. New York, NY, Springer New York.

Honeychurch, W. and C.A. Makarewicz 2016 The Archaeology of Pastoral Nomadism. *Annual Review of Anthropology* 45(1):341–359.

Honeychurch, W., J. Wright, and C. Amartuvshin 2007 A Nested Approach to Survey in the Egiin Gol Valley, Mongolia. *Journal of Field Archaeology* 32(4):369–383.

Honeychurch, William. and Ch. (Chunagiĭn) Amartüvshin 2007 Hinterlands, Urban Centers, and Mobile Settings: The 'New' Old World Archaeology from the Eurasian Steppe. *Asian Perspectives* 46(1):36–64.

Horiuchi, K., K. Minoura, K. Hoshino, T. Oda, T. Nakamura, and T. Kawai 2000 Palaeoenvironmental history of Lake Baikal during the last 23000 years. *Palaeogeography, Palaeoclimatology, Palaeoecology* 157(1–2):95–108.

Houle, J.-L. 2010 Emergent Complexity on the Mongolian Steppe: Mobility, Territoriality, and the Development of Early Nomadic Polities. Pittsburgh, University of Pittsburgh.

Houle, J.-L. 2016 Bronze Age Mongolia. In Oxford Handbooks Editorial Board (ed.). *The Oxford Handbook of Topics in Archaeology*. First edition. Oxford University Press.

Howard, A.J., A.G. Brown, C.J. Carey, K. Challis, L.P. Cooper, M. Kincey, and P. Toms 2008 Archaeological resource modelling in temperate river valleys: a case study from the Trent Valley, UK. *Antiquity* 82(318):1040–1054.

Imai, T., T. Sakayama, and T. Kanemori 1987 Use of ground-probing radar and resistivity surveys for archaeological investigations. *Geophysics* 52(2):137–150.

Jacobson-Tepfer, E. 2001 Cultural Riddles: Stylized Deer and Deer Stones of the Mongolian Altai. *Bulletin of the Asia Institute* 15:31–56.

Janz, L. 2012 Chronology of Post-Glacial Settlement in the Gobi Desert and the Neolithization of Arid Mongolia and China. Tucson, The University of Arizona.

Janz, L., D. Odsuren, and D. Bukhchuluun 2017 Transitions in Palaeoecology and Technology: Hunter-Gatherers and Early Herders in the Gobi Desert. *Journal of World Prehistory* 30(1):1–80.

Janz, L., A.M. Rosen, D. Bukhchuluun, and D. Odsuren 2021 Zaraa Uul: An archaeological record of Pleistocene-Holocene palaeoecology in the Gobi Desert. *PLOS One* 16(4):e0249848.

Jeong, C., K. Wang, S. Wilkin, W.T.T. Taylor, B.K. Miller, J.H. Bemmann, R. Stahl, C. Chiovelli, F. Knolle, S. Ulziibayar, D. Khatanbaatar, D. Erdenebaatar, U. Erdenebat, A. Ochir, G. Ankhsanaa, C. Vanchigdash, B. Ochir, C. Munkhbayar, D. Tumen, A. Kovalev, N. Kradin, B.A. Bazarov, D.A. Miyagashev, P.B. Konovalov, E. Zhambaltarova, A.V. Miller, W. Haak, S. Schiffels, J. Krause, N. Boivin, M. Erdene, J. Hendy, and C. Warinner 2020 A Dynamic

6,000-Year Genetic History of Eurasia's Eastern Steppe. *Cell* 183(4):890–904.

Jeong, C., S. Wilkin, T. Amgalantugs, A.S. Bouwman, W.T.T. Taylor, R.W. Hagan, S. Bromage, S. Tsolmon, C. Trachsel, J. Grossmann, J. Littleton, C.A. Makarewicz, J. Krigbaum, M. Burri, A. Scott, G. Davaasambuu, J. Wright, F. Irmer, E. Myagmar, N. Boivin, M. Robbeets, F.J. Rühli, J. Krause, B. Frohlich, J. Hendy, and C. Warinner 2018 Bronze Age population dynamics and the rise of dairy pastoralism on the eastern Eurasian steppe. *Proceedings of the National Academy of Sciences* 115(48):E11248–E11255.

Jones, R., A. Roberts, C. Westell, I. Moffat, G. Jacobsen, and R. Rudd 2022 Aboriginal earth mounds of the Calperum Floodplain (Murray Darling Basin, South Australia): New radiocarbon dates, sediment analyses and syntheses, and implications for behavioural change. *The Holocene* 32(8):816–834.

Karkanas, P. 2021 All about wood ash: Long term fire experiments reveal unknown aspects of the formation and preservation of ash with critical implications on the emergence and use of fire in the past. *Journal of Archaeological Science* 135:105476.

Keay, S., G. Earl, S. Hay, S. Kay, J. Ogden, and K.D. Strutt 2009 The role of integrated geophysical survey methods in the assessment of archaeological landscapes: the case of Portus. *Archaeological Prospection* 16(3):154–166.

Keller, G.V. 1971 Electrical Characteristics of the Earth's Crust. In J.R. Wait (ed.), pp.13–76. *Electromagnetic Probing in Geophysics*. Boulder, Colorado, The Golem Press.

Kelly, T.B., M.N. Angel, D.E. O'Connor, C.C. Huff, L.E. Morris, and G.D. Wach 2021 A novel approach to 3D modelling ground-penetrating radar (GPR) data – A case study of a cemetery and applications for criminal investigation. *Forensic Science International* 325:110882.

Khatsenovich, A.M., E.P. Rybin, B. Gunchinsuren, J.W. Olsen, R.A. Shelepaev, L.V. Zotkina, T. Bolorbat, A.Y. Popov, and D. Odsuren 2017 New evidence for Paleolithic human behavior in Mongolia: The Kharganyn Gol 5 site. *Quaternary International* 442:78–94.

Khazanov, A.M. 1994 *Nomads and the outside world*. (J. Crookenden, tran.). 2nd ed. Madison, University of Wisconsin Press.

Khuut, T., O. Ayudai, T. Kawai, I. Byanmunkh, and B. Khuut 2015a Geophysical integrated survey result of ancient Turkic tombs in Bulgan province, Mongolia. pp.72–75. *Proceedings of the 12th SEGJ International Symposium, Tokyo, Japan, 18-20 November 2015*. Tokyo, Japan, Society of Exploration Geophysicists of Japan.

Khuut, T., L. Erdenebold, and T.-A. Nyambayar 2015b Archaeology and geophysical integrated survey results for Xiongnu period site, Mongolia *IEICE Tech. Rep.*

Khuut, T. and M. Sato 2009 Evaluation of Van Khan Tooril's castle, an archaeological site in Mongolia, by Ground Penetrating Radar. *Exploration Geophysics* 40(1):69–76.

Khuut, T., O. Tserendorj, B. Dashdondog, B. Khuut, and B. Khuut 2018 Integrated Geophysical Investigations at the Khaya Khudag Ritual Complex in Eastern Part of Mongolia. Irkutsk.

Khuut, T., O. Tserendorj, B. Jamsranjav, B. Khuut, and B. Khuut 2019 Integrated geophysical survey results to detect buried ritual

complex structures in eastern Mongolia. pp.406–409. *Proceedings of the 13th SEGJ International Symposium, Tokyo, Japan, 12–14 November 2018*. Tokyo, Japan, Society of Exploration Geophysicists and Society of Exploration Geophysicists of Japan.

King, J.A., B.W. Bevan, and R.J. Hurry 1993 The reliability of geophysical surveys at historic-period cemeteries: An example from the plains cemetery, mechanicsville, Maryland. *Historical Archaeology* 27(3):4–16.

Klanica, R., R. Křivánek, H. Grison, P. Tábořík, and J. Šteffl 2022 Capabilities and limitations of electrical resistivity tomography for mapping and surveying hillfort fortifications. *Archaeological Prospection* 29(3):401–416.

Komatsu, G., S.G. Arzhannikov, A.R. Gillespie, R.M. Burke, H. Miyamoto, and V.R. Baker 2009 Quaternary paleolake formation and cataclysmic flooding along the upper Yenisei River. *Geomorphology* 104(3–4):143–164.

Komatsu, G., V.R. Baker, S.G. Arzhannikov, R. Gallagher, A.V. Arzhannikova, A. Murana, and T. Oguchi 2016 Catastrophic flooding, palaeolakes, and late Quaternary drainage reorganization in northern Eurasia. *International Geology Review* 58(14):1693–1722.

Kovesi, P. 2015, September 11 Good Colour Maps: How to Design Them. arXiv.

Kowlessar, J., I. Moffat, D. Wesley, M. Willis, S. Wrigglesworth, T. Jones, A. Nayinggul, and the Njanjma Rangers 2023 Reconstructing archaeological palaeolandscapes using geophysical and geomatic

survey techniques: An example from Red Lily Lagoon, Arnhem Land, Australia. *PLOS One* 18(5):e0283006.

Kozłowski, S.K. 2009 *Thinking Mesolithic*. Oxbow Books.

Kravchinsky, V.A., V.S. Zykina, and V.S. Zykin 2008 Magnetic indicator of global paleoclimate cycles in Siberian loess–paleosol sequences. *Earth and Planetary Science Letters* 265(3–4):498–514.

Krivonogov, S.K., V.S. Sheinkman, and A.A. Mistruykov 2005 Stages in the development of the Darhad dammed lake (Northern Mongolia) during the Late Pleistocene and Holocene. *Quaternary International* 136(1):83–94.

Krivonogov, S.K., S. Yi, K. Kashiwaya, J.C. Kim, T. Narantsetseg, T. Oyunchimeg, I.Y. Safonova, A.Y. Kazansky, T. Sitnikova, J.Y. Kim, and N. Hasebe 2012 Solved and unsolved problems of sedimentation, glaciation and paleolakes of the Darhad Basin, Northern Mongolia. *Quaternary Science Reviews* 56:142–163.

Kuzmin, Y.V. 2010 The Neolithic of the Russian Far East and Neighbouring East Asia: Definition, Chronology, and Origins. *Bulletin of the Indo-Pacific Prehistory Association* 30:157–162.

Kuzmin, Y.V. 2013a The Patterns of Neolithization in the North Eurasian Forest Zone: A Comment on Hartz et al. (2012). *Radiocarbon* 55(1):*201*–203.

Kuzmin, Y.V. 2013b Two Trajectories in the Neolithization of Eurasia: Pottery versus Agriculture (Spatiotemporal Patterns) *Radiocarbon* 55(2-3):1304–1313.

Kuzmin, Y.V. 2013c The beginnings of prehistoric agriculture in the Russian Far East: Current evidence and concepts. *Documenta Praehistorica* 40:1–12.

Lamb, M.P. and M.A. Fonstad 2010 Rapid formation of a modern bedrock canyon by a single flood event. *Nature Geoscience* 3(7):477–481.

Lattimore, O. 1940 *Inner Asian Frontiers of China*. New York, American Geographical Society.

Le Borgne, E. 1955 Susceptibilité magnétique anormale du sol superficiel. *Annales de Geophysique* 11:399–419.

Lees, S.H. and D.G. Bates 1974 The Origins of Specialized Nomadic Pastoralism: A Systemic Model. *American Antiquity* 39(2Part1):187–193.

Lin, A.Y.-M., A. Novo, S. Har-Noy, N.D. Ricklin, and K. Stamatiou 2011 Combining GeoEye-1 Satellite Remote Sensing, UAV Aerial Imaging, and Geophysical Surveys in Anomaly Detection Applied to Archaeology. *IEEE Journal of Selected Topics in Applied Earth Observations and Remote Sensing* 4(4):870–876.

Linford, N.T. and M.G. Canti 2001 Geophysical evidence for fires in antiquity: preliminary results from an experimental study. Paper given at the EGS XXIV General Assembly in The Hague, April 1999. *Archaeological Prospection* 8(4):211–225.

Linzen, S., S. Reichert, J. Bemmann, and R. Stolz 2019 What magnetic prospection, topographic mapping and archaeology can tell us about urbanism in the Mongolian steppes.

Loke, D.M.H. 2004 *Tutorial : 2-D and 3-D electrical imaging surveys*.

Loke, M.H., J.E. Chambers, D.F. Rucker, O. Kuras, and P.B. Wilkinson 2013 Recent developments in the direct-current geoelectrical imaging method. *Journal of Applied Geophysics* 95:135–156.

Loke, M.H. and T. Dahlin 2002 A comparison of the Gauss–Newton and quasi-Newton methods in resistivity imaging inversion. *Journal of Applied Geophysics* 49(3):149–162.

Lubbock, J. 1865 *Pre-Historic Times as Illustrated by Ancient Remains and the Manners and Customs of Modern Savages*. London, Williams and Norgate.

Ma, Y., K. Liu, Z. Feng, H. Meng, Y. Sang, W. Wang, and H. Zhang 2013 Vegetation changes and associated climate variations during the past ~38,000 years reconstructed from the Shaamar eolian-paleosol section, northern Mongolia. *Quaternary International* 311:25–35.

Maher, B.A. 2011 The magnetic properties of Quaternary aeolian dusts and sediments, and their palaeoclimatic significance. *Aeolian Research* 3(2):87–144.

Margui, E. and R. Van Grieken 2013 *X-Ray Fluorescence Spectrometry and Related Techniques : An Introduction*. New York, Momentum Press.

Maringer, J. 1963 Mongolia before the Mongols. *Arctic Anthropology* 1(2):75–85.

Marmet, E., M. Bina, N. Fedoroff, and A. Tabbagh 1999 Relationships between human activity and the magnetic properties of soils: a case study in the medieval site of Roissy-en-France. *Archaeological Prospection* 6:161–170.

Mats, V.D. and T.I. Perepelova 2011 A new perspective on evolution of the Baikal Rift. *Geoscience Frontiers* 2(3):349–365.

Miller, B.K., M. Furholt, J. Bayarsaikhan, T. Tüvshinjargal, L. Brandtstätter, J. Wright, T. Ayush, and T. Wunderlich 2019 Proto-Urban Establishments in Inner Asia: Surveys of an Iron Age Walled Site in Eastern Mongolia. *Journal of Field Archaeology* 44(4):267–286.

Miller, C.E., S.M. Mentzer, C. Berthold, P. Leach, B. Ligouis, C. Tribolo, J. Parkington, and G. Porraz 2016 Site-formation processes at Elands Bay Cave, South Africa. *Southern African Humanities* 29:69-128.

Moffat, I. 2015 Locating Graves with Geophysics. In A. Sarris (ed.), pp.45–53. *Best practices of geoinformatic technologies for the mapping of archaeolandscapes*. Oxford, Archaeopress Publishing Ltd.

Moffat, I., B. David, B. Barker, A. Kuaso, R. Skelly, and N. Araho 2011 Magnetometer surveys in archaeological research in Papua New Guinea: Keveoki 1, Gulf Province. *Archaeology in Oceania* 46(1):17–22.

Moffat, I., J. Linsell, A. Vella, B. Duke, J. Kowlessar, J.G. Griffith, and A. Down 2020 Mapping unmarked graves with Ground Penetrating Radar at the Walkerville Wesleyan Cemetery, Adelaide. *Australian Archaeology* 86(1):57–62.

Moník, M., Z. Lenďáková, J.J. Ibáñez, J. Muñiz, F. Borell, E. Iriarte, L. Teira, and F. Kuda 2018 Revealing early villages - Pseudo-3D ERT geophysical survey at the pre-pottery Neolithic site of Kharaysin, Jordan. *Archaeological Prospection* 25(4):339–346.

Morrish, A. 1965 *The Physical Principles of Magnetism*. New York, John Wiley & Sons.

Mufti, I.R. 1976 Finite-Difference Resistivity Modeling for Arbitrarily Shaped Two-Dimensional Structures. *Geophysics* 41(1):62–78.

Mugnier, fford J. 2003 Grids & Datums: Mongolia. *Photogrammetric Engineering and Remote Sensing* 69(1):20–21.

Murakami, T., N. Katsuta, K. Yamamoto, N. Takamatsu, M. Takano, T. Oda, G.I. Matsumoto, K. Horiuchi, and T. Kawai 2010 A 27-kyr record of environmental change in central Asia inferred from the sediment record of Lake Hovsgol, northwest Mongolia. *Journal of Paleolimnology* 43(2):369–383.

Narantsetseg, Ts., S.K. Krivonogov, O. Ts., U. B., G.S. Burr, T. D., and D. Kh. 2013 Late Glacial to Middle Holocene climate and environmental changes as recorded in Lake Dood sediments, Darhad Basin, northern Mongolia. *Quaternary International* 311:12–24.

Negri, S., G. Leucci, and F. Mazzone 2008 High resolution 3D ERT to help GPR data interpretation for researching archaeological items in a geologically complex subsurface. *Journal of Applied Geophysics* 65(3–4):111–120.

Ni, Z., E. Zhang, S. Yi, W. Sun, X. Meng, D. Ning, and J.C. Kim 2022 A Chironomid Record of Early-Middle Holocene Environmental Evolution in the Darhad Basin, Northern Mongolia. *Insects* 13(5):461.

Nishiyama, R., A. Ariga, T. Ariga, A. Lechmann, D. Mair, C. Pistillo, P. Scampoli, P.G. Valla, M. Vladymyrov, A. Ereditato, and F. Schlunegger 2019 Bedrock sculpting under an active alpine glacier revealed from cosmic-ray muon radiography. *Scientific Reports* 9(1):6970.

Noel, M. and B. Xu 1991 Archaeological investigation by electrical resistivity tomography: a preliminary study. *Geophysical Journal International* 107(1):95–102.

Nowaczinski, E., G. Schukraft, S. Hecht, K. Rassmann, O. Bubenzer, and B. Eitel 2012 A Multimethodological Approach for the Investigation of Archaeological Ditches - Exemplified by the Early Bronze Age Settlement of Fidvár Near Vráble (Slovakia): Multimethodological Investigation of Archaeological Ditches. *Archaeological Prospection* 19(4):281–295.

Nowaczinski, E., G. Schukraft, K. Rassmann, S. Reiter, N. Müller-Scheeßel, S. Hecht, B. Eitel, O. Bubenzer, and J. Bátora 2015 A Multidimensional Research Strategy for the Evaluation of Settlement Pits: 3D Electrical Resistivity Tomography, Magnetic Prospection and Soil Chemistry: A Research Strategy for the Evaluation of Settlement Pits. *Archaeological Prospection* 22(4):233–253.

Okladnikov, A.P. and A.P. Derevianko 1970 Tamsag-Bulak. Neoliticeskaja kul'tura Vostocnoj Mongolii. *Materiali po istorii i filologii Tsetral'noy Azii* 5:3–20.

Orkhonselenge, A., M. Uuganzaya, and T. Davaagatan 2022 *Lakes of Mongolia: Geomorphology, Geochemistry and Paleoclimatology*. Cham, Springer International Publishing.

Orlando, L. 2013 GPR to constrain ERT data inversion in cavity searching: Theoretical and practical applications in archeology. *Journal of Applied Geophysics* 89:35–47.

Papadimitrios, K.S., C.-G. Bank, S.J. Walker, and M. Chazan 2019 Palaeotopography of a Palaeolithic landscape at Bestwood 1, South Africa, from ground-penetrating radar and magnetometry. *South African Journal of Science* 115(1/2).

Papadopoulos, N.G., A. Sarris, W.A. Parkinson, A. Gyucha, R.W. Yerkes, P.R. Duffy, and P. Tsourlos 2014 Electrical Resistivity Tomography for the Modelling of Cultural Deposits and Geomophological Landscapes at Neolithic Sites: a Case Study from Southeastern Hungary: Electrical Resistivity Tomography in Palaeoenvironmental Modelling. *Archaeological Prospection* 21(3):169–183.

Park, J.-S., W. Honeychurch, and A. Chunag 2011 Ancient bronze technology and nomadic communities of the Middle Gobi Desert, Mongolia. *Journal of Archaeological Science* 38(4):805–817.

Pennington, B.T., M.A. Hamdan, B.R. Pears, and H.I. Sameh 2019 Aridification of the Egyptian Sahara 5000–4000 cal BP revealed from x-ray fluorescence analysis of Nile Delta sediments at Kom al-Ahmer/Kom Wasit. *Quaternary International* 514:108–118.

Polymenakos, L. 2019 Searching for prehistoric small-sized graves in complex geoarchaeological conditions: Ayios Vasilios North Cemetery (Peloponnese, Greece). *Journal of Archaeological Science: Reports* 24:1–15.

Prokopenko, A.A., G.K. Khursevich, E.V. Bezrukova, M.I. Kuzmin, X. Boes, D.F. Williams, S.A. Fedenya, N.V. Kulagina, P.P. Letunova, and A.A. Abzaeva 2007 Paleoenvironmental proxy records from Lake Hovsgol, Mongolia, and a synthesis of Holocene climate

change in the Lake Baikal watershed. *Quaternary Research* 68(1):2–17.

Prothero, D.R. and F.L. Schwab 2013 *Sedimentary geology: an introduction to sedimentary rocks and stratigraphy*. Third edition. New York, W.H. Freeman.

Putnam, D. 2016 Preliminary Interpretation of the Soyo Site. Geological report, Nomad Science.

Reichert, S., N.-O. Erdene-Ochir, S. Linzen, Lkh. Munkhbayar, and J. Bemmann 2022 Overlooked—Enigmatic—Underrated: The City Khar Khul Khaany Balgas in the Heartland of the Mongol World Empire. *Journal of Field Archaeology* 47(6):397–420.

Reimer, P.J., W.E.N. Austin, E. Bard, A. Bayliss, P.G. Blackwell, C. Bronk Ramsey, M. Butzin, H. Cheng, R.L. Edwards, M. Friedrich, P.M. Grootes, T.P. Guilderson, I. Hajdas, T.J. Heaton, A.G. Hogg, K.A. Hughen, B. Kromer, S.W. Manning, R. Muscheler, J.G. Palmer, C. Pearson, J. Van Der Plicht, R.W. Reimer, D.A. Richards, E.M. Scott, J.R. Southon, C.S.M. Turney, L. Wacker, F. Adolphi, U. Büntgen, M. Capano, S.M. Fahrni, A. Fogtmann-Schulz, R. Friedrich, P. Köhler, S. Kudsk, F. Miyake, J. Olsen, F. Reinig, M. Sakamoto, A. Sookdeo, and S. Talamo 2020 The IntCal20 Northern Hemisphere Radiocarbon Age Calibration Curve (0–55 cal kBP). *Radiocarbon* 62(4):725–757.

Retallack, G.J. 1990 *Soils of the Past: An Introduction to Paleopedology*. Boston, Unwin Hyman.

Richter, T. and L.A. Maher 2013 Terminology, process and change: reflections on the Epipalaeolithic of South-west Asia. *Levant* 45(2):121–132.

Ristić, A., M. Govedarica, L. Pajewski, M. Vrtunski, and Ž. Bugarinović 2020 Using Ground Penetrating Radar to Reveal Hidden Archaeology: The Case Study of the Württemberg-Stambol Gate in Belgrade (Serbia). *Sensors* 20(3):607.

Rogers, L.L. and F.A. Kaestle 2022 Analysis of mitochondrial DNA haplogroup frequencies in the population of the slab burial mortuary culture of Mongolia (ca. 1100–300 BCE). *American Journal of Biological Anthropology* 177(4):644–657.

Rücker, C. 2010 Advanced Electrical Resistivity Modelling and Inversion using Unstructured Discretization. Leipzig, Leipzig University.

Rybin, E.P., A.M. Khatsenovich, B. Gunchinsuren, J.W. Olsen, and N. Zwyns 2016 The impact of the LGM on the development of the Upper Paleolithic in Mongolia. *Quaternary International* 425:69–87.

Sandmeier, K.J. 2020 Reflexw: Version 9.5.

Schmidt, A. 2013 *Earth Resistance for Archaeologists*. Lanham, AltaMira Press.

Schneider, A., F. Hirsch, K.-P. Wechler, A. Raab, and T. Raab 2017 Reconstruction of a Palaeosurface and Archaeological Site Location in an Anthropogenic Drift Sand Area: Reconstruction of a palaeosurface and archaeological site location. *Archaeological Prospection* 24(4):297–310.

Schneider, J.S., T. Yadmaa, J.M. Farquhar, and P. Hadel 2020 Entering new territory: The results of a random-sample archaeological inventory

at Ikh Nartiin Chuluu Nature Reserve, Dornogovi Aimag, Mongolia. *Archaeological Research in Asia* 25:100251.

Schneider, J.S., T. Yadmaa, T.C. Hart, A.M. Rosen, and A. Spiro 2016 Mongolian "Neolithic" and Early Bronze Age ground stone tools from the northern edge of the Gobi Desert. *Journal of Lithic Studies* 3(3):479–497.

Schumm, S.A. 1971 Experimental Study of Channel Patterns. *Nature* 233:407–409.

Schumm, S.A. 1993 River Response to Baselevel Change: Implications for Sequence Stratigraphy. *The Journal of Geology* 101(2):279–294.

Séfériadès, M.L. 2004 An aspect of Neolithisation in Mongolia: the Mesolithic-Neolithic site of Tamsagbulag (Dornod district). *Documenta Praehistorica* 31:139–149.

Seitsonen, O., J.-L. Houle, L.G. Broderick, P. Woodley, and J. Bayarsaikhan 2018 Lithics in the steppe landscape: An off-site spatial analysis of stone artefacts in the Khanuy Valley, Mongolia. *Archaeological Research in Asia* 16:1–13.

Shackley, M.S., editor 2011 *X-Ray Fluorescence Spectrometry (XRF) in Geoarchaeology*. New York, NY, Springer New York.

Shelach-Lavi, G., M. Teng, Y. Goldsmith, I. Wachtel, C.J. Stevens, O. Marder, X. Wan, X. Wu, D. Tu, R. Shavit, P. Polissar, H. Xu, and D.Q. Fuller 2019 Sedentism and plant cultivation in northeast China emerged during affluent conditions. *PLOS One* 14(7):e0218751.

Sherratt, A. 1981 Ploughs and Pastoralism: Aspects of the Secondary Products Revolution. In I. Hodder, G. Isaac, and N. Hammond

(eds), pp.261–305. *Patters of the Past: Studies in Honour of David Clarke*. Cambridge, Cambridge University Press.

Similox-Tohon, D., K. Vanneste, M. Sintubin, P. Muchez, and M. Waelkens 2004 Two-dimensional resistivity imaging: a tool in archaeoseismology. An example from ancient Sagalassos (Southwest Turkey). *Archaeological Prospection* 11(1):1–18.

Simyrdanis, K., N. Papadopoulos, and G. Cantoro 2016 Shallow Off-Shore Archaeological Prospection with 3-D Electrical Resistivity Tomography: The Case of Olous (Modern Elounda), Greece. *Remote Sensing* 8(11):897.

Slater, L.D., N.D. Hamilton, S. Sandberg, and M. Jankowski 2000 Magnetic prospecting at a prehistoric and historic settlement in Maine. *Archaeol. Prospect.* 7:31–41.

Smith, R.C. and D.B. Sjogren 2006 An evaluation of electrical resistivity imaging (ERI) in Quaternary sediments, southern Alberta, Canada. *Geosphere* 2(6):287–298.

Stern, N. 2008 Stratigraphy, Depositional Environments, and Palaeolandscape Reconstruction in Landscape Archaeology. In B. David and J. Thomas (eds), pp.365–378. *Handbook of Landscape Archaeology*. Walnut Creek, California, Left Coast Press.

Takakura, J. 2020 Rethinking the Disappearance of Microblade Technology in the Terminal Pleistocene of Hokkaido, Northern Japan: Looking at Archaeological and Palaeoenvironmental Evidence. *Quaternary* 3(3):21.

Tarasov, P., E. Bezrukova, E. Karabanov, T. Nakagawa, M. Wagner, N. Kulagina, P. Letunova, A. Abzaeva, W. Granoszewski, and F. Riedel

2007 Vegetation and climate dynamics during the Holocene and Eemian interglacials derived from Lake Baikal pollen records. *Palaeogeography, Palaeoclimatology, Palaeoecology* 252(3–4):440–457.

Taylor, R. 1987 *Radiocarbon Dating: An Archaeological Perspective*. Orlando, Academic Press.

Taylor, W.T.T., B. Jargalan, K.B. Lowry, J. Clark, T. Tuvshinjargal, and J. Bayarsaikhan 2017 A Bayesian chronology for early domestic horse use in the Eastern Steppe. *Journal of Archaeological Science* 81:49–58.

Taylor, W., S. Wilkin, J. Wright, M. Dee, M. Erdene, J. Clark, T. Tuvshinjargal, J. Bayarsaikhan, W. Fitzhugh, and N. Boivin 2019 Radiocarbon dating and cultural dynamics across Mongolia's early pastoral transition. *PLOS One* 14(11):1–20.

Taylor, W., M. Fantoni, C. Marchina, S. Lepetz, J. Bayarsaikhan, J.-L. Houle, V. Pham, and W. Fitzhugh 2020a Horse sacrifice and butchery in Bronze Age Mongolia. *Journal of Archaeological Science: Reports* 31:102313.

Taylor, W.T.T., J. Clark, J. Bayarsaikhan, T. Tuvshinjargal, J.T. Jobe, W. Fitzhugh, R. Kortum, R.N. Spengler, S. Shnaider, F.V. Seersholm, I. Hart, N. Case, S. Wilkin, J. Hendy, U. Thuering, B. Miller, A.R.V. Miller, A. Picin, N. Vanwezer, F. Irmer, S. Brown, A. Abdykanova, D.R. Shultz, V. Pham, M. Bunce, K. Douka, E.L. Jones, and N. Boivin 2020b Early Pastoral Economies and Herding Transitions in Eastern Eurasia. *Scientific Reports* 10(1):1001.

Taylor, W.T.T. and C.I. Barrón-Ortiz 2021 Rethinking the evidence for early horse domestication at Botai. *Nature Scientific Reports* 11(1):7440.

Taylor, W.T.T., M. Pruvost, C. Posth, W. Rendu, M.T. Krajcarz, A. Abdykanova, G. Brancaleoni, R. Spengler, T. Hermes, S. Schiavinato, G. Hodgins, R. Stahl, J. Min, S. Alisher kyzy, S. Fedorowicz, L. Orlando, K. Douka, A. Krivoshapkin, C. Jeong, C. Warinner, and S. Shnaider 2021 Evidence for early dispersal of domestic sheep into Central Asia. *Nature Human Behaviour* 5(9):1169–1179.

Tonkov, N. and M.H. Loke 2006 A resistivity survey of a burial mound in the 'Valley of the Thracian Kings'. *Archaeological Prospection* 13(2):129–136.

Tsydenova, N., D. Andreeva, and W. Zech 2017 Early pottery in Transbaikal Siberia: New data from Krasnaya Gorka. *Quaternary International* 441:81–90.

Tsypukova, S.S., A.B. Perepelov, E.I. Demonterova, A.V. Ivanov, S.I. Dril, M.I. Kuzmin, A.V. Travin, Yu.D. Shcherbakov, M.Yu. Puzankov, and S.V. Kanakin 2022 Two Stages of the Cenozoic Alkaline-Basalt Volcanism in the Darkhad Depression (Northern Mongolia) - Geochronology, Geochemistry, and Geodynamic Consequences. *Geodynamics & Tectonophysics* 13(3):0613.

Ufland, A.K., A.B. Ilin, A.I. Spirkin, and G.N. Shilova 1971 Osnovniye cherty stratigrafii i usloviya formirovanya Kainozoiskikh obrazovanii Prikosogolya. *Bulletin of the Moscow Society of Naturalists* 46:54–69.

Ungureanu, C., A. Priceputu, A.L. Bugea, and A. Chirică 2017 Use of electric resistivity tomography (ERT) for detecting underground

voids on highly anthropized urban construction sites. *Procedia Engineering* 209:202–209.

Urban, T.M., J. Rasic, I. Buvit, R.W. Jacob, J. Richie, S. Hackenberger, S. Hanson, W. Ritz, E. Wakeland, and S.W. Manning 2016 Geophysical investigation of a Middle Holocene archaeological site along the Yukon River, Alaska. *The Leading Edge* 35(4):345–349.

Urban, T.M., J.T. Rasic, C. Alix, D.D. Anderson, L. Chisholm, R.W. Jacob, S.W. Manning, O.K. Mason, A.H. Tremayne, and D. Vinson 2019 Magnetic detection of archaeological hearths in Alaska: A tool for investigating the full span of human presence at the gateway to North America. *Quaternary Science Reviews* 211:73–92.

Vanwezer, N., S.F.M. Breitenbach, F. Gázquez, J. Louys, A. Kononov, D. Sokol'nikov, E. Avirmed, A. Burguet-Coca, A. Picin, A. Cueva-Temprana, J. Sánchez-Martínez, W.T.T. Taylor, N. Boivin, J. Bayarsaikhan, and M.D. Petraglia 2021a Archaeological and environmental cave records in the Gobi-Altai Mountains, Mongolia. *Quaternary International* 586:66–89.

Vanwezer, N., W. Timothy Treal Taylor, J. Bayarsaikhan, S.F.M. Breitenbach, N. Amano, J. Louys, M. Del Val, N. Boivin, and M. Petraglia 2021b Hunting, herding, and people in the rock art of Mongolia: New discoveries in the Gobi-Altai Mountains. *Archaeological Research in Asia* 26:100267.

Vella, A. 2018 On the Mongolian Steppe: A Subsurface Investigation of Soyo, Northern Mongolia. Adelaide, Flinders University.

Ventresca Miller, A.R., S. Wilkin, J. Bayarsaikhan, A. Ramsøe, J. Clark, B. Byambadorj, S. Vanderwarf, N. Vanwezer, A. Haruda, R. Fernandes,

B. Miller, and N. Boivin 2023 Permafrost preservation reveals proteomic evidence for yak milk consumption in the 13th century. *Communications Biology* 6(1):351.

Vogel, C.R. 1996 Non-convergence of the L-curve regularization parameter selection method. *Inverse Problems* 12(4):535–547.

Vogel, J.S., J.R. Southon, D.E. Nelson, and T.A. Brown 1984 Performance of Catalytically Condensed Carbon for Use in Accelerator Mass Spectrometry. *Nuclear Instruments and Methods in Physics Research* 5(2):289–93.

Volkov, V. 1995 Early Nomads of Mongolia. In J. Davis-Kimball, V.A. Bashilov, and L.T. Yablonsky (eds), pp.319–333. *Nomads of the Eurasian Steppes in the Early Iron Age*. Berkeley, Zinat Press.

Weber, A. 1995 The neolithic and early bronze age of the Lake Baikal Region: A review of recent research. *Journal of World Prehistory* 9(1):99–165.

Welc, F. and P. Bobrowski 2020 Results of Geophysical Survey in Bargat El-Shab in Southern Egypt. Insight into the Early Holocene Settlement Pattern of the El Nabta / Al Jerar Interphase. *Archaeologia Polona* 58:221–234.

Westoby, M.J., J. Brasington, N.F. Glasser, M.J. Hambrey, and J.M. Reynolds 2012 'Structure-from-Motion' photogrammetry: A low-cost, effective tool for geoscience applications. *Geomorphology* 179:300–314.

Wilkin, S., A. Ventresca Miller, W.T.T. Taylor, B.K. Miller, R.W. Hagan, M. Bleasdale, A. Scott, S. Gankhuyg, A. Ramsøe, S. Uliziibayar, C. Trachsel, P. Nanni, J. Grossmann, L. Orlando, M. Horton, P.W.

Stockhammer, E. Myagmar, N. Boivin, C. Warinner, and J. Hendy 2020 Dairy pastoralism sustained eastern Eurasian steppe populations for 5,000 years. *Nature Ecology & Evolution* 4(3):346–355.

Witten, A. 2006 *Handbook of Geophysics and Archaeology*. London, Equinox Publishing.

Worm, H.-U. and M. Jackson 1999 The superparamagnetism of Yucca Mountain Tuff. *Journal of Geophysical Research: Solid Earth* 104(B11):415–425.

Wright, J. 2006 The Adoption of Pastoralism in Northeast Asia: Monumental Transformation in the Egiin Gol Valley, Mongolia. Cambridge, Harvard University.

Wright, J. 2014 Landscapes of Inequality?: A Critique of Monumental Hierarchy in the Mongolian Bronze Age. *Asian Perspectives* 51(2):139–163.

Wright, J. 2017 The honest labour of stone mounds: monuments of Bronze and Iron Age Mongolia as costly signals. *World Archaeology* 49(4):547–567.

Wright, J. 2021 Prehistoric Mongolian Archaeology in the Early 21st Century: Developments in the Steppe and Beyond. *Journal of Archaeological Research* 29(3):431–479.

Wright, J., G. Ganbaatar, W. Honeychurch, B. Byambatseren, and A. Rosen 2019 The earliest Bronze Age culture of the south-eastern Gobi Desert, Mongolia. *Antiquity* 93(368):393–411.

Wright, J., W. Honeychurch, and C. Amartuvshin 2009 The Xiongnu settlements of Egiin Gol, Mongolia. *Antiquity* 83(320):372–387.

Yanshina, O.V. and S.V. Kovalenko 2022 New data and insights into how pottery appeared along the Amur river. *Quaternary International* 608–609:154–177.

Yelf, R. and D. Yelf 2004 Where is True TIme Zero? pp.279–282. *Proceedings of the Tenth International Conference on Ground Penetrating Radar*.

Yi, M., X. Gao, F. Li, and F. Chen 2016 Rethinking the origin of microblade technology: A chronological and ecological perspective. *Quaternary International* 400:130–139.

Zhao, C., L. Janz, D. Bukhchuluun, and D. Odsuren 2021 Neolithic pathways in East Asia: early sedentism on the Mongolian Plateau. *Antiquity* 95(379):45–64.

Zwyns, N. 2021 The Initial Upper Paleolithic in Central and East Asia: Blade Technology, Cultural Transmission, and Implications for Human Dispersals. *Journal of Paleolithic Archaeology* 4(3):19.

Zwyns, N., S.A. Gladyshev, B. Gunchinsuren, T. Bolorbat, D. Flas, T. Dogandžić, A.V. Tabarev, J.C. Gillam, A.M. Khatsenovich, S. McPherron, D. Odsuren, C.H. Paine, K.-E. Purevjal, and J.R. Stewart 2014 The open-air site of Tolbor 16 (Northern Mongolia): Preliminary results and perspectives. *Quaternary International* 347:53–65.

Zwyns, N., C.H. Paine, B. Tsedendorj, S. Talamo, K.E. Fitzsimmons, A. Gantumur, L. Guunii, O. Davakhuu, D. Flas, T. Dogandžić, N. Doerschner, F. Welker, J.C. Gillam, J.B. Noyer, R.S. Bakhtiary, A.F. Allshouse, K.N. Smith, A.M. Khatsenovich, E.P. Rybin, G. Byambaa, and J.-J. Hublin 2019 The Northern Route for Human dispersal in

Central and Northeast Asia: New evidence from the site of Tolbor-16, Mongolia. *Scientific Reports* 9(1):11759.

Appendix A

Inverted ERT Profiles

Map of ERT Line Locations

(All lines start south and end north)

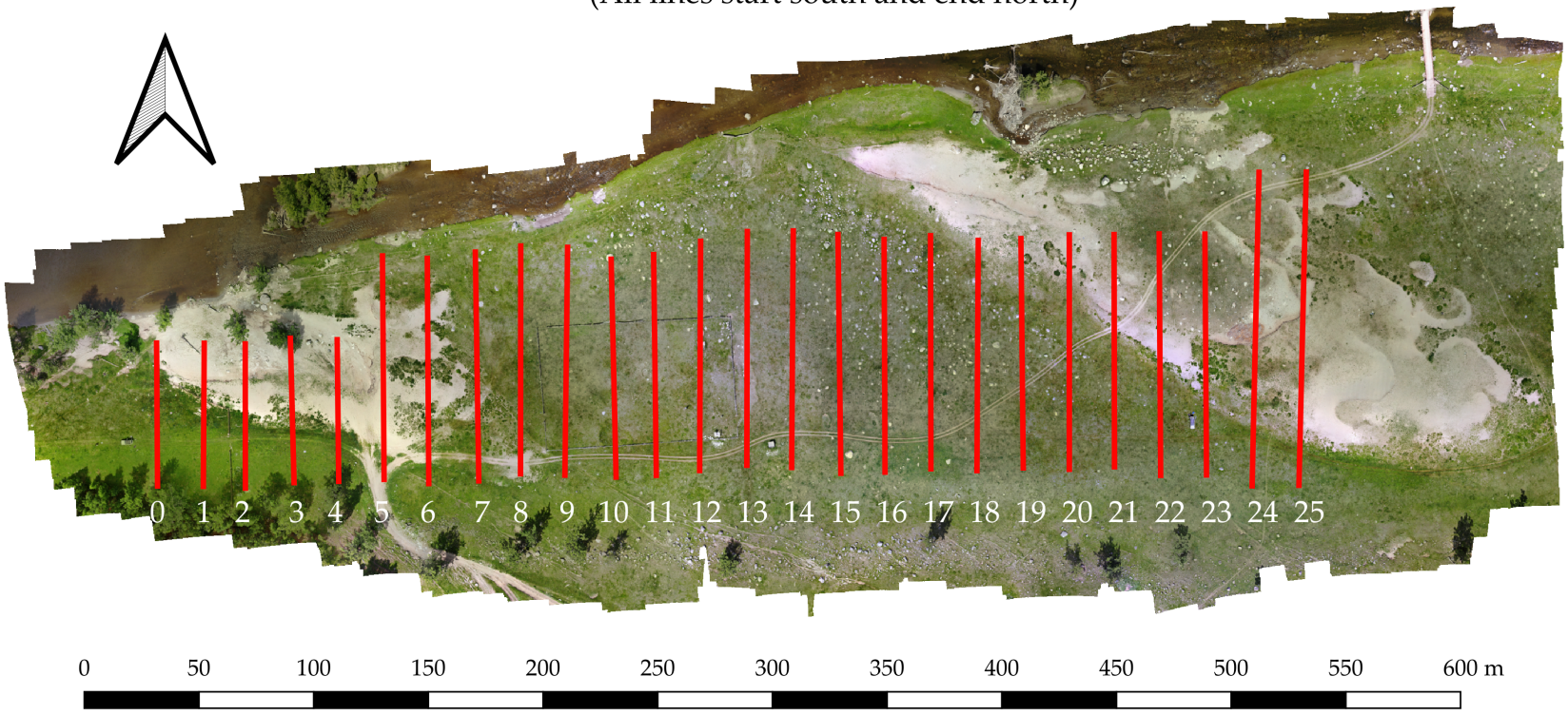

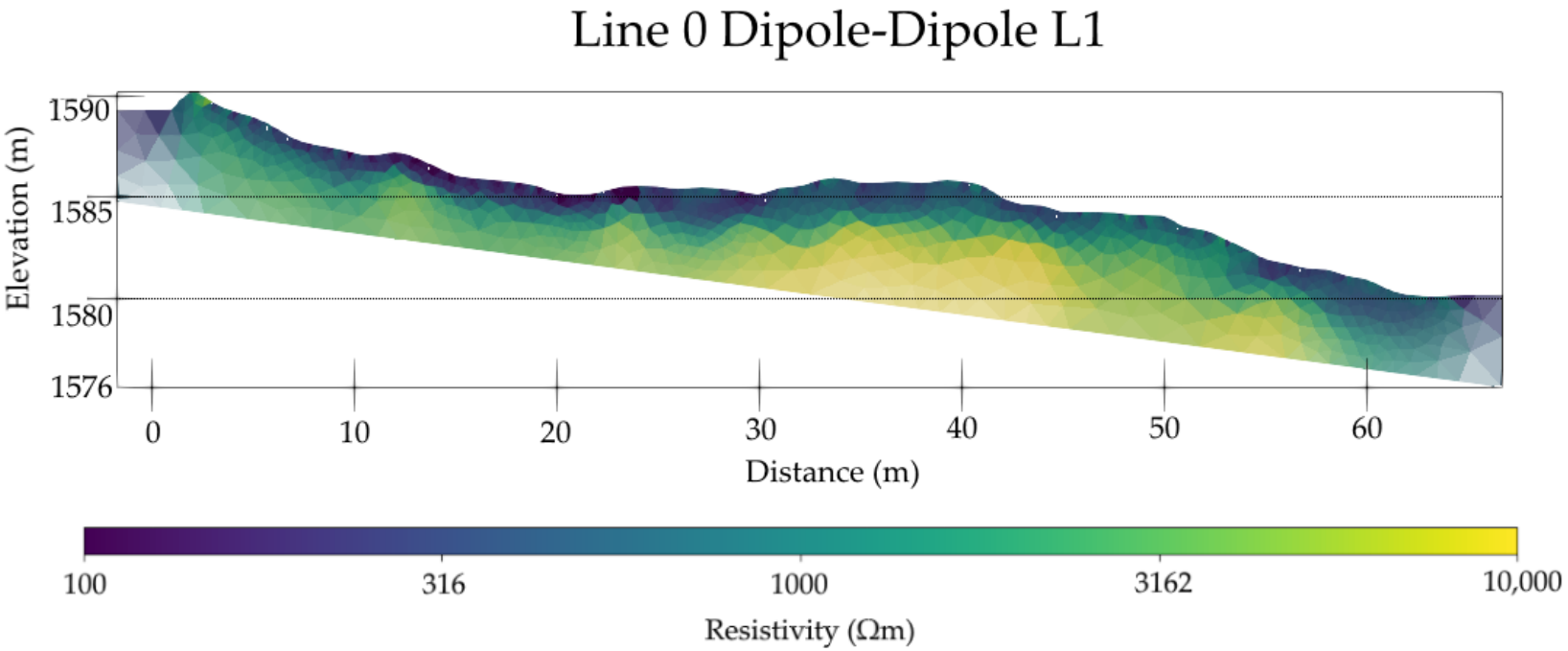
Line 0 Dipole-Dipole L1
Elevation (m)
1590
1585
1580
1576
0
10
20
30
40
50
60
Distance (m)
100
316
1000
3162
10,000
Resistivity (Ωm)

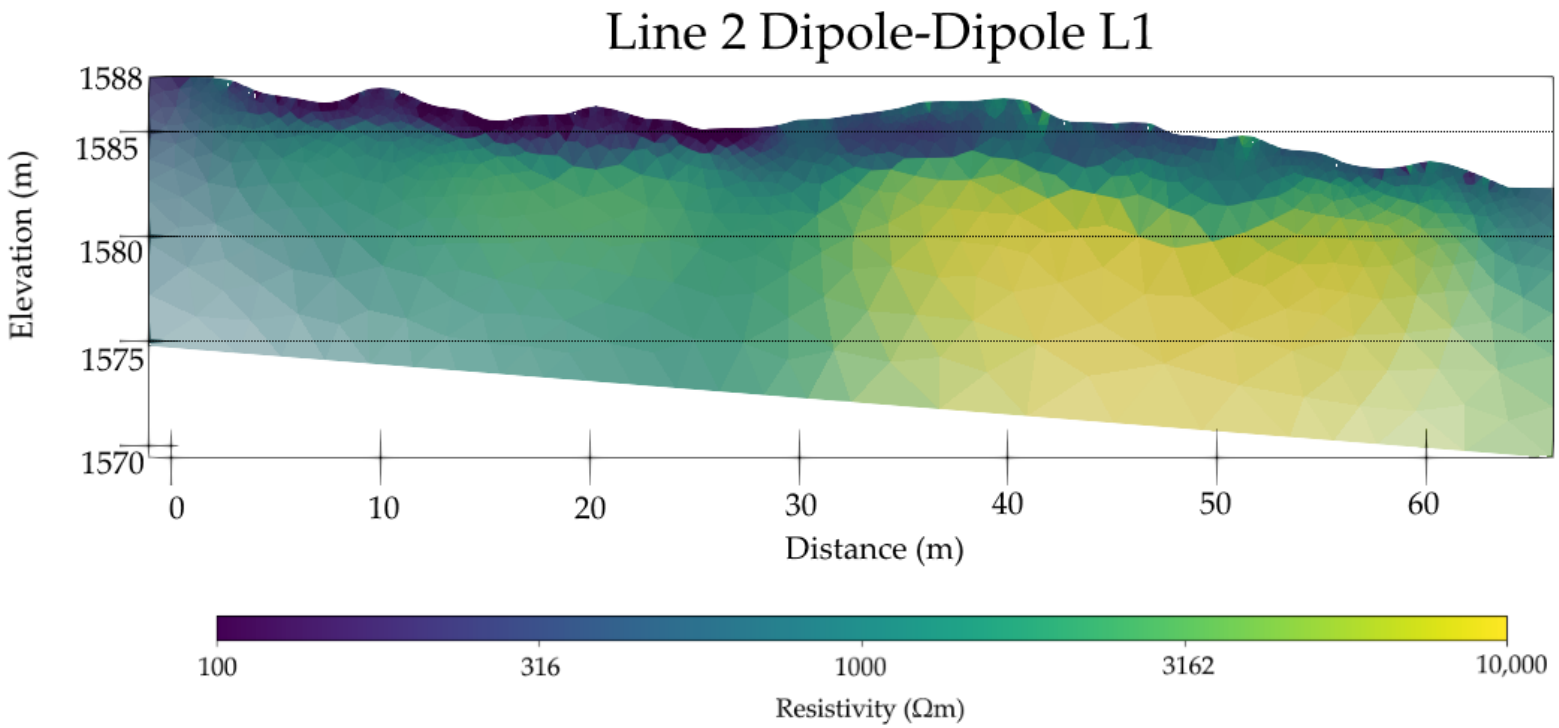
Line 2 Dipole-Dipole L1
Elevation (m)
1588
1585
1580
1575
1570
0
10
20
30
40
50
60
Distance (m)
100
316
1000
3162
10,000
Resistivity (Ωm)

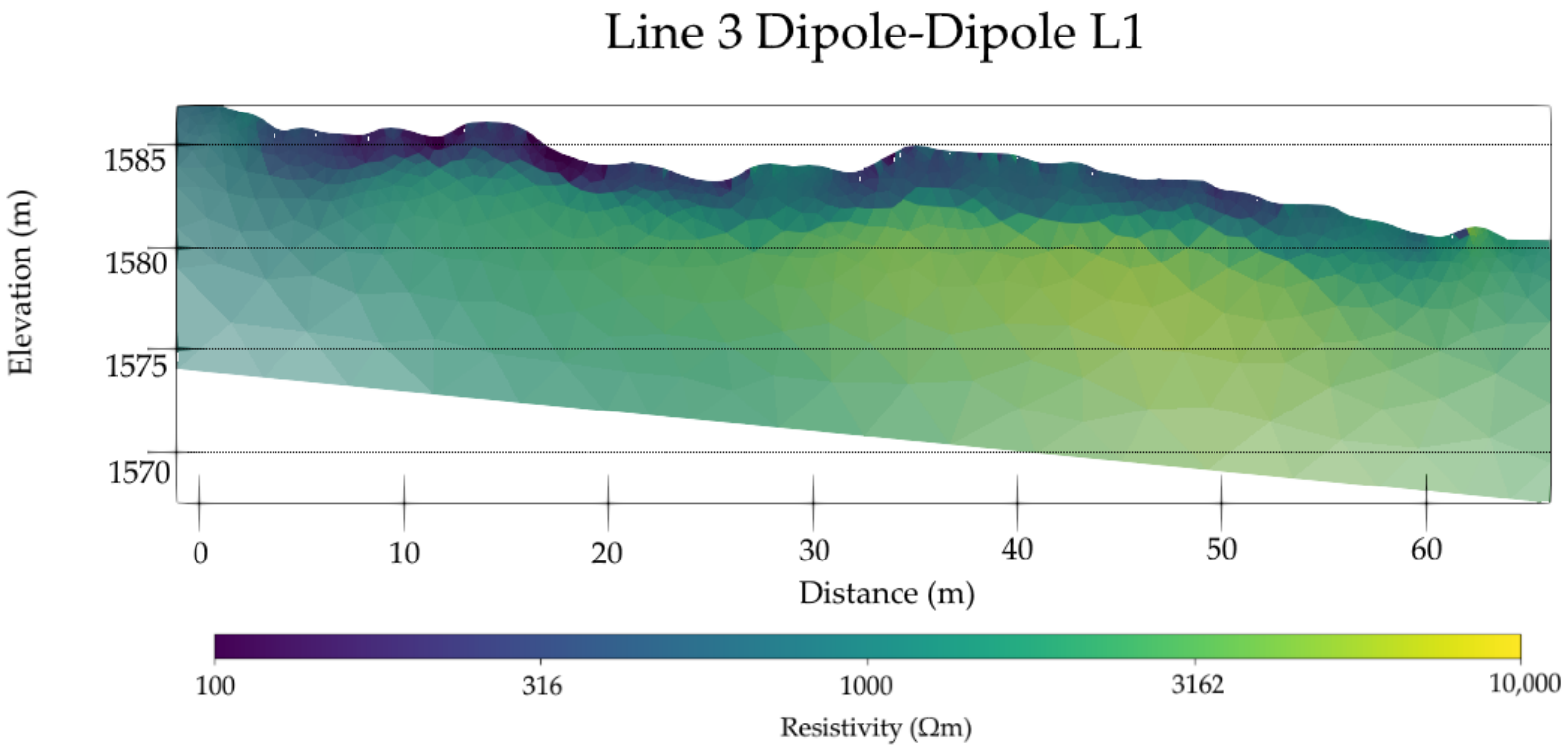
Line 3 Dipole-Dipole L1
Elevation (m)
1585
1580
1575
1570
0
10
20
30
40
50
60
Distance (m)
100
316
1000
3162
10,000
Resistivity (Ωm)

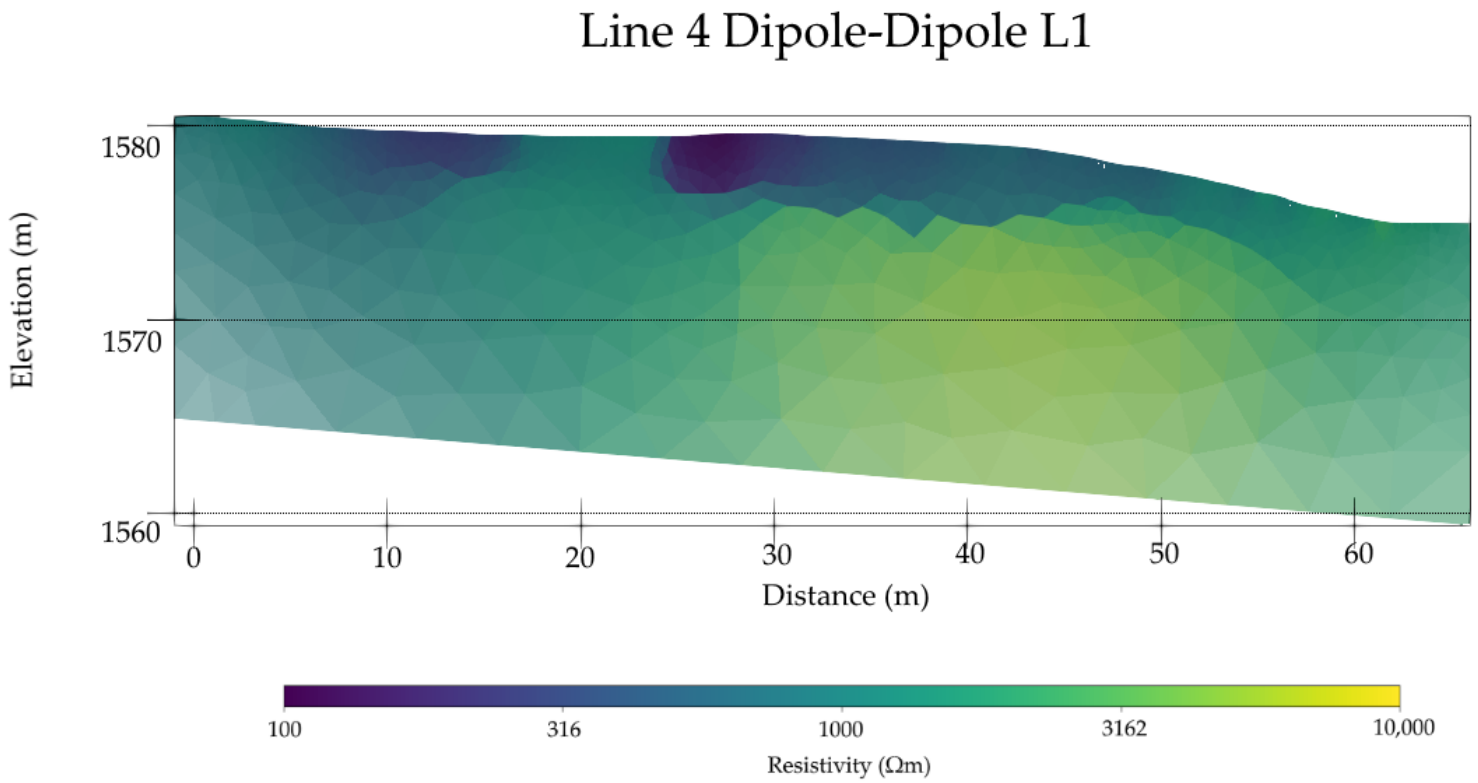
Line 4 Dipole-Dipole L1
Elevation (m)
1580
1570
1560
0
10
20
30
40
50
60
Distance (m)
100
316
1000
3162
10,000
Resistivity (Ωm)

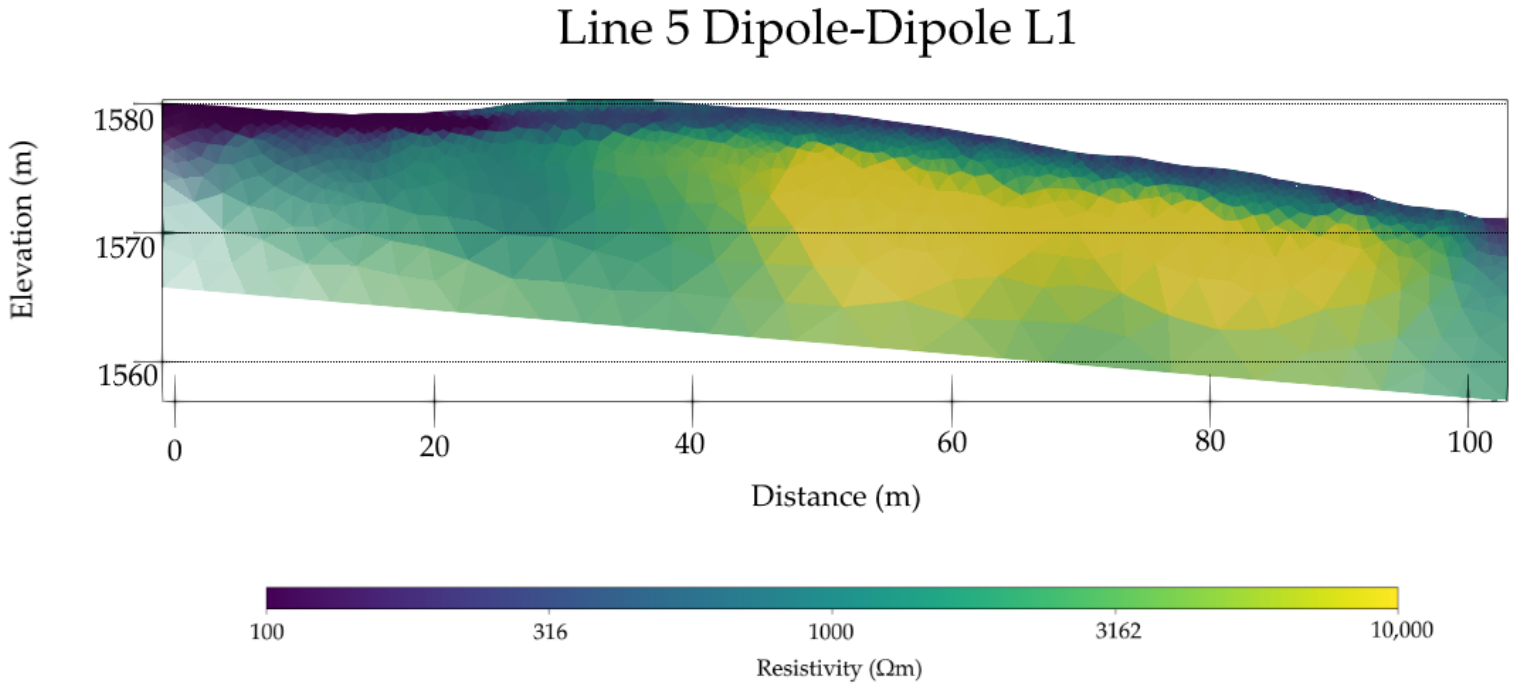
Line 5 Dipole-Dipole L1
Elevation (m)
1580
1570
1560
0
20
40
60
80
100
Distance (m)
100
316
1000
3162
10,000
Resistivity (Ωm)

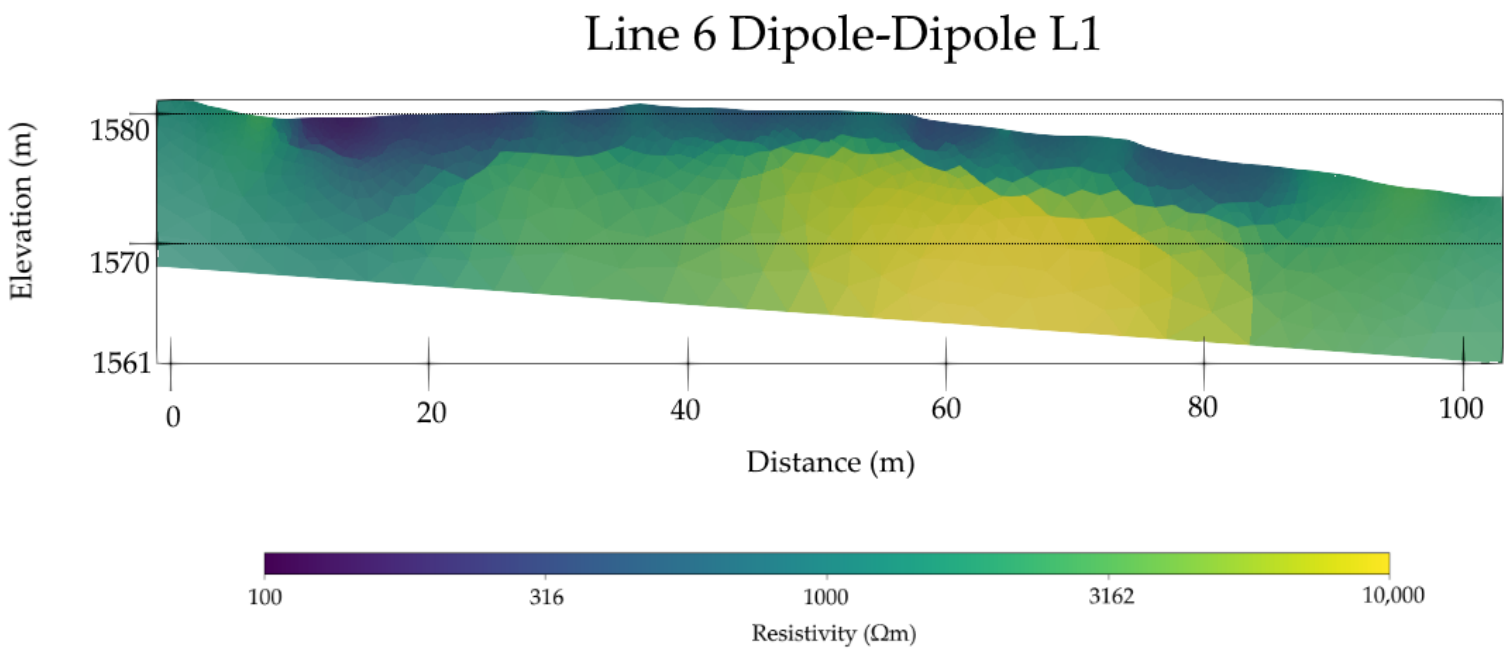
Line 6 Dipole-Dipole L1
Elevation (m)
1580
1570
1561
0
20
40
60
80
100
Distance (m)
100
316
1000
3162
10,000
Resistivity (Ωm)

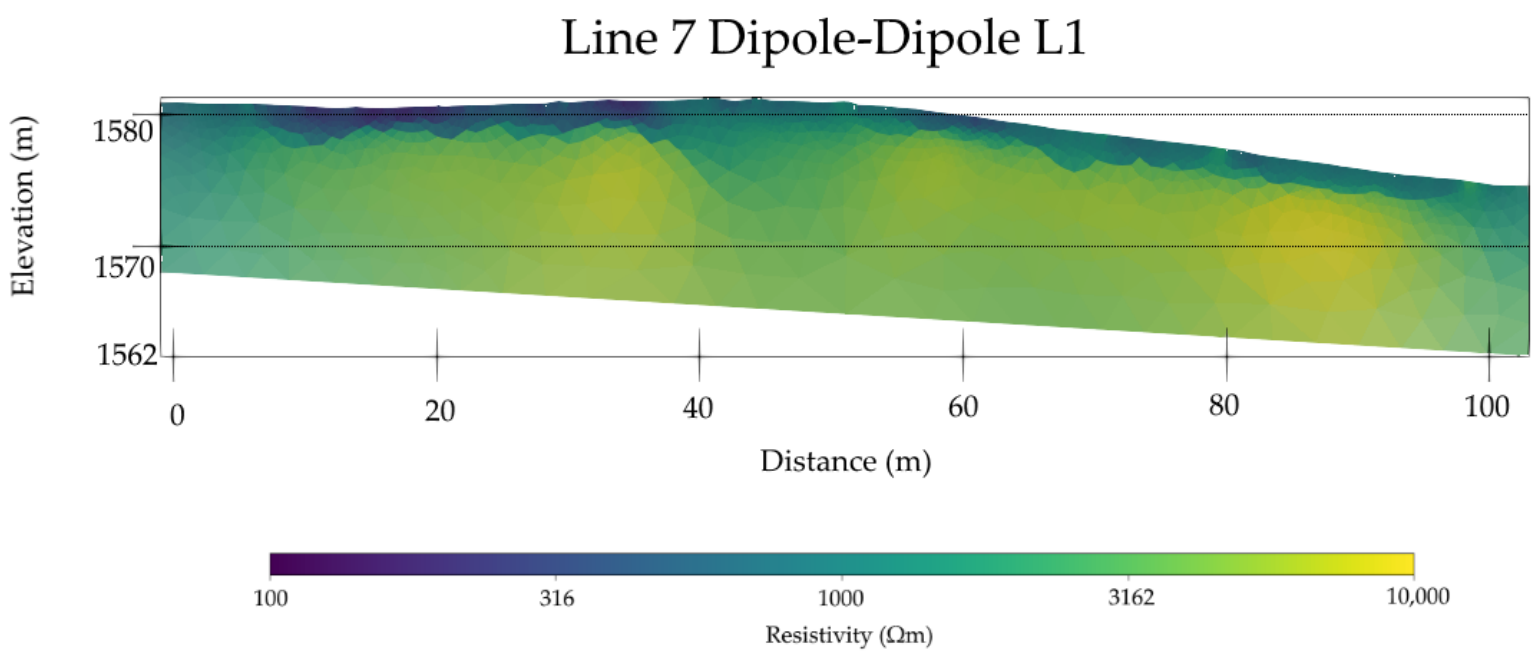
Line 7 Dipole-Dipole L1
Elevation (m)
1580
1570
1562
0
20
40
60
80
100
Distance (m)
100
316
1000
3162
10,000
Resistivity (Ωm)

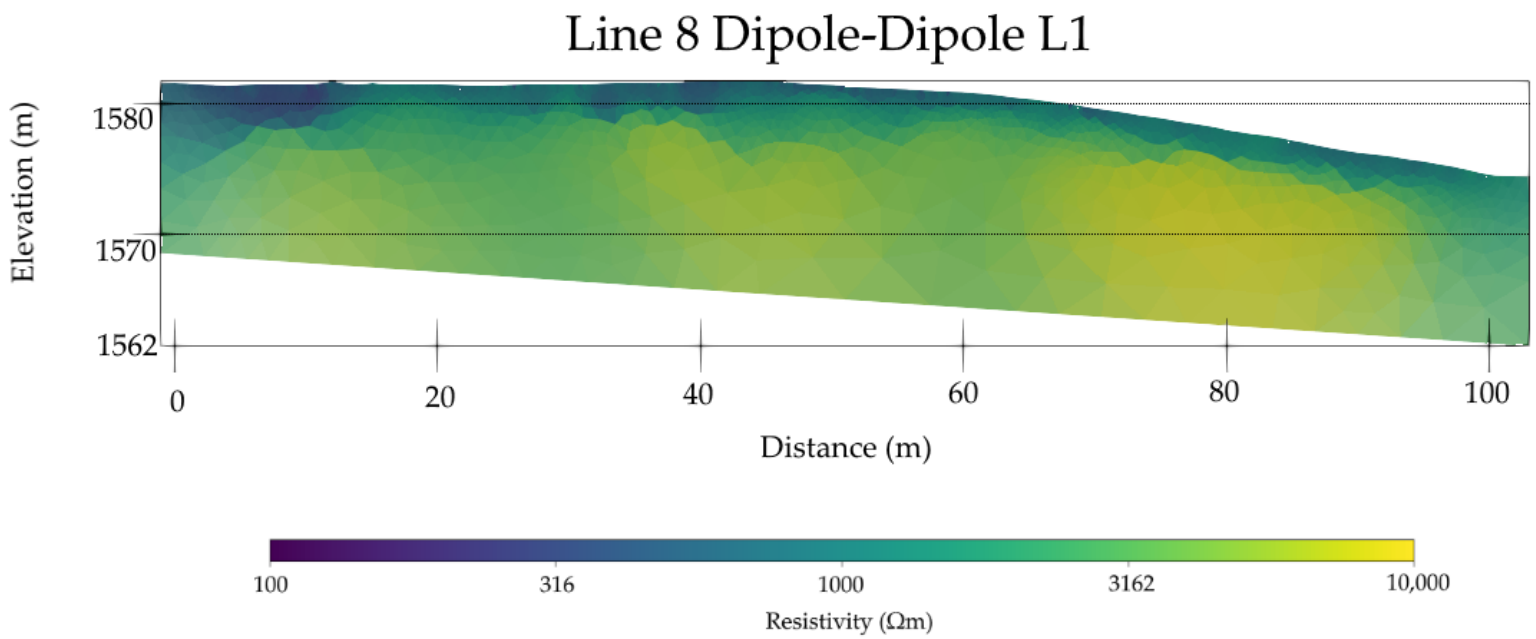
Line 8 Dipole-Dipole L1
Elevation (m)
1580
1570
1562
0
20
40
60
80
100
Distance (m)
100
316
1000
3162
10,000
Resistivity (Ωm)

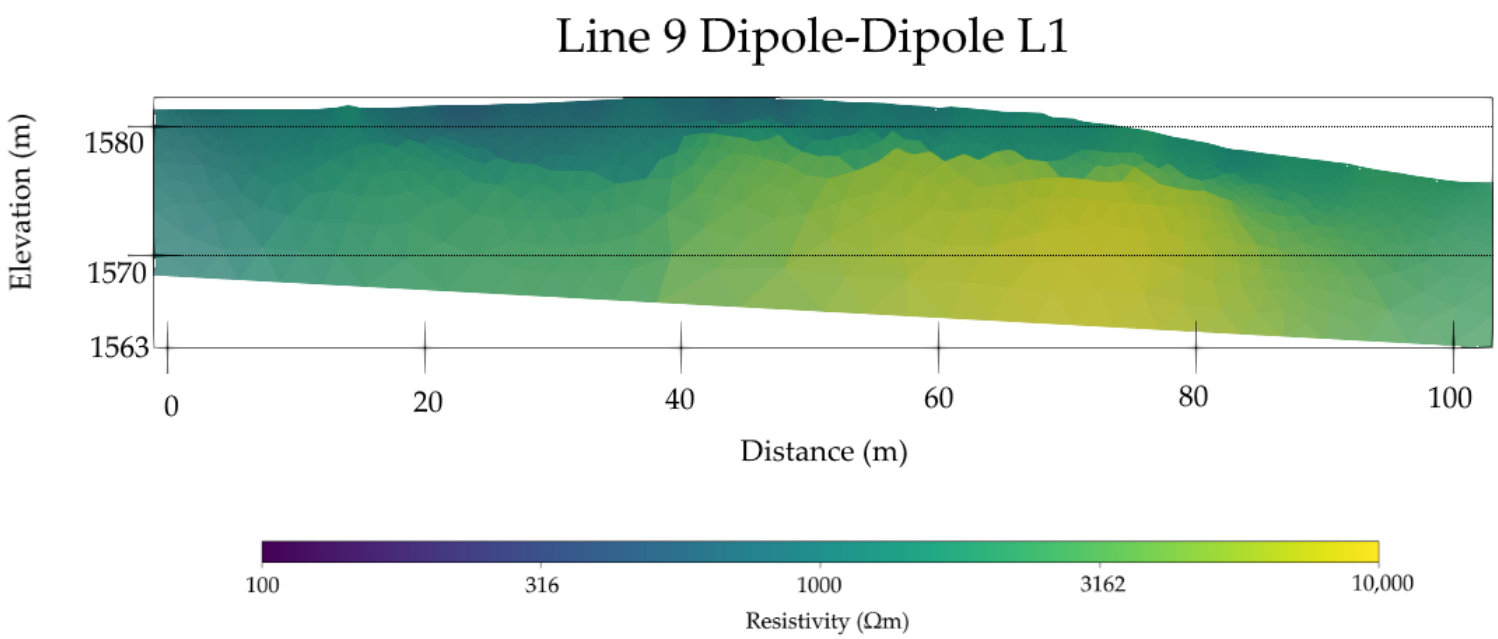
Line 9 Dipole-Dipole L1
Elevation (m)
1580
1570
1563
0
20
40
60
80
100
Distance (m)
100
316
1000
3162
10,000
Resistivity (Ωm)

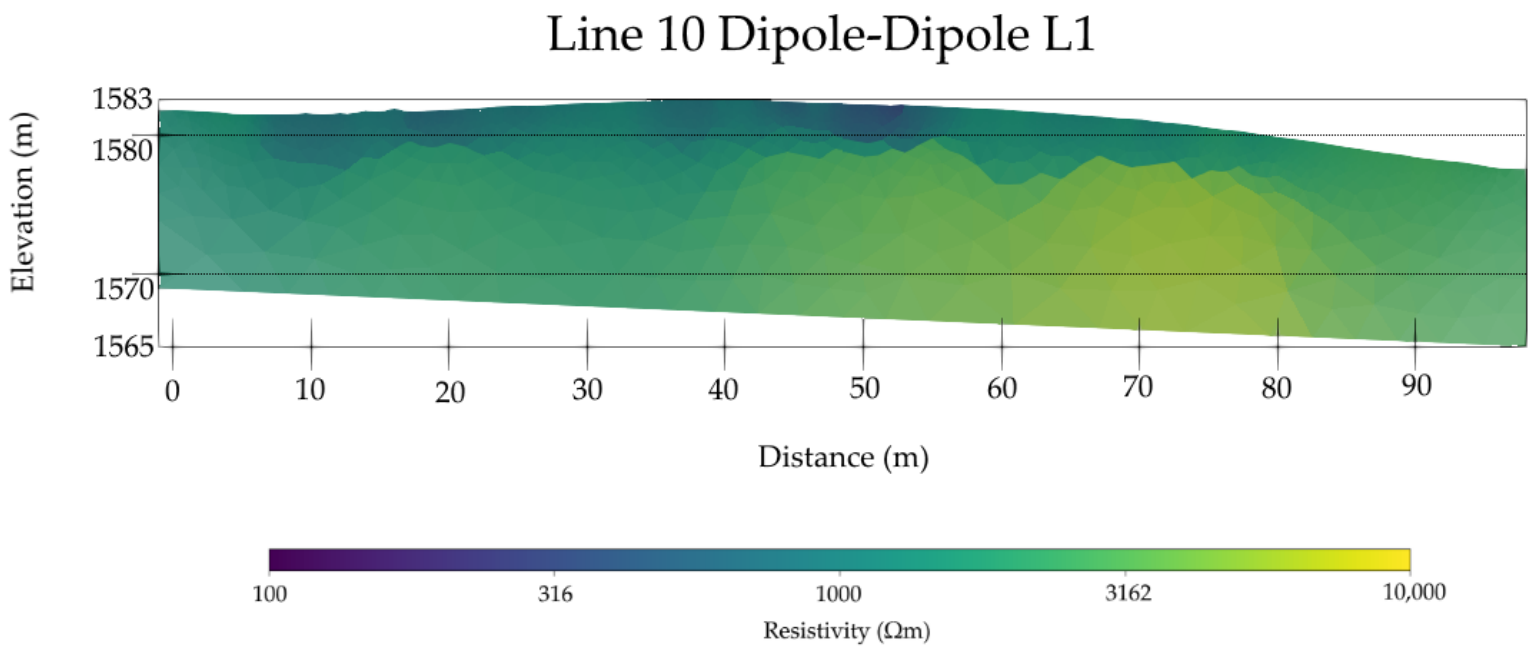
Line 10 Dipole-Dipole L1
Elevation (m)
1583
1580
1570
1565
0
10
20
30
40
50
60
70
80
90
Distance (m)
100
316
1000
3162
10,000
Resistivity (Ωm)

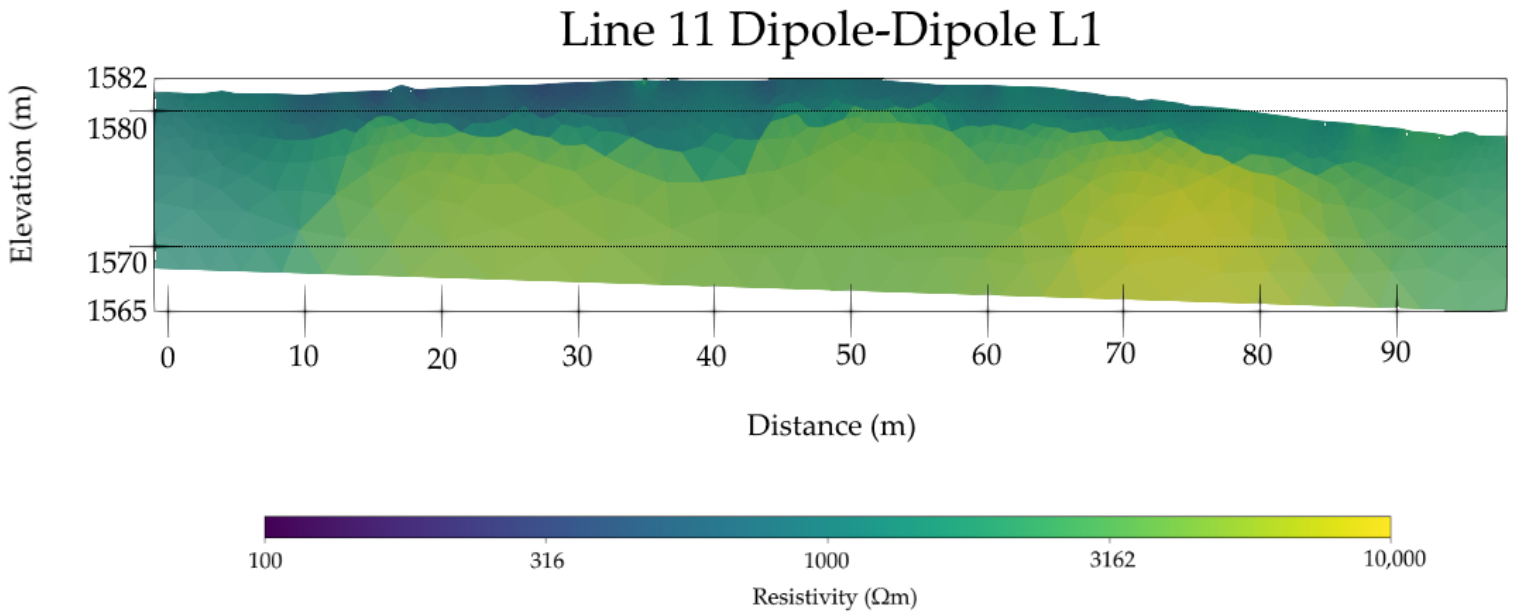
Line 11 Dipole-Dipole L1
Elevation (m)
1582
1580
1570
1565
0
10
20
30
40
50
60
70
80
90
Distance (m)
100
316
1000
3162
10,000
Resistivity (Ωm)

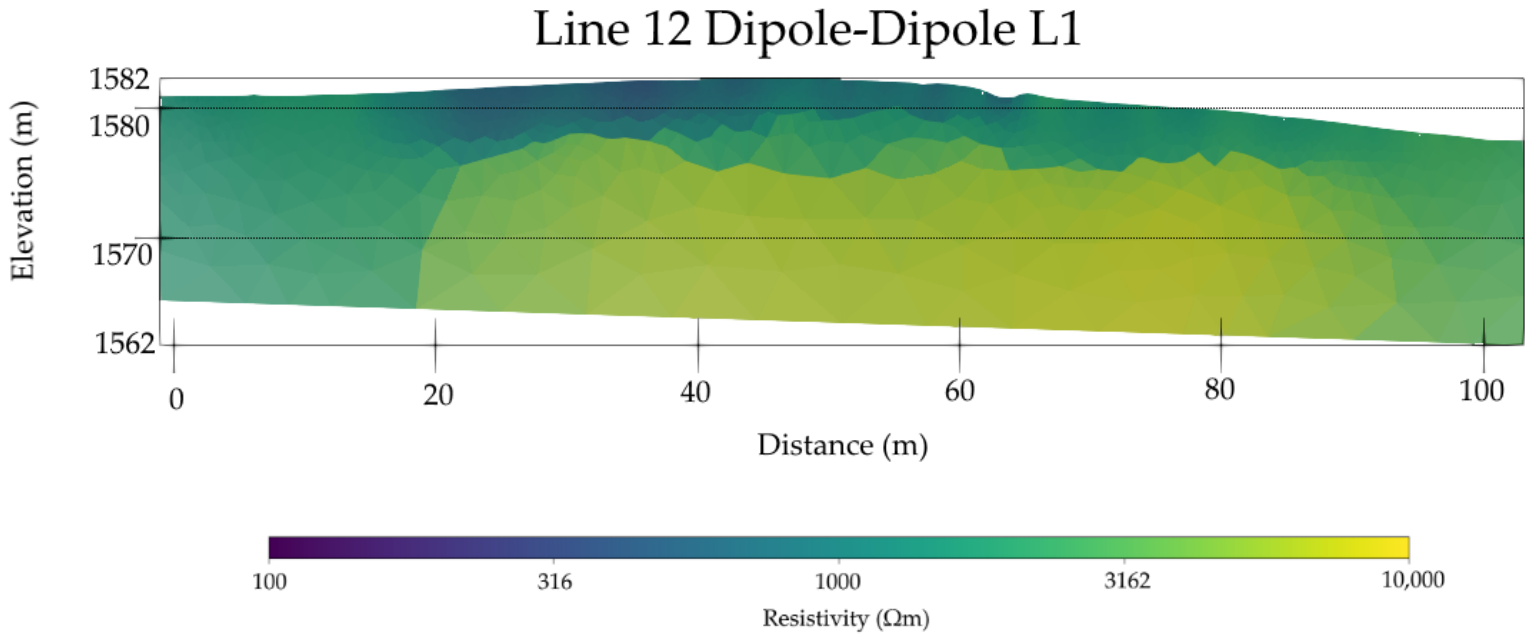
Line 12 Dipole-Dipole L1
Elevation (m)
1582
1580
1570
1562
0
20
40
60
80
100
Distance (m)
100
316
1000
3162
10,000
Resistivity (Ωm)

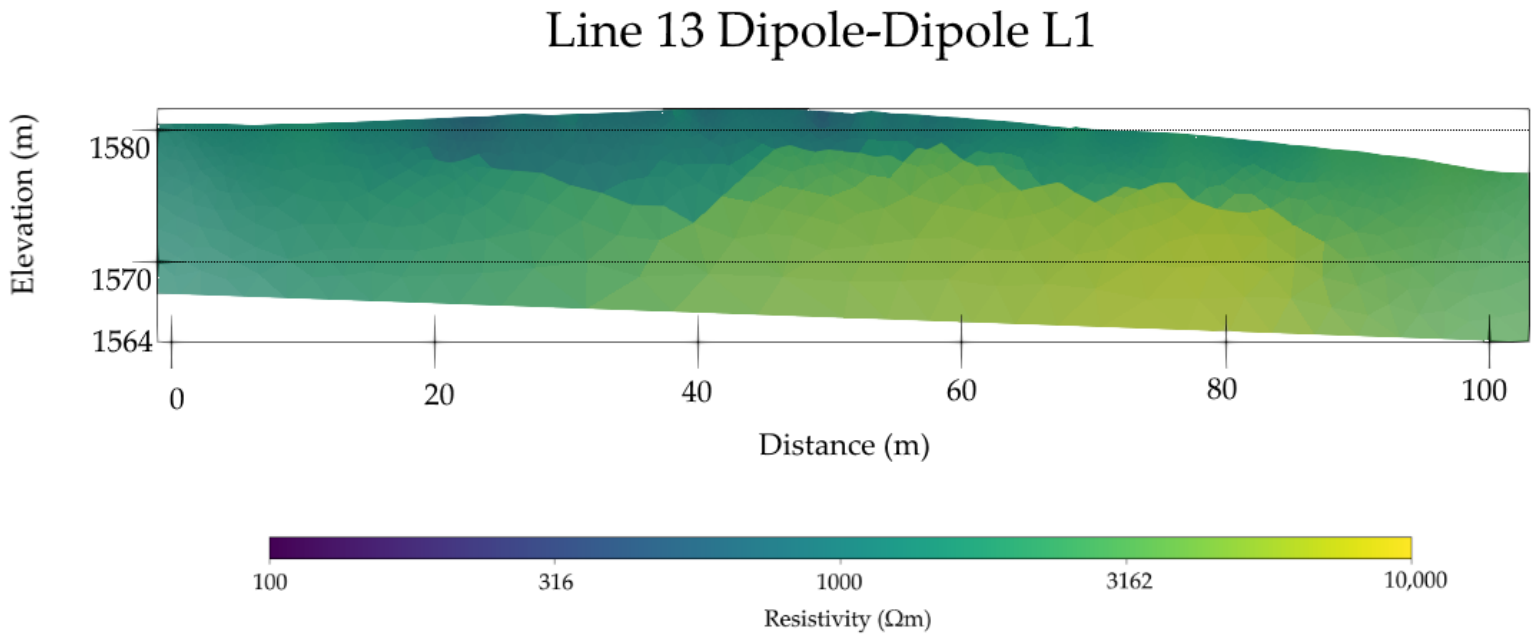
Line 13 Dipole-Dipole L1
Elevation (m)
1580
1570
1564
0
20
40
60
80
100
Distance (m)
100
316
1000
3162
10,000
Resistivity (Ωm)

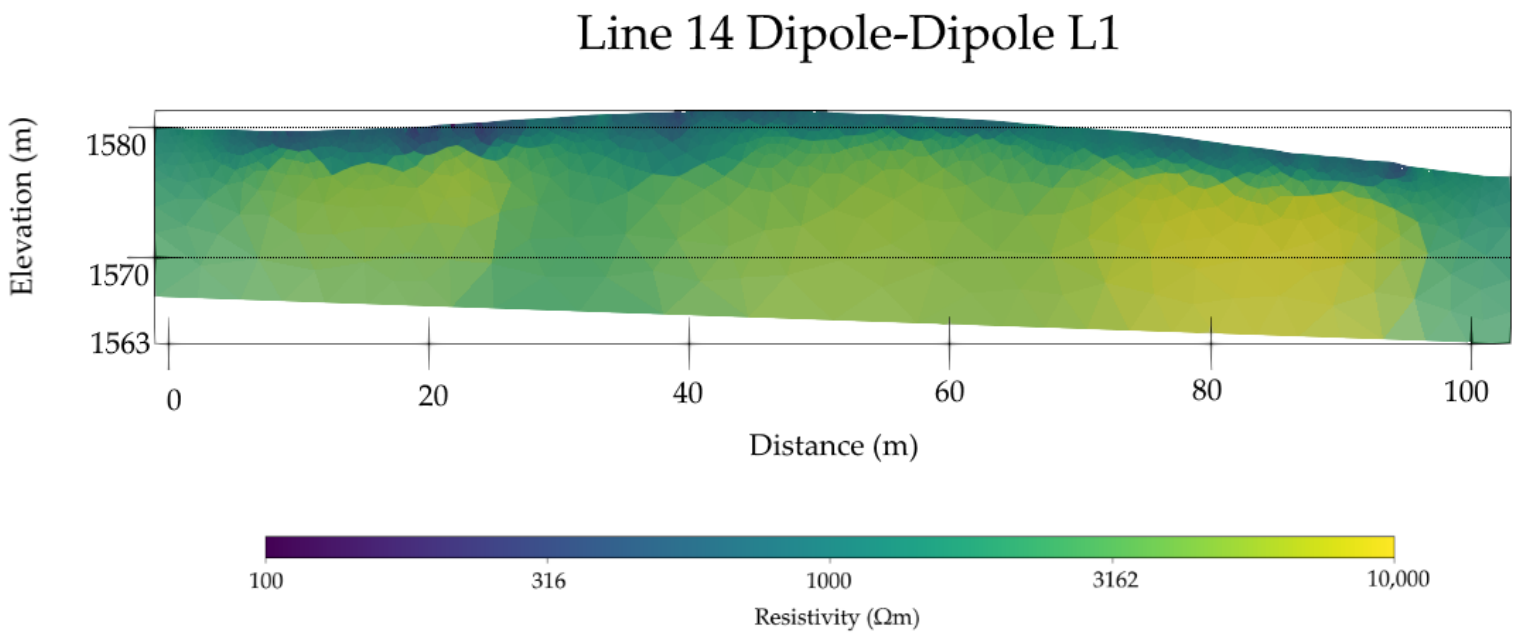
Line 14 Dipole-Dipole L1
Elevation (m)
1580
1570
1563
0
20
40
60
80
100
Distance (m)
100
316
1000
3162
10,000
Resistivity (Ωm)

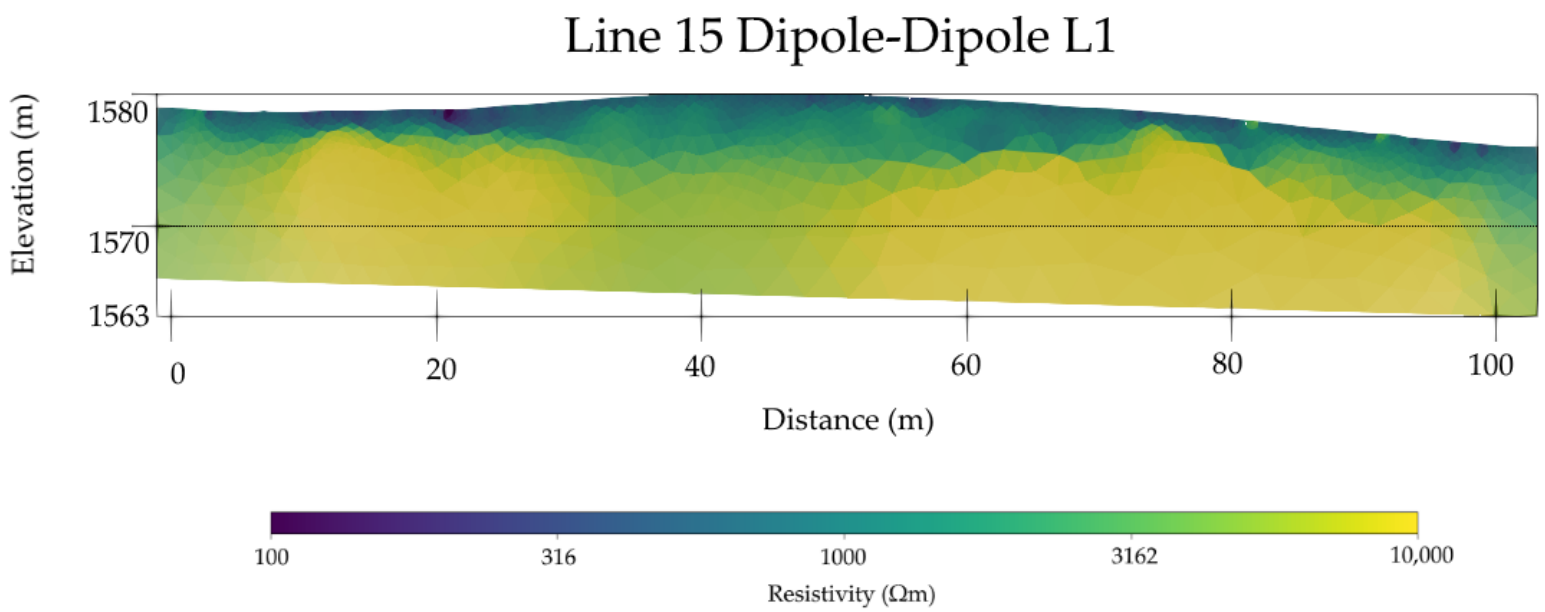
Line 15 Dipole-Dipole L1
Elevation (m)
1580
1570
1563
0
20
40
60
80
100
Distance (m)
100
316
1000
3162
10,000
Resistivity (Ωm)

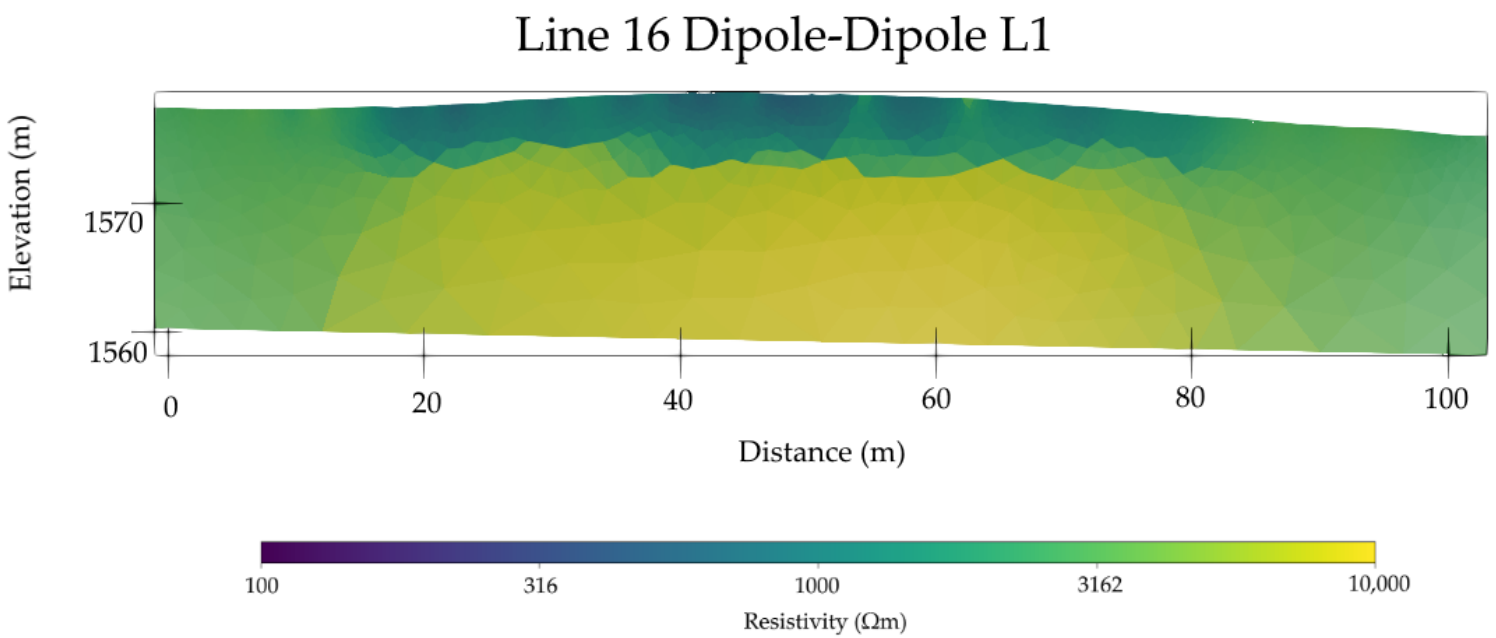
Line 16 Dipole-Dipole L1
Elevation (m)
1570
1560
0
20
40
60
80
100
Distance (m)
100
316
1000
3162
10,000
Resistivity (Ωm)

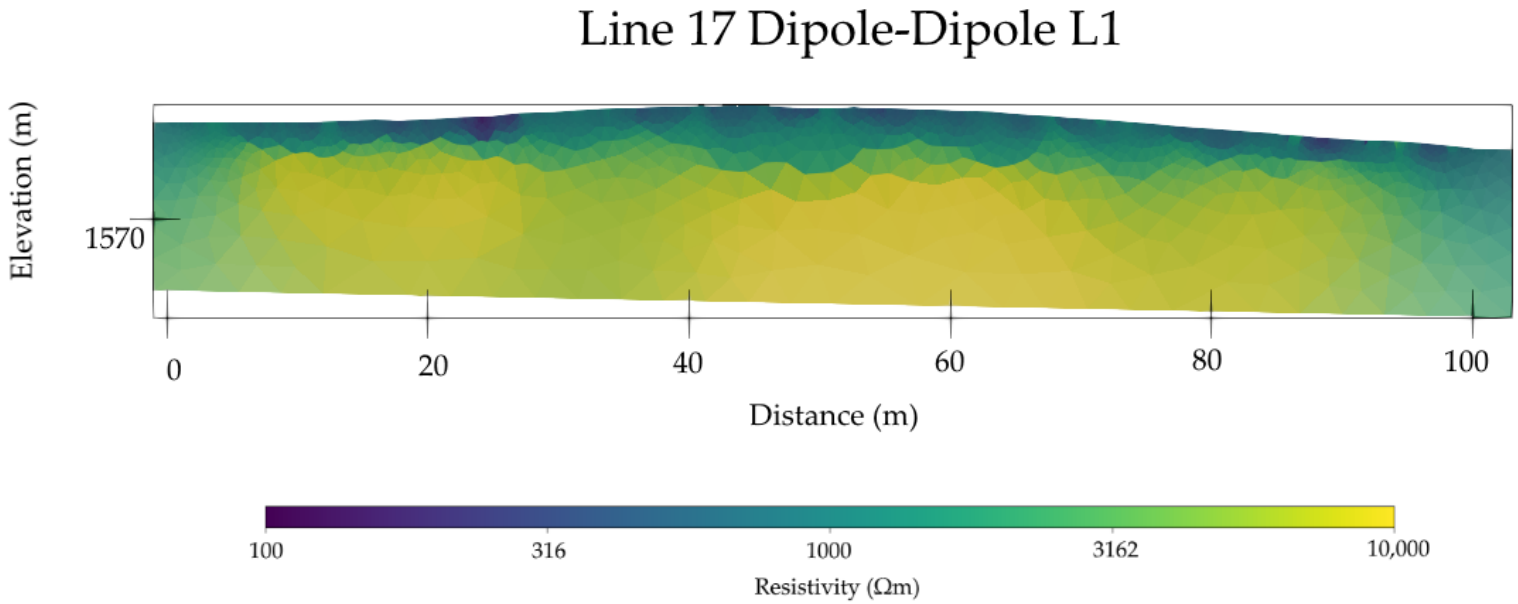
Line 17 Dipole-Dipole L1
Elevation (m)
1570
0
20
40
60
80
100
Distance (m)
100
316
1000
3162
10,000
Resistivity (Ωm)

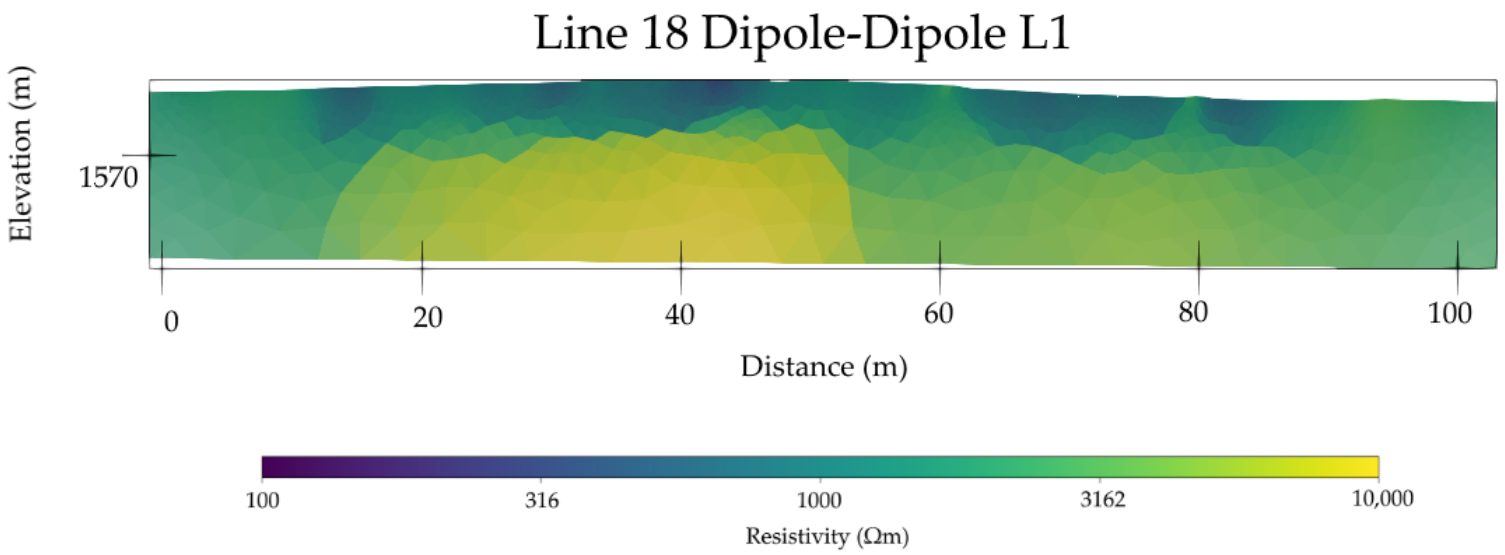
Line 18 Dipole-Dipole L1
Elevation (m)
1570
0
20
40
60
80
100
Distance (m)
100
316
1000
3162
10,000
Resistivity (Ωm)

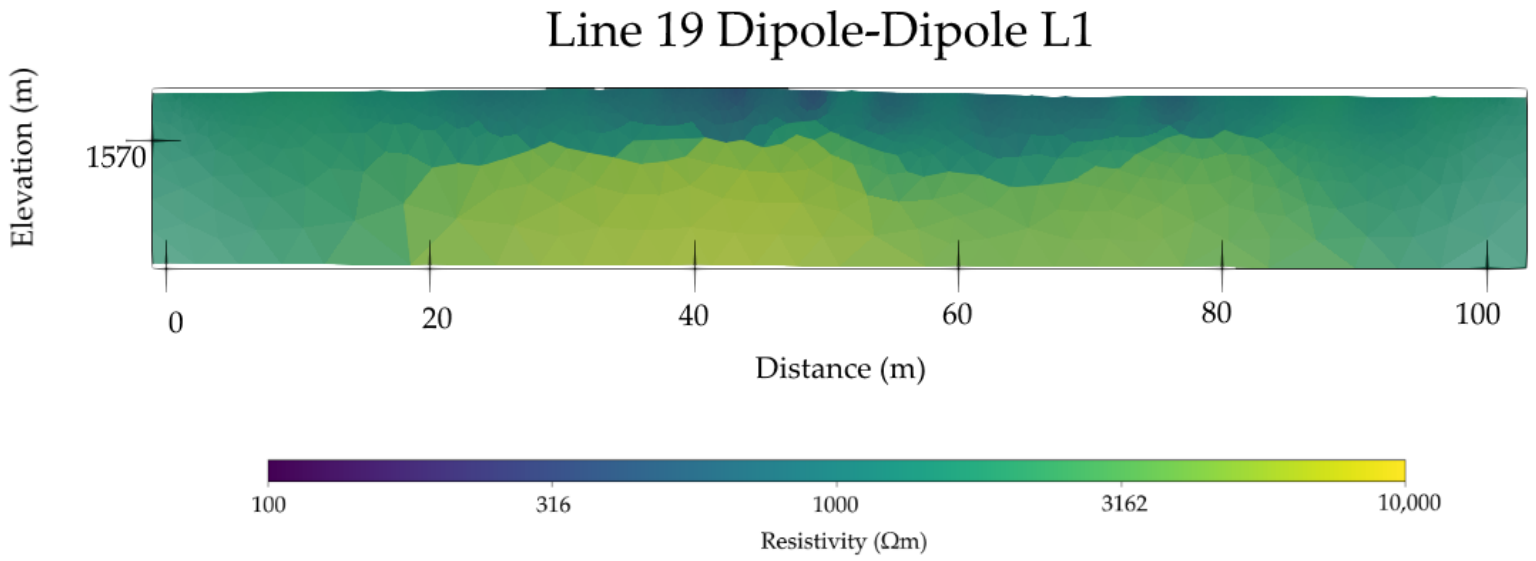
Line 19 Dipole-Dipole L1
Elevation (m)
1570
0
20
40
60
80
100
Distance (m)
100
316
1000
3162
10,000
Resistivity (Ωm)

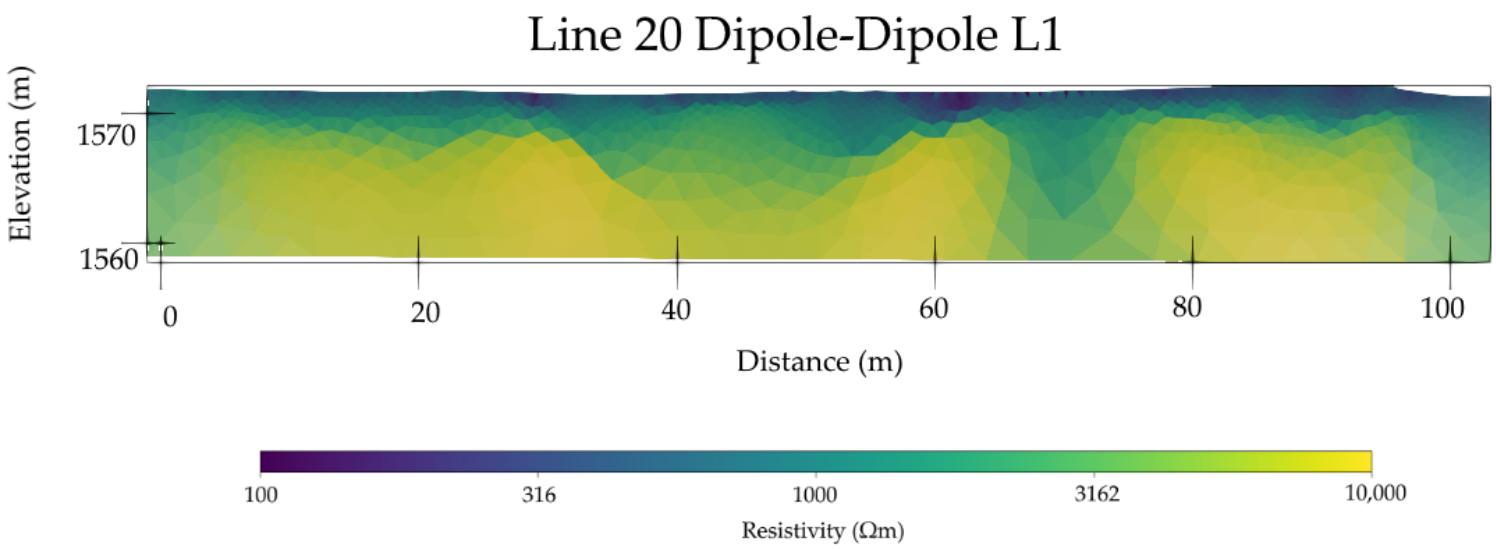
Line 20 Dipole-Dipole L1
Elevation (m)
1570
1560
0
20
40
60
80
100
Distance (m)
100
316
1000
3162
10,000
Resistivity (Ωm)

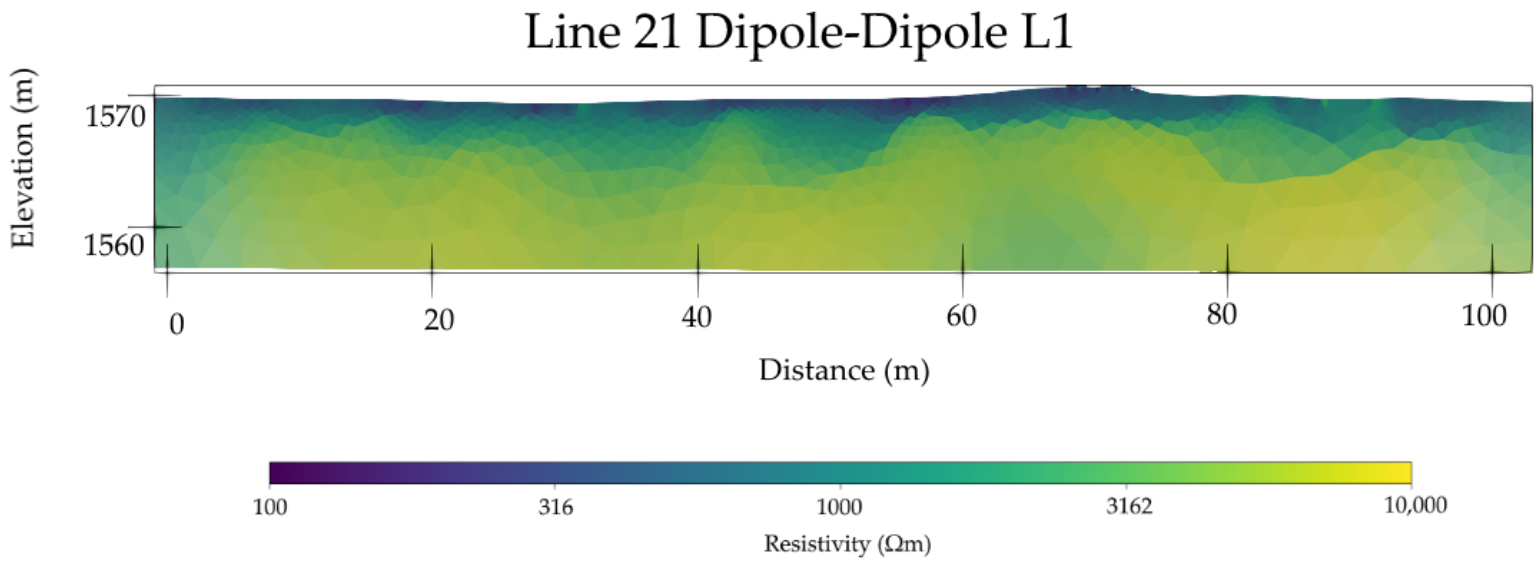
Line 21 Dipole-Dipole L1
Elevation (m)
1570
1560
0
20
40
60
80
100
Distance (m)
100
316
1000
3162
10,000
Resistivity (Ωm)

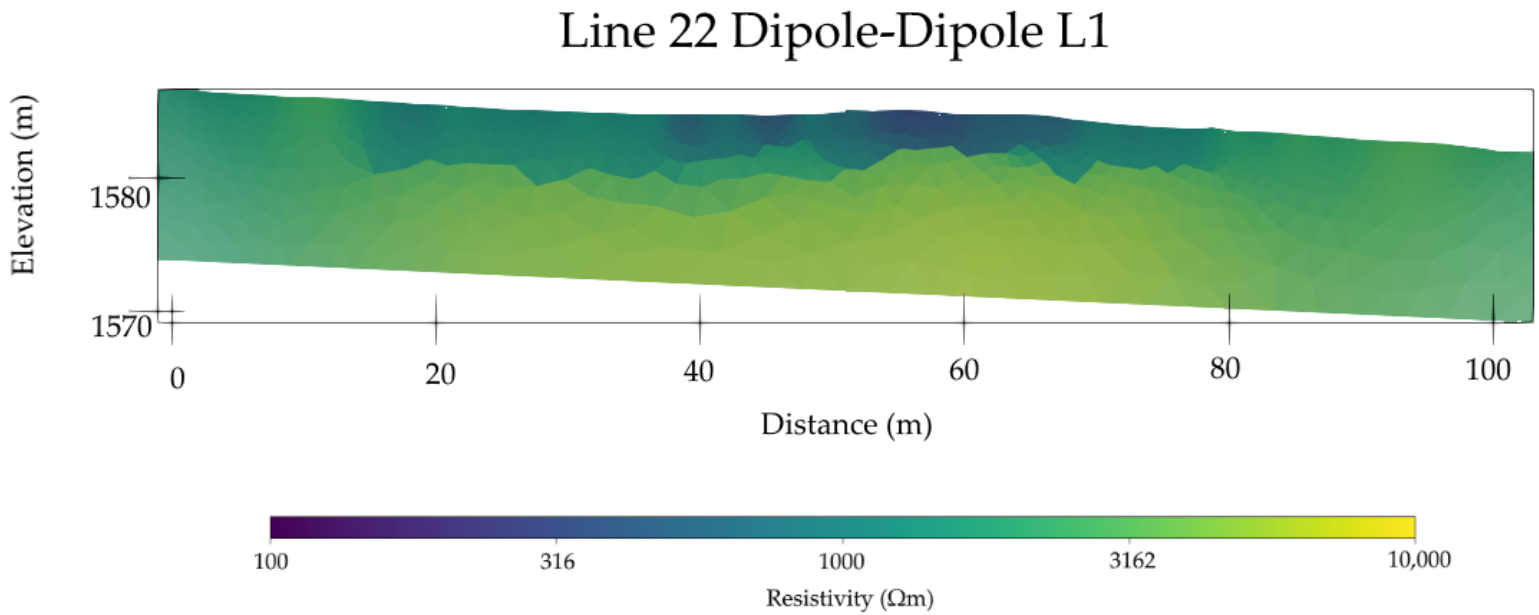
Line 22 Dipole-Dipole L1
Elevation (m)
1580
1570
0
20
40
60
80
100
Distance (m)
100
316
1000
3162
10,000
Resistivity (Ωm)

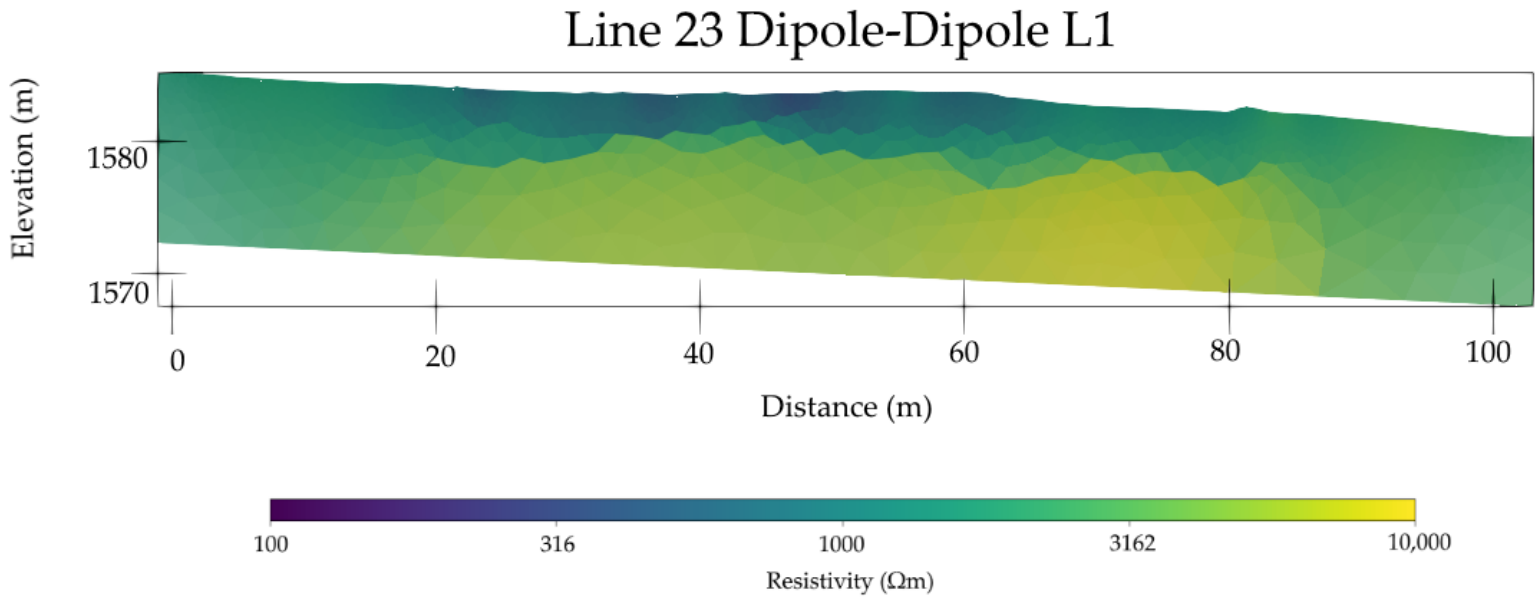
Line 23 Dipole-Dipole L1
Elevation (m)
1580
1570
0
20
40
60
80
100
Distance (m)
100
316
1000
3162
10,000
Resistivity (Ωm)

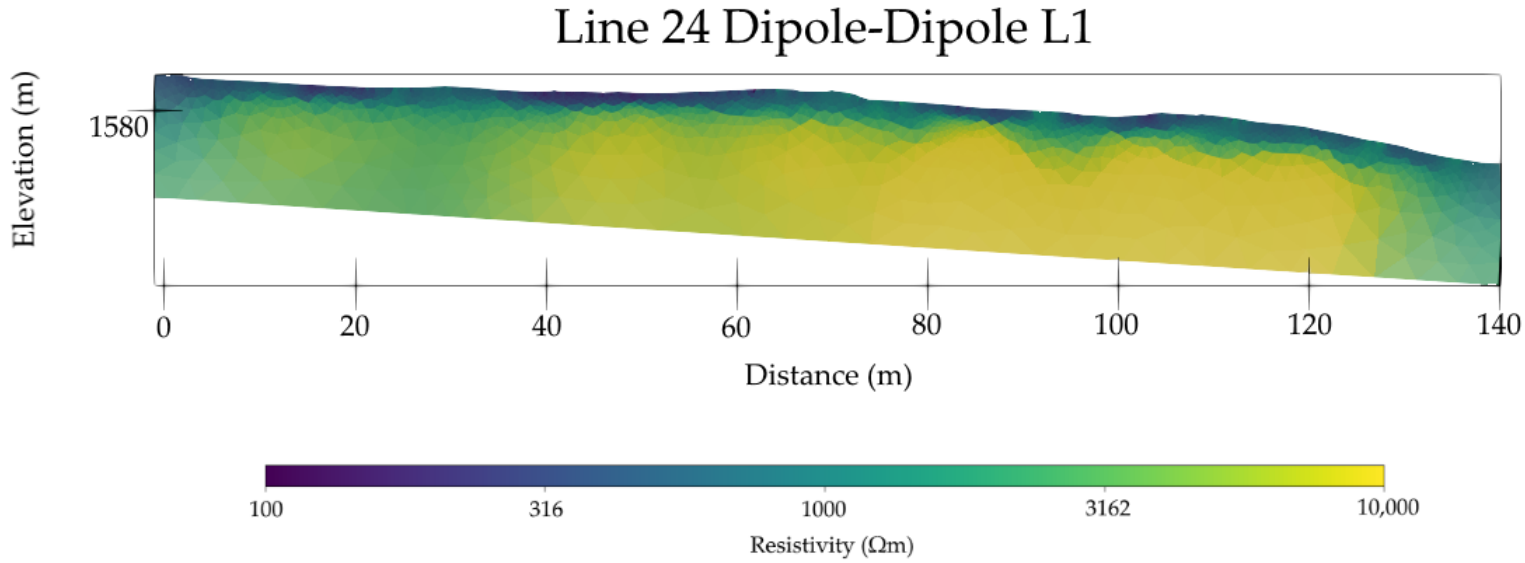
Line 24 Dipole-Dipole L1
Elevation (m)
1580
0
20
40
60
80
100
120
140
Distance (m)
100
316
1000
3162
10,000
Resistivity (Ωm)

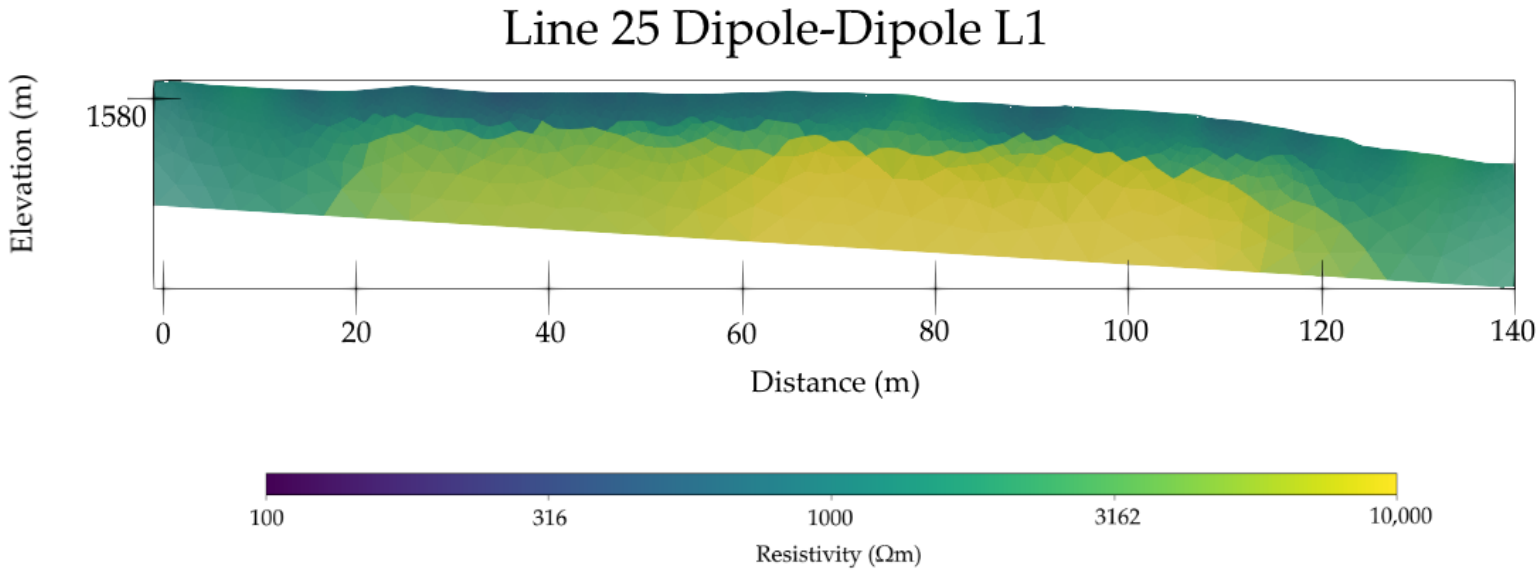
Line 25 Dipole-Dipole L1
Elevation (m)
1580
0
20
40
60
80
100
120
140
Distance (m)
100
316
1000
3162
10,000
Resistivity (Ωm)

Appendix B

Examples of Picked GPR Profiles

GPR Line A85

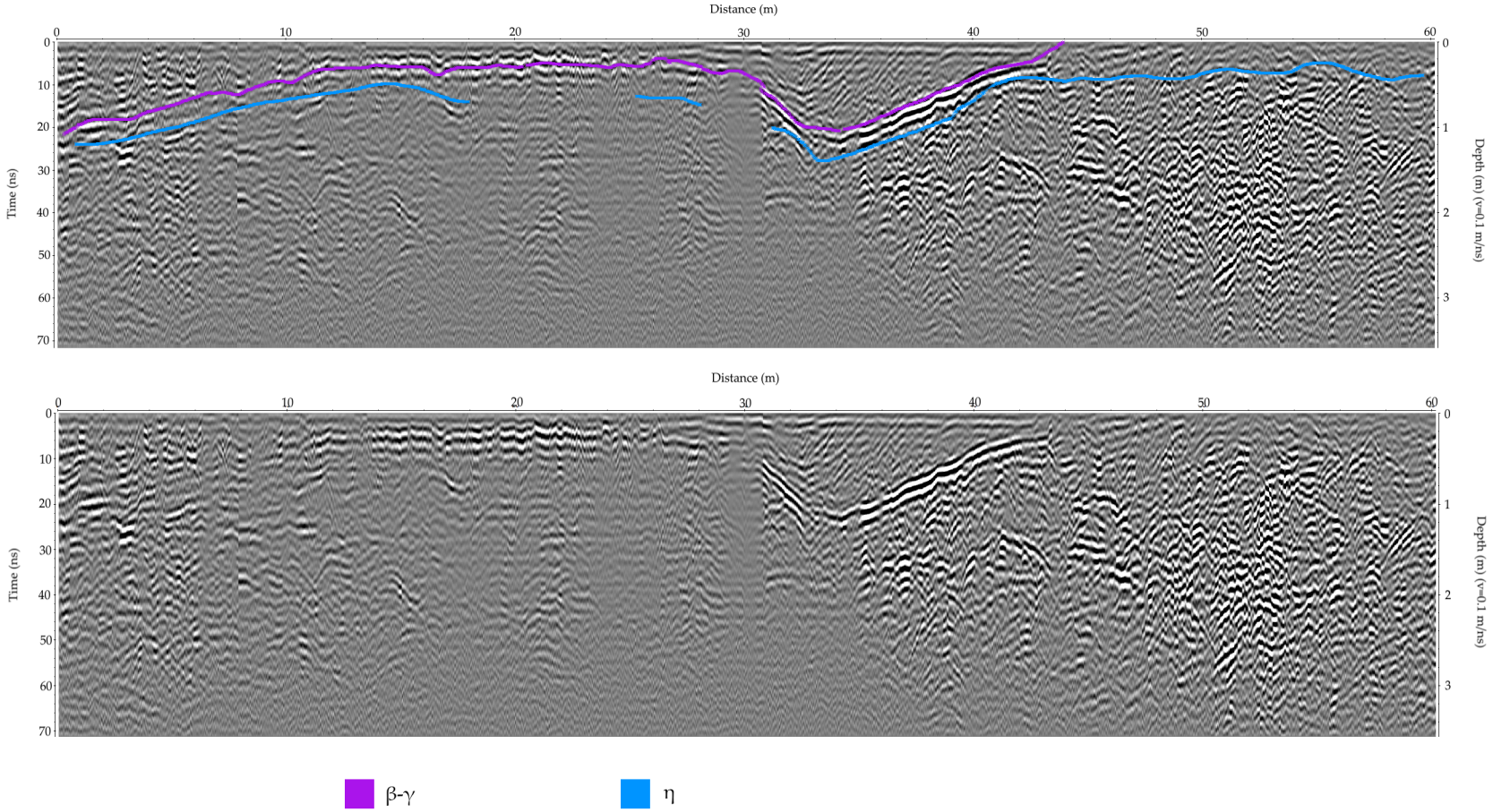
Distance (m)
0
10
20
30
40
50
60
Time (ns)
0
10
20
30
40
50
60
70
Depth (m) (v=0.1 m/ns)
0
1
2
3
Distance (m)
Time (ns)
Depth (m) (v=0.1 m/ns)
β-γ
η

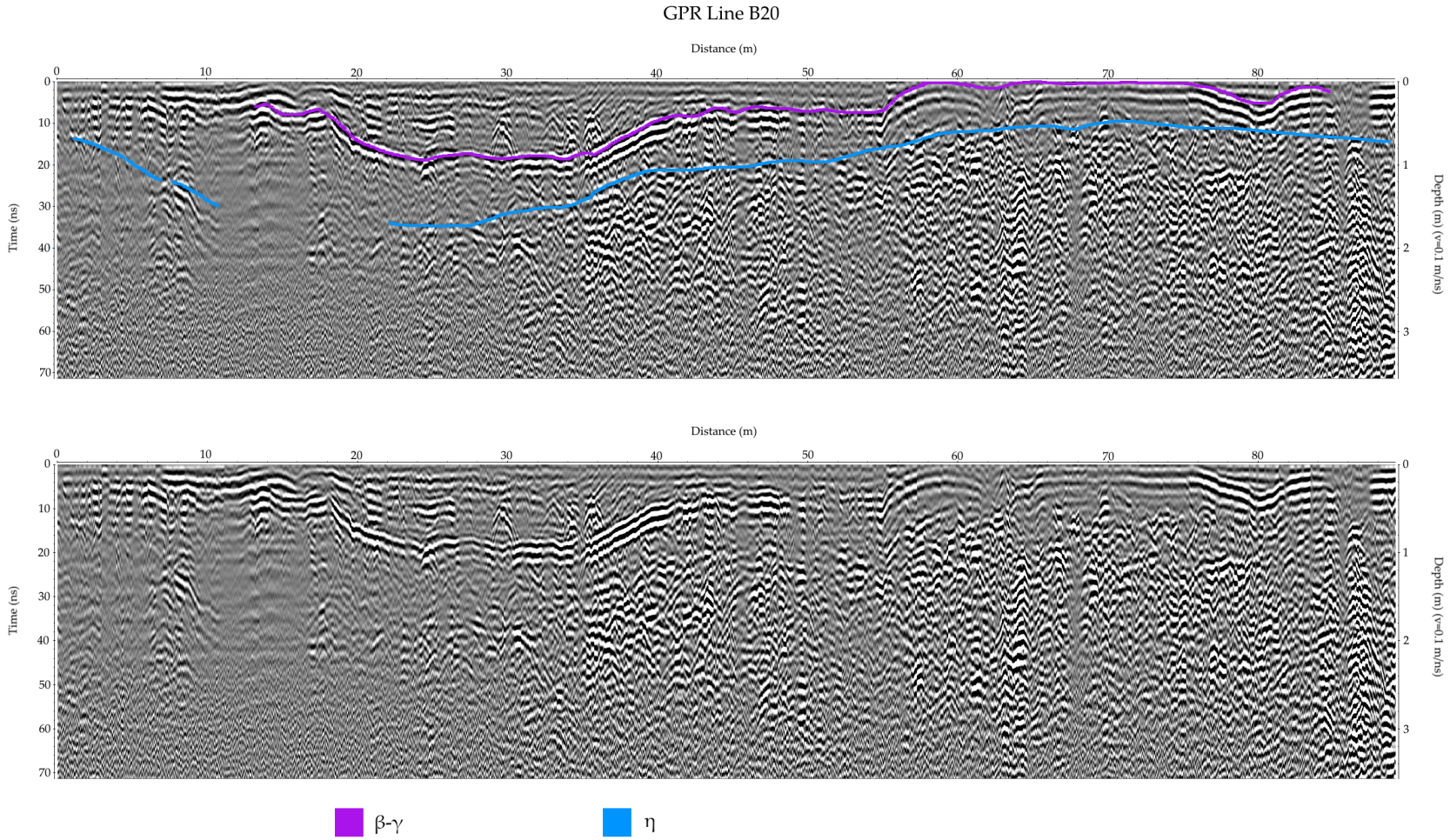
GPR Line B20
Distance (m)
0
10
20
30
40
50
60
70
80
Time (ns)
0
10
20
30
40
50
60
70
Depth (m) (v=0.1 m/ns)
0
1
2
3
Distance (m)
Time (ns)
Depth (m) (v=0.1 m/ns)
β-γ
η

GPR Line B81

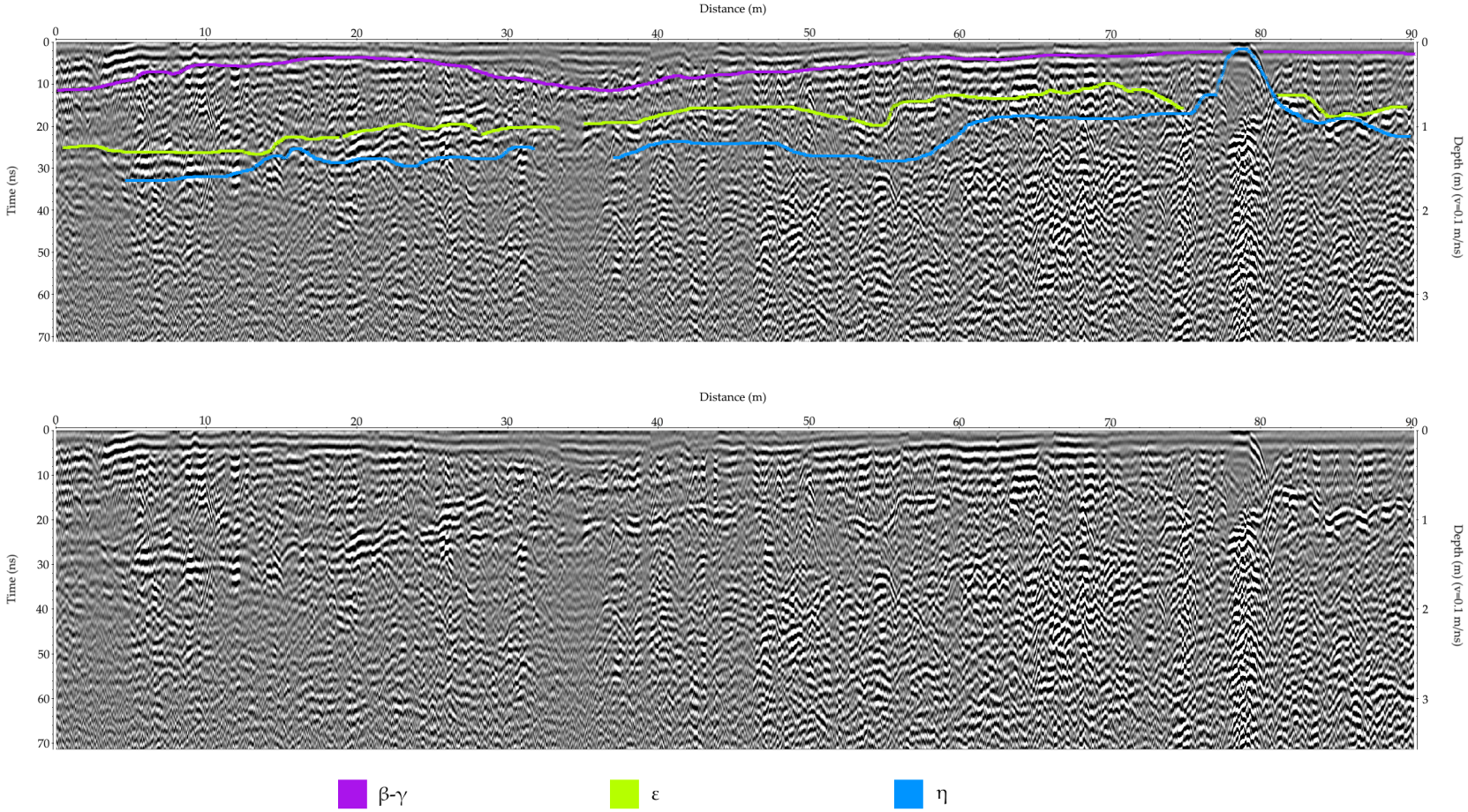
Distance (m)
0
10
20
30
40
50
60
70
80
90
Time (ns)
0
10
20
30
40
50
60
70
Depth (m) (v=0.1 m/ns)
0
1
2
3
Distance (m)
Time (ns)
Depth (m) (v=0.1 m/ns)
β-γ
ε
η

GPR Line B105

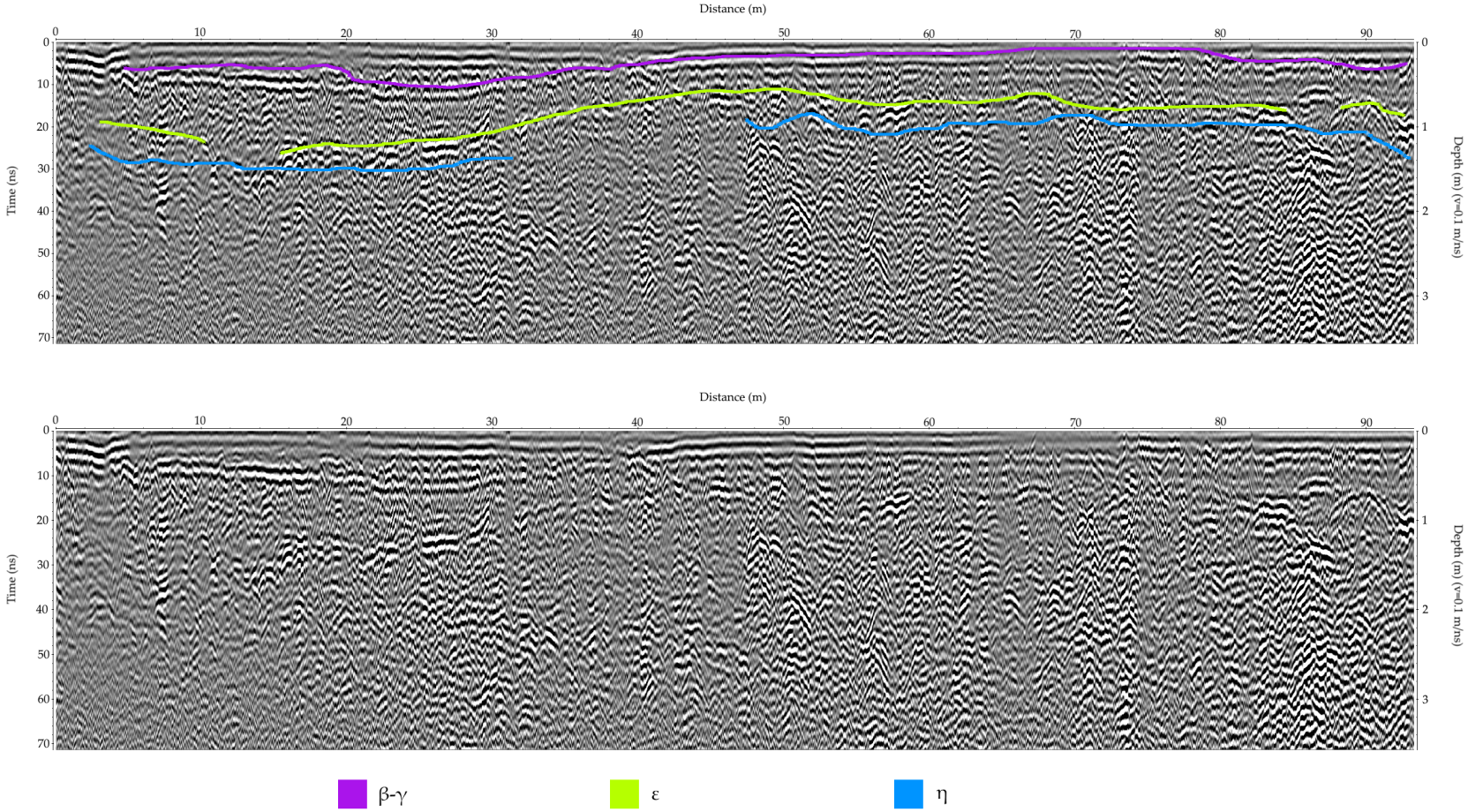

GPR Line B110

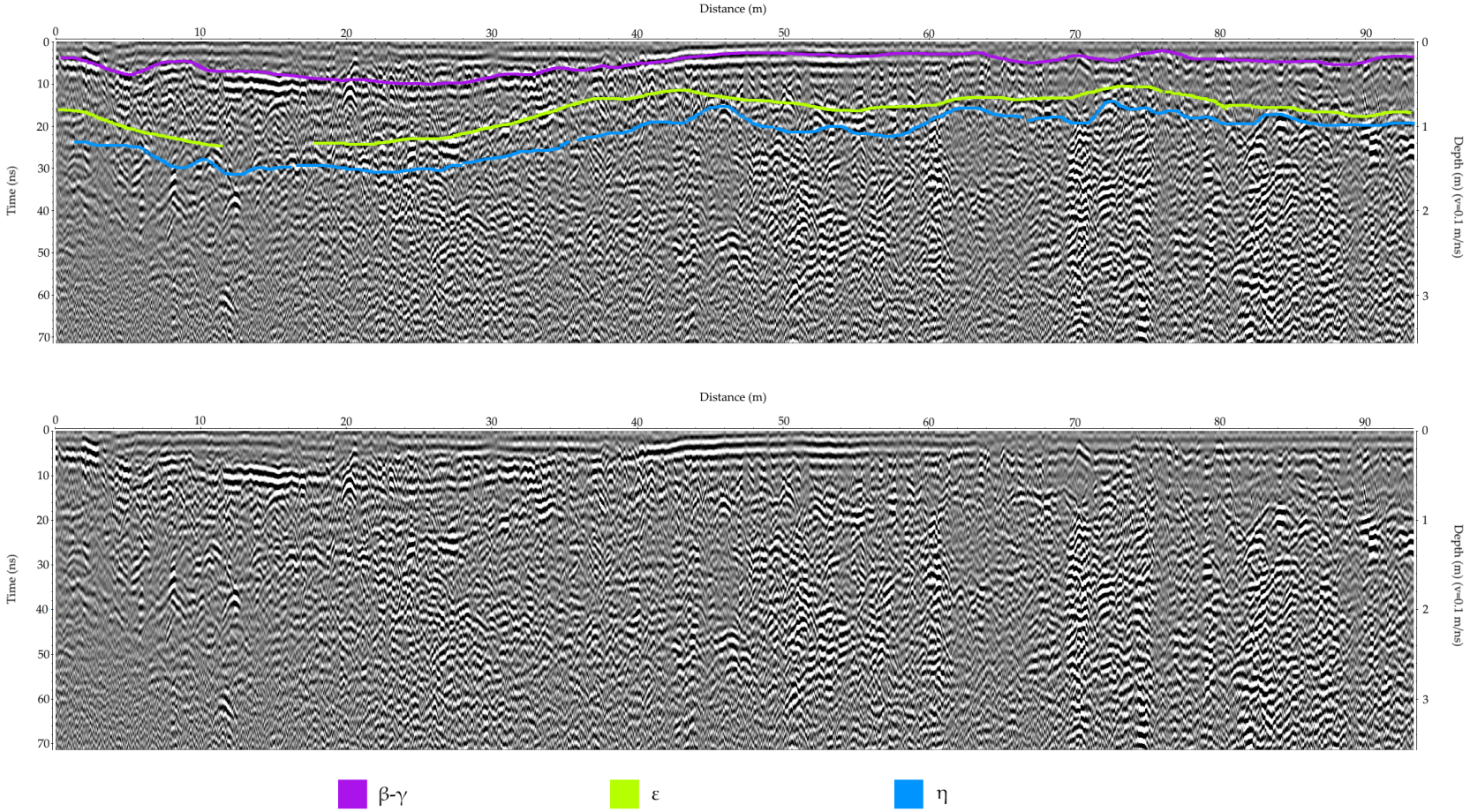

GPR Line C10

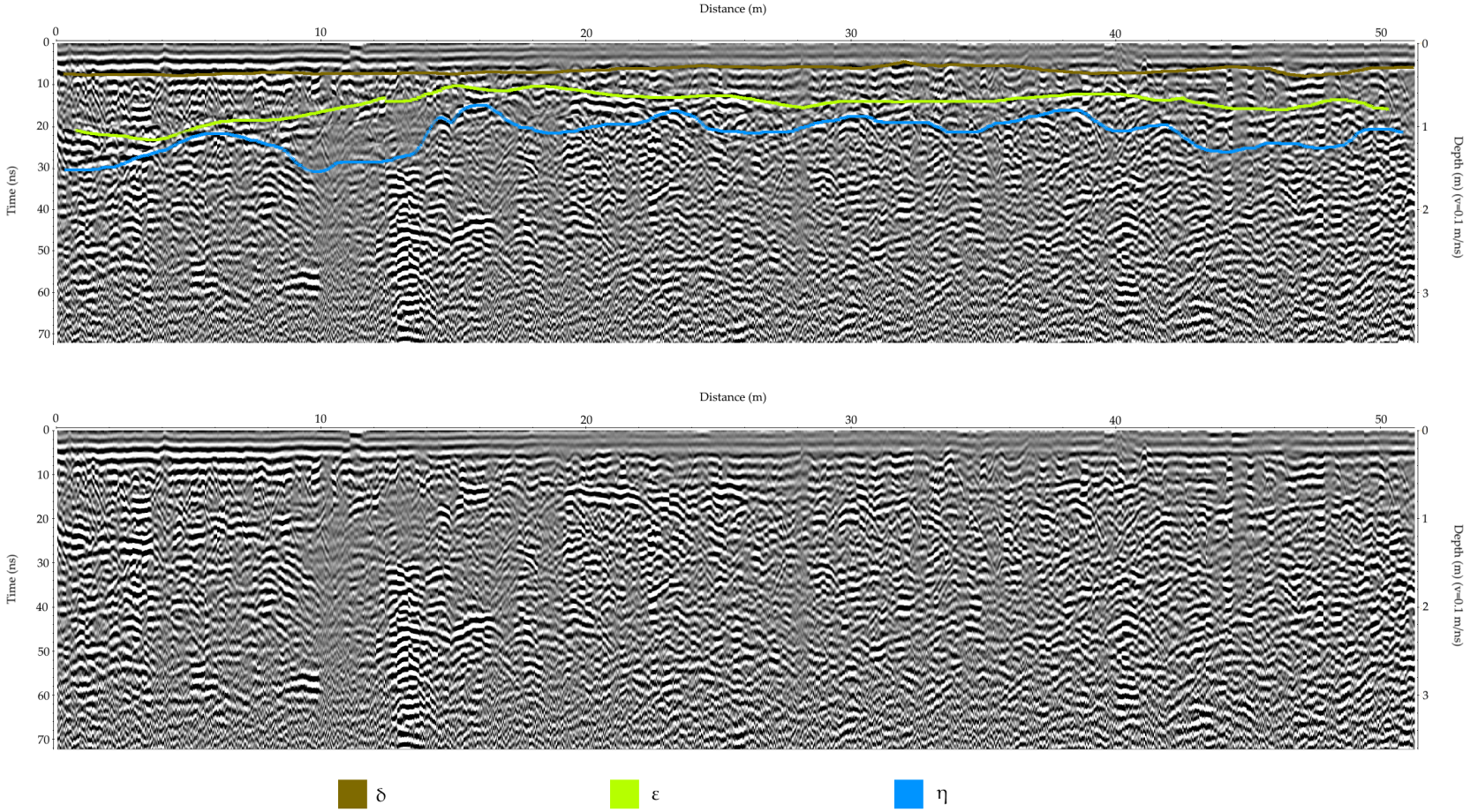
Distance (m)
0
10
20
30
40
50
Time (ns)
0
10
20
30
40
50
60
70
Depth (m) (v=0.1 m/ns)
0
1
2
3
Distance (m)
Time (ns)
Depth (m) (v=0.1 m/ns)
δ
ε
η

GPR Line C60

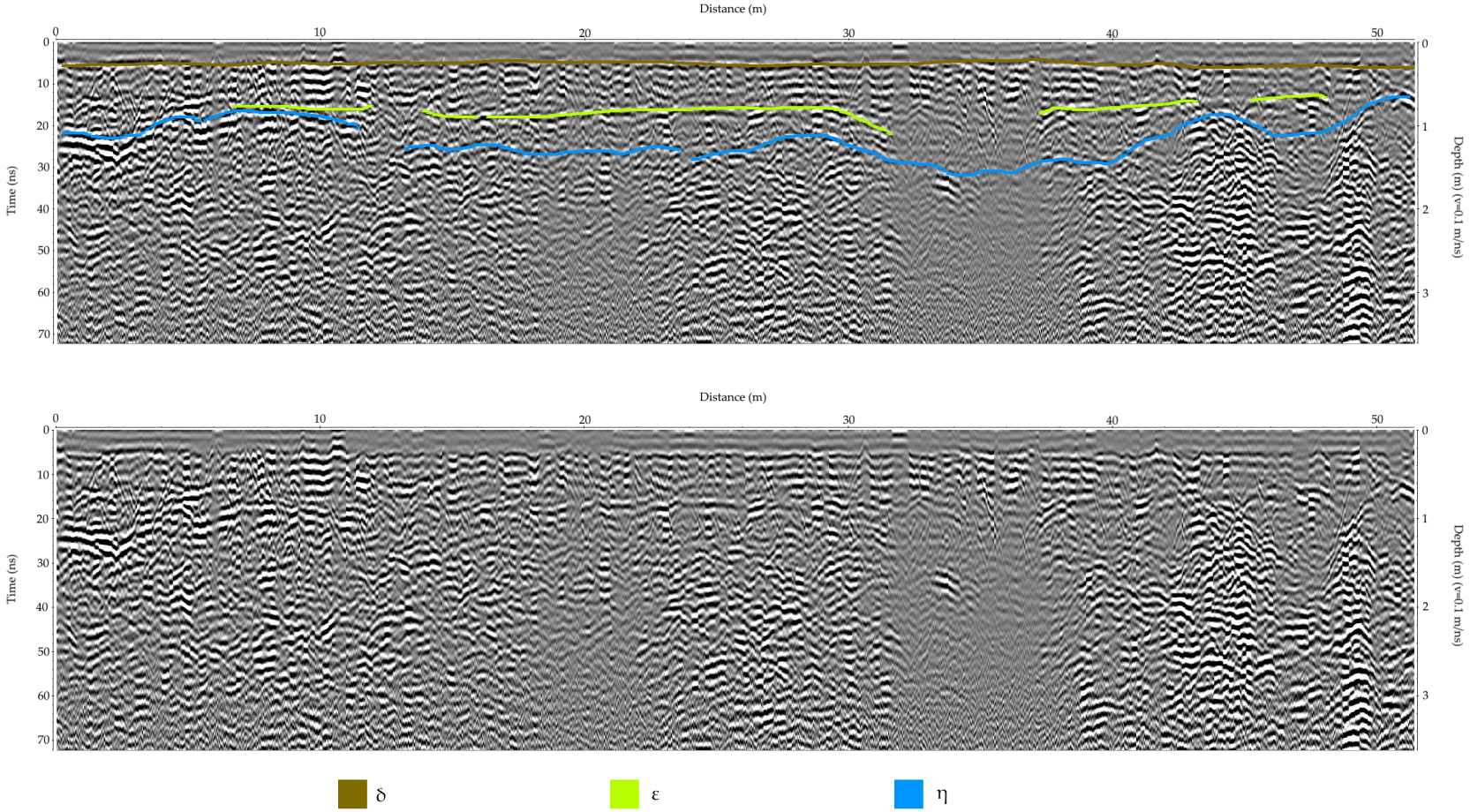
Distance (m)
0
10
20
30
40
50
Time (ns)
0
10
20
30
40
50
60
70
Depth (m) (v=0.1 m/ns)
0
1
2
3
Distance (m)
Time (ns)
Depth (m) (v=0.1 m/ns)
δ
ε
η

GPR Line C70

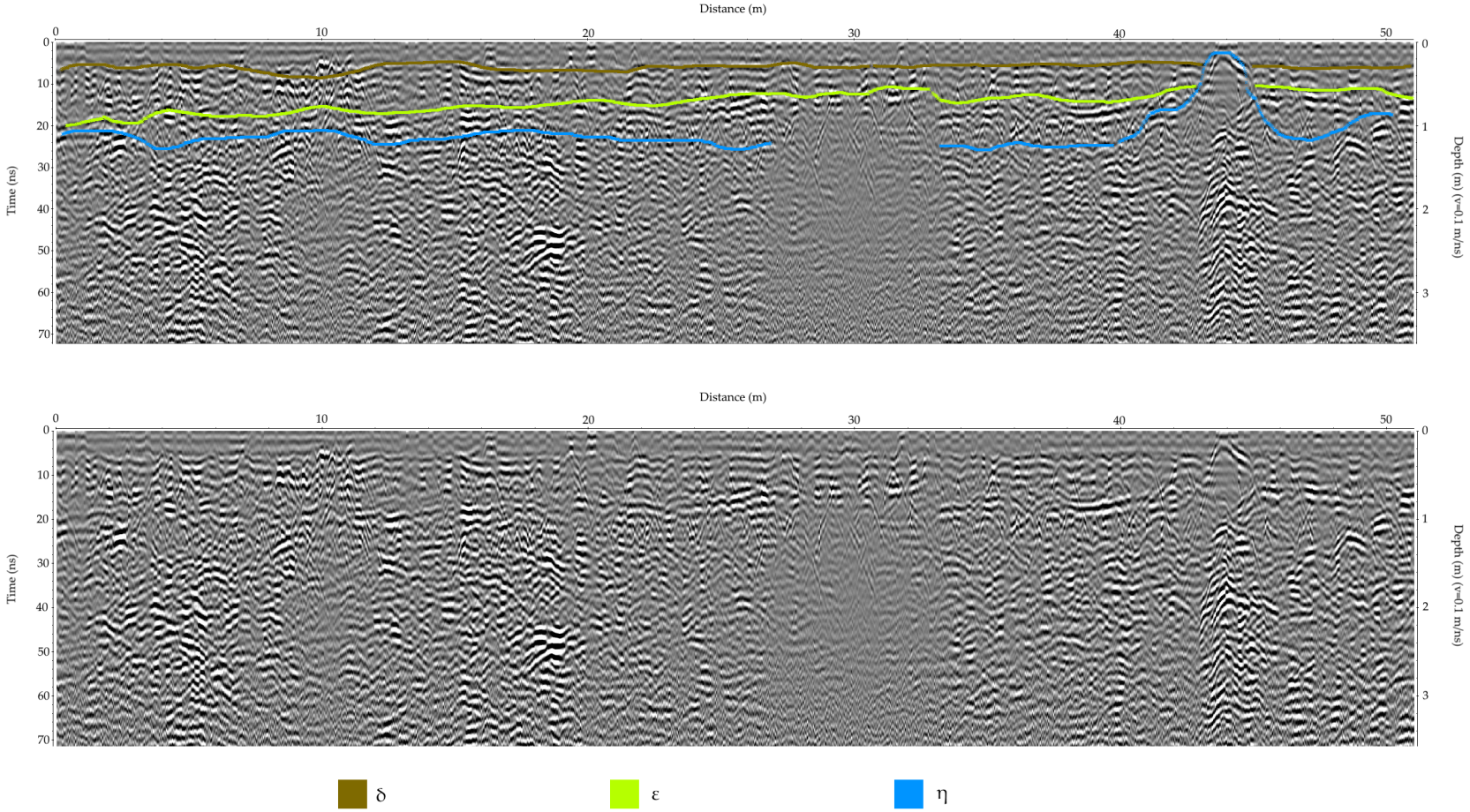
Distance (m)
0
10
20
30
40
50
Time (ns)
0
10
20
30
40
50
60
70
Depth (m) (v=0.1 m/ns)
0
1
2
3
Distance (m)
Time (ns)
Depth (m) (v=0.1 m/ns)
δ
ε
η

GPR Line C150

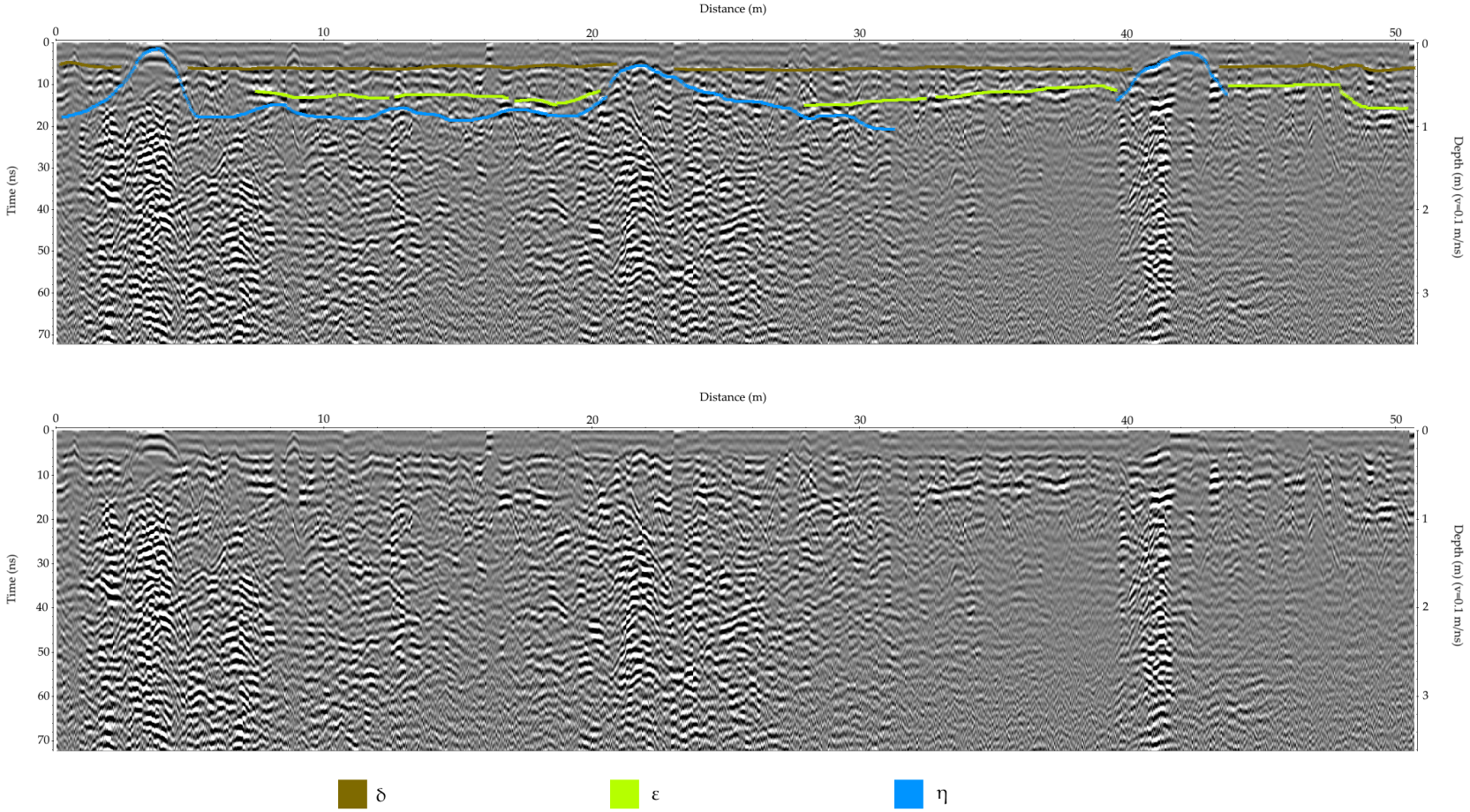

Appendix C

Sediment Result Plots

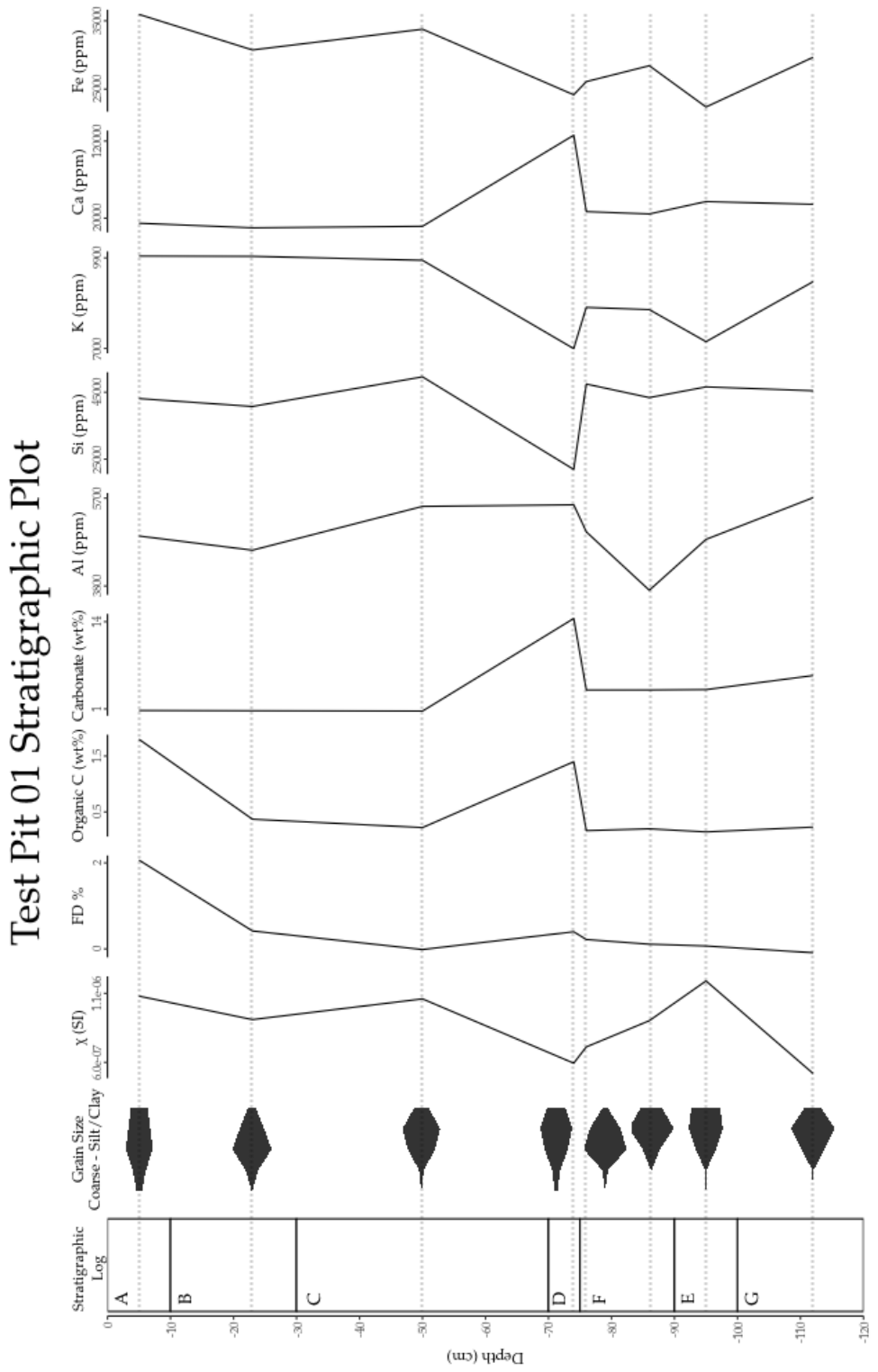

Figure C.1: Stratigraphic plot showing sediment analysis results for test pit 01.

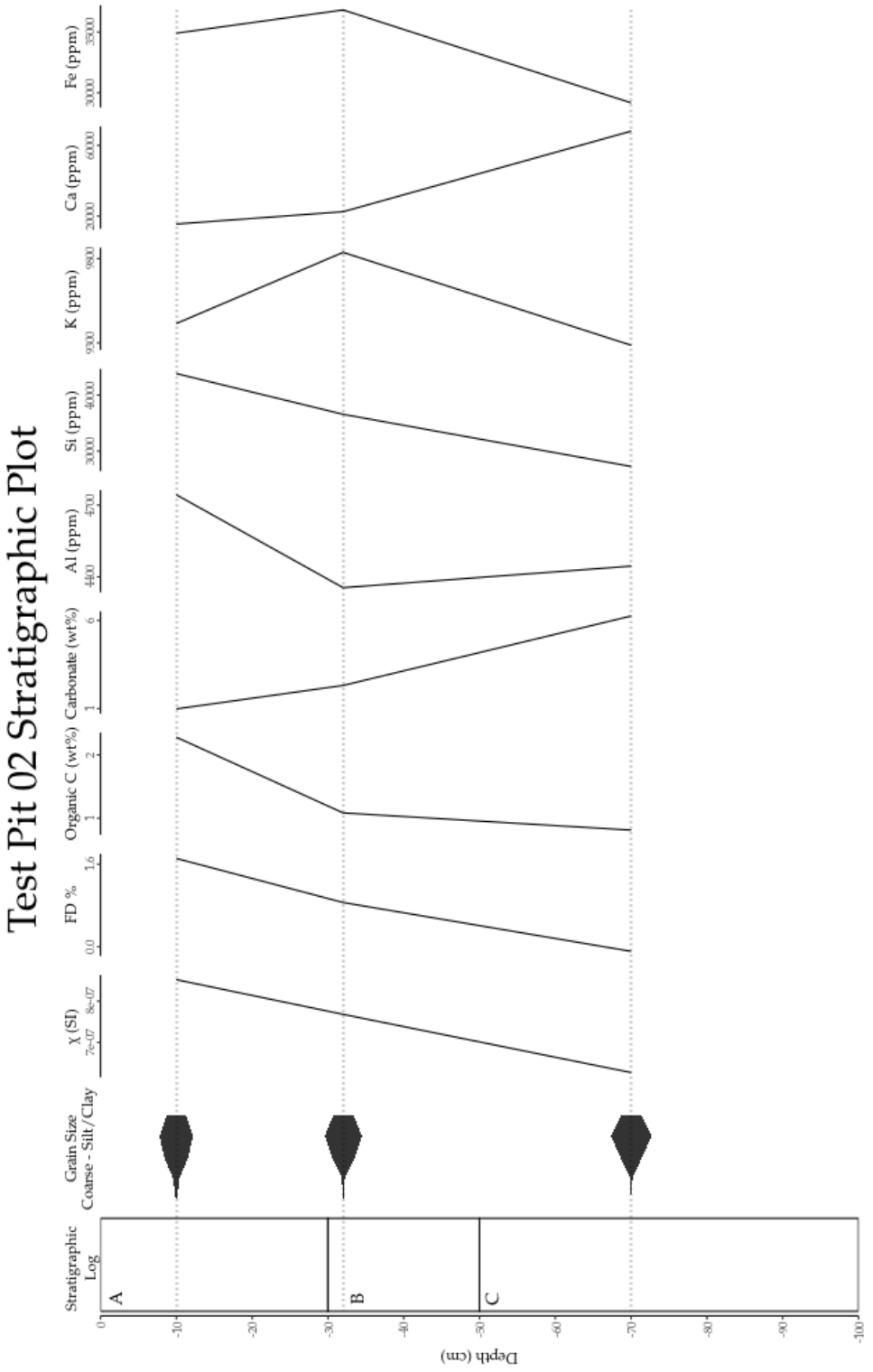

Figure C.2: Stratigraphic plot showing sediment analysis results for test pit 02.

Figure C.3: Stratigraphic plot showing sediment analysis results for test pit 03.

Figure C.4: Stratigraphic plot showing sediment analysis results for test pit 05.

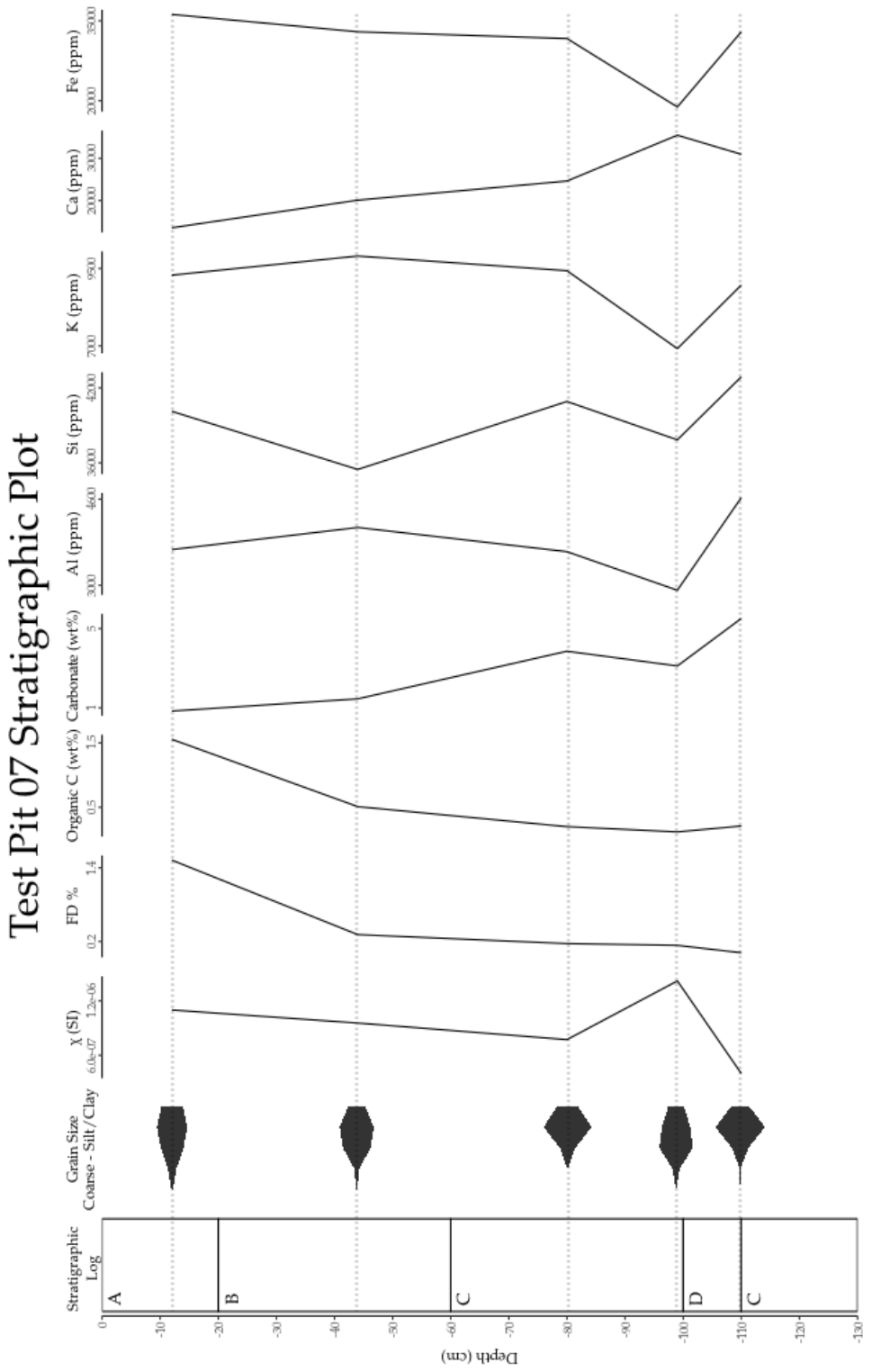

Figure C.5: Stratigraphic plot showing sediment analysis results for test pit 07.

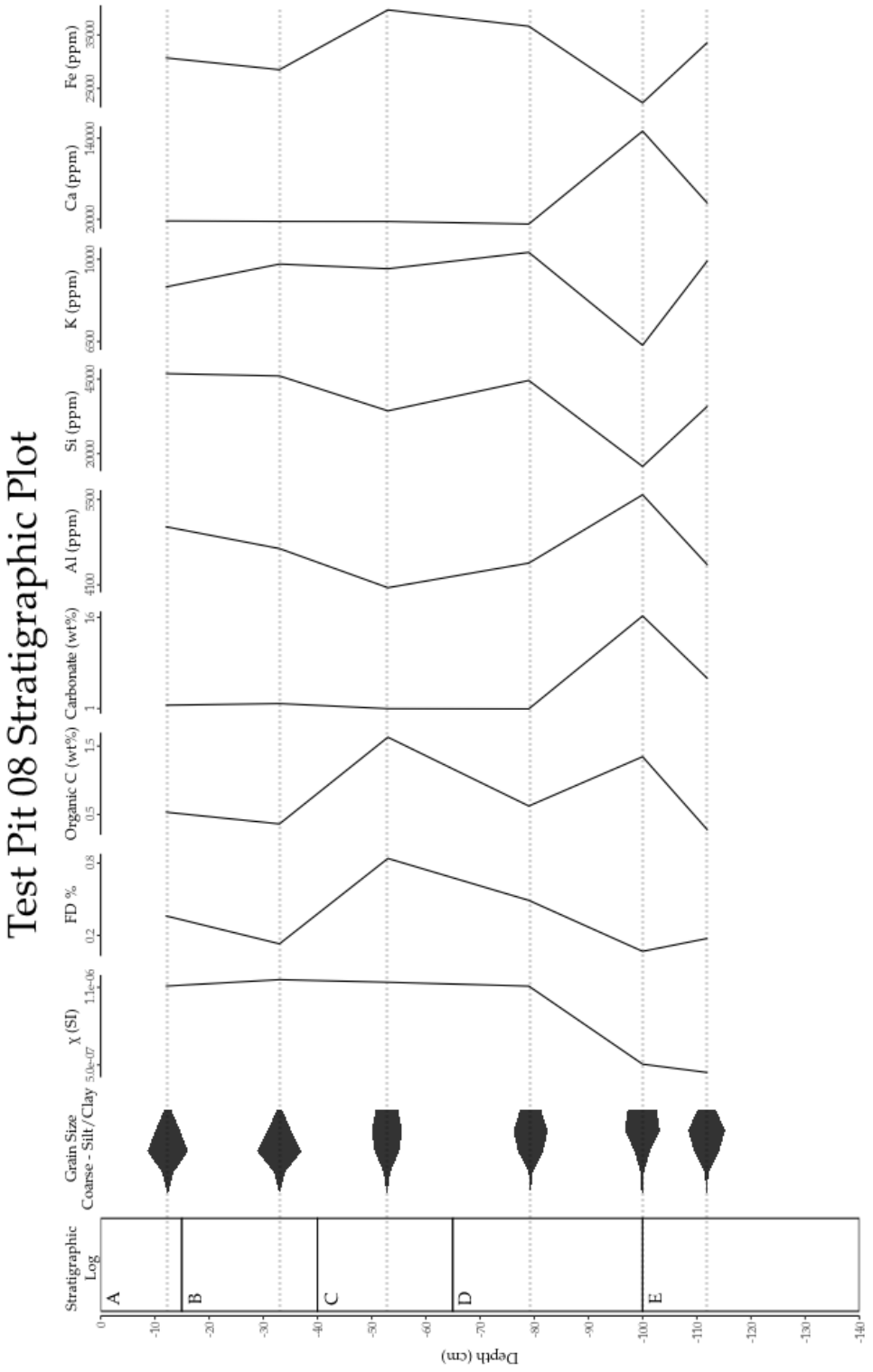

Figure C.6: Stratigraphic plot showing sediment analysis results for test pit 08.

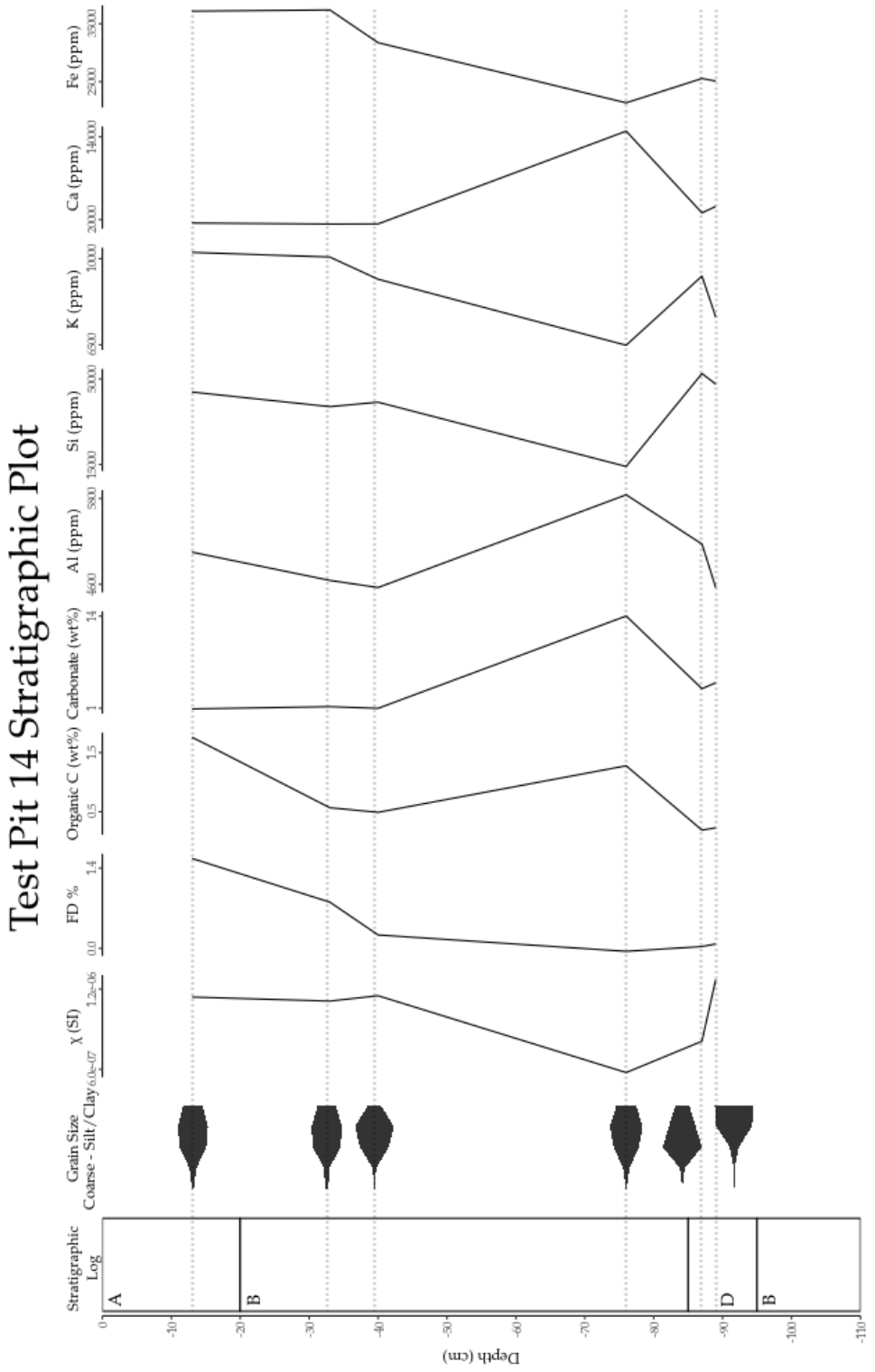

Figure C.7: Stratigraphic plot showing sediment analysis results for test pit 14.

Appendix D

ERT Profiles with GPR Picks

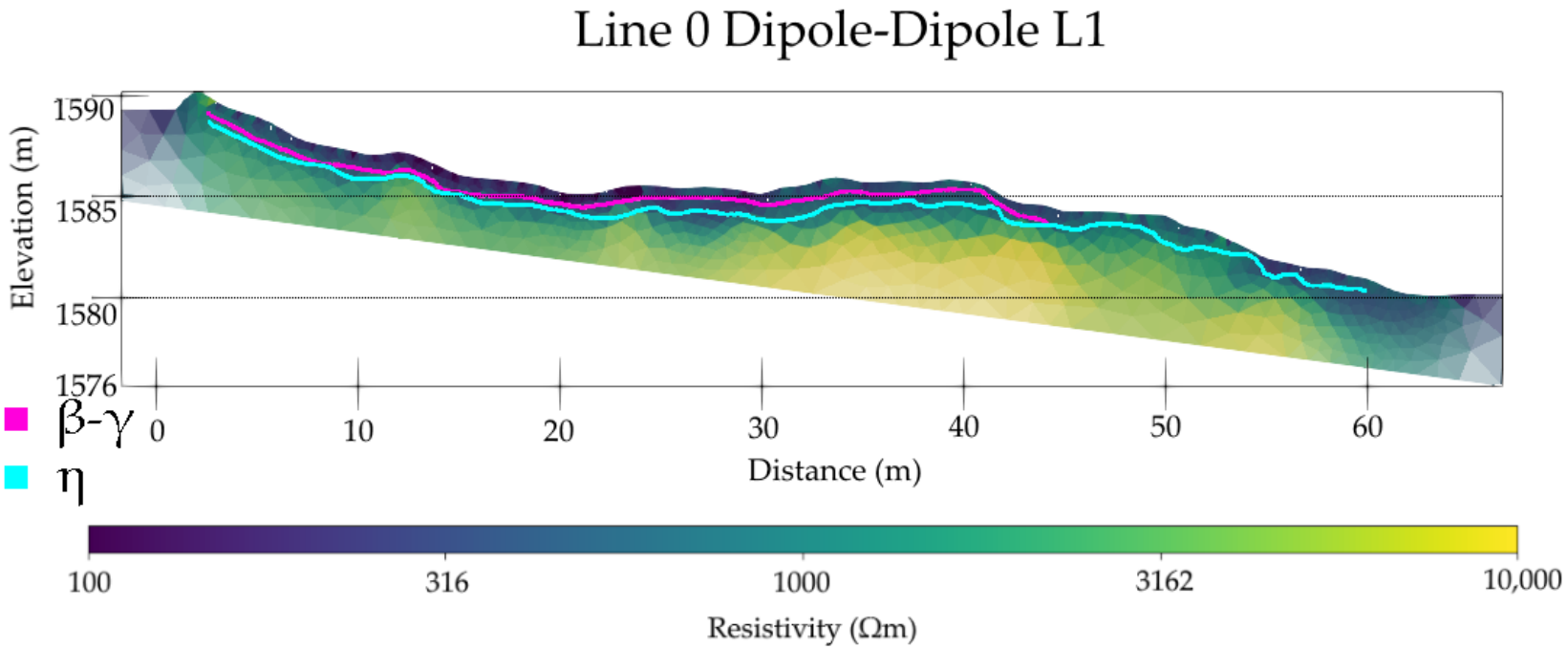
Line 0 Dipole-Dipole L1
Elevation (m)
1590
1585
1580
1576
β-γ
η
0
10
20
30
40
50
60
Distance (m)
100
316
1000
3162
10,000
Resistivity (Ωm)

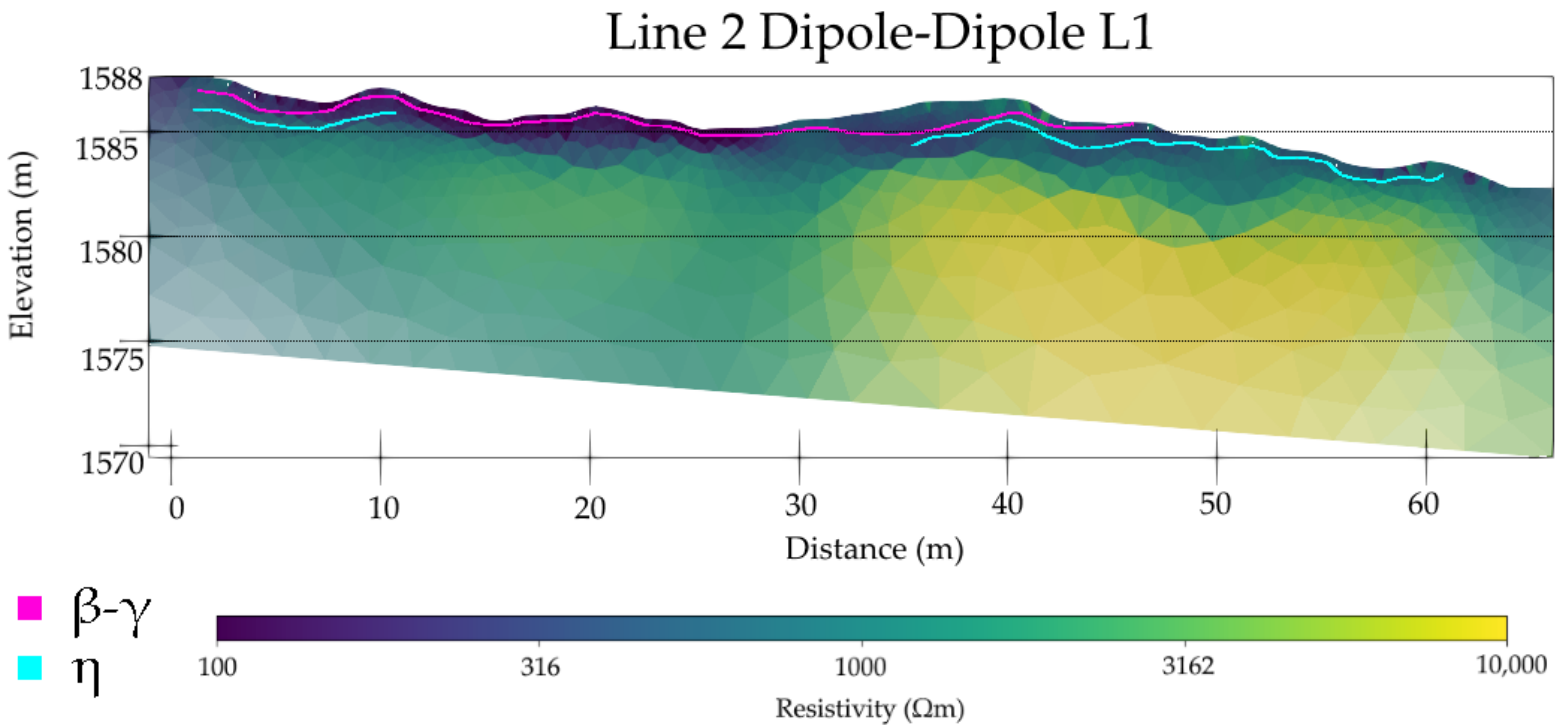
Line 2 Dipole-Dipole L1
Elevation (m)
1588
1585
1580
1575
1570
0
10
20
30
40
50
60
Distance (m)
β-γ
η
100
316
1000
3162
10,000
Resistivity (Ωm)

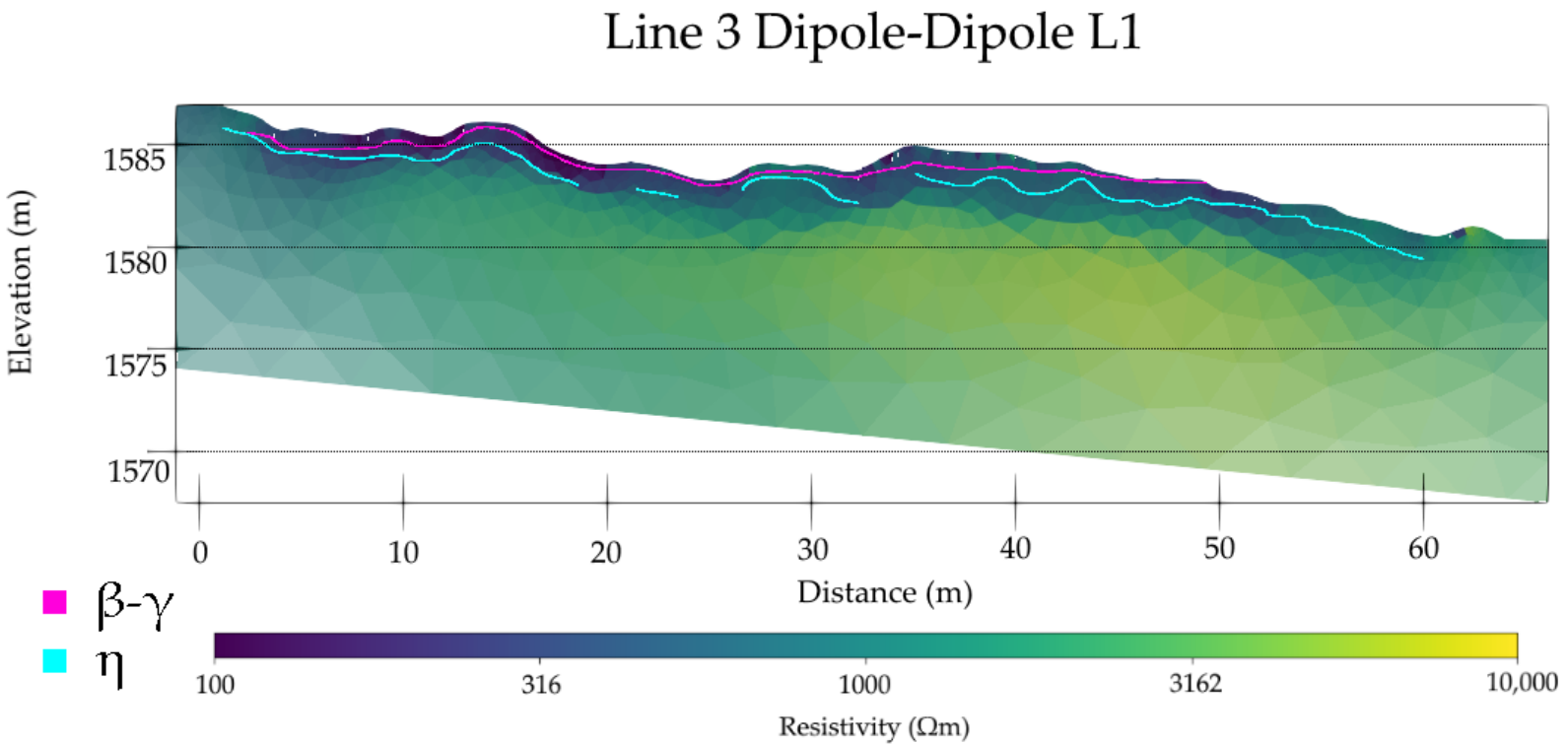
Line 3 Dipole-Dipole L1
Elevation (m)
1585
1580
1575
1570
0
10
20
30
40
50
60
Distance (m)
β-γ
η
100
316
1000
3162
10,000
Resistivity (Ωm)

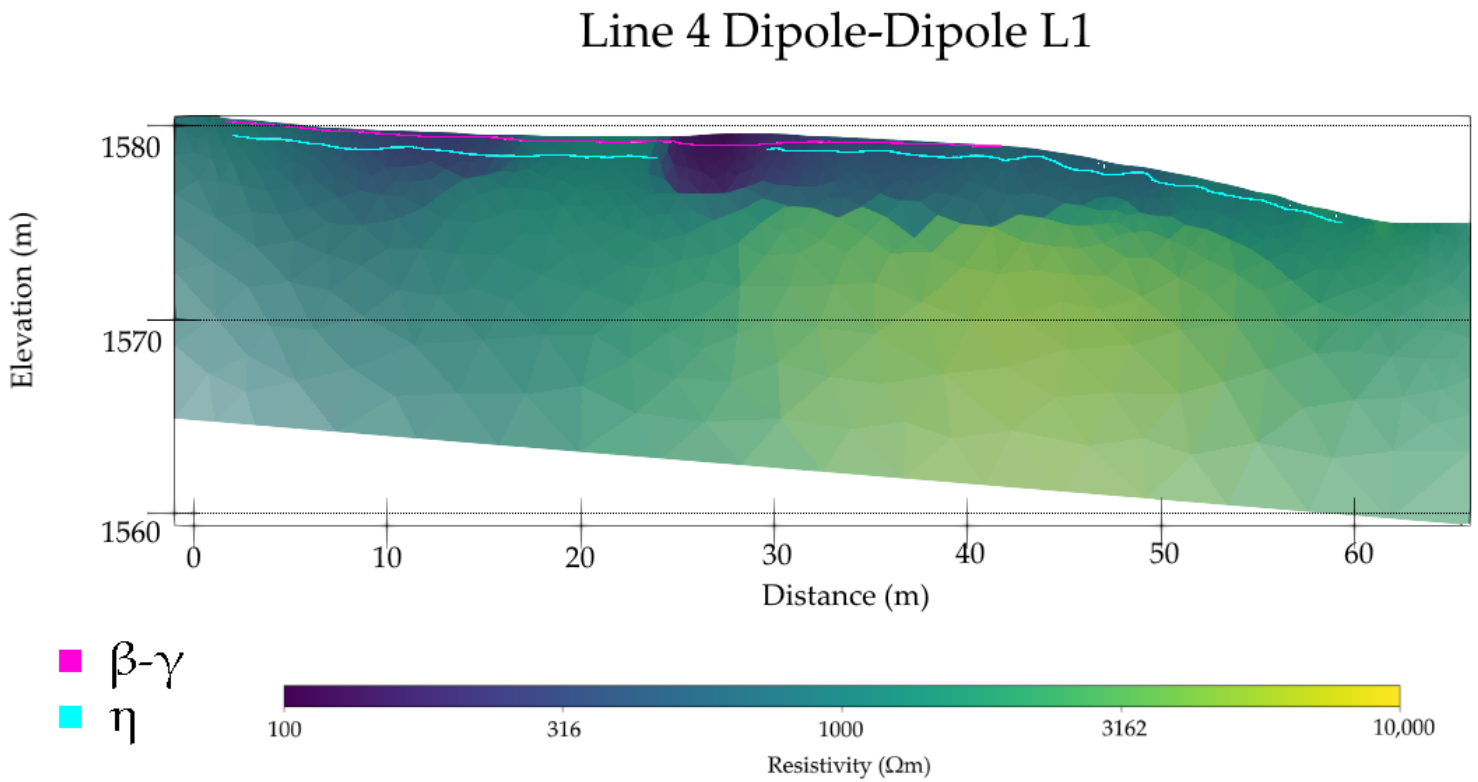
Line 4 Dipole-Dipole L1
Elevation (m)
1580
1570
1560
0
10
20
30
40
50
60
Distance (m)
β-γ
η
100
316
1000
3162
10,000
Resistivity (Ωm)

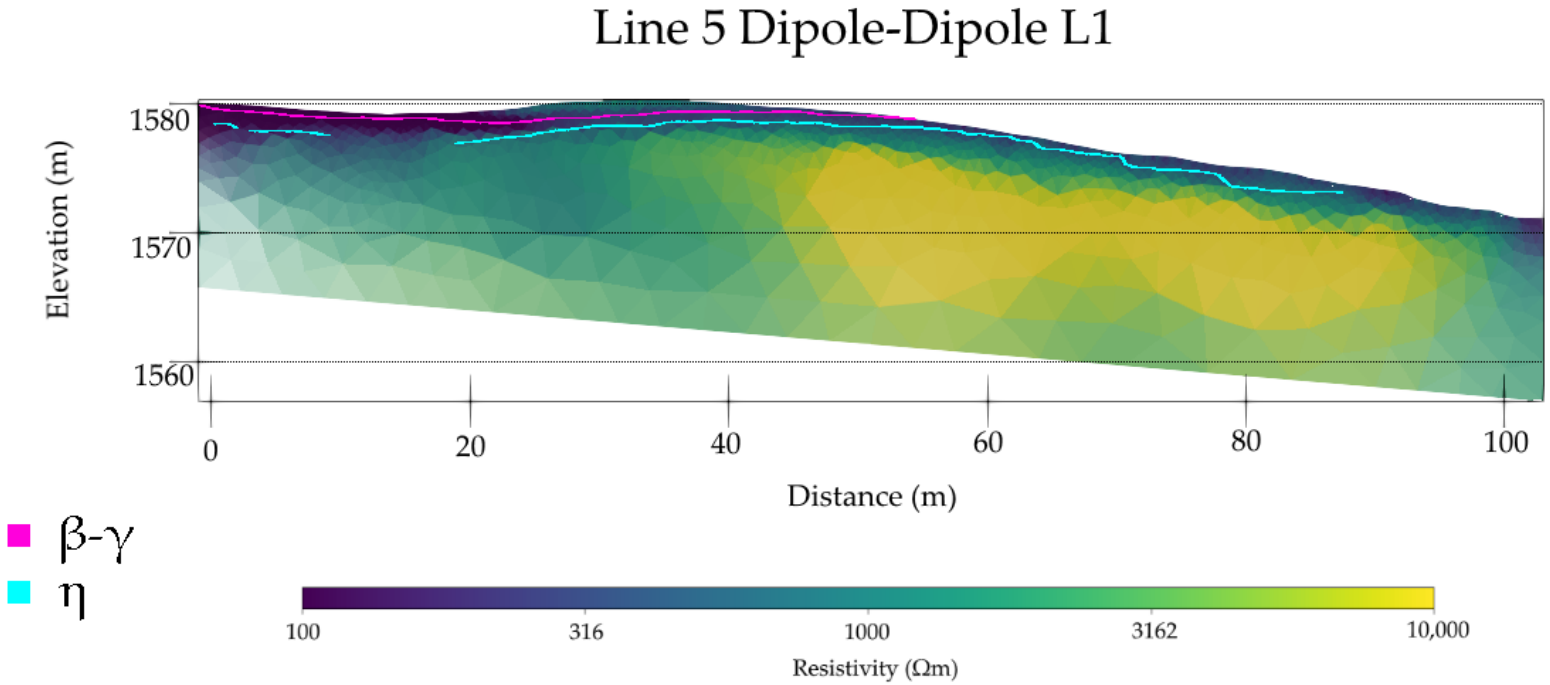
Line 5 Dipole-Dipole L1
Elevation (m)
1580
1570
1560
0
20
40
60
80
100
Distance (m)
β-γ
η
100
316
1000
3162
10,000
Resistivity (Ωm)

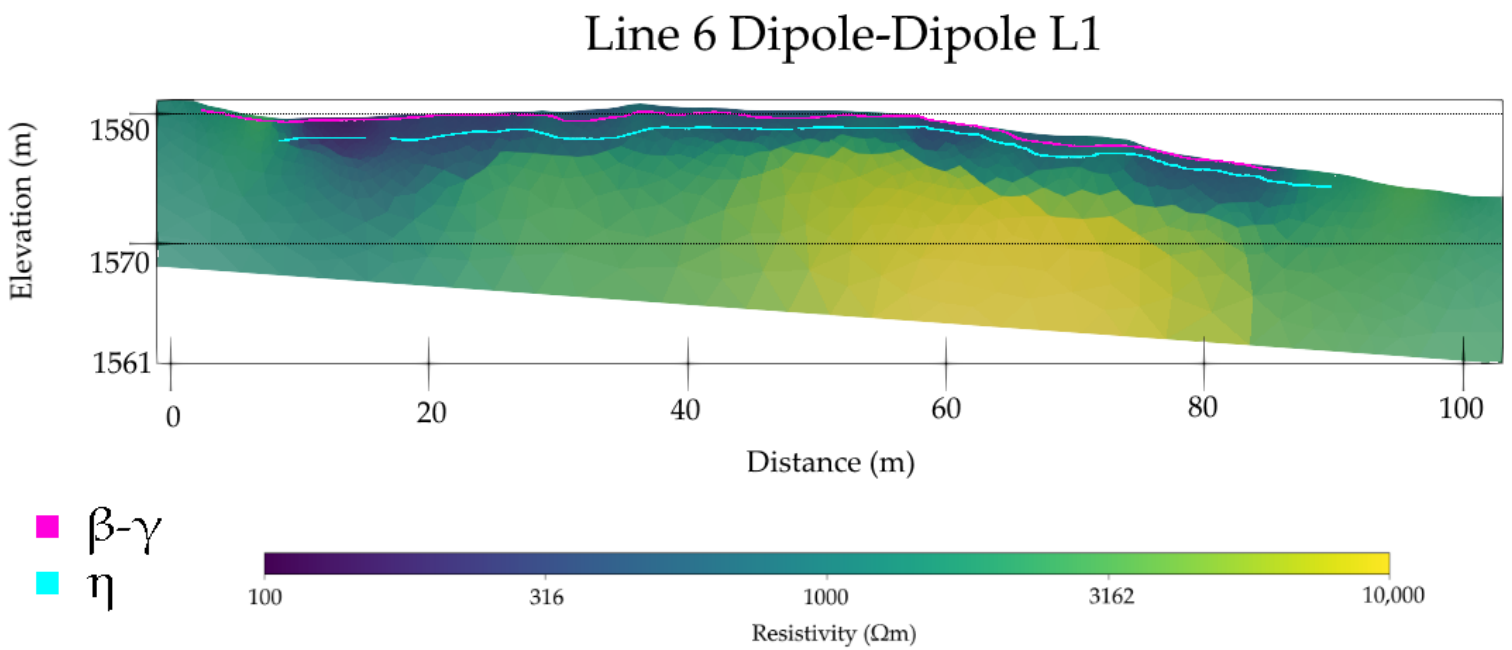
Line 6 Dipole-Dipole L1
Elevation (m)
1580
1570
1561
0
20
40
60
80
100
Distance (m)
β-γ
η
100
316
1000
3162
10,000
Resistivity (Ωm)

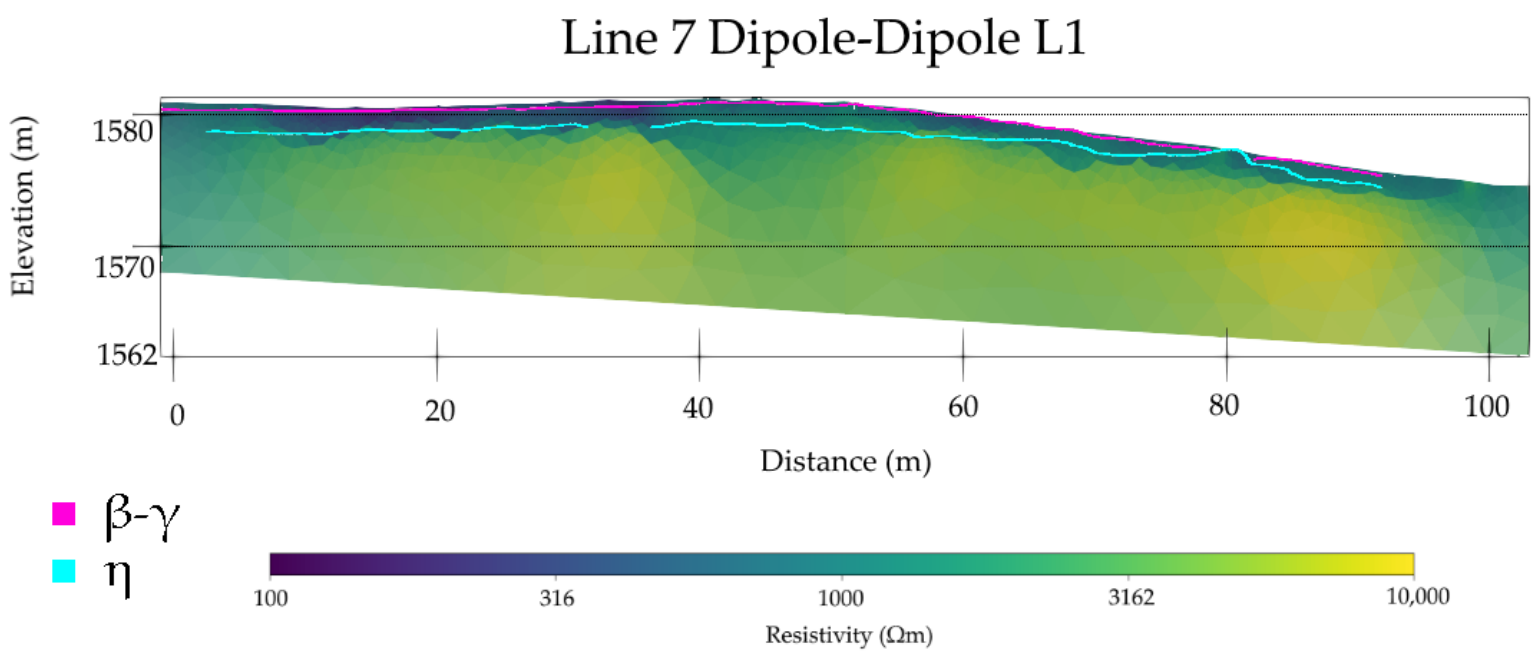
Line 7 Dipole-Dipole L1
Elevation (m)
1580
1570
1562
0
20
40
60
80
100
Distance (m)
β-γ
η
100
316
1000
3162
10,000
Resistivity (Ωm)

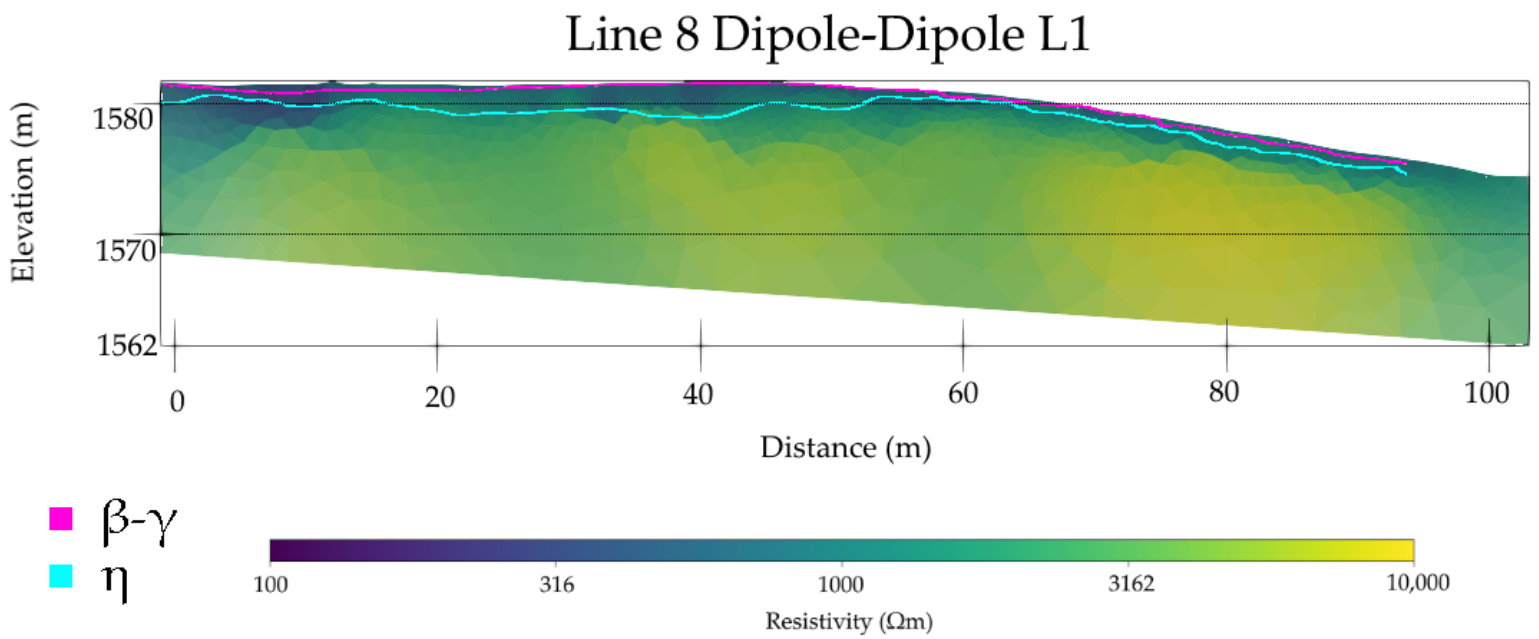
Line 8 Dipole-Dipole L1
Elevation (m)
1580
1570
1562
0
20
40
60
80
100
Distance (m)
β-γ
η
100
316
1000
3162
10,000
Resistivity (Ωm)

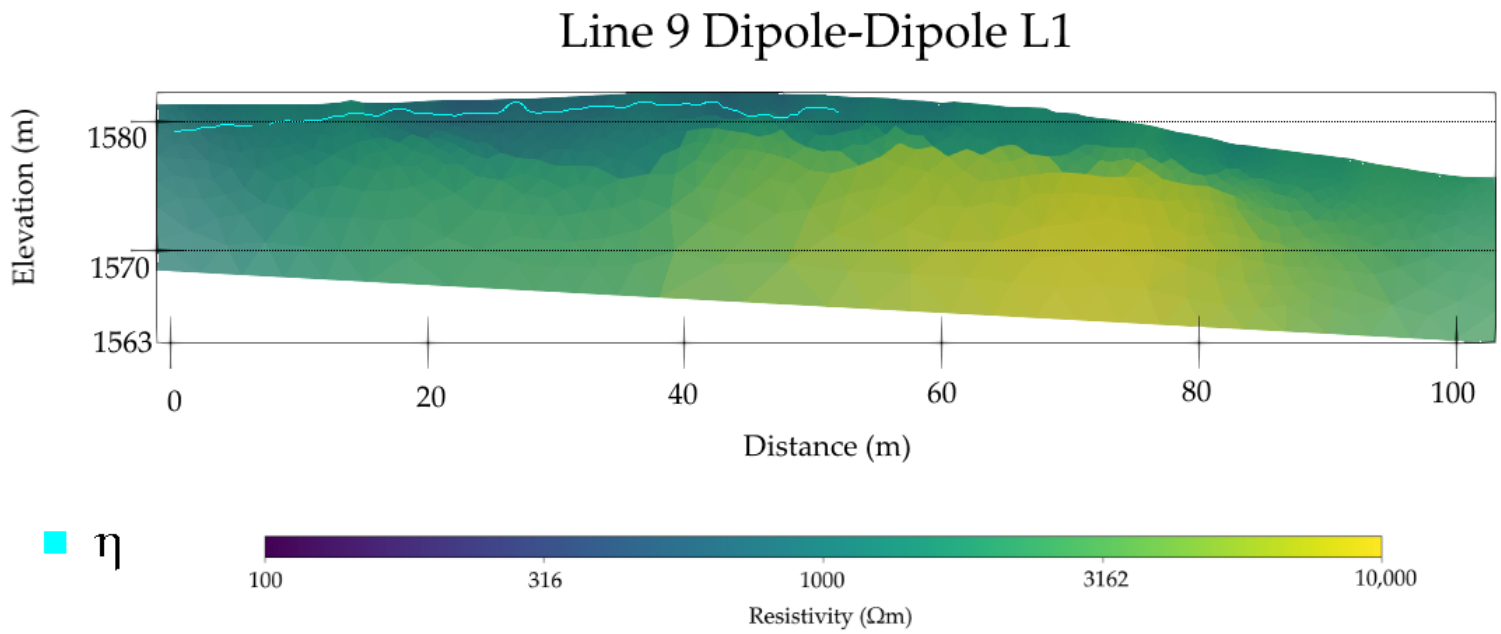
Line 9 Dipole-Dipole L1
Elevation (m)
1580
1570
1563
0
20
40
60
80
100
Distance (m)
η
100
316
1000
3162
10,000
Resistivity (Ωm)

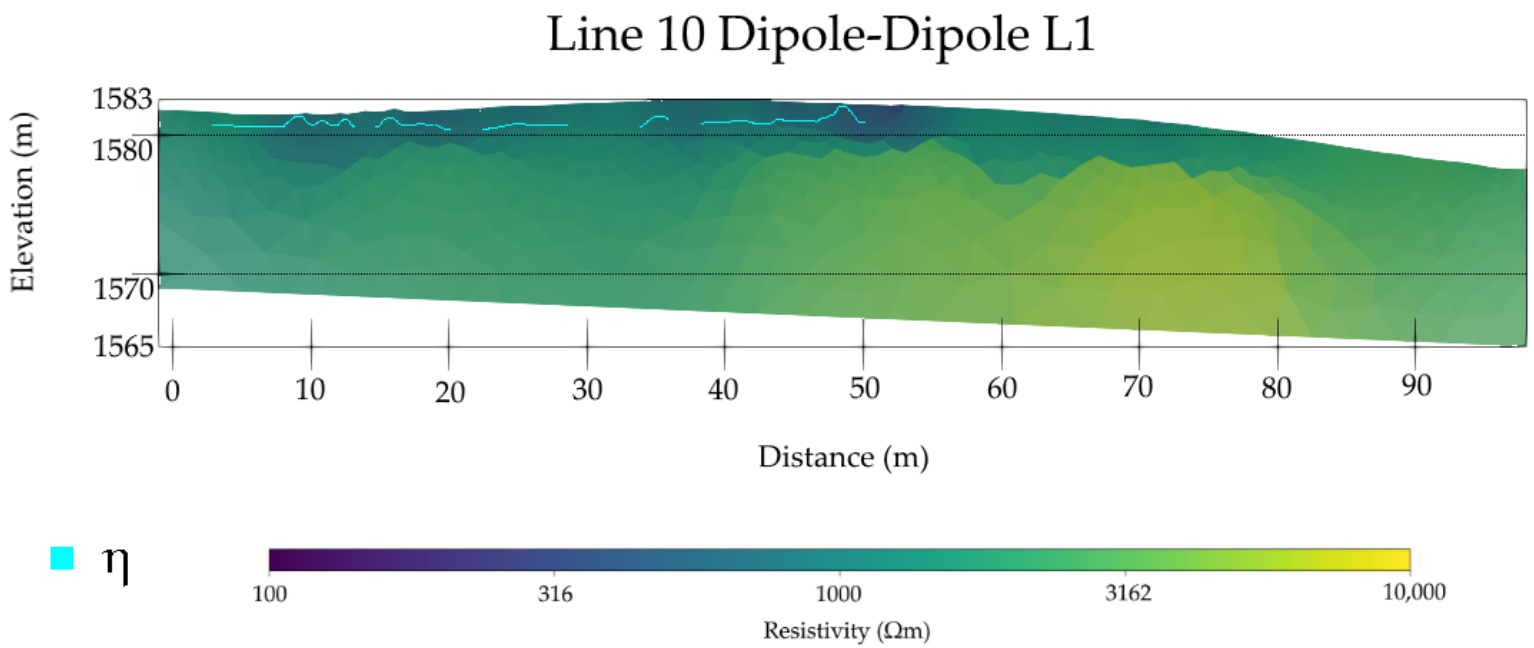
Line 10 Dipole-Dipole L1
Elevation (m)
1583
1580
1570
1565
0
10
20
30
40
50
60
70
80
90
Distance (m)
η
100
316
1000
3162
10,000
Resistivity (Ωm)

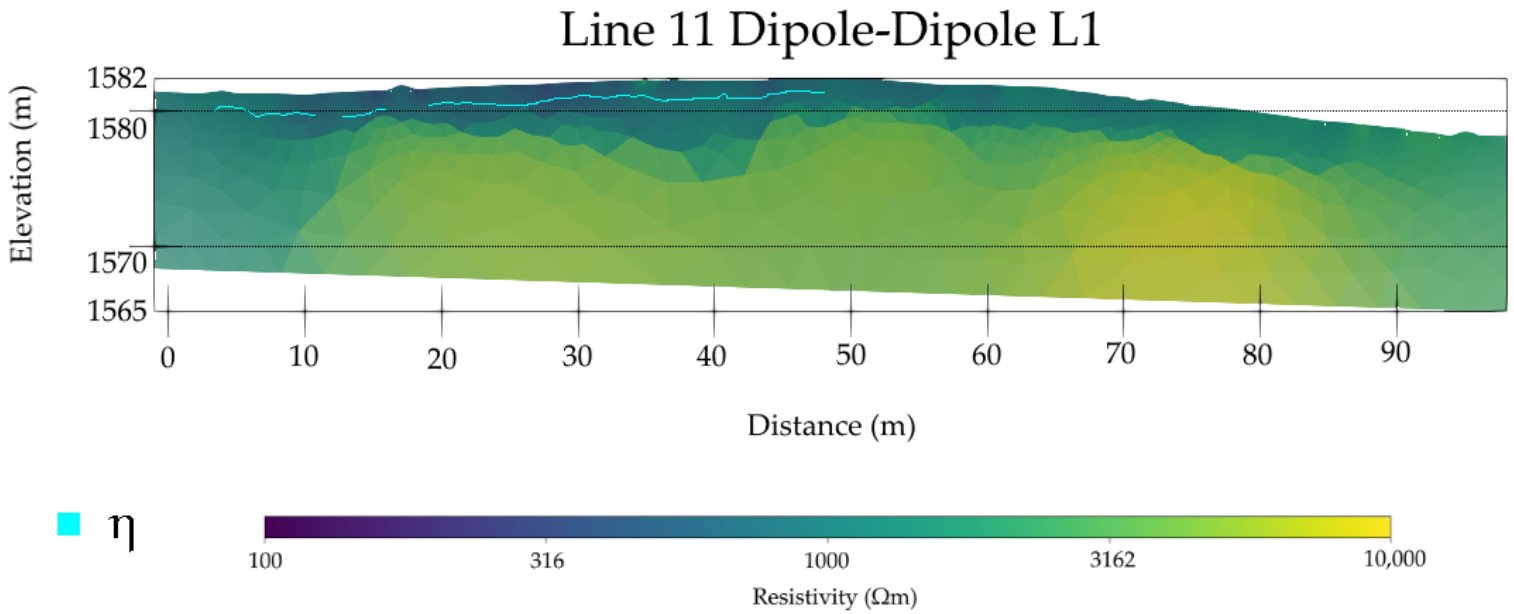
Line 11 Dipole-Dipole L1
Elevation (m)
1582
1580
1570
1565
0
10
20
30
40
50
60
70
80
90
Distance (m)
η
100
316
1000
3162
10,000
Resistivity (Ωm)

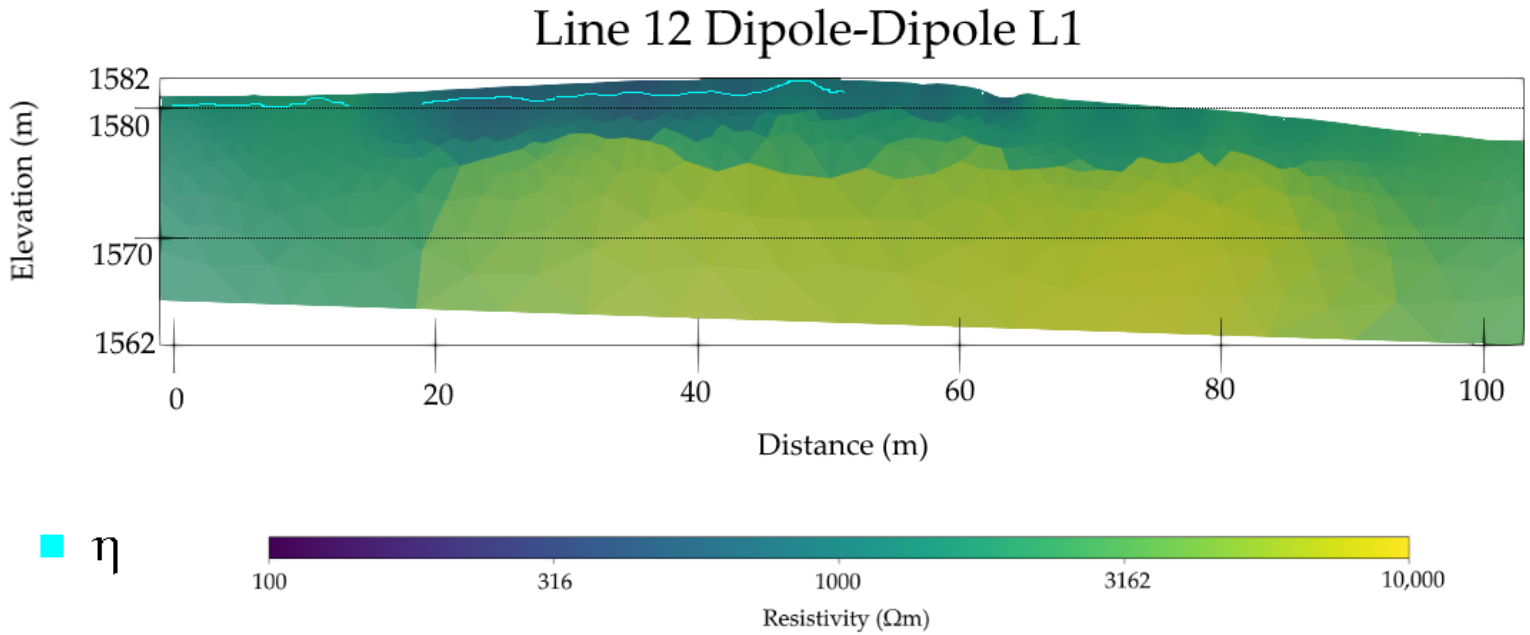
Line 12 Dipole-Dipole L1
Elevation (m)
1582
1580
1570
1562
0
20
40
60
80
100
Distance (m)
η
100
316
1000
3162
10,000
Resistivity (Ωm)

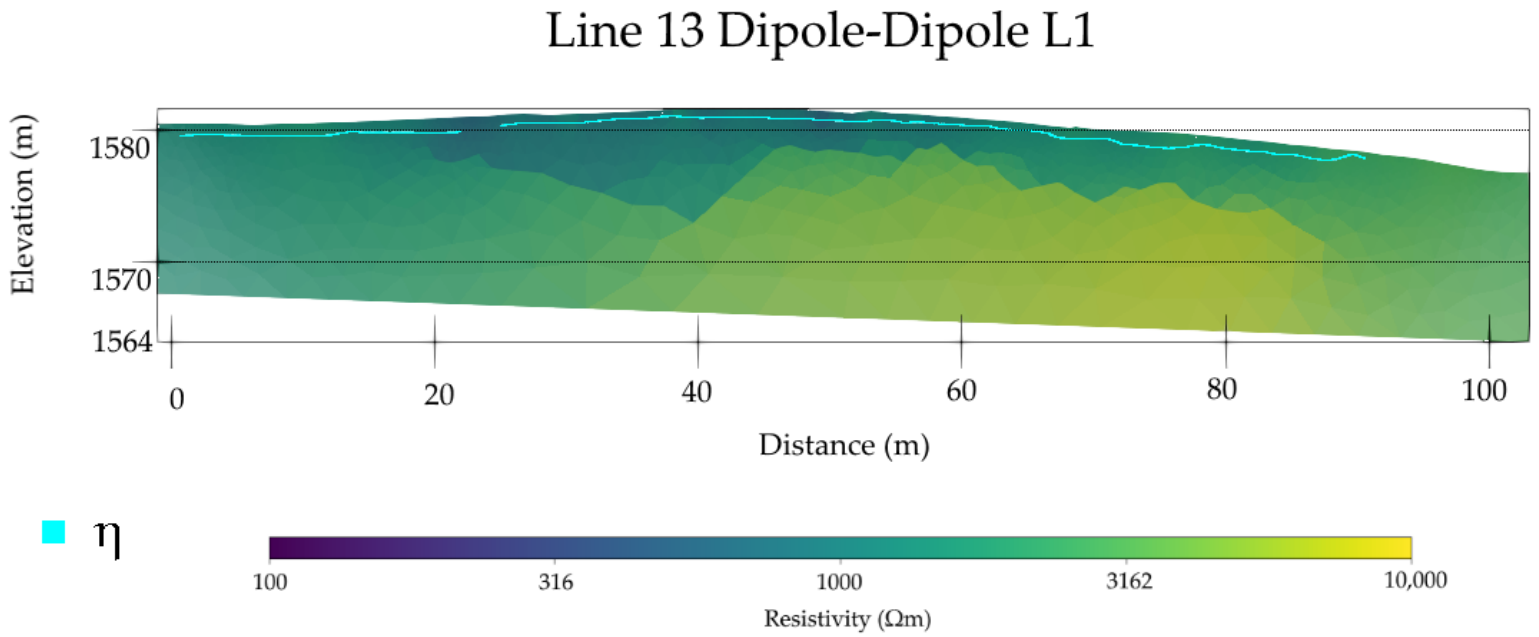
Line 13 Dipole-Dipole L1
Elevation (m)
1580
1570
1564
0
20
40
60
80
100
Distance (m)
η
100
316
1000
3162
10,000
Resistivity (Ωm)

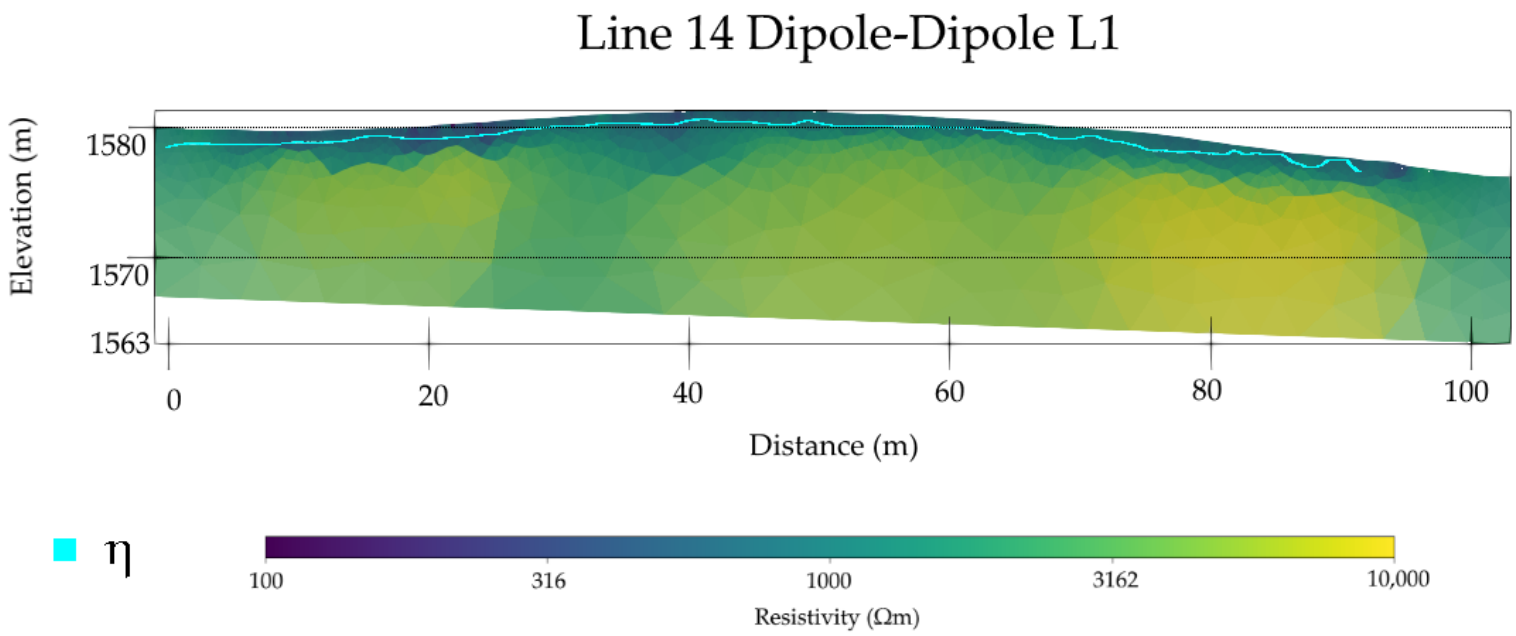
Line 14 Dipole-Dipole L1
Elevation (m)
1580
1570
1563
0
20
40
60
80
100
Distance (m)
η
100
316
1000
3162
10,000
Resistivity (Ωm)

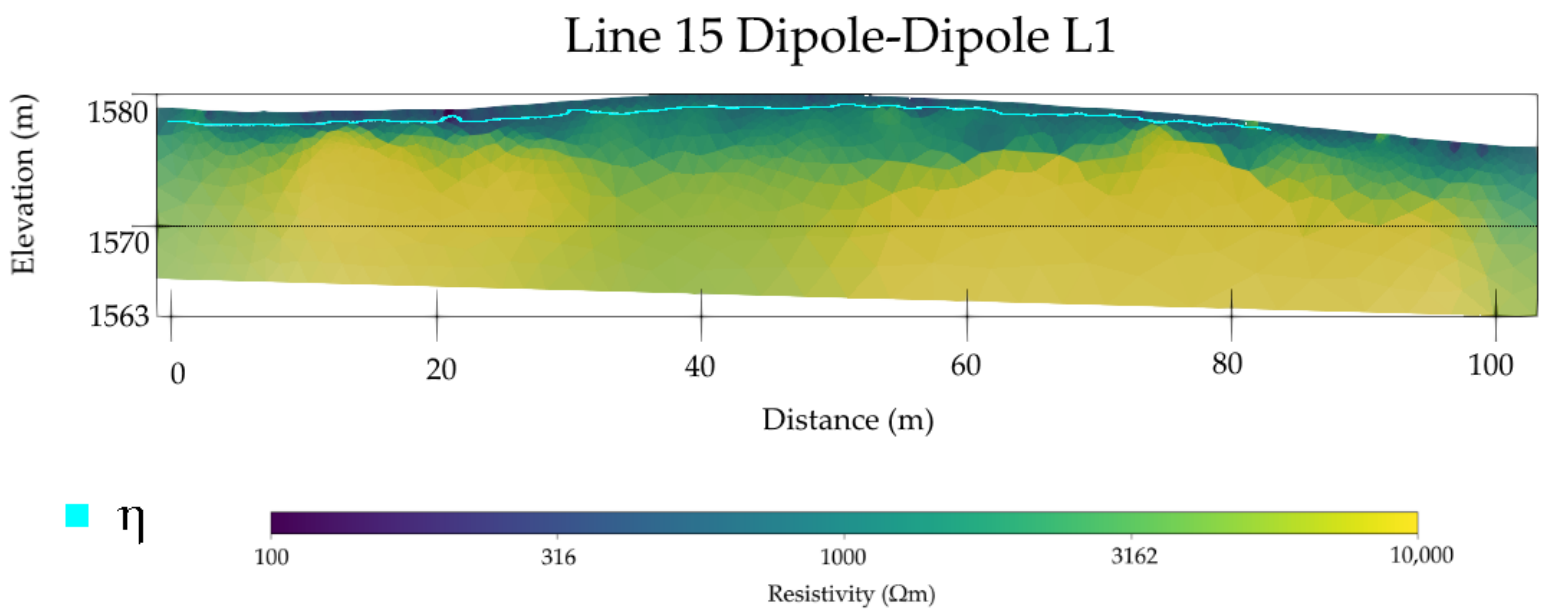
Line 15 Dipole-Dipole L1
Elevation (m)
1580
1570
1563
0
20
40
60
80
100
Distance (m)
η
100
316
1000
3162
10,000
Resistivity (Ωm)

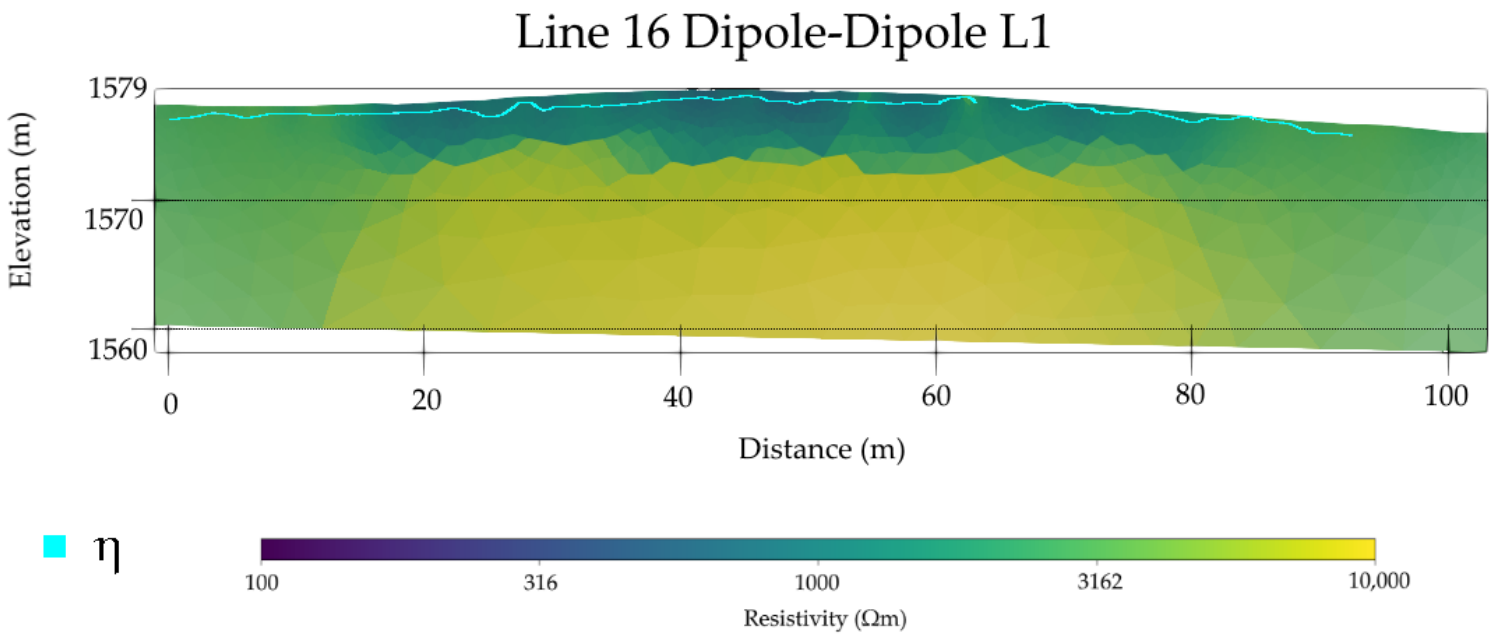
Line 16 Dipole-Dipole L1
Elevation (m)
1579
1570
1560
0
20
40
60
80
100
Distance (m)
η
100
316
1000
3162
10,000
Resistivity (Ωm)

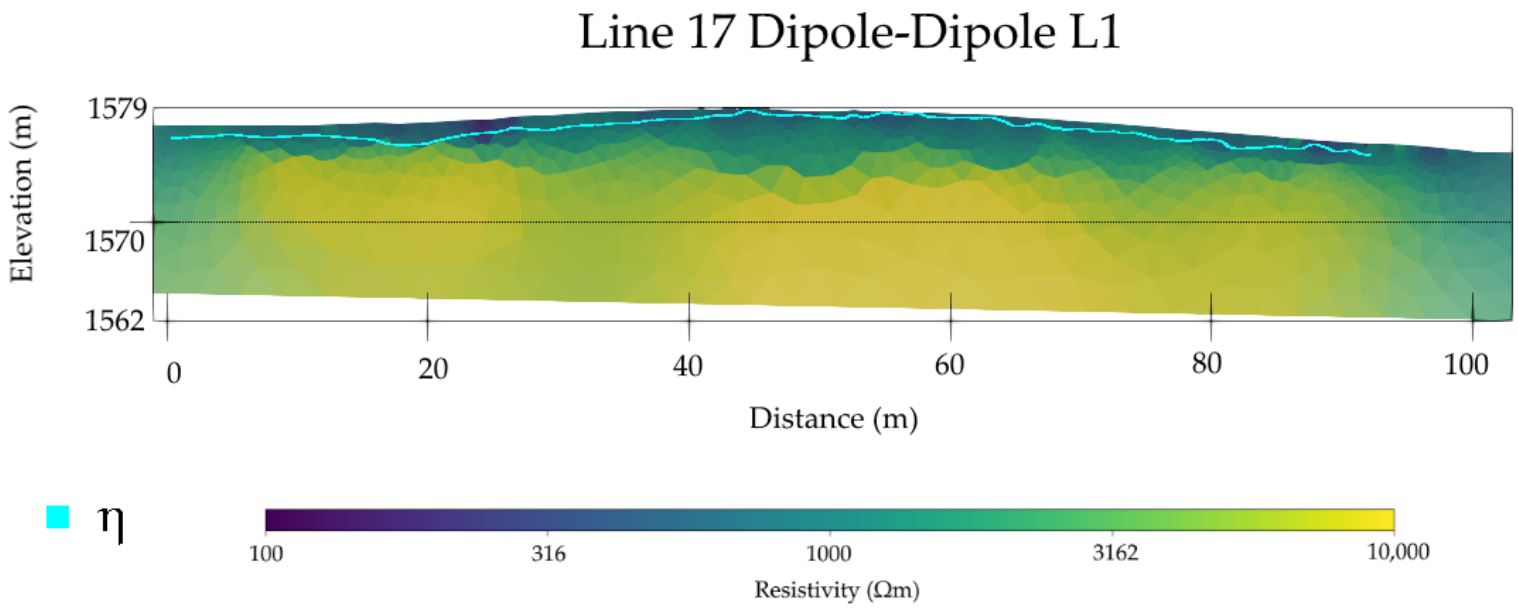
Line 17 Dipole-Dipole L1
Elevation (m)
1579
1570
1562
0
20
40
60
80
100
Distance (m)
η
100
316
1000
3162
10,000
Resistivity (Ωm)

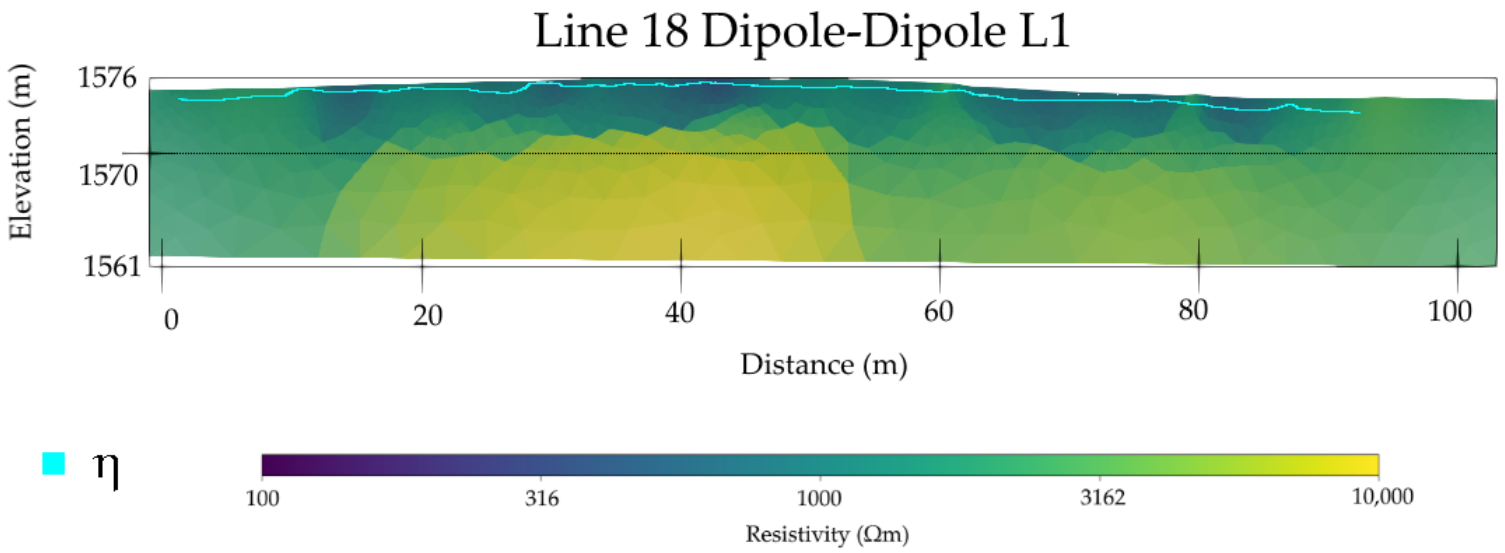
Line 18 Dipole-Dipole L1
Elevation (m)
1576
1570
1561
0
20
40
60
80
100
Distance (m)
η
100
316
1000
3162
10,000
Resistivity (Ωm)

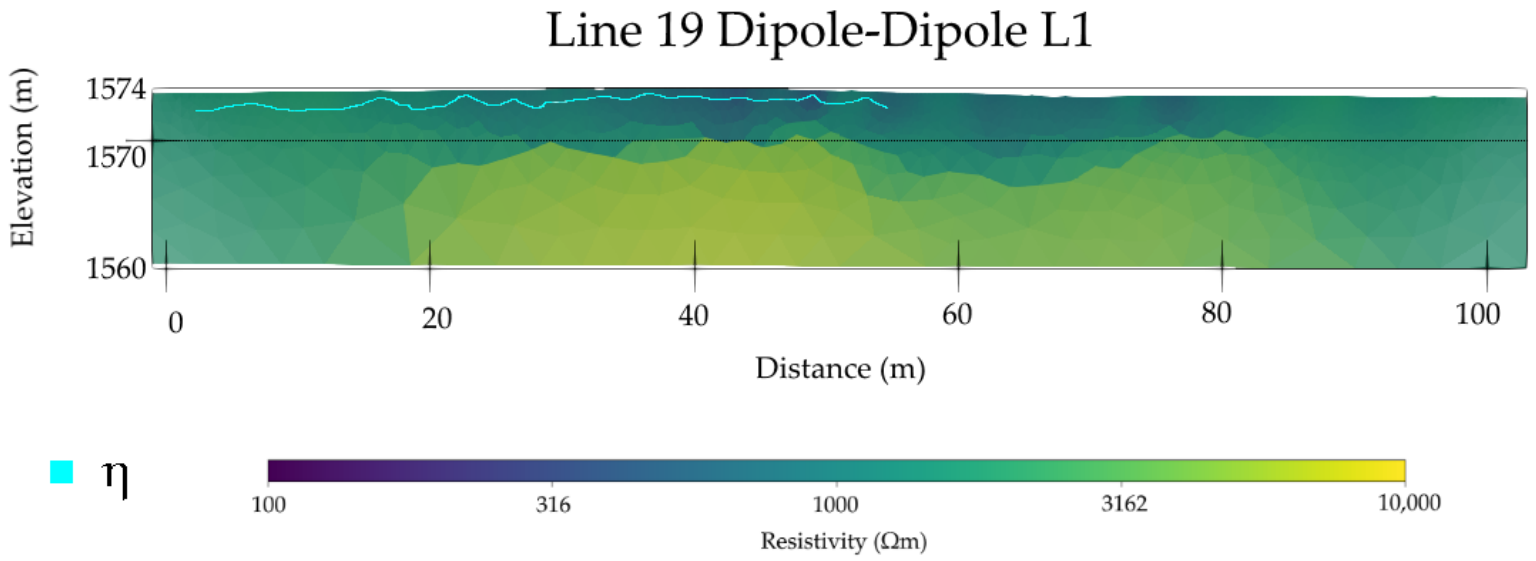
Line 19 Dipole-Dipole L1
Elevation (m)
1574
1570
1560
0
20
40
60
80
100
Distance (m)
η
100
316
1000
3162
10,000
Resistivity (Ωm)

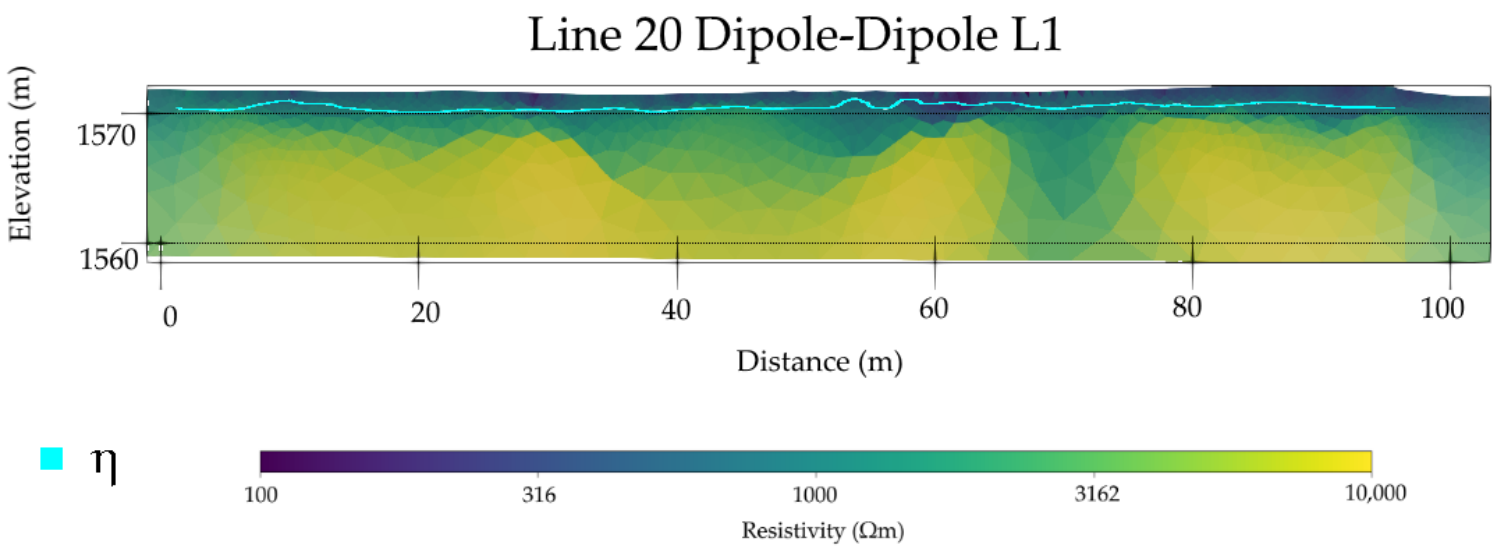
Line 20 Dipole-Dipole L1
Elevation (m)
1570
1560
0
20
40
60
80
100
Distance (m)
η
100
316
1000
3162
10,000
Resistivity (Ωm)

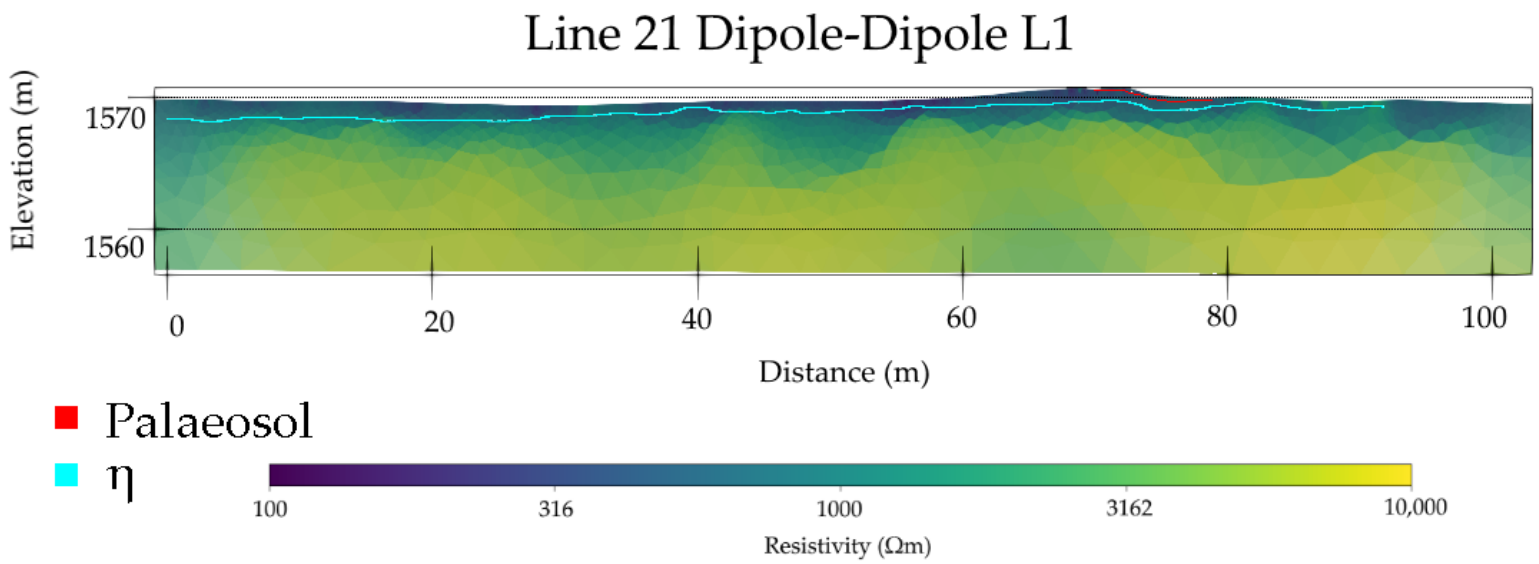
Line 21 Dipole-Dipole L1
Elevation (m)
1570
1560
0
20
40
60
80
100
Distance (m)
Palaeosol
η
100
316
1000
3162
10,000
Resistivity (Ωm)

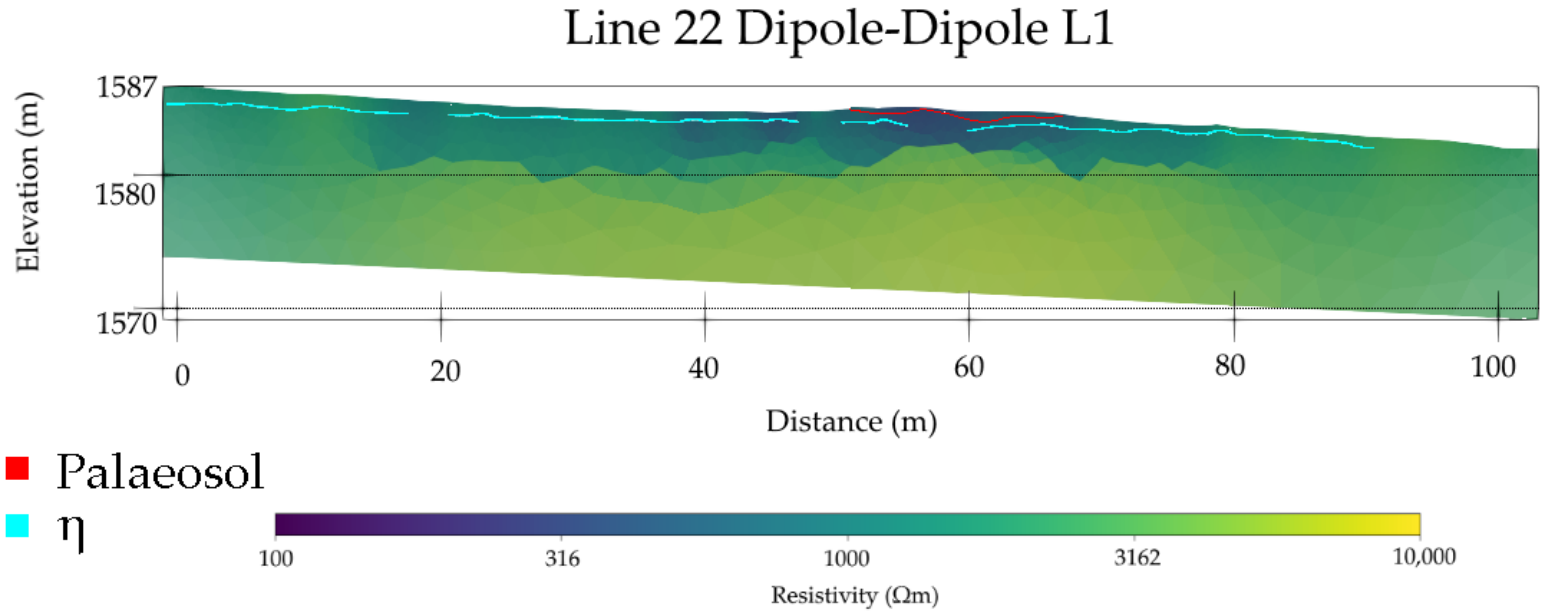
Line 22 Dipole-Dipole L1
Elevation (m)
1587
1580
1570
0
20
40
60
80
100
Distance (m)
Palaeosol
η
100
316
1000
3162
10,000
Resistivity (Ωm)

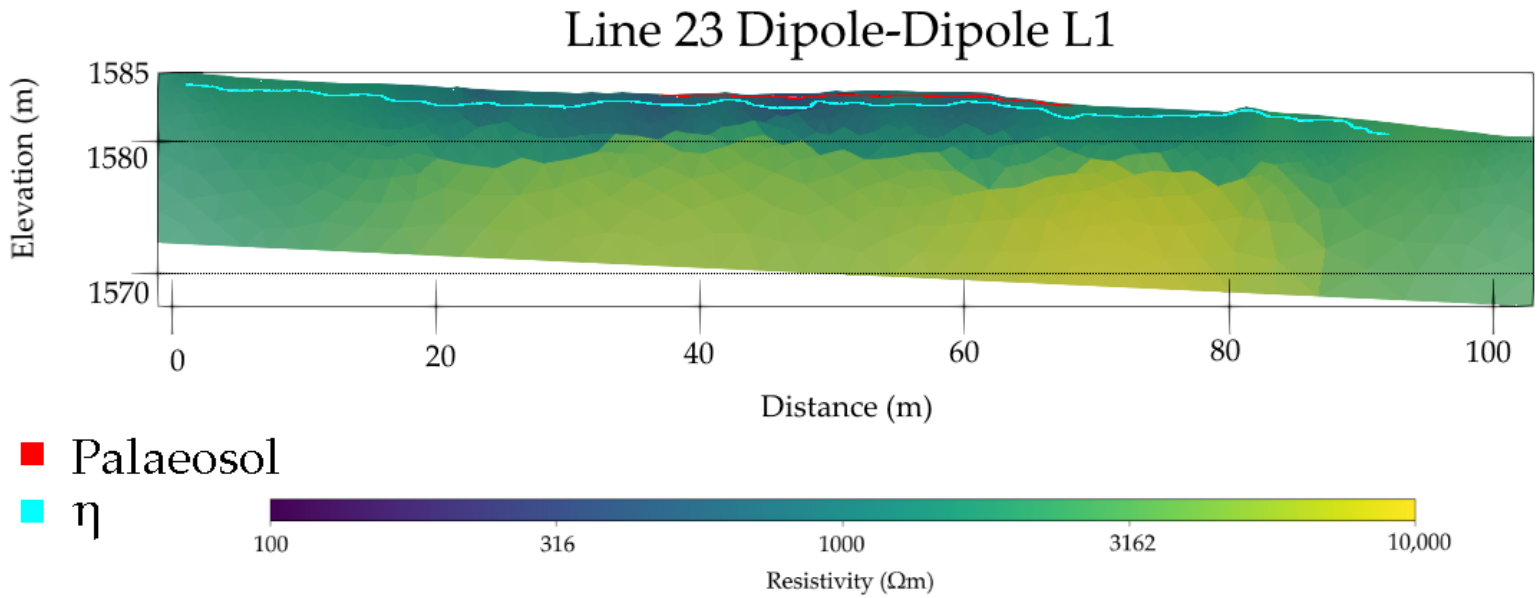
Line 23 Dipole-Dipole L1
Elevation (m)
1585
1580
1570
0
20
40
60
80
100
Distance (m)
Palaeosol
η
100
316
1000
3162
10,000
Resistivity (Ωm)

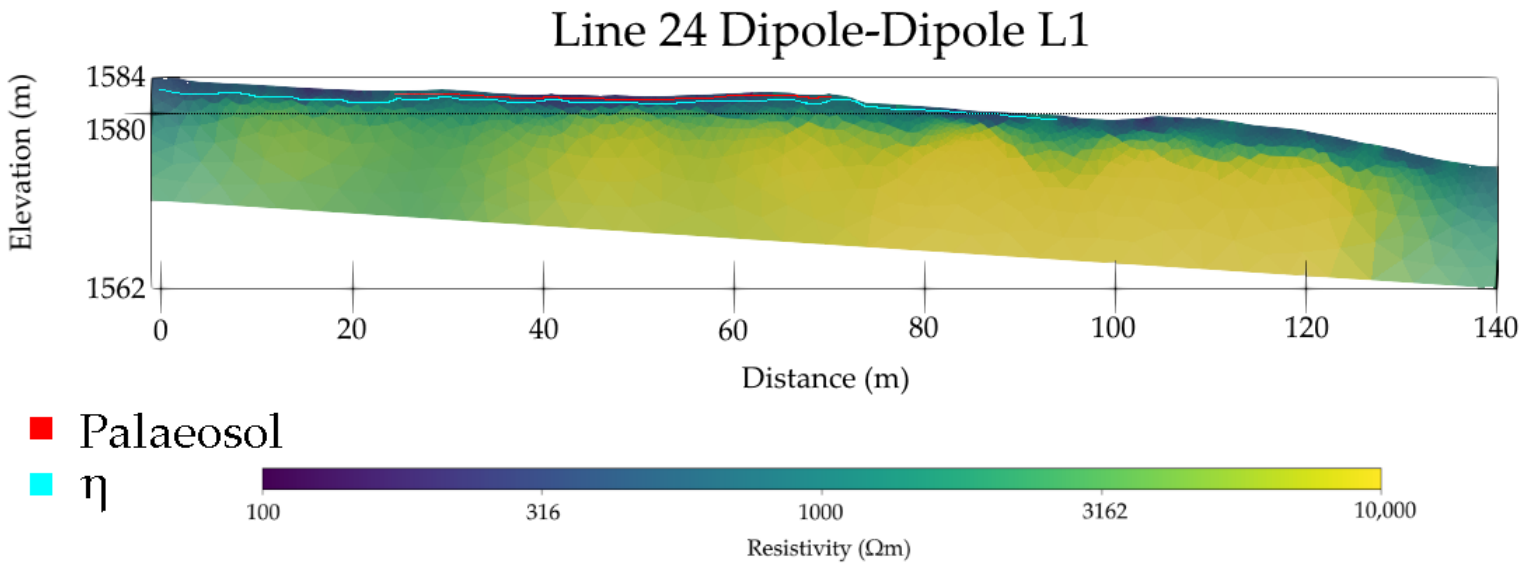
Line 24 Dipole-Dipole L1
Elevation (m)
1584
1580
1562
0
20
40
60
80
100
120
140
Distance (m)
Palaeosol
η
100
316
1000
3162
10,000
Resistivity (Ωm)

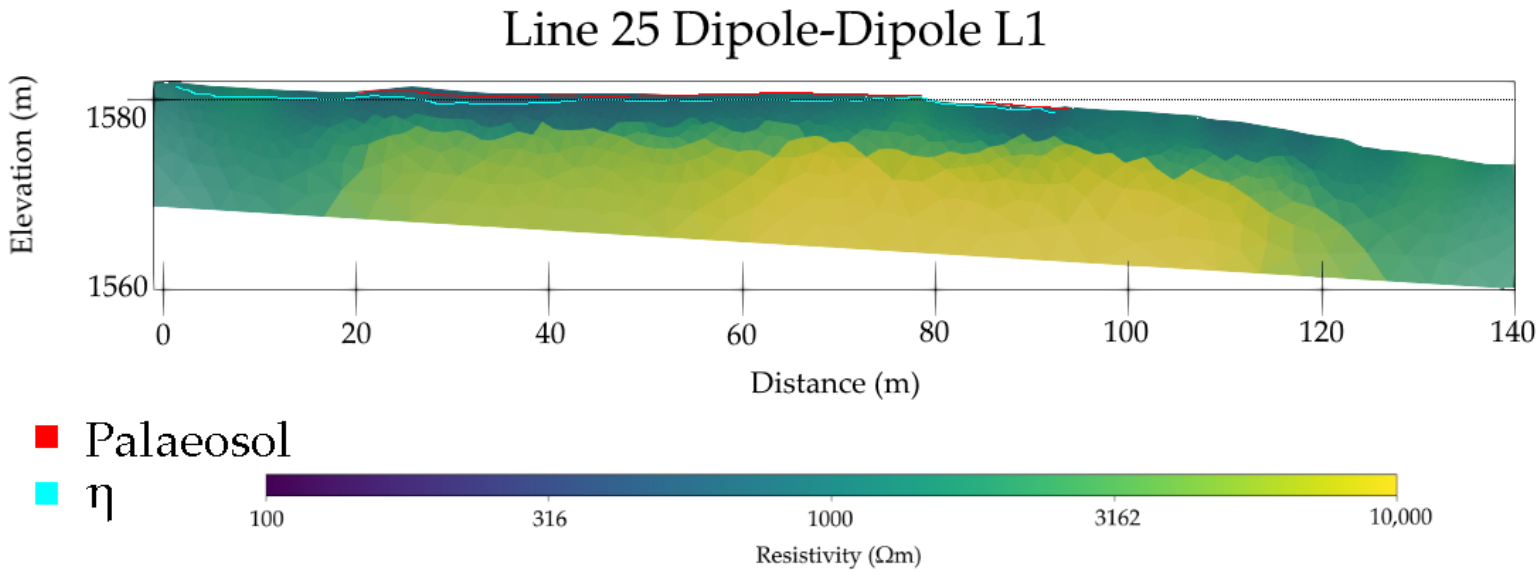
Line 25 Dipole-Dipole L1
Elevation (m)
1580
1560
0
20
40
60
80
100
120
140
Distance (m)
Palaeosol
η
100
316
1000
3162
10,000
Resistivity (Ωm)